MIXED-CONVECTION HEAT TRANSFER IN VERTICAL CHANNELS WITH ARBITRARY WALL CONDITIONS

by

Reza Sarmast
B.Sc., M.Sc., D.I.C.

Thesis submitted for the degree of
Doctor of Philosophy
of the
University of London

November, 1978

Thermal Power Section,
Department of Mechanical Engineering,
Imperial College of Science and Technology,
London, SW7 2BX

To:

Judith,

Margery,

Joseph.

ABSTRACT

This thesis describes a theoretical and experimental study of mixed forced-free laminar convection in vertical channels with an arbitrary prescribed wall heat-flux or temperature.

The problem is solved for two different cross-sections: rectangular and circular. The results are based on a numerical solution of the conservation equations of mass, momentum and energy using a finite-difference method. No restriction on the profiles of wall heat-flux or temperature is made, solutions being obtained for various profiles. The scope of application of the method is wider for the rectangular cross-section than for the circular one, because in the former case, the computer program is written in such a way that the profiles of heat-flux or temperature on the opposite walls may differ. The method is applied to predict different cases of wall heat-flux profiles and of continuously developing flow along the channel. Special reference is made to models simulating plate-type nuclear fuel elements, as contained in the core of the University of London Reactor, at different power levels. The pressure drop and the nature of the flow inside channels of these elements are obtained. The problem relates to the maximum safe power at which the reactor can be operated.

A search for a relevant parameter to represent the mixed-convection flows is pursued and as a result, the parameter Gr_D/Re_D^2 is found to be suitable. Using this parameter, a plan is proposed for a general representation of the pure-forced convection, pure free-convection and mixed-convection regimes.

In order to gain more confidence in the adequacy of the theoretical method, the predictions are compared with available

published results for prescribed uniform or sinusoidal heating cases. There is always good agreement between the results, which were further checked by considering a wall heat-flux profile for a typical channel and obtaining the corresponding wall temperature profile. Then, this profile is considered as data for the same channel and the wall heat-flux is re-obtained. A comparison between the two wall heat-flux profiles adds to the confidence about the present method.

The possibility of the inception of an inflexion point in the axial velocity profile under various profiles of heating is also examined. For flow in round tubes, a tentative transition parameter, based on the published experimental results for uniform heating cases, is used to predict the possibility of transition from laminar flow into an unstable flow.

The effects of different entrance conditions (e.g. Reynolds number, entrance velocity profile, water inlet temperature) on the flow are also investigated.

The results for mixed-convection cases are compared with the corresponding forced-convection cases and it is concluded that because of continuously changing velocity and temperature profiles, a mixed-convection flow never becomes fully-developed.

ACKNOWLEDGEMENTS

Very many people have contributed to the successful completion of this thesis. I would like to acknowledge first the invaluable help of my supervisor, Professor W. Murgatroyd, for his encouragement and guidance throughout the work.

Thanks are also due to Dr. A. A. El-Shirbini for his helpful advice, particularly on the experimental part of the project. The financial help of the University of London Reactor Centre (ULRC) towards the expenses of part of the test-rig, together with the valuable technical advice of Mr. G. D. Burholt are gratefully acknowledged.

My thanks are extended to Mr. K. Graham, HEDIN Limited, for his helpful advice on the design of the simulating heaters and for providing the special insulating material (FILAMIC) for their construction. The making of substantial portions of the test-rig was very ably performed by Mr. K. Barham (Mech. Eng. Workshop) to whom I owe many thanks.

I would like to express my appreciation to Messrs. J. Knight, N. Wood and J. Martin of the Steam Plant for their assistance and efforts in operating the test-rig. Mr. D. Bloxham has also been very helpful in the discussions about the electrical parts of the apparatus.

Special thanks are due to Miss D. Day who has been so helpful in administration matters and Miss E. Archer for her continuous interest in providing the references. I also thank Dr. B. Mitchell and Mrs. H. A. Bastin for their outstanding help in the preparation of the final manuscript.

Finally, I express my deepest gratitude to my fellow students with whom I discussed this project. The work was supported throughout by the British Council during a period of leave of absence from Arya-Mehr Univerisity, IRAN.

R. Sarmast,

November, 1978

TABLE OF CONTENTS

NOMENCLATURE

List of Symbols

a : Coefficient for the numerical integration in Eq. (3.36)

a´ : Element of the "Flow-Field" matrix, |PVU| in Eq. (3.44)

a´´ : Element of the "Temperature" matrix, |T| in Eq. (3.45)

b : A constant used in Eq. (8.30)

b´ : Element of the right-hand matrix, Eq. (3.44)

b´´ : Element of the right-hand matrix, Eq. (3.45)

c : A constant used in Eq. (8.30)

C´ : $ZDT/(Pr \cdot Re_D)$

C_1, C_2, C_3 : Constants defined by Eq. (3.5a)

CO1 : $1/(C_5 \cdot C_2)$

CO2 : $(t_{in} + C_1)/C_2$

CO3 : C_3

C_4, C_5, C_6 : Constants defined by Eq. (3.6)

CO4 : $C_4 - C_5 \cdot t_{in} + C_6 \cdot t_{in}^2$

CO5 : $2t_{in} \cdot C_6/C_5 - 1$

CO6 : $C_6/(C_5^2 \cdot G)$

C_p : Specific heat of the fluid at constant pressure

d : Gap between the walls of test-channel, Fig. (6.5a)

d´ : Coefficient for the numerical differentiation, Eq. (3.37)

D : Effective diameter of the channel;

$\begin{cases} D = 2d \rightarrow \text{For flat duct} \\ D = 2R \rightarrow \text{For round tube} \end{cases}$

E : $d/(2L)$

f_p : Pressure loss factor = $-\frac{\partial P_{mean}}{\partial Z}$

f_s : Shear loss factor = $\frac{\tau_w}{\frac{1}{2}\rho_m \cdot u_o^2}$

g : Gravitational acceleration

G : A dimensionless parameter = $d^3 \cdot g/\nu_B^2$

G_r : G parameter for round tubes = $R^3 \cdot g/\nu_B^2$

h : Heat transfer coefficient

$\Delta h'$: Effective level-difference between the Supply and the Discharge Tanks, Fig. (6.1)

$\Delta h'_e$: $(\Delta p_{tot} - \Delta p_{gain})/(\rho_m \cdot g)$

i : Mixed-convection index defined in Section (a.5) of (5.3.3). For forced convection; i = 0 while for free convection; i = 100

I : Electric current through each simulating plate

J : An index to represent intermediate points for the numerical integration, Eq. (3.36)

k : Thermal conductivity

ℓ : Dummy coordinate

L : Length of the channel

L' : Extrapolated length of the channel, Fig. (6.11)

m : Horizontal parameter shown on Figs. (3.4) and (8.2)

$\dot{m}$: Mass flow rate through the test-channel

M : Number of horizontal divisions in the finite-difference approximation as shown on Figs. (3.4) and (8.2)

n : Axial parameter as shown on Figs. (3.4) and (8.2)

N : Number of divisions considered for the numerical integration, Eq. (3.36)

N' : Number of divisions considered for the numerical differentiation, Eq. (3.37)

p : Pressure

$p_{o.extra}$: Extra pressure needed at the entrance to the test-channel for forcing the fluid through the channel

$\Delta p_{t.s}$: Pressure drop in the test-section

Δp_{gain} : Pressure gain in the test-section

Δp_{tot} : Total pressure drop throughout the water circuit, Fig. (6.1)

P : Dimensionless pressure parameter = $\frac{p}{\rho_m \cdot u_o^2}$

$\dot{q}''_w$: Heat-flux rate at wall, Fig. (7.2)

$\dot{q}''_{cd}$: Rate of longitudinal heat conduction, Fig. (7.2)

$\dot{Q}_n$: Heat rating of the division "n", Table (6.1)

$\dot{Q}_{tot}$: Total heat rating of the test-channel

r : Dimensionless radial coordinate = r'/R

r' : Radial coordinate

r_t : Ratio of wall temperatures = $\frac{t_{wo} - t_{in}}{t_{wi} - t_{in}}$

r_q : Ratio of wall heat-fluxes = $\dot{q}''_{wo}/\dot{q}''_{wi}$

R : Tube radius

R_1, R_2 : Conversion ratios of the transformers, Fig. (6.17)

R' : Electrical resistance of a simulating plate (Ω)

S : Parameter indicating the direction of the flow;

$$\begin{cases} \text{Upward flow} \rightarrow S = 1 \\ \text{Downward flow} \rightarrow S = -1 \\ \text{Adiabatic flow} \rightarrow S = 0 \end{cases}$$

t : Temperature

t_1 : Selected temperature for water in the Heater Tank

t_{in} : Fluid temperature at the inlet to the test-section

t_{out} : Fluid temperature at the exit of the test-section

T : Dimensionless temperature parameter = $G \cdot C_s(t - t_{in})$

U : Axial velocity parameter = u/u_o

U^* : $d/(2\alpha) \cdot u$

v : Horizontal velocity

V : Horizontal velocity parameter = v/u_o

w : Width of the test-channel

x : Third coordinate (across the simulating plates)

X : x/w

y : Horizontal coordinate in flat duct

Y : Horizontal parameter = y/d

z : Axial coordinate measured from the entrance of the channel

z' : Axial coordinate measured from the middle of the channel

Z : Axial parameter;

$$\begin{cases} \text{For flat duct, } Z = z/d \\ \text{For round tube, } Z = z/R \end{cases}$$

Z_D : $Z/2$

Greek Symbols

α : Average thermal diffusivity of the fluid = $\dfrac{k}{\rho \cdot C_p}$

β : $\dot{q}''_{w.Max}/\dot{q}''_{w.av}$

β' : Bulk expansion coefficient

δ : Dummy axial coordinate

δ' : Thickness of the simulating plate

ρ : Density

ρ' : Specific resistance (Ω/unit length)

μ : Viscosity

ν : Kinematic viscosity = μ/ρ

θ^* : Dimensionless temperature = $(t - t_{in} - \frac{1}{2} \cdot \frac{\partial t_{mean}}{\partial z} \cdot L) / (\frac{\dot{q}''' \cdot d}{2k})$

η_A : (CO1 . T/G + CO2)

η_B : $\frac{d}{dT} (\eta_A)$

ξ : {CO4 . G + T (CO5 + CO6 . T)}

τ_w : Shear stress at wall

Dimensionless Numbers

Gr_D : Grashof number = $\frac{\beta_o' \cdot g \cdot \dot{q}'''_{w.av} \cdot D^4}{\nu_m^2 \cdot k_m}$

Gr_t : Grashof number based on the temperature
= $\beta_o' \cdot g \cdot (t - t_{in}) \cdot D^3/\nu_m^2$

Nu : Nusselt number = $D \cdot h/k_m$

Nu_i : Nusselt number at the "inner" wall
= $\frac{D \cdot h_{wi}}{k_m}$

Nu_o : Nusselt number at the "outer" wall
= $\frac{D \cdot h_{wo}}{k_m}$

Pe : Peclet number = $Re \cdot Pr$

Pr : Prandtl number = $\mu_B \cdot (\frac{C_p}{k})_m$

Ra : Rayleigh number = $Pr \cdot Gr_D$

Re : Flow Reynolds number = $\rho_m \cdot u_o \cdot d/\mu_B$

Re_m : Bulk Reynolds number = $u_o \cdot d/\nu_m$

Re_o : Entrance Reynolds number = $u_o \cdot d/\nu_o$

Subscripts

Av : Average

B : Base

C : Coolant

℄ : Centreline

D : Based on the effective diameter, D

f : Frictional

H : Based on constant $\dot{q}''_w$ case

i : Measured at the inner wall (Y = 0 RL)

m : Measured halfway through the channel

mean : Integrated throughout the cross-section

o : Measured at the outer wall (Y = 1 RL)

p : Peak

tot : Total

T : Based on constant t_w case

0 : Entrance to the test-channel

∞ : A reference point

w : Wall

Abbreviations

CIRCLE : The computer program to solve for round tube geometry

DUCT : The computer program to solve for flat duct geometry

DVM : Digital Volt Meter

F : Dummy function

FI : Prescribed function at the inner wall

FO : Prescribed function at the outer wall

HFLUX : Dimensionless parameter for heat-flux rate in round tube geometry

$$= \frac{R^4 \cdot g \cdot C_s}{\nu_B^2 \cdot k_m \cdot M} \cdot \dot{q}''_w$$

HFI : Dimensionless parameter for heat-flux rate in flat duct at the inner wall

$$= \frac{d^4 \cdot g \cdot C_s}{\nu_B^2 \cdot k_m \cdot M} \cdot q''_{wi}$$

HFO : The same as HFI but at the outer wall

ICCC : Imperial College Computer Centre

PL : Plate

T/C : Thermocouple

TWALL : Dimensionless parameter for t_w in round tube geometry

$= G_r \cdot C_s (t_w - t_{in})$

TWI : Dimensionless parameter for t_{wi} in flat duct geometry

$= G \cdot C_s (t_{wi} - t_{in})$

TWO : The same as TWI but for t_{wo}

ULCC : University of London Computer Centre

ULR : University of London Reactor

ULRC : University of London Reactor Centre

ZDT : Z_D for the Thermal Entry Length

ZDU : z_D for the Hydrodynamic Entry Length

NB (i) For forced-convection cases where; ρ = Cte., the constant C_s must be replaced by $1/t_{in}$

(ii) Notation of the parameters used in the Flow-Charts of DUCT and CIRCLE computer programs is given in Chapter (4). The listing of these two programs is available at:-

Thermal Power Section, Imperial College of Science and Technology, London, SW7 2BX

CHAPTER 1

INTRODUCTION

Most studies of laminar convective heat transfer in vertical channels were done in channels in which the longitudinal heating was uniform. Moreover, the problem has been simplified by assuming that either "free" or "forced" convection effects dominate the mode of heat transfer. In view of several practical situations which involve a mode of heat transfer which is neither free nor forced-convection but a mixture of these two, together with non-uniform prescribed heating on the wall, it has been decided to seek a method of solution which will be general in so far as solving for a mixed-convection regime with arbitrary wall conditions is concerned. For practical applications, the case of a plate-type fuel element in a low-power nuclear reactor, where the prescribed wall heat-flux along its channel is almost sinusoidal, has been solved for with special interest.

In order to gain more confidence about the present theoretical method, an experimental test-rig has been designed and successfully tested. Water has been used as the working fluid and the tests, and in fact the study as a whole, have been directed to deal only with one-phase flow regimes.

In Chapter (2) a review on the available literature on the forced and the mixed-convection regimes has been presented. Theoretical models, as well as experimental investigations on the subject, have been explained in detail. In particular, several methods of simulation of sinusoidal heating profiles have been reviewed. Towards the end of the chapter, the shortcomings of the existing methods in dealing with mixed-convection regimes and non-uniform heating cases have been pointed

out together with the possibility of considering them in the present study.

In Chapter (3), the present theoretical model and the formulation of the problem have been described. Three principal conservation equations of mass, momentum and energy have been used in a form which preserves the representative terms for variations of viscosity and density with temperature. Arbitrary wall boundary conditions have been dealt with and it has been shown how they can be transformed into uniform wall conditions by employment of the present method. For the solution, the finite-difference method has been used which leads to the Matrix form of the above-mentioned equations.

In Chapter (4), the numerical solution technique has been explained, leading to the writing of the computer program DUCT to solve for vertical flat ducts with arbitrary wall conditions. Input functions together with Input and Output parameters and a Flow-Chart have also been given. In the discussion which closes the chapter, a comparison has been made between the computer time consumption for solution of a typical flat duct with two different values of horizontal increments.

Chapter (5) has been written to represent the present theoretical predictions for a set of arbitrary prescribed wall conditions in the forced and the mixed-convection regimes. To gain more confidence, a selected number of these results have been compared with the published theoretical and experimental results of other workers on the subject. In particular, the results for a typical "hot-channel" of a plate-type fuel element at two different heat ratings have been predicted. The contributions of mixed-convection effects on their corresponding forced-convection cases has been shown. Non-symmetrical heating cases have also been dealt with and the differences in these results and those

of the symmetrical heating cases have been pointed out. Two parameters which can be representative of the forced and the mixed-convection case have been introduced and their variations for different cases have been studied. Conclusions for forced and mixed-convection regimes have been given near the middle and the end of the chapter respectively. A cross-checking of the present predictions for a typical flat duct has been presented at the end of the chapter.

In Chapter (6), the experimental test-rig with its special features and its design has been described. The functions of each part of the rig together with necessary design drawings for them have also been given. Towards the end of the chapter, the measurements which have been executed for each typical test and the reasons for their utility in the confirmation of the present theoretical results have been mentioned.

In Chapter (7), the experimental results of the test-rig have been given in comparison with their corresponding theoretical predictions. These consist of the results of four typical mixed-convection tests which have been executed together with one test for a typical natural-convection test. In order to facilitate the representation of these results, a plan has been proposed which distinguishes the forced, free and mixed-convection regimes by means of defining two boundary curves. In the conclusions which have been given at the end of the chapter, the present experimental and theoretical results and their differences have been given and the factors which are thought to be the causes of these differences have been pointed out.

Chapter (8) has been written to show how the present method can also solve for vertical channels with circular cross-section and the computer program CIRCLE has been developed for the purpose. By making

use of the existing experimental results for a round tube with prescribed uniform heating, it has been shown that the present predictions are reliable and accurate. Variations of the predicted results for different profiles of heating have been obtained together with the possibility of transition from a laminar into an unstable flow in certain cases. Towards the end of the chapter, the theoretical results of two other authors for a set of sinusoidal heating cases have been accurately reproduced with the contributions of the mixed-convection effects to these results. As for flat duct in Chapter (5), Chapter (8) includes the cross-checking of a typical solution for a prescribed heating case, and the effects of the different entrance conditions on the present theoretical predictions.

Finally, in Chapter (9), general remarks about the present theoretical and experimental results have been made. Suggestions for continuation of the present work in future have also been included.

CHAPTER 2

SURVEY OF THE LITERATURE

2.1 Introduction

Several practical situations involve a mode of heat transfer which is neither "forced" convection nor "free" convection in nature. These arise when a fluid is forced to move adjacent to a heated surface at a rather low velocity. Coupled with this velocity, there is a convective velocity due to buoyancy forces. As a result, design parameters as friction factors and heat-transfer coefficients cannot be obtained from either free or forced convective flows. This type of heat transfer is referred to as "free-forced convection" or "combined-convection". However, the term "mixed-convection" is used in this thesis referring to this situation.

Mixed-convective flows may be classified as: laminar, transitional or turbulent. The present work is concerned with the first and, to some extent, with the second classes, in vertical channels with arbitrary heating. Of particular interest is the case of an open-ended vertical flat duct which is heated by a sinusoidal wall heat-flux along its vertical axis.

2.2 Review of Theoretical Work

There has been ever-increasing attention paid to the problem of mixed-convective heat transfer during the last three decades. Possible equipment in which this method of heat transfer occurs are liquid-cooled turbines, boilers, transformers and low-power nuclear reactors. Earlier investigations on the problem are reported among others by Hallman (1956), Hanratty et al (1961) and Chato (1963).

2.2.1 Boundaries of the Flow

According to Metais et al (1964), the existence of mixed-convective flow is characterized by two dimensionless numbers: Reynolds number (Re) and Rayleigh number (Ra). They mention that large Re implies forced-flow and, hence, less influence of free-convection. On the other hand, at larger Ra, one would expect free-convection effects to prevail. The limits of the forced and the free-convection flows are defined so that the actual heat-flux under the combined influence of the forces does not deviate by more than 10% from the heat-flux that would be caused by the external forces alone or by the body forces alone.

Holman (1968) presents a general suggestion that the predominance of heat transfer mode is governed by the fluid velocity associated with that mode. He proposes a general criterion for determining whether free-convection effects predominate, which is that when, $Gr/Re^2 > 1$, free-convection is of primary importance.

2.2.2 Forced-Convection Flow

Pure forced-convection flow can be regarded as a limiting case of mixed-convection flow. Then the continuity and momentum equations may be solved independently of the energy equation. Early attempts to predict heat-transfer characteristics were centred about fully-developed velocity and temperature profiles far from the duct entrance. Hallman's (1958) results were presented in terms of local Nusselt number (Nu), for forced-convective flow in a round tube with uniform wall heat-flux, $\dot{q}''_w$. His solution consists of a series expansion similar to that

obtained by Graetz (1885) for the isothermal wall case. Graetz's work is reported by Jakob (1949). Solutions of this type are of limited value since in a channel of finite-length, the conditions under which they are valid may never exist. To be useful, these solutions must be backed by experiments or be arrived at numerically. In this regard, works of Schiller (1921), Campbell et al (1936) and Langhaar (1942) are more general in the sense that they consider the existence of a hydrodynamic entry length in the channel. Schiller (1921) analysed the hydrodynamic entrance region of round tubes and also of flat ducts by the use of an integral technique. This technique, in a modified form, is also used by Campbell et al (1936). Their results, according to Hornbeck (1964), seem to give reasonable agreement with the available experimental data but, because of the wide variations in these data, no conclusive statement is made as to the accuracy of his solution. Langhaar (1942) proposed an approach in which the axial momentum equation is linearised.

Employment of the digital computer for solving the governing equations accentuated approaches based on numerical solutions. The finite-difference method is used by Hornbeck (1964). His approach consists of a marching forward procedure in which the velocities and the pressure at any axial position in the pipe are determined by making use of the values upstream from that point. Zeldin et al (1970) employed a numerical solution based on the method proposed by Allen et al (1955) to solve the energy equation for both round tubes and flat ducts. In their work, however, axial conduction is neglected.

2.2.3 Free-Convection Flow

Pure free-convection heat transfer is another limit of a

mixed-convective flow. This problem was first studied by Elenbaas (1942a) for vertical flat ducts. Later, Elenbaas (1942b) also established the heat dissipation characteristics of tubes of circular and other shapes of cross-section, with isothermal walls. However, by following his reported technique, it is not possible to obtain the temperature and the velocity profiles explicitly. Vernier (1962) obtained these profiles for natural-convection flow of water in vertical flat ducts with constant $\dot{q}''_w$. By his method, which is similar to that of Ostrach (1952), he produces the velocity and the temperature profiles, for several sets of spacings and heat ratings, at the end of the duct. Dyer (1968) calculates U and T profiles by making use of a finite-difference technique in the study of the development of the flow in vertical round tubes with uniform wall temperature/heat-flux. His method of solution is similar to that of Bodoia et al (1962) who used it for their study of an isothermal flat duct. Davis et al (1971) have also investigated the development of the U and T profiles for uniform $\dot{q}''_w$ in flat ducts.

Dyer (1975) gives a more recent account of a theoretical, and also experimental, study of the flow in heated flat ducts and round tubes. In this paper, T and U profiles, and also the relationship between Nu and Ra, are obtained by solving the governing equations with a step-by-step numerical technique. Also, two types of Rayleigh numbers - one expressed in terms of uniform $\dot{q}''_w$ and another in terms of the mean wall temperature, $t_{w_{mean}}$. Many features of natural-convection heat transfer, including the influence of Pr on the relationship between Nu and Ra, and also effects of three different inlet conditions on these relationships are examined. He concludes that the relationship remains the same for small values of Ra, and the difference

between the relationships obtained for large values of Ra are only small.

2.2.4 Mixed-Convection Flow

Various aspects of the problem have been investigated, e.g. cases of axially symmetric flow in vertical flat ducts or round tubes which are uniformly heated or cooled. In most instances, the existence of a fully-developed flow is assumed. This is followed by considering similarity solutions for the U and T profiles, which means that the "entrance region effects" are neglected. Hallman (1956) reports similarity solutions for both upflow and downflow with constant $\dot{q}''_w$. Theoretical similarity solutions were also attempted by Hanratty et al (1958). In a succeeding paper, Hanratty et al (1960) visualised the effects of heating, or cooling, on the water flow in a vertical round tube by dye injection. They observed that under relatively mild conditions of heating or cooling ($Re < 2300$), the distortions were sufficient to change the parabolic velocity profile to an extent that the flow became turbulent. In a following paper, Hanratty et al (1961), used the integral method of Pigford (1955) for their solution of an initially fully-developed flow in an isothermal pipe. In this paper, they allowed for linear variations with temperature of both density and viscosity, but their method could only produce overall characteristics of the flow and not the U and T profiles explicitly.

Lawrence et al (1966) considered a developing flow in a pipe with uniform $\dot{q}''_w$. In addition to obtaining a numerical solution to the boundary-layer-type conservation equations, an experiment using water was performed. In their numerical analysis, the entrance velocity and temperature are assumed to be uniform. Later, Collins (1971), continued

the study of the problem with the same developing-model as Lawrence et al (1966). In his study, the four main alternatives, (of upward or downward flow with heating or cooling), with constant t_w or constant $\dot{q}''_w$, were investigated. He compared the results for water and air as working fluids and concluded that the mixed-convection effects are stronger in water than in air. Zeldin et al (1972) included the effects of the axial conduction and also of axial momentum change. Their results, backed by their experiments with air, are presented for both uniform and parabolic U_o profiles. Their findings confirm that as a consequence of the presence of gravity, density gradients induced by heat transfer, though small, may significantly alter the flow characteristics (particularly the U profile). Also, they show that the rate of heat transfer improves with increasing Gr. Collins (1975) extends his study of the mixed-convection problem, to cover several working fluids, vertical annuli and also the effects of the viscous dissipation. Iqbal et al (1970) also showed that viscous dissipation effects reduce the Nusselt numbers, Nu. However, these effects are found to be important only when the working fluid has a high Pr (e.g. oils).

Chen et al (1975) made an analytical study of the effects of the buoyancy forces along an isothermally heated pipe. For the range of their study, $0 \leq Gr/Re^2 \leq 2$, they report that the heat transfer rate increases with increase in the buoyancy force and also with the curvature of the surface. Patankar et al (1976) showed analytically that the effects of the buoyancy on the laminar forced-convection adjacent to a heated vertical plate are accentuated by the presence of an unheated length. Chen et al (1976) extend their study to cover the

constant $\dot{q}''_w$ case. They confirmed, as did Oosthuizen (1973), that similar to the isothermal cases, local Nusselt numbers and the friction-factors increase with higher degrees of mixed-convection.

2.2.5 Non-Uniform Heating

The introduction of arbitrary prescribed thermal conditions on the wall adds considerably to the difficulties of solving the mixed-convection problem. Available literature on this type of heating is rather limited. The first published study of convective heat transfer in a channel with arbitrary prescribed heating at the wall is that of Graetz (1885). His analytical method solves the case of fully-developed laminar flow in a pipe with a step-change in t_w. He obtained a solution by the technique of separation of variables leading to the solution of the Sturm-Liouville type equation. Graetz (1885) originally obtained the first three terms of the infinite series solution for the local Nu in a flat duct with constant t_w. Sellars et al (1956) extended Graetz's approach to solve the prescribed $\dot{q}''_w$ cases. Fully-developed forced convection in flat ducts with uniform-equal, and also uniform-unequal $\dot{q}''_w$ s, are solved by Cess et al (1958) and (1960). They use a method based on a series expansion similar to that of Graetz (1885) and is proposed by Hallman et al (1958). McCuen (1962) solved laminar and also turbulent heat transfer flows in flat ducts of arbitrarily prescribed t_w or $\dot{q}''_w$. His solutions are based on the "four fundamental - solutions method" proposed by Reynolds et al (1960). These fundamental solutions were considered to be: a step change in the temperature or heat-flux at one wall combined with the opposite wall being either insulated or kept at the inlet temperature of the working fluid. At

this period, the solution for laminar heat transfer in flat ducts with uniform or non-uniform heating and fully-developed velocity profile, seemed to be complete. But the effort involved in calculating the necessary eigenfunctions, eigenvalues and also the coefficients was enormous. Lundberg et al (1963) and Kays et al (1964) published the generalised form of the above mentioned "four fundamental-solutions" for annular tubes in four successive papers. In the first three papers, they consider only the fully-developed U profile in the heated region of the annulus. The fourth paper, however, deals with simultaneous development of the U and also T profiles in the annuli of constant $\dot{q}''' _w$. These four papers also include results for flat ducts and round tubes as the two extreme limits of a vertical annulus. It should also be mentioned that in these papers, the study is restricted to laminar incompressible flows. This assumption along with the assumption that other properties are not temperature dependent allowed an independent solution of the hydrodynamic problem, since the momentum and the energy equations were not coupled. Bankston et al (1969) pointed out that the superposition procedure used in the Lundberg et al (1963) and Kays et al (1964) gives rise to a very slowly converging series solution for the local Nu. The error, due to truncation of this series near the entry, may be great if a sufficient number of terms is not considered. A less attractive feature of these analytical approaches is that quite a substantial amount of numerical computation work, connected with the eigenvalues and eigenfunctions, which requires considerable skill, must be carried out. This may be the reason that although the approach is widely used in heat transfer text-books, it does not seem to be extensively applied in design.

An alternative approach is based on expressing the governing

equations in a finite-difference form which can be solved in a straightforward manner. This approach is proposed by Kays (1955) and used by Grigull et al (1965). For high accuracy, a fine mesh size is desirable, entailing large computational times. Nijsing et al (1973) pointed out that the explicit computational procedures applied in the two papers just mentioned further require, because of stability restrictions, that the axial distance increment in the finite-difference formulation, does not exceed a critical size. This size, in turn, is related to the distance increment in the direction normal to the wall. In comparison with the analytical methods, the numerical methods have the drawback that they yield solutions of which the details cannot be obtained explicitly.

2.2.6 Sinusoidal Heating

Of particular interest in this thesis is the case of laminar heat transfer to a fluid flowing in a vertical flat duct with sinusoidal wall heat-flux. At the first sight, the problem, with the assumption of fully-developed velocity profile, seems to have been completely solved by making use of the general formulae given in the two papers by Sellars et al (1956) and Tribus et al (1957), the former deals with the laminar and the latter with the turbulent flows. The solutions appear to be general but, as also mentioned by Dzung (1958a), their method can be applied reasonably only to the cases of prescribed t_w. If $\dot{q}''_w$ is prescribed, the method becomes very laborious, since the relevant eigenvalues and also the coefficients of the rather slowly converging series are themselves calculated from another set of eigenvalues and coefficients. Dzung (1958), in two successive papers - one for a round tube and another for a flat duct - represents a more direct method for sinusoidal heat-flux. By following his method, any arbitrary prescribed

$\dot{q}''_w$ can be treated by Fourier series expansion, instead of the superposition method of Sellars et al (1956). Dzung's approach, although sound, requires the eigenvalues and the associated constants to be evaluated according to approximate asymptotic solutions. Hsu (1965) solved the same problem in a more straightforward manner by utilizing the thermal-entrance region's solution for uniform $\dot{q}''_w$ obtained by Hallman (1958). Hsu (1965) uses digital computers to calculate the first twenty eigenvalues, eigenfunctions and the coefficients for the series expansion. His analytical results near the entrance region for slug flow agree closely with the experimental results obtained by Petrovichev (1960) for turbulent flow. Bankston et al (1969) applied the superposition method of Sellars et al (1956) in a developed form for prediction of t_w. As a special case, they treated forced-convective flow with sinusoidal $\dot{q}''_w$ along a round tube. By comparing the local Nusselt numbers calculated according to the two methods, they concluded that the method of Sellars et al (1956) should not be applied for design predictions. This is because, for the same number of terms in the series solution, the numerical method of Bankston et al (1969) predicts results with lower percentage errors. In dealing with the sinusoidal $\dot{q}''_w$ case, it is generally expected that if the wavelength of $\dot{q}''_w$ (z) is long, compared to the distance which the basic constant $\dot{q}''_w$ solution requires for the desired accuracy with the available eigenvalues, then reasonable results will be obtained by the superposition method of Sellars et al (1956). Stein (1966) has partially quantified this aspect of the problem for the first-order approximation for a sinusoidal distribution. Nijsing (1972) and (1973) proposes a "hybrid-method" which lies between the superposition method of Sellars et al (1956) and the numerical method of Bankston et al (1969). The essential feature of his method is

that the fluid region is discretized only in the section normal to the flow direction. Local energy balances which are set up for each element yield a system of linear first-order differential equations with the axial coordinate as the sole independent variable. This system of equations is solved analytically using a matrix method. Cases of flat ducts and round tubes are dealt with by Nijsing (1972) and (1973). The results, in the form of local Nusselt numbers, seem to be in agreement with those of Grigull et al (1965) and Schmidt (1967).

2.2.7 Limitations of the Existing Literature

The main assumptions of the afore-mentioned literature for arbitrarily heated channels, including the sinusoidal $\dot{q}''_w$ cases, are:-

(a) The velocity profile is fully-developed, i.e.

$$u/u_o = 6 \cdot y/d \ (1 - y/d) \quad \text{For flat ducts}$$

or:-

$$u/u_o = 2 \cdot \{1 - (r/R)^2\} \quad \text{For round tubes}$$

(b) There is no natural-convection effect on the forced-convection flow.

(c) The horizontal component of the fluid velocity is not significant, i.e.: $V = 0$.

These assumptions are shown to be valid only for low heat transfer rates to the flow and as a consequence, the results are reasonable only for forced-convection flows. As mentioned earlier, Hanratty et al (1960) showed that by taking into account the variations of density and viscosity, the velocity profile is distorted and does not have a parabolic form. Lawrence (1965) reports similar effects of the buoyancy force for a constant $\dot{q}_w''$ case. He actually measured T profiles and also centreline velocities along the pipe and confirmed the continuously developing model for them. These results show that neither the fully-developed U profile nor constant ρ and μ assumptions are valid for the solution of the mixed-convection problem. Schmitz et al (1965) reported that for constant t_w or $\dot{q}_w''$ cases, the effects of the horizontal velocity V lead to a significant decrease in the calculated values of Nu in the entrance region from those obtained by Kays (1955). Hwang et al (1974) investigated the effects of V in flat ducts and their results are similar to those of Schmitz et al (1965).

As will be seen from the other chapters, the intention of this thesis is to tackle the arbitrary heating case for mixed-convection, in a general form, avoiding the three limitations mentioned earlier. The solution is to cover all the three flows: pure-forced, pure-free and mixed-convection, in a laminar situation. Among the cases considered, a vertical flat duct with sinusoidal $\dot{q}_w''$ is solved for and discussed with particular interest.

2.3 Review of Experimental Work

Experimental results in the literature are mainly for vertical

round tubes or flat ducts in which either t_w or $\dot{q}''_w$ are constant. Working fluids considered are either water or oil for medium and high Prandtl numbers respectively. Limited experimental results are available for liquid metals (low Pr) and the only gas tested is air (Pr ≅ 0.7).

2.3.1 Experiments with Uniform Heating

Hallman (1961) experimentally analysed the convective heat transfer in vertical round tubes with constant $\dot{q}''_w$ and confirmed the three following points:-

(a) Existence of a thermal entrance region;

(b) Free convection effects on the forced-convection results;

(c) Transition to an "unstable-flow" at certain conditions.

Hanratty et al (1960) and (1962) obtained similar results for the constant t_w case. Kemeny et al (1962) extended the experiments of Hallman (1961) to oil and produced pressure drop data for the mixed-convection cases.

Lawrence (1965) measured developing T profiles, centreline velocities, and the pressure drop along a pipe with constant $\dot{q}''_w$. These results were in good agreement with his analytical results and confirmed the necessity of developing U and T models along the channel. His study also includes the definition of a tentative transition criterion, which depends only on the developing velocity

profiles, the fluid viscosity, and the entrance Reynolds number (Re_o).

Flat vertical ducts with constant $\dot{q}''_w$ were experimentally investigated by Vernier (1962). He measured the U and T profiles at the exit of the duct for a set of spacings between the parallel plates. His results are in agreement with those of Riley (1970).

Zeldin et al (1972) experimentally investigated the forced and also the mixed-convection flows with air as the working fluid. Their results, obtained for a vertical-isothermal pipe, include determination of the developing U and T profiles explicitly.

2.3.2 Experiments with Sinusoidal and Non-Uniform Heating Cases

Experimental results for sinusoidal heating, or generally non-uniform heating, are not extensive. The difficulty in producing these types of heat distributions, in comparison with uniform heating, may be the main reason. The earliest attempt, known to the author, is that of Petrovichev (1960). He made heat transfer measurements for turbulent flow of mercury in a horizontal pipe with a sinusoidal $\dot{q}''_w$ distribution along the axis. Results of this work are presented in the form of the local Nu, and also empirical correlations relating $t_{w_{max}}$ and the Peclet number, Pe. A sinusoidal $\dot{q}''_w$ was achieved in Petrovichev (1960) by winding an electric heater over the outside surface of the test-pipe, with variable spacing. The "correctness" of the experimental set-up in his work is checked by replacing the sinusoidal heating element with a similar element but with a constant $\dot{q}''_w$, to produce similar results to those of Johnson et al (1954).

McCuen (1962) produced experimental data for the forced turbulent heat transfer in air with non-uniform heating. Broad-sides of the flat duct in his tests were each composed of a number of narrow

rectangular copper cells, each separated from its neighbours by thermal insulators. The cells, forming the broad-sides, were subjected to heating, or cooling, individually to a range of desired temperatures. An adiabatic entry length was provided to minimise hydrodynamic-entry effects. Prescribed t_w profiles of constant or linear variation were tested by McCuen (1962).

Dijkman (1969) reports experiments with sinusoidal heat-flux for a boiling water channel. His simulation model is based on the concept of "continuous variation of the wall thickness" in the test-pipe. Because of lack of machine tools, he divided the pipe into a number of pieces welded together. Every piece was internally turned with a tapering diameter. His results are of little interest to this thesis. Therefore, only his simulation method is mentioned.

Muzzy et al (1974) used the same method as Dijkman (1969). By taking advantage of highly sophisticated tools, they achieved an accurately simulated chopped-sinusoidal $\dot{q}''_w$ profile. They concluded that a heater element as such has a thermal response that is representative of a nuclear fuel element in the core of a nuclear reactor. (This conclusion is, of course, subject to satisfying certain specifications which are inherent to the analysis, e.g. geometry and thermal properties).

Ornatskiy et al (1975), in their experiments of the "burn-out problem" in annuli, also used the concept of "variable wall thickness" to simulate a chopped-sinusoidal $\dot{q}''_w$. In their work, several profiles of the sinusoidal $\dot{q}''_w$ with different $\dot{q}''_{w_{Max}}/\dot{q}''_{w_{av}}$ ratios were experimented.

Reisman et al (1977) obtained experimental results for laminar forced flow in a horizontal pipe with sinusoidal $\dot{q}''_w$. Their method of simulation was based on the concept of "step-change" in $\dot{q}''_w$ which was

proposed by Sellars et al (1956). To approximate the sinusoidal $\dot{q}''_w$ with a step-varying flux, Reisman et al (1977) divided the sine-wave into three rows. The heating cable of the simulating pipe consisted of three separate windings, one for each row, and the test fluid was an organic liquid (Oil 10C, General Electric). Their conclusion, backed by numerical calculations of the Sellars et al (1956) formulae, was that the step varying model leads to a good approximation of the sinusoidal wall heat-flux.

CHAPTER 3

THEORETICAL ANALYSIS

3.1 Discussion of the Problem

As mentioned in Chapter 2, it is the purpose of this study to develop a solution to the problem of mixed-convective heat transfer in vertical flat ducts (or round tubes at a later stage), for a variety of prescribed wall conditions.

Major attention is devoted to cases with upflow heating, although the equations are developed in such a way that other configurations, such as downflow, or adiabatic flow, may also be tackled by manipulation of the buoyancy term.

Among the different wall conditions, cases of uniform wall temperature or heat-flux are the basic cases upon which the solutions for arbitrary conditions are founded. In other words, profiles of arbitrary wall conditions are divided into infinitesimal lengths and treated as uniform heating along the length of each of the divisions.

In the search for a general solution, it should be recalled that according to the studies of Hanratty et al (1961), and also Lawrence et al (1966), any solution claiming generality must include viscosity and density variations with temperature. Density variations are normally allowed for only in the buoyancy term of the axial momentum-equation. This condition is sometimes termed "quasi-incompressible". Also, because of the modest temperature changes frequently associated with the mixed-convection cases, other properties are assumed constant. As will follow, these points are taken into account in the present formulation of the theoretical model.

3.2 The Theoretical Model

The theoretical model is to represent the "laminar convective heat transfer in vertical flat ducts with arbitrary wall conditions". For the purpose of this study, the ducts with large aspect-ratios are to be considered. Therefore, a two-dimensional model is sought. Fig. (3.1) shows such a model with its vertical and horizontal co-ordinates, z and y respectively. Thermal boundary conditions, such as wall temperature or heat-flux, may only vary in the vertical direction.

3.3 General Formulation

The solution is to be based on the three principal conservation equations of mass, momentum and energy in a two-dimensional form. According to Kays (1966), these equations in the differential form are:-

(a) Continuity Equation

$$\frac{\partial u}{\partial z} + \frac{\partial v}{\partial y} = 0 \qquad (3.1)$$

(b) Momentum Equation in the Axial Direction, z

$$\rho \left(u \frac{\partial u}{\partial z} + v \frac{\partial u}{\partial y} \right) = - \frac{\partial p}{\partial z} - S.\rho.g + \frac{\partial}{\partial z} \left(2\mu \frac{\partial u}{\partial z} \right) + \frac{\partial}{\partial y} \left\{ \mu \left(\frac{\partial u}{\partial y} + \frac{\partial v}{\partial z} \right) \right\} \qquad (3.2)$$

(c) Momentum Equation in the Horizontal Direction, y

$$\rho \left(u \frac{\partial v}{\partial z} + v \frac{\partial v}{\partial y} \right) = - \frac{\partial p}{\partial y} + \frac{\partial}{\partial y} \left(2\mu \frac{\partial v}{\partial y} \right) + \frac{\partial}{\partial z} \left\{ \mu \left(\frac{\partial v}{\partial z} + \frac{\partial u}{\partial y} \right) \right\} \qquad (3.3)$$

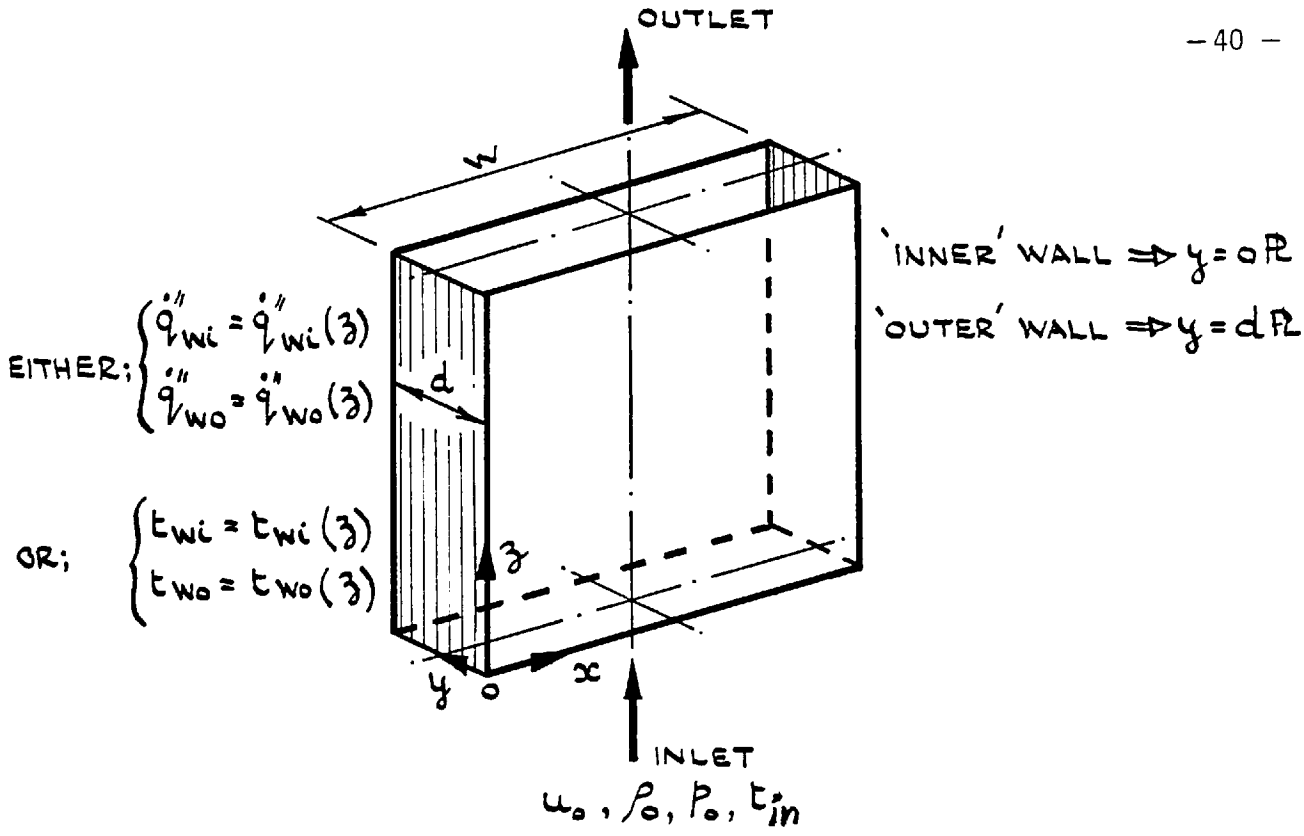

FIG(3.1) THE THEORETICAL MODEL.

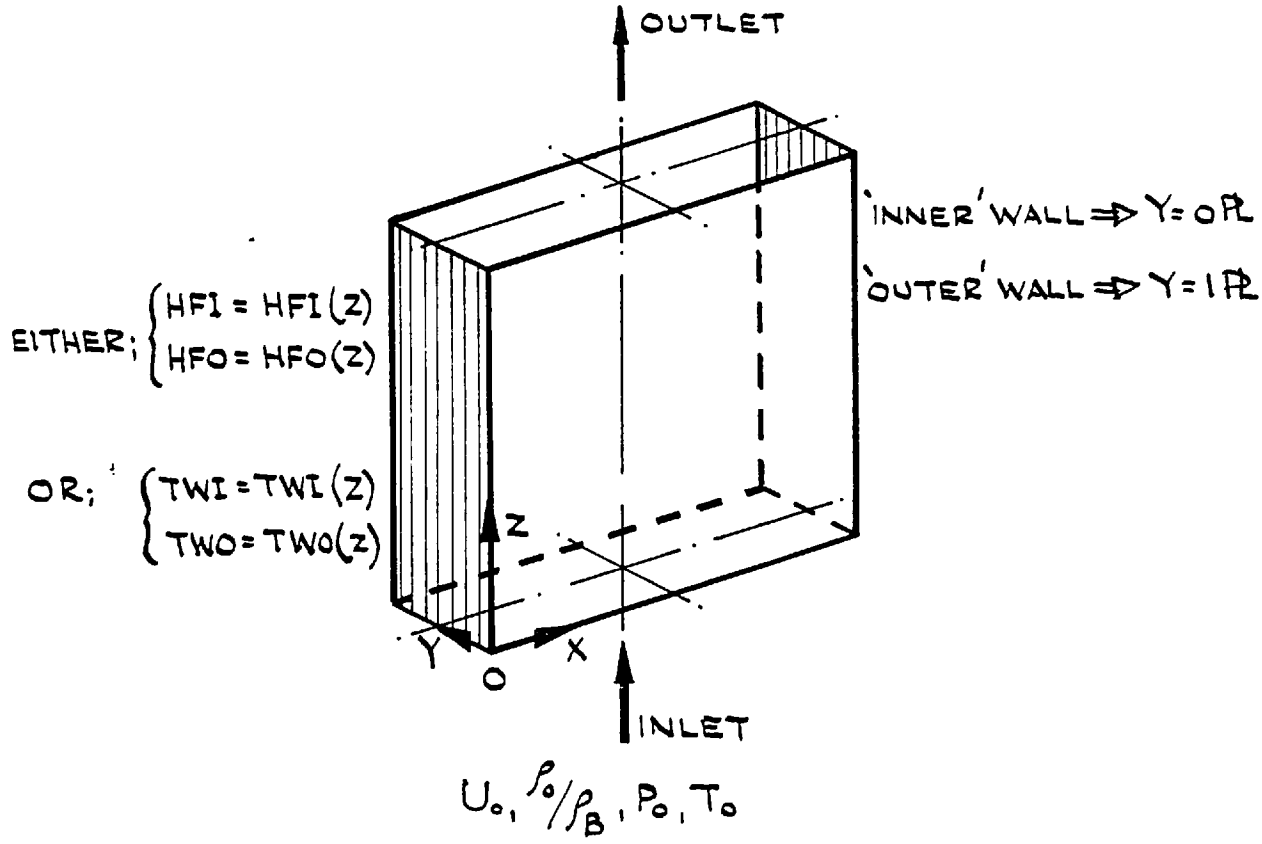

FIG(3.2) THE THEORETICAL MODEL IN DIMENSIONLESS FORM.

(d) Energy Equation

$$u \frac{\partial t}{\partial z} + v \frac{\partial t}{\partial y} = \frac{k}{\rho \cdot C_p} \left(\frac{\partial^2 t}{\partial z^2} + \frac{\partial^2 t}{\partial y^2}\right) \qquad (3.4)$$

The assumptions in Equations (3.1) - (3.4) are:-

1. The flow is steady and laminar.

2. The ratio w/d is large enough to minimize the effects of the third co-ordinate x on the flow. Therefore, the flow specifications parallel to the y - z plate do not change for the model.

3. Viscous energy dissipation is negligible.

4. Wall thermal conditions, i.e. temperature or heat-flux, are prescribed on the parallel boundaries distance d apart. For the flat duct, these two boundaries are referred to an "Inner" and "Outer" plates respectively (y = 0 or y = d).

5. C_p and k are constant, but the viscosity μ varies with temperature.

6. The density, ρ, is constant except in the buoyancy term of Equation (3.2). This assumption is justified for the liquid and for the conditions of interest by comparing the effects of density variations in the terms of Equations (3.2) - (3.3).

The buoyancy term in Equation (3.2) represents natural-convection effects. This is done by assuming:-

$S = 1$	For upward flow
$S = -1$	For downward flow
$S = 0$	For pure-forced or adiabatic flow

Choice of the viscosity-function of temperature, within the temperature range of the problem, depends on the test-fluid. Collins (1975) proposes the following three correlations:-

(i) $$\mu = \mu_B\left(\frac{t + C_1}{C_2}\right)^{-C_3} \tag{3.5a}$$

(For water, water/glycerol mixture and some oils)

(ii) $$\mu = \mu_B(t/t_B)^{-C_1} \tag{3.5b}$$

(For S.A.E. 600 oil, suggested by Martin . 1973)

(iii) $$\mu = \mu_B(C_1 + C_2 \,.\, t - C_3 \,.\, t^2) \tag{3.5c}$$

(For air)

In these correlations, μ_B and t_B are base viscosity and temperature respectively, while C_1, C_2 and C_3 are constants.

An exponential approximation to the viscosity-function for water is proposed by Lawrence et al (1966) which facilitates the

differentiations occurring in Equations (3.2) - (3.3). This approximation is:-

$$\mu = \mu_{\infty} + (\mu_B - \mu_{\infty}) \cdot \exp\{- C_1 (t - t_B)\} \qquad (3.5d)$$

where μ_{∞} and μ_B are water viscosities at two finite temperatures and C_1 is a constant.

For the purpose of this study, Equations (3.5a) and (3.5d) were considered and compared with actual values reported by Kemeny et al (1962). This comparison is shown on Table (3.1) which leads to the selection of Equation (3.5a) for the results computed in this thesis.

In regard to the approximation of the density-function of temperature for water, Lawrence et al (1966), who studied upflow heating in a round tube with uniform heat-flux, showed that in order to obtain a good fit with their experimental data, it was necessary to use a quadratic expression for the density. Traditionally, a linear expression has been used where the bulk coefficient is calculated at the temperature halfway between the entrance and exit temperatures of the channel. Lawrence et al (1966) concluded that this leads to velocity and temperature profiles along the channel which only match at one point with the actual values and diverge elsewhere. Table (3.2) shows approximate values of water density according to the following form of quadratic function which is used for the numerical calculation of this thesis:-

$$\rho = \rho_B(C_4 - C_5 \cdot t + C_6 \cdot t^2) \qquad (3.6)$$

where ρ_B is water density at a finite temperature and $C_4 - C_6$ are constants.

TABLE (3.1)

WATER VISCOSITY AS A FUNCTION OF TEMPERATURE

Temperature $t(F^o)$	Kemeny et al (1962) μ(lbm/ft.hr.)	Lawrence et al (1966) μ(lbm/ft.hr.)	Collins (1975) μ(lbm/ft.hr.)
70	2.372	2.372	2.372
80	2.084	2.085	2.079
90	1.847	1.846	1.843
100	1.650	1.648	1.650
110	1.487	1.483	1.490
120	1.353	1.346	1.354
130	1.236	1.232	1.239
140	1.137	1.137	1.139
170	0.900	0.938	0.909
200	0.740	0.824	0.750

Column 2 : Experimental values of μ.

Column 3 : Exponential approximation:

$$\mu = 0.67 + 1.702\ \mathrm{Exp}\{-0.01848\ (t - 70)\}\ \text{(lbm/ft.hr.)}$$

Column 4 : Power approximation:

$$\mu = 2.372\ \left(\frac{t + 30}{70 + 30}\right)^{-1.38239}\ \text{(lbm/ft.hr.)}$$

The power approximation is used for the calculations in this thesis.

In C.G.S. units, this approximation is:-

$$\mu = 0.9805\ \left(\frac{t + 34.444}{55.555}\right)^{-1.38239}$$

(t and μ are in ^oC and Cent. Poise respectively)

TABLE (3.2)

WATER DENSITY AS A FUNCTION OF TEMPERATURE

Temperature $t(F^{O})$	C.R.P. Handbook (1956) $\rho(lbm/ft^3)$	Approximation $\rho(lbm/ft^3)$
50	62.407	62.430
68	62.314	62.314
86	62.153	62.151
104	61.940	61.940
122	61.680	61.683
140	61.378	61.377
158	61.039	61.024
176	60.667	61.626
200	60.130	60.020

The approximation is calculated from the function:-

$$\rho = 62.314\ (1.003063 + 3.444 \times 10^{-5} \cdot t - 1.169 \times 10^{-6} \cdot t^2)$$

This function in C.G.S. units is:-

$$\rho = 0.99817\ (1.0029654 - 7.2677 \times 10^{-5} \cdot t - 3.7875 \times 10^{-6} \cdot t^2)$$

(t and ρ are in ^{O}C and gr/cm^3 respectively)

The integral continuity equation may be used as an additional equation for numerical solution of the problem. For the theoretical model, this equation is:-

$$\rho_o \cdot u_o \cdot w \cdot d = \int_0^d w \cdot u \cdot \rho \cdot dy \qquad (3.7)$$

In the calculations which follow, Equation (3.7) is used as part of the analysis, rather than as a mass balance check - a procedure proposed by Bodoia et al (1959).

Wall thermal boundary conditions are specified either as temperature or heat-flux at the "Inner" and "Outer" walls, i.e. :-

Either:

$$t_{wi} = t_{wi}(z) \qquad (3.8)$$

$$t_{wo} = t_{wo}(z) \qquad (3.9)$$

Prescribed wall temperatures

Or:

$$\dot{q}''_{wi} = \dot{q}''_{wi}(z) \qquad (3.10)$$

$$\dot{q}''_{wo} = \dot{q}''_{wo}(z) \qquad (3.11)$$

Prescribed wall heat-fluxes

The overall energy balance over an infinitesimal vertical length, dz, which is used as part of the analysis rather than as a heat balance check, is written as either:-

$$u_o \cdot w \cdot d \cdot \rho \cdot C_p \cdot \Delta t_{mean} = w \cdot \int_z^{z+dz} \{\dot{q}''_{wi}(z) + \dot{q}''_{wo}(z)\} \cdot dz \qquad (3.12)$$

(For prescribed $\dot{q}''_{wi}(z)$ and $\dot{q}''_{wo}(z)$)

or:-

$$u_o \cdot w \cdot d \cdot \rho \cdot C_p \cdot \Delta t_{mean} = w \cdot dz \cdot k\{- \left.\frac{\partial t}{\partial y}\right|_{y=0} + \left.\frac{\partial t}{\partial y}\right|_{y=d}\} \qquad (3.13)$$

(For prescribed t_{wi} (z) and t_{wo} (z))

where Δt_{mean} is the increase in the mixed-mean temperature, t_{mean}, for the length dz. This temperature is defined as:-

$$t_{mean} = \frac{\int_o^d u \cdot \rho \cdot t \cdot dy}{\int_o^d u \cdot \rho \cdot dy} \qquad (3.14)$$

3.4 Boundary Conditions

Boundary conditions of the problem may be classified into the following three groups:-

(i) Entrance conditions: $(z = 0,\ 0 \leq y \leq d)$

$u = u_o,\ v = 0,\ p = p_o,\ t = t_{in}$

(ii) Wall flow conditions: $(0 \leq z \leq L,\ y = 0 \text{ or } d)$

$u = 0,\ v = 0$

An additional assumption is necessary in order to start the finite-difference solution of Equations (3.1) - (3.4) from the "Inner" wall. This is assumed to be $- \left.\frac{\partial p}{\partial y}\right|_{y=0}$ = Const. - which is consistent with known round-tube results (The assumption was

checked by solving for a symmetrically heated vertical channel and confirming that p(y) has the same behaviour near the "Outer" wall also. Therefore:-

$$\left.\frac{dp}{dy}\right|_{y=0} = \left.\frac{dp}{dy}\right|_{y=\varepsilon}$$

where ε is an infinitesimal value).

(iii) Wall thermal conditions: $(0 < z \leq L,\ y = 0 \text{ or } d)$

Either:-

$$t_{wi} = t_{wi}(z)$$

$$t_{wo} = t_{wo}(z)$$

For prescribed wall temperatures

or:-

$$\dot{q}''_{wi} = \dot{q}''_{wi}(z) = -k \left.\frac{\partial t}{\partial y}\right|_{y=0}$$

$$\dot{q}''_{wo} = \dot{q}''_{wo}(z) = k \left.\frac{\partial t}{\partial y}\right|_{y=d}$$

For prescribed wall heat-fluxes

3.5 Transformation Into a Non-Dimensional Form

The above equations and boundary conditions may be transformed by the substitutions defined in the nomenclature.

3.5.1 Equations

As follows, Equations (3.1) - (3.14) transform into Equations (3.15) - (3.28) respectively:-

$$\frac{\partial U}{\partial Z} + \frac{\partial V}{\partial Y} = 0 \tag{3.15}$$

$$U \frac{\partial U}{\partial Z} + V \frac{\partial U}{\partial Y} = - \frac{\partial P}{\partial Z} - S \frac{\rho_m}{\rho_B} \xi/Re^2 + \frac{1}{Re} \left[\eta_A \left(\frac{\partial^2 U}{\partial Z^2} + \frac{\partial^2 U}{\partial Y^2}\right) + \right.$$

$$\left. + \eta_B \left\{2 \frac{\partial T}{\partial Z} \cdot \frac{\partial U}{\partial Z} + \frac{\partial T}{\partial Y} \left(\frac{\partial U}{\partial Y} + \frac{\partial V}{\partial Z}\right)\right\} \right] \tag{3.16}$$

$$U \frac{\partial V}{\partial Z} + V \frac{\partial V}{\partial Y} = - \frac{\partial P}{\partial Y} + \frac{1}{Re} \left[\eta_A \left(\frac{\partial^2 V}{\partial Y^2} + \frac{\partial^2 V}{\partial Z^2}\right) + \right.$$

$$\left. + \eta_B \left\{2 \frac{\partial T}{\partial Y} \cdot \frac{\partial V}{\partial Y} + \frac{\partial T}{\partial Z} \left(\frac{\partial V}{\partial Z} + \frac{\partial U}{\partial Y}\right)\right\} \right] \tag{3.17}$$

$$U \frac{\partial T}{\partial Z} + V \frac{\partial T}{\partial Y} = \frac{1}{Pr \cdot Re} \left(\frac{\partial^2 T}{\partial Z^2} + \frac{\partial^2 T}{\partial Y^2}\right) \tag{3.18}$$

$$\frac{\mu}{\mu_B} = (CO1 \cdot T/G + CO2)^{(- CO3)} \tag{3.19}$$

$$\frac{\rho}{\rho_B} = (CO4 + CO5/G \cdot T + CO6/G \cdot T^2) \tag{3.20}$$

$$1 = \int_0^1 \rho/\rho_o \cdot U \cdot dY \tag{3.21}$$

$$TWI\ (Z) = \frac{d^3 \cdot g \cdot C_5}{\nu_B^2}\ (t_{wi}\ (z) - t_{in}) \tag{3.22}$$

$$TWO\ (Z) = \frac{d^3 \cdot g \cdot C_5}{\nu_B^2}\ (t_{wo}\ (z) - t_{in}) \tag{3.23}$$

$$HFI\ (Z) = \frac{d^4 \cdot g \cdot C_5}{\nu_B^2 \cdot k \cdot M} \cdot \dot{q}''_{wi}\ (z) \tag{3.24}$$

$$HFO\ (Z) = \frac{d^4 \cdot g \cdot C_5}{\nu_B^2 \cdot k \cdot M} \cdot \dot{q}''_{wo}\ (z) \tag{3.25}$$

$$\int_0^1 U \cdot T \cdot \frac{\rho}{\rho_o} \cdot dY = \frac{\Delta Z \cdot M^2}{Pr \cdot Re} \Big| (HFI + HFO) \Big|_{Av.\ (between\ Z\ and\ Z + dZ)} \tag{3.26}$$

$$\int_0^1 U \cdot T \cdot \frac{\rho}{\rho_o} \cdot dY = \frac{\Delta Z \cdot M}{Pr \cdot Re} \left\{ \left| \frac{\partial T}{\partial Y} \right|_{Y=0} + \left| \frac{\partial T}{\partial Y} \right|_{Y=1} \right\}_{At\ level\ "Z"} \tag{3.27}$$

$$TMEAN_n = \int_0^1 \frac{\rho}{\rho_o} \cdot U_n \cdot T_n \cdot dY \tag{3.28}$$

In Equations (3.16) - (3.17), it is assumed that:-

$$\frac{\partial \mu}{\partial y} = \frac{d\mu}{dt} \cdot \frac{\partial t}{\partial y}$$

$$\eta_A \equiv (CO1 \cdot T/G + CO2)^{(-\ CO3)}$$

$$\eta_B \equiv \frac{d}{dT}\ (\eta_A) = \frac{CO1}{G}\ (CO1 \cdot T/G + CO2)^{-\ (CO3\ +\ 1)}$$

Also:-

$$\xi \equiv \{CO4 \cdot G + T\,(CO5 + CO6 \cdot T)\}$$

3.5.2 Boundary Conditions

Boundary conditions in dimensionless form are:-

(1) Entrance conditions: $(Z = 0,\ 0 \leq Y \leq 1)$

$$U = 1,\ V = 0,\ P = P_o,\ T = T_o$$

(2) Wall flow conditions: $(0 < Z \leq L/d,\ Y = 0 \text{ or } 1)$

$$U = 0,\ V = 0,\ \left.\frac{\partial P}{\partial Y}\right|_{\text{near walls}} = \text{Const.}$$

(3) Wall thermal conditions: $(0 < Z \leq L/d,\ Y = 0 \text{ or } 1)$

Either:-

$$\left.\begin{aligned} TWI &= TWI\,(Z) \\ TWO &= TWO\,(Z) \end{aligned}\right\} \quad \text{Prescribed wall temperatures}$$

or:-

$$\left.\begin{aligned} HFI &= HFI\,(Z) \\ HFO &= HFO\,(Z) \end{aligned}\right\} \quad \text{Prescribed wall heat-fluxes}$$

Figs. (3.2) - (3.3) show the general configuration and the cross-section of the theoretical model in dimensionless form.

3.6 Choice of the Method of Solution

So far, the relevant equations for the theoretical model of the problem have been written and normalized together with the boundary conditions. The question now appears to be: "What method of solution may be adopted to these equations?" As mentioned in Chapter 2, analytical solutions of these equations are limited to the simple cases of fully-developed flow with uniform heating which are proposed, among others, by Sellars et al (1956) and McCuen (1962). Even these solutions involve a great deal of mathematical work. With recent developments in digital computers with high storage capacity, a numerical solution with the aid of these machines seems to be a natural choice.

Numerical solution of Equations (3.15) - (3.28) may be attempted by the finite-difference or the finite-element methods. Both of these methods are DISCRETISATION techniques by which one approximates a problem with a large number of algebraic equations which may be solved by digital-computers. Olusoji et al (1977) applied the finite-element method to solve the case of natural-convection heat transfer in an open-ended vertical channel. Their results, in term of correlations between Nusselt and Reynolds numbers, compared very closely with those for the finite-difference solution obtained by Bodoia et al (1962).

Nayak et al (1975) compared the finite-element and the finite-difference methods when they computed the fully-developed Nusselt number using both techniques. For the comparison, they first applied the finite-element method to solve for a square-duct with twenty-five

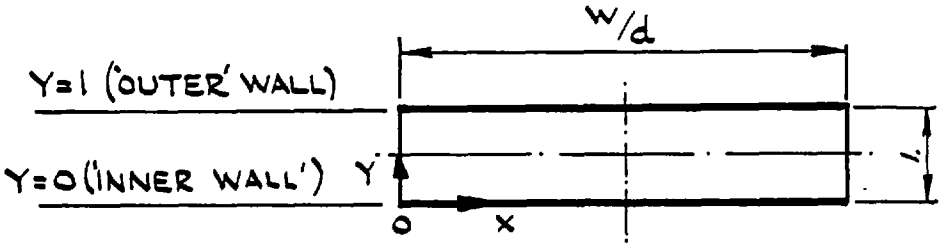

FIG(3.3) CROSS SECTION OF THE DUCT IN THE DIMENSIONLESS FORM.

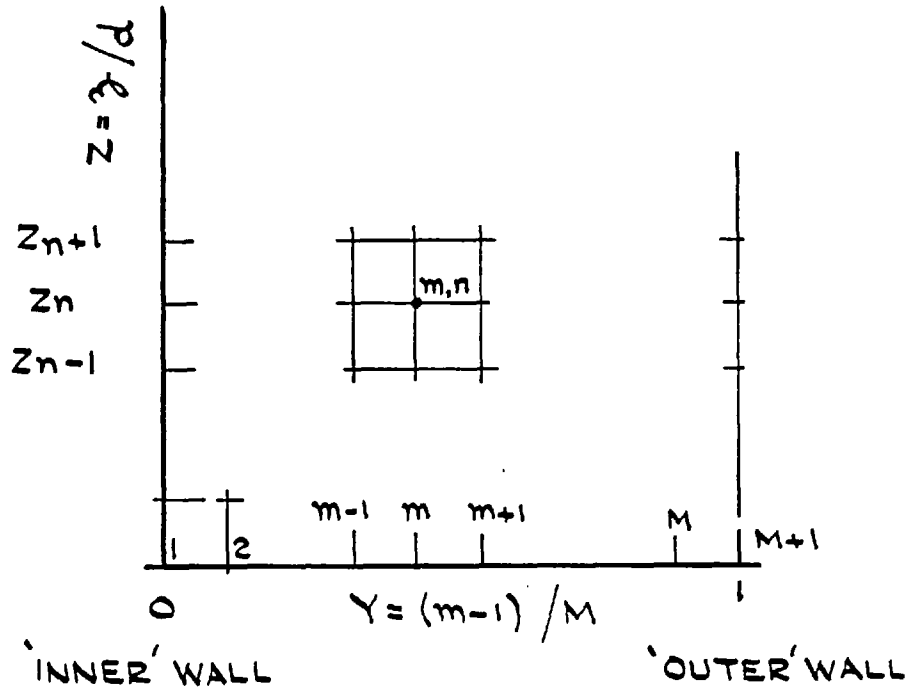

FIG(3.4) GRID FOR THE FINITE-DIFFERENCE METHOD.

nodes. In addition to this, numerical calculations for the same duct based on the standard five-point formula of the finite-difference method were also carried out. Comparison of the results obtained by both of the methods showed that the finite-difference method is more accurate than the finite-element when a relatively small number of nodes are used. In fact, while the finite-difference method always gives symmetric results for symmetric boundary conditions, the finite-element method, with triangular elements and linear interpolation polynominals, sometimes gives slightly unsymmetric results for symmetric boundary conditions. However, these results become more and more symmetric as more nodes are used. On the other hand, the finite-element method has advantages of its own. For instance, unequal mesh sizes do not introduce additional complexity in the computations. This characteristic can be utilised to advantage by allowing greater density of elements in the critical region where changes in the dependent variables are rapid. This consideration is desirable from the standpoint of economy, namely, it will give the investigator more information in the critical region with less computer time than a more refined grid with uniform size.

In passing, it may be stated that according to Zienkiewicz et al (1975), within a broad definition, the finite-difference techniques fall into a "subclass" of the general finite-element methodology which, indeed, embraces many other classical approximation procedures.

In conclusion, it may be argued that within the existing literature on these two methods, it is not quite certain which of them should be used for a particular problem. For the solution of Equations (3.15) - (3.28) in this thesis, a finite-difference method, similar to that used by Lawrence et al (1966) and Collins (1971) for round tubes is used.

3.7 Solution Procedure

3.7.1 The Finite-Difference Method

A rectangular grid, shown on Fig. (3.4) with axial and horizontal co-ordinates (suffix n and m respectively), is used. The channel spacing, d, is divided into M divisions. Therefore:-

$$Y = (m - 1)/M$$

According to this definition:-

For the "Inner" wall : $m = 1 \rightarrow Y = 0$

For the "Outer" wall : $m = M + 1 \rightarrow Y = 1$

In order to solve Equations (3.15) - (3.18), a set of linear equations may be written for the unknown level "n + 1". Then, these equations may be solved by making use of the known values at the level "n". Whenever products of two unknowns occur in the solution, linearity may be achieved by putting one unknown at its value of the previous step, $(Z_{n+1} \rightarrow Z_n)$. Provision should be made to check that this approximation does not have a considerable effect on the solution.

In order to express Equations (3.15) - (3.18) in the finite-difference form, the derivatives should be approximated also in the finite-difference form. The following two general formulae are useful in economising the space of presentation, for approximation of the derivatives:-

$$\left.\frac{\partial F}{\partial \ell}\right|_{\substack{n+1 \\ m}} = \frac{F_{n+1,\,m} - F_{n,\,m}}{\Delta \ell}$$

$$\left.\frac{\partial^2 F}{\partial \ell^2}\right|_{\substack{n+1 \\ m}} = \frac{F_{n+1,\,m} - 2F_{n,\,m} + F_{n-1,\,m}}{\Delta \ell^2}$$

where F and ℓ represent a flow characteristic and a co-ordinate respectively.

3.7.2 Finite-Difference Form of the Equations

(a) Mass Conservation

Define:-

$$\left.\frac{\partial U}{\partial Z}\right|_{n+1,\,m} = \frac{U_{n+1,\,m} + U_{n+1,\,m-1} - U_{n,\,m} - U_{n,\,m-1}}{2\Delta Z}$$

$$\left.\frac{\partial V}{\partial Y}\right|_{n+1,\,m} = \frac{V_{n+1,\,m} - V_{n+1,\,m-1}}{1/M}$$

By substitution of these approximations into Equation (3.15), one obtains:-

$$M \cdot V_{n+1,\,m} - M \cdot V_{n+1,\,m-1} + \frac{U_{n+1,\,m}}{2\Delta Z} + \frac{U_{n+1,\,m-1}}{2\Delta Z} = \frac{(U_{n,\,m} + U_{n,\,m-1})}{2\Delta Z} \qquad (3.29)$$

(b) Momentum Conservation in Z Direction

In Equation (3.16), $\partial U/\partial Z$, $\partial P/\partial Z$, $\partial T/\partial Z$, $\partial V/\partial Z$ and also $\partial^2 U/\partial Z^2$, $\partial^2 U/\partial Y^2$ may be approximated by the general two and three point formulae mentioned above.

The remaining derivatives are approximated as follows:-

$$\left.\frac{\partial U}{\partial Y}\right|_{n+1,\ m} = \frac{U_{n+1,\ m+1} - U_{n+1,\ m-1}}{2/M}\ ,\ \text{the same for}\ \frac{\partial T}{\partial Y}\ \text{and}\ \frac{\partial U}{\partial Y}$$

Introducing these approximations into Equation (3.16) yields:-

$$U_{n+1,\ m+1}\left[\frac{M^2}{2Re}\{2\eta_A + \frac{\eta_B}{2}(T_{n+1,\ m+1} - T_{n+1,\ m-1})\} - \frac{M}{2}\cdot V_{n,\ m}\right] +$$

$$+ U_{n+1,\ m}\left[\frac{1}{Re}\{\eta_A\left(\frac{1}{\Delta Z^2} - 2M^2\right) + \frac{2\eta_B}{\Delta Z^2}(T_{n+1,\ m} - T_{n,\ m})\} - \frac{U_{n,\ m}}{\Delta Z}\right] +$$

$$+ U_{n+1,\ m-1}\left[\frac{M^2}{2Re}\{2\eta_A - \frac{\eta_B}{2}(T_{n+1,\ m+1} - T_{n+1,\ m-1})\} + \frac{M}{2}V_{n,\ m}\right] -$$

$$- P_{n+1,\ m}/\Delta Z = -\frac{S}{Re^2}\cdot\frac{\rho_m}{\rho_B}\cdot\xi - \frac{P_{n,\ m}}{\Delta Z} - \frac{U^2_{n,\ m}}{\Delta Z} +$$

$$+ \frac{2U_{n,\ m}}{Re\ .\ \Delta Z^2}\{\eta_A + \eta_B\,(T_{n+1,\ m} - T_{n,\ m})\} \qquad (3.30)$$

where:-

$$\eta_A = (CO1\ \frac{T_{n+1,\ m}}{G} + CO2)^{-CO3}$$

$$\eta_B = \frac{CO1}{G}\{CO1\ \frac{T_{n+1,\,m}}{G} + CO2\}^{-(CO3+1)}$$

$$\xi = \{CO4\ .\ G + T_{n+1,\,m}\ (CO5 + CO6\ .\ T_{n+1,\,m})\}$$

(c) Momentum Conservation in Y Direction

In Equation (3.17), $\partial V/\partial Z$, $\partial T/\partial Z$ and also $\partial^2 V/\partial Z^2$, $\partial^2 V/\partial Y^2$ may be approximated according to the general two and three-point formulae respectively. The rest of the derivatives in this equation are approximated as follows:-

$$\left.\frac{\partial V}{\partial Y}\right|_{n+1,\,m} = \frac{V_{n+1,\,m+1} - V_{n+1,\,m-1}}{2/M}\ ,\ \text{the same for}\ \frac{\partial P}{\partial Y},\ \frac{\partial T}{\partial Y},\ \frac{\partial V}{\partial Y}\ \text{and}\ \frac{\partial U}{\partial Y}$$

By employing these approximations, one obtains:-

$$V_{n+1,\,m+1}\left[\frac{M^2}{2Re}\{\eta_A + \frac{\eta_B}{2}\ (T_{n+1,\,m+1} - T_{n+1,\,m-1})\} - \frac{M}{2}\ V_{n,m}\right] +$$

$$+\ V_{n+1,\,m}\left[\frac{1}{Re}\{\eta_A\ (\frac{1}{\Delta Z^2} - 2M^2) + \frac{\eta_B}{\Delta Z^2}\ (T_{n+1,\,m} - T_{n,\,m})\} - \frac{U_{n,\,m}}{\Delta Z}\right] +$$

$$+\ V_{n+1,\,m-1}\left[\frac{M^2}{2Re}\{2\eta_A - \eta_B\ (T_{n+1,\,m+1} - T_{n+1,\,m-1})\} + \frac{M}{2}\ V_{n,\,m}\right] +$$

$$+ M \cdot P_{n+1,\,m-1} - M \cdot P_{n+1,\,m+1} = - \frac{U_{n,\,m} \cdot V_{n,\,m}}{\Delta Z} + \frac{2 \cdot V_{n,\,m} \cdot \eta_A}{\Delta Z^2 \cdot Re} +$$

$$+ \frac{V_{n-1,\,m}}{\Delta Z^2 \cdot Re} \left\{ \frac{\eta_B}{2} (T_{n+1,\,m} - T_{n,\,m}) - \eta_A \right\} -$$

$$- \frac{M \cdot \eta_B}{2\Delta Z \cdot Re} (T_{n+1,\,m} - T_{n,\,m}) \cdot (U_{n,\,m+1} - U_{n,\,m-1}) \qquad (3.31)$$

where η_A and η_B are the same as for Equation (3.30).

(d) Energy Conservation

In Equation (3.18), $\partial T/\partial Z$ and $\partial^2 T/\partial Z^2$, $\partial^2 T/\partial Y^2$ may be approximated according to the general two and three points formulae respectively. The remaining derivative is approximated by:-

$$\left.\frac{\partial T}{\partial Y}\right|_{n+1,\,m} = \frac{T_{n+1,\,m+1} - T_{n+1,\,m-1}}{2/M}$$

Introduction of these substitutions into Equation (3.18) yields:-

$$T_{n+1,\,m+1} \left(\frac{M}{2} V_{n,\,m} - \frac{M^2}{Pr \cdot Re}\right) + T_{n+1,\,m} \left(\frac{U_{n,\,m}}{\Delta Z} + \frac{2M^2 - 1/\Delta Z^2}{Pr \cdot Re}\right) +$$

$$+ T_{n+1,\,m-1} \left(-\frac{M}{2} V_{n,\,m} - \frac{M^2}{Pr \cdot Re}\right) = T_{n,\,m} \left(\frac{U_{n,\,m}}{\Delta Z} - \frac{2}{\Delta Z^2 \cdot Pr \cdot Re}\right) +$$

$$+ T_{n-1,\,m} \left(\frac{1}{\Delta Z^2 \cdot Pr \cdot Re}\right) \qquad (3.32)$$

(e) Viscosity and Density Functions

Equations (3.19) - (3.20) transform into the following two equations:-

$$\mu = \mu_B \left(CO1 \frac{T_{n+1,\,m}}{G} + CO2\right)^{-CO3} \tag{3.33}$$

$$\rho = \rho_B \left\{CO4 + \frac{T_{n+1,\,m}}{G} (CO5 + CO6 \cdot T_{n+1,\,m})\right\} \tag{3.34}$$

(f) The Integral Continuity Equation

If numerical integration in Equation (3.21) is carried out by a third order approximation, one obtains:-

$$1 = \frac{2}{6M} \left(U_{n+1,\,1} + 4U_{n+1,\,2} + 2U_{n+1,\,3} + 4U_{n+1,\,4} + \cdots\cdots\right.$$

$$\left. \cdots\cdots + 2U_{n+1,\,M-1} + 4U_{n+1,\,M} + U_{n+1,\,M+1}\right)$$

But:-

$$U_{n+1,\,M+1} = U_{n+1,\,1} = 0$$

By using these boundary conditions in the equation and re-arranging:-

$$\frac{3M}{2} = 2 \sum_{m=1}^{M/2} \frac{\rho}{\rho_o} \cdot U_{2m} + \sum_{m=1}^{M/2 - 1} \frac{\rho}{\rho_o} \cdot U_{2m+1} \tag{3.35}$$

(g) Overall Energy Balance

In the following, it is shown how Equations (3.26) - (3.27) may be transformed into Equations (3.36) - (3.37) respectively by making use of the finite-difference approximations.

(g.1) When wall heat-fluxes are prescribed

$$\sum_{m=2}^{M} \frac{\rho}{\rho_o} \cdot U_{n+1,\,m} \cdot T_{n+1,\,m} - \sum_{m=2}^{M} \frac{\rho}{\rho_o} \cdot U_{n,\,m} \cdot T_{n,\,m} =$$

$$= \frac{\Delta Z \,.\, M^2}{Pr \,.\, Re} \Big| (HFI + HFO) \Big|_{\text{Integrated between Z and Z + dZ}}$$

The functions HFI (Z) and HFO (Z) on the right-hand side of this equation may be numerically integrated for the solution. According to the method mentioned in Singer (1964), these integrations may be carried out by the formula:-

$$\frac{1}{\Delta Z} \int_{Z}^{Z + \Delta Z} HFI\ (Z)\ .\ dZ = a \sum_{J=0}^{N} C_J\ .\ HFI\ (Z_J)$$

where:-

N = Number of divisions considered for the integration interval.

a = Overall coefficient of the integration depending on N.

J = A parameter to represent intermediate points for the integration.

C_J = Partial coefficients depending on N.

Table (I.1) in the Appendix (I), reproduced from Singer (1964), shows values of these coefficients against their parameters.

The function HFO (Z) may be similarly integrated. Therefore, the overall energy balance for this case becomes:-

$$\sum_{m=2}^{M} \frac{\rho}{\rho_o} \cdot U_{n+1,\,m} \cdot T_{n+1,\,m} - \sum_{m=2}^{M} \frac{\rho}{\rho_o} \cdot U_{n,\,m} \cdot T_{n,\,m} =$$

$$= \frac{M^2 \cdot \Delta Z}{Pr \cdot Re} \left\{ \left| a \sum_{J=0}^{N} C_J \cdot HFI\,(Z_J) \right|_{\substack{\text{"Inner"} \\ \text{Wall}}} + \left| a \sum_{J=0}^{N} C_J \cdot HFO\,(Z_J) \right|_{\substack{\text{"Outer"} \\ \text{Wall}}} \right\} \quad (3.36)$$

(g.2) <u>When wall temperatures are prescribed</u>

In this case, the integral energy equation is:-

$$\sum_{m=2}^{M} \frac{\rho}{\rho_o} \cdot U_{n+1,\,m} \cdot T_{n+1,\,m} - \sum_{m=2}^{M} \frac{\rho}{\rho_o} \cdot U_{n,\,m} \cdot T_{n,\,m} =$$

$$= \frac{M \cdot \Delta Z}{Pr \cdot Re} \left\{ \left| \frac{dT}{dY} \right|_{Y=0} + \left| \frac{dT}{dY} \right|_{Y=1} \right\}$$

The right-hand side differentiations may be carried out numerically. According to Singer (1964):-

$$\left| \frac{dT}{dY} \right|_{Y=0} = M \left\{ \left| d' \sum_{J=0}^{N'} C_J \cdot T(Y_J) \right|_{Y=0} \right\}$$

where:-

N' = Total number of points used for the differentiation.

d' = Overall coefficient of the differentiation depending on N'.

J = A parameter which signifies the points used for the differentiation.

C_J = Partial coefficients depending on N'.

Table (I.2), in Appendix (I), reproduced from Singer (1964), shows values of these coefficients against their parameters.

The other derivative:-

$$\left|\frac{dT}{dY}\right|_{Y=1}$$

may be similarly treated. Therefore, the overall energy balance equation for this case is:-

$$\sum_{m=2}^{M} \frac{\rho}{\rho_o} \cdot U_{n+1,\,m} \cdot T_{n+1,\,m} - \sum_{m=2}^{M} \frac{\rho}{\rho_o} \cdot U_{n,\,m} \cdot T_{n,\,m} =$$

$$= \frac{M^2 \cdot \Delta Z}{Pr \cdot Re} \left\{ \left| d' \sum_{J=0}^{N'} C_J \cdot T(Y_J) \right|_{Y=0} + \left| d' \sum_{J=0}^{N'} C_J \cdot T(Y_J) \right|_{Y=1} \right\} \qquad (3.37)$$

3.7.3 Finite-Difference Form of the Boundary Conditions

(1) Entrance conditions: $(Z = 0,\ 0 \leq Y < 1)$

$$U_{1,\,m} = 1,\ V_{1,\,m} = 0,\ P_{1,\,m} = P_o,\ T_{1,\,m} = T_o$$

(2) Wall flow conditions: $(0 < Z \leq L/d,\ Y = 0 \text{ or } 1)$

$$U_{n,\,1} = U_{n,\,M+1} = 0$$

$$V_{n,\,1} = V_{n,\,M+1} = 0$$

Additional assumption necessary to start the solution from the "Inner" wall:-

$$P_{n,\,1} - P_{n,\,2} = P_{n,\,2} - P_{n,\,3}$$

$$\text{or: } P_{n,\,2} = \frac{P_{n,\,1} + P_{n,\,3}}{2}$$

(3) Wall thermal boundary conditions: $(0 < Z \leq L/d,\ Y = 0 \text{ or } 1)$

In order to make wall thermal conditions, $\dot{q}''_w(z)$ or $t_w(z)$ suitable for the finite-difference approximation, their profile is divided into infinitesimal axial strips and dealt with as follows:-

(i) <u>Wall heat-flux prescribed</u>

In this case, an average wall heat-flux is used. Define for the $\dot{q}''_{wi}(z)$ profile:-

$$HFI\Big|_{\text{Av. for } \Delta Z} = \frac{\int_{Z_n}^{Z_{n+1}} HFI\ (Z)\ .\ dZ}{Z_{n+1} - Z_n} \qquad (3.38)$$

On the other hand, for differentiation with one adjacent point:-

$$HFI\Big|_{\text{Av. for } \Delta Z} = \frac{\partial T}{\partial Y}\Big|_{Y = 0} = \frac{T_{n,\,1} - T_{n,\,2}}{1/M} \tag{3.39}$$

Combining Equations (3.38) and (3.39):-

$$T_{n,\,1} = T_{n,\,2} + \frac{1}{M} \cdot HFI\Big|_{\text{Av. for } \Delta Z}$$

By substituting $TWI_n = T_{n,1}$ and

$$HFI\ (z) = \frac{d^4 \cdot g \cdot C_5}{\nu_B^2 \cdot k_m} \cdot \dot{q}''_{wi}\ (z) :-$$

$$TWI_n = T_{n,2} + \frac{d^4 \cdot g \cdot C_5}{\nu_B{}^2 \cdot k_m \cdot M} \cdot \dot{q}''_{wi}\ (z)\Big|_{\text{Av. integrated between Z and Z + dZ}} \tag{3.40}$$

The "Outer" wall may be dealt with similarly to obtain:-

$$TWO_n = T_{n,\,M} + \frac{d^4 \cdot g \cdot C_5}{\nu_B{}^2 \cdot k_m \cdot M} \cdot \dot{q}''_{wo}\Big|_{\text{Av. integrated between Z and Z + dZ}} \tag{3.41}$$

Equations (3.40) and (3.41) show how a prescribed wall heat-flux profile is turned into a boundary

condition problem. Now if the flow specifications at the point Z are known, their corresponding values at Z_{n+1} may be calculated. In other words, the flow specifications (U, V, P and T), obtained for the level "Z" are treated as initial conditions for the level "Z + dZ". Also, the heat added to the model is the integrated value of the HFI and HFO profiles over the length dZ. Thus, a prescribed non-uniform $\dot{q}''_w$ (z) turns into a uniform wall heat-flux problem for the distance dz. Here, the only prerequisite is the integrability of $\dot{q}''_w$ (z), either analytically or numerically. For the solutions reported in this thesis, these integrations are carried out numerically as mentioned for Equation (3.36).

(ii) Wall temperature prescribed

A similar procedure as for the case of prescribed $\dot{q}''_w$ may be followed to obtain:-

$$TWI_n = \frac{d^3 \cdot g \cdot C_5}{\nu_B^2} (t_{wi}(z_n) - t_{in}) \tag{3.42}$$

$$TWO_n = \frac{d^3 \cdot g \cdot C_5}{\nu_B^2} (t_{wo}(z_n) - t_{in}) \tag{3.43}$$

3.7.4 Method of Solution

From examination of Equations (3.29) - (3.32), it may be observed that where the product of two unknowns has occurred,

linearity is achieved by putting one of the unknowns equal to its value at the previous position. It can also be seen that these equations may be classified into two sets: one for the flow-field (i.e. U, V and P) and the other one for the temperature, T. In other words, the equations of conservation of mass and momentum are distinguished from the "energy equation" as the "flow-field" equations. These two sets of equations are linked to each other by the effects of temperature on the "flow-field" and vice versa. Therefore, the solution of Equations (3.29) - (3.32) may begin with the solution for either of the "sets". In the calculations which follow, it is assumed that the effect of temperature on the flow-field is of second-order. Therefore, the solution is started by solving the "flow-field" equations first. The solution is continued by using these results for the energy equation.

In order to take into account the dependence of the coefficients of each of the above-mentioned "sets" on each other, the solution is to be repeated at each step to make sure that they have their "correct" values for the final solution. This repetition is to be stopped when the difference between two immediate solutions is negligible. In more detail, Equations (3.29) - (3.31) and (3.35) are written for each horizontal position. At the first axial step from the channel entry, the coefficients and also the right-hand side values are evaluated from the entrance boundary conditions. This produces (3M - 2) unknowns, (U, V, P for each horizontal position and P at the "Outer" wall) and the same number of equations.

3.7.5 Matrix Form of the Flow-Field and the Energy Equations

Equations (3.29) - (3.31), together with Equation (3.35) may

be written in the following Matrix form:-

$$\begin{vmatrix} a'_{1,1} & a'_{1,2} & \cdots & a'_{1,3M-2} \\ a'_{2,1} & \cdots & \cdots & \cdots \\ \vdots & \vdots & \vdots & \vdots \\ a'_{3M-2,1} & \cdots & \cdots & a'_{3M-2,3M-2} \end{vmatrix} \times \begin{vmatrix} P_2 \\ \vdots \\ P_{M+1} \\ V_2 \\ \vdots \\ V_M \\ U_2 \\ \vdots \\ U_M \end{vmatrix} = \begin{vmatrix} b'_1 \\ \vdots \\ b'_{3M-2} \end{vmatrix}$$

where:-

a'_{ij} = Coefficients depending on the flow-field and also the temperature values at the previous steps.

b'_i = Known values in the right-hand side of each of the equations.

This Matrix form may also be represented as:-

$$|A'| \times |PVU| = |B'| \qquad \text{(For the flow-field)} \qquad (3.44)$$

Equation (3.32) together with either Equation (3.36) or (3.37) may be similarly treated to obtain the following Matrix form:-

$$\begin{vmatrix} a''_{1,1} & a''_{1,2} & \cdots & a''_{1,M-1} \\ a''_{2,1} & \cdots & & \\ \vdots & & & \\ a''_{M-1,1} & \cdots & & a''_{M-1,M-1} \end{vmatrix} \times \begin{vmatrix} T_2 \\ \vdots \\ T_M \end{vmatrix} = \begin{vmatrix} b''_1 \\ \vdots \\ b''_{M-1} \end{vmatrix}$$

where:-

a''_{ij} = A coefficient depending on PVU values obtained from the solution of Equation (3.44) and also the temperature values at the previous steps.

b''_i = Known values at the right-hand side of each of the equations.

This equation may be represented also as:-

$$|A''| \times |T| = |B''| \qquad \text{(For energy)} \qquad (3.45)$$

CHAPTER 4

THE NUMERICAL SOLUTION TECHNIQUE AND THE COMPUTER PROGRAM 'DUCT'

4.1 Introduction

In Chapter (3), conservation equations of mass, momentum and energy were written for the theoretical model. Later, these were transformed into the finite-difference form which led to the matrix Equation (3.44) for the "flow-field" equations (i.e. PVU) and the matrix Equation (3.45) for the temperature, T. This chapter is concerned with the solution of these two sets of equations by the computer program, DUCT specially written for the purpose.

4.2 The Numerical Solution Technique

Recalling the matrix Equation (3.44):-

$$|A'| \cdot |PVU| = |B'| \qquad (3.44)$$

Solution of this type of equation may be attempted, among other methods, by inversion of the matrix $|A'|$ and later multiplying it by the matrix $|B'|$. In this thesis, however, the solution is obtained by a standard Gaussian Elimination Method suggested by McCormack et al (1964).

The matrix Equation (3.45):-

$$|A''| \cdot |T| = |B''| \qquad (3.45)$$

is also similarly treated.

As mentioned in Chapter (3), Equations (3.44) and (3.45) are coupled together because of the effects of the temperature, T on the

flow-field, PVU and vice versa. Thus, after obtaining a solution for Equation (3.44), this solution should be used for the solution of Equation (3.45). In order to make sure the effects of the dependence of the $|A'|$ and $|A''|$ matrices on the PVU and T solutions is being catered for, these joint solutions are repeated until the difference between two successive solutions is negligible. The marching is carried out by progressing to the next axial distance until the total length of the tube is covered.

The computer program DUCT is written for the solution of the matrix Equations (3.44) - (3.45). The listing of this program is available at:-

Imperial College of Science and Technology, Thermal Power Section

A discussion of the strategy of the computer program and also its parameters, plus a Flow-Chart are given in the following.

4.3 The Computer Program DUCT

This program is written in FORTRAN 4 and consists of the main program DUCT and the subroutine, MRV for the Gaussian Elimination Method.

The main program DUCT has two basic parts.

(i) In the first part, the coefficients a'_{ij} for (3M - 2) rows of the matrix $|A'|$, are calculated. The coefficients b_i of the matrix $|B'|$ are also calculated by making use of the boundary conditions. At the end of the first part of DUCT, the subroutine MRV is called to solve for PVU values.

(ii) In the second part of DUCT, the coefficients a''_{ij} of the (M - 1)

rows of the matrix $|A''|$ are calculated. In these calculations, PVU values, obtained at the first part of the main program are used. The subroutine MRV is called at the end of this part also to solve for the T values.

In order to take into effect the dependence of the PVU and T solutions on each other, a semi-iterative operation is carried out. This is done by using the T solutions, at the end of the DUCT program, to obtain another PVU solution which in turn is followed by another solution for T. This iteration is repeated until the difference between two successive solutions for T falls within the criterion pre-selected for the problem. Having completed the iteration, the PVU and the T solutions are declared final and are written in the output list.

4.4 The Computer Program's Notation and Definition of its Terms

4.4.1 Input Functions

In order to prescribe the functions according to which wall temperature or heat-flux on both walls vary, provision is made to give two functions, FI(Z) and FO(Z), as input directives for the computer program.

4.4.2 Input Parameters

CO1, CO2, CO3 — These three parameters represent the coefficients of the viscosity function of temperature, Equation (3.19). (The program DUCT may be used for other viscosity functions than Equation (3.19), by replacing the η_A and η_B terms which are used in it with the relevant new terms).

C04, C05, C06 — These parameters represent the coefficients of the density function of temperature, Equation (3.20). The term ξ should be adjusted if density functions other than Equation (3.20) are to be used.

DELTZ — The axial increment in the marching-forward procedure is given by this parameter. It should be assumed rather small, e.g. DELTZ = 0.625, near the entrance region of the channel. However, provision is made in the program for DELTZ to be doubled at particular axial positions, should this be required.

EPSYLN — The criterion for iterative PVU and T solutions is specified by this parameter. The value of this parameter depends on the accuracy desired in the calculations. In DUCT, the iterative procedure is stopped when:-

$$\frac{TWO_{i+1} - TWO_i}{TWO_i} \leq \text{EPSYLN} \rightarrow \text{for IFTOQ = 2 or 3}$$

or:-

$$\frac{HFO_{i+1} - HFO_i}{HFO_i} \leq \text{EPSYLN} \rightarrow \text{for IFTOQ = 1}$$

where i is the number of iterations already executed.

GNUMBRY — A dimensionless number related to the geometry of the

theoretical model and the base temperature, t_B:-

GNUMBRY ≡ G = d^3 . g/ν_B^2

IDR — The number of points for the numerical differentiation in Equation (3.13) is specified by this index.

IFTOQ — This index specifies whether the wall temperature profiles or wall heat-fluxes are prescribed. Different cases are assumed by the program according to the following values of IFTOQ:-

1 → { FI(Z) = TWI(Z); FO(Z) = TWO(Z)

2 → { FI(Z) = HFI(Z); FO(Z) = HFO(Z)

3 → { FI(Z) = TWI(Z); FO(Z) = HFO(Z) = 0 (Thermally insulated wall)

ILASTY — This is an index which controls the total number of axial steps in the marching-forward procedure.

ISTEP — This index specifies after how many axial steps the writing of the results in the output list should take place.

ISUNUY — The program assumes the following two U_o profiles according to the value of this index:-

(i) Uniform U_o, i.e. $U_o = 1 \rightarrow$ For ISUNUY = 1

(ii) Parabolic U_o, i.e. $U_o = 6Y(1 - Y) \rightarrow$ For ISUNUY = 2

KLASTY — Provision is made in the program that at some axial positions, the axial increment, DELTZ is doubled. This is done to economize on the computer time after small increments which are necessary near the channel entry.

LD — Elements of this array specify the axial positions at which the axial increment, DELTZ is doubled. The maximum number of its elements is equal to ILASTY.

MAXY — This index specifies the number of divisions in the channel spacing, d (M ≡ MAXY). Due to the nature of the finite-difference approximation used for Equation (3.35), MAXY must be an even number. Choice of this index depends on the capacity of the computer system. For the CDC 7600 (ULCC), it could be increased up to: MAXY = 90.

NIM — This index is used to limit the number of successive iterations at a particular axial position.

PENTRY — This parameter represents the pressure at the entrance to the channel. For convenience, it may be assumed zero. Later, p at any axial level may be adjusted by adding the

actual p_o value to it.

PRNDTL, RYNLDS — These two parameters are the modified Prandtl and Reynolds numbers defined in the nomenclature.

RATIOY — The ratio, ρ_m/ρ_B is specified by this parameter.

S — This parameter specifies the sign of the buoyancy term. Its value is:-

1 → For upward flow

- 1 → For downward flow

0 → For adiabatic or pure-forced flow

4.4.3 Output Parameters

f_p, $f_{p_{av}}$ (Pressure-factors): These two parameters represent the local and the average pressure drops and are calculated based on the formulae:

$$f_p = \frac{\text{PMEANY}\Big|_{\text{ZBAR}} - \text{PMEANY}\Big|_{(\text{ZBAR-DELTZ})}}{\text{DELTZ}}$$

$$f_{p_{av}} = \frac{\text{PMEANY}\Big|_{\text{ZBAR}}}{\text{ZBAR}}$$

f_{s_i}, f_{s_o} (Shear loss-factors): These two parameters represent local shear stress factors at the "Inner" and the "Outer" walls respectively. For the "Inner" wall:-

$$f_{s_i} = \frac{\tau_{s_i}}{\frac{1}{2}\rho_m \cdot u_o^2} = \frac{\mu_{wi} \cdot \frac{\partial u}{\partial y}\Big|_{y=0}}{\frac{1}{2}\rho_m \cdot u_o^2}$$

$$f_{s_i} = \frac{2}{Re} \cdot \left.\frac{\partial U}{\partial Y}\right|_{Y=0} \cdot \frac{\mu_{wi}}{\mu_B}$$

$$f_{s_i} = \frac{2 \cdot \eta_{A(wi)}}{Re} \cdot \left.\frac{\partial U}{\partial Y}\right|_{Y=0}$$

Similarly, for the "Outer" wall:-

$$f_{s_o} = \frac{2 \cdot \eta_{A(wo)}}{Re} \cdot \left.\frac{\partial U}{\partial Y}\right|_{Y=1}$$

Differentiations on the right-hand side of these formulae are numerically executed in the DUCT computer program. Local friction and shear-loss factors, f_p and f_s, are important performance data. These two coincide only when density is constant,i.e. there is no momentum change.

GRAETZ Graetz number is calculated according to the formula:-

$$GRAETZ = Re_D \cdot Pr/Z_D$$

HEADM This parameter represents the total pressure head which is needed at each axial position. It is calculated from the formula:-

$$HEADM = \frac{\int_o^z (\rho_{mean} - \rho_o) \cdot g \cdot dz - \Delta p_f}{\rho_m \cdot u_o^2}$$

It can be noted that the right-hand side of this is the

difference between the "friction" and "buoyancy" pressure terms, where the buoyancy term is the difference between the static pressure drop which actually occurs with the heated fluid and the static pressure drop which would occur in the channel if the fluid density remained at its entrance value. This parameter is chosen, similar to that of Lawrence et al (1966), because it has physical significance in a mixed-convection regime.

HFLUXI, HFLUXO — Wall heat-fluxes at the "Inner" and the "Outer" walls are represented by these two parameters respectively. When t_w is prescribed, (IFTOQ = 1), these parameters are calculated according to the formulae:-

$$\dot{q}''_{wi} = -k \left.\frac{\partial t}{\partial y}\right|_{y=0}, \quad \dot{q}''_{wo} = + k \left.\frac{\partial t}{\partial y}\right|_{y=d}$$

or in the dimensionless form:-

$$\text{HFLUXI} = \frac{-1}{M} \cdot \left.\frac{\partial T}{\partial Y}\right|_{Y=0}$$

$$\text{HFLUXO} = \frac{1}{M} \cdot \left.\frac{\partial T}{\partial Y}\right|_{Y=1}$$

The differentiation on the right-hand side of these equations is performed by the method of Singer (1964) shown in Table (I.2) of Appendix (I).

MCPCM — This parameter specifies the "degree" of mixed-convection which is to be referred as "mixed-convection index" in Chapter (5). It is calculated from the formula:-

$$MCPCM = \frac{\int_0^z (\rho_{mean} - \rho_o) \cdot g \cdot dz}{p_o - p_{mean}\Big|_z} \times 100$$

Therefore, it assumes values 0 and 100 for pure-forced and pure-free convection regimes respectively.

NUSSLTI, NUSSLTO

These two parameters are Nu_i and Nu_o respectively. The following relations show how Nu_i is calculated:-

$$Nu_i = \frac{2d}{k} \cdot h_{wi} = \frac{2d}{k} \cdot \frac{\dot{q}''_{wi}}{(t_{wi} - t_{mean})}$$

or in the normalized form:-

$$NUSSLTI = \frac{2 \cdot MAXY \cdot HFLUXI}{(TWALLI - TMEANY)}$$

A similar method is adopted for the calculation of NUSSLTO.

PMEANY

The pressure is integrated throughout the cross-section according to the formula:-

$$w \cdot d \cdot p_{mean} = \int_0^d p \cdot w \cdot dy$$

or:-

$$P_{mean} = M \cdot \int_0^1 P \cdot dY$$

By execution of the integral numerically:-

$$PMEANY = \sum_{m=2}^{M} P_m + \frac{1}{2}(P_1 + P_{M+1})$$

REDZD, REDZDPR — These two parameters are modified forms of the axial coordinate, Z. They are calculated from the formulae:-

$$REDZD = \frac{Re_D}{Z_D}$$

$$REDZDPR = \frac{Re_D \cdot Pr}{Z_D}$$

TBARY — This parameter is the mixed-mean temperature which is calculated based on the total heat input to the theoretical model, Equation (3.12) or (3.13).

TMEANY — This parameter is the mixed-mean temperature which is calculated based on the temperature profile across the cross-section. Recalling from Equation (3.14):-

$$t_{mean} = \frac{\int_o^d u \cdot \rho \cdot t \cdot dy}{\int_o^d \rho \cdot u \cdot dy} \qquad (3.14)$$

which after normalization and the numerical integration becomes:-

$$TMEAN\Big|_{n+1} = \frac{1}{M} \sum_{m=2}^{M} U_{n+1,m} \cdot T_{n+1,m} \cdot \frac{\rho}{\rho_o}$$

As mentioned in Chapter (2), the overall energy balance equations, Equation (3.12) or Equation (3.13), are used in the solution procedure as part of the equations in the PVU and the T solutions. Thus, TMEANY and TBARY should be the same. As a check, these two parameters are calculated independently to show the accuracy of the method of solution.

TWALLI, TWALLO — These two parameters represent t_w at the "Inner" and the "Outer" walls, (Y = 0 and 1) respectively. When $\dot{q}_w''$ is prescribed, IFTOQ = 2, these parameters are calculated based on a curve-fitting exercise to the solved temperature profile. For "Inner" wall with three adjacent points:-

$$TWALLI = (6 \cdot HFLUXI + 18 \cdot T_2 - 9 \cdot T_3 + 2 \cdot T_4)/11$$

For higher accuracies, more points are used according to the method of Singer (1964), see Table (I.2) of Appendix (I). The "Outer" wall is similarly treated to obtain TWALLO.

U, V, T and P — The output list contains the normalized values of the axial and horizontal velocities, the temperature and the pressure across the cross-section at each axial position. The outline of the output is arranged such that the first value for each of these is the value at Y = 0 and the rest are the values at horizontal increments of 1/M.

ZBAR — This parameter represents the axial coordinate in dimensionless form.

ZDRED, ZDREDPR — These two parameters are modified forms of the axial coordinate, Z. They are calculated from the formulae:-

$$ZDRED = \frac{Z_D}{Re_D}$$

$$ZDREDPR = \frac{Z_D}{Re_D \cdot Pr}$$

4.4.4 Input Parameters' Format

(a) Card 1: ILASTY, KLASTY, MAXY, ISUNUY, IFTOQ, NIM, ISTEP, IDR are entered as integer numbers with maximum of three digits.

(b) Cards 2 and 3: CO1, CO2, CO3, CO4, CO5/CO6, GNUMBRY, PENTRY, DELTZ, PRNDTL, RYNLDS are entered as decimal numbers.

(c) Cards 4 and 5: These cards explain the specifications of the functions FI(Z) and FO(Z) to be used as the head-lines in the output list. Due to the type of characters used in these cards, they are entered with "alpha-numeric" format.

(d) Card 6: S, RATIOY, EPSYLN are entered as decimal numbers.

(e) Card 7: LD(1) .... LD(KLASTY) are entered as integer numbers. The last element of the array LD must be equal to ILASTY.

4.4.5 Execution of the Program DUCT

In order to facilitate execution of this computer program whilst reserving the possibility of inserting the new FI(Z) and FO(Z) functions in the program,and also any necessary modifications for any particular mixed-convection problem, the UPDATE filing system is used. By making use of this system, developed by Sinclair et al (1975), the computer program is stored in an initial form. Later, by a set of directives, the new functions FI(Z) and FO(Z) are inserted by deleting their corresponding functions which exist in the stored version. After the insertion of the new functions FI(Z) and FO(Z), and also the necessary modifications, the program turns into a new version ready to be compiled for the new set of data which follows the input-directives. This new version of the computer program does not remain permanently in the stored file and is purged as soon as the execution is over.

4.5 Discussion About the Flow-Chart of the DUCT Computer Program

For the Flow-Chart (given at the end of this chapter), four variables, in addition to those already mentioned, are used. These internal variables are:-

ITALLY An index representing the number of axial steps already taken. The program stops when:- ITALLY = ILASTY

N12 This index shows the number of iterations executed for the PVU and T solutions. Iteration stops when this index equals NIM.

NITER Iteration, for the PVU and T solutions, starts when this index is zero and finishes when it equals 1.

PTWO This parameter represents the value of TWALLO or HFLUXO at the last iteration as follows:-

IFTOQ = 1 → PTWO = HFLUXO

IFTOQ = 2 or 3 → PTWO = TWALLO

At the end of this chapter, the Flow-Chart of the computer program DUCT, with utilization of the UPDATE system, is given. For straightforward running of the program with a deck of cards, the two cards for the FI(Z) and FO(Z) functions must be inserted beforehand.

4.6 Consumption of Computer Time for a Typical Run of the Computer Program DUCT

A single run of the DUCT computer program on the CDC 7600 (ULCC), for a uniform heating case with 40 horizontal divisions and 16 axial steps, uses 6.088 (sec) of the Central-Processing time, CP. This time increases to 119.114 (sec) for the same problem, but with 90 horizontal divisions.

For the CDC 6400 (ICCC), which is a much slower machine, CP time for the above-mentioned problem with 40 horizontal divisions and

24 axial steps, is 83.112 (sec). It increases to 310.811 (sec) when the number of horizontal divisions increases to 60.

4.7 Flow-Chart of DUCT

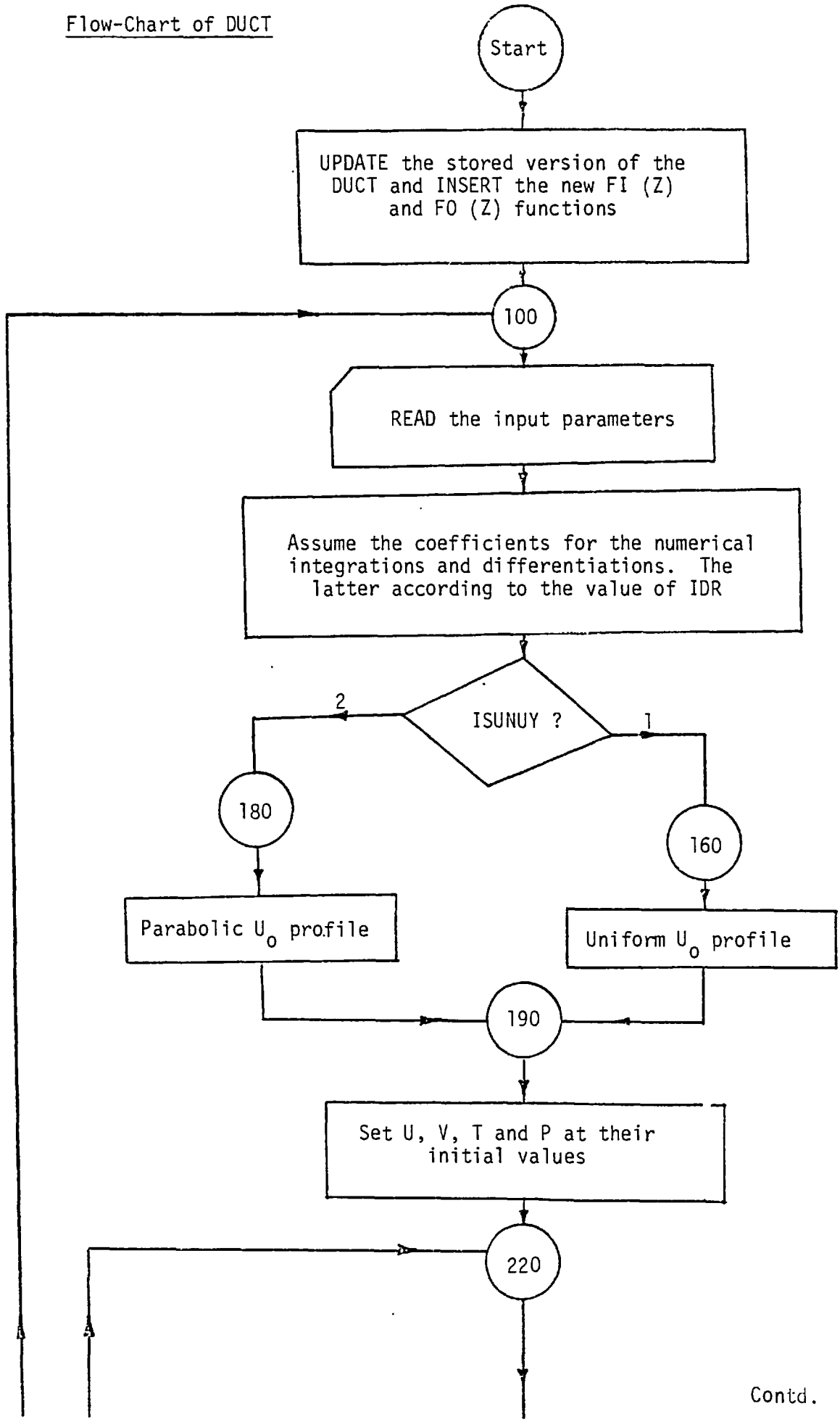

Contd.

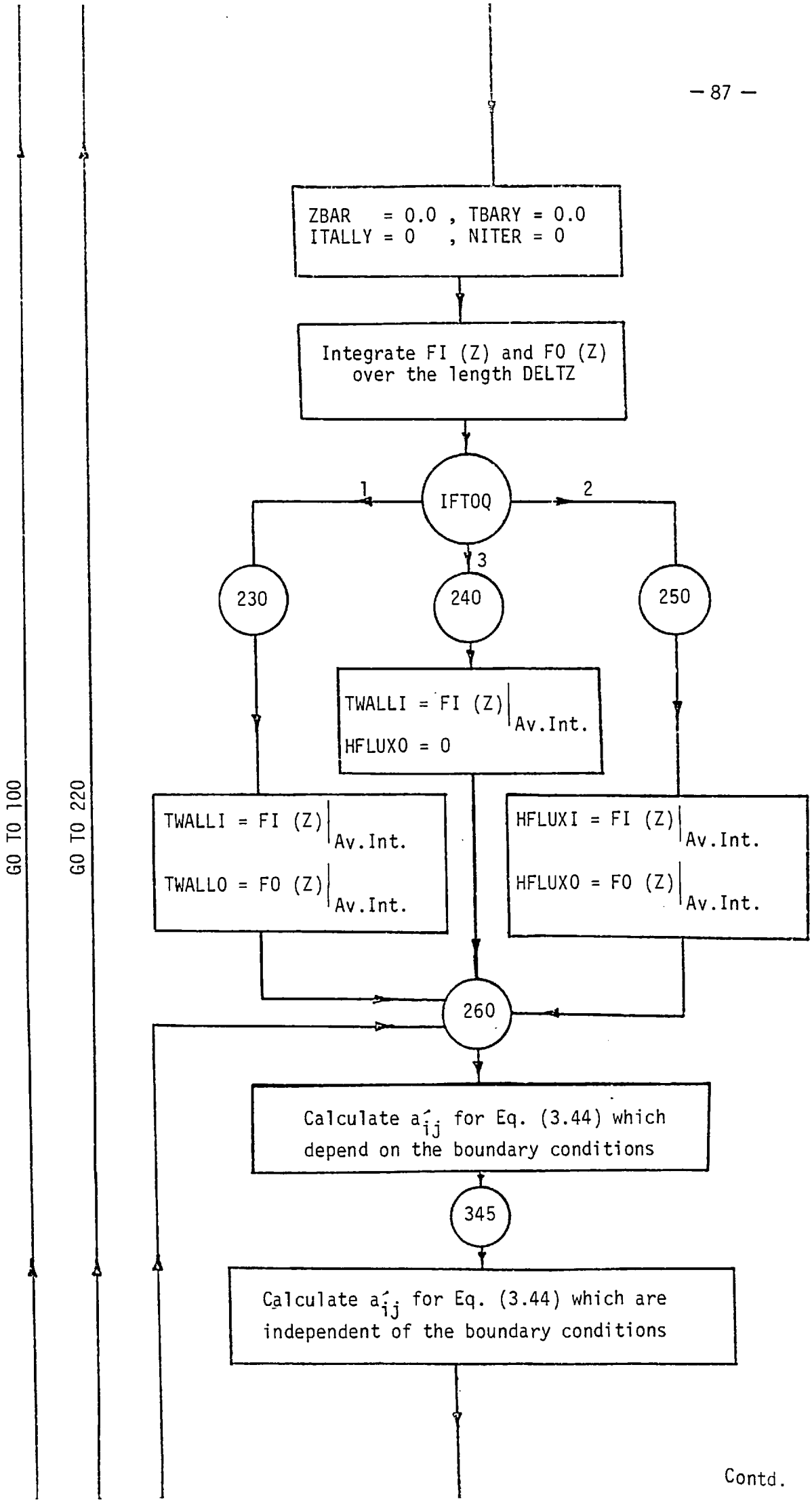
ZBAR = 0.0 , TBARY = 0.0
ITALLY = 0 , NITER = 0
Integrate FI (Z) and FO (Z) over the length DELTZ
IFTOQ
1
2
3
230
240
250
TWALLI = FI (Z) | Av.Int.
HFLUXO = 0
TWALLI = FI (Z) | Av.Int.
TWALLO = FO (Z) | Av.Int.
HFLUXI = FI (Z) | Av.Int.
HFLUXO = FO (Z) | Av.Int.
260
Calculate a'ij for Eq. (3.44) which depend on the boundary conditions
345
Calculate a'ij for Eq. (3.44) which are independent of the boundary conditions
GO TO 100
GO TO 220

Contd.

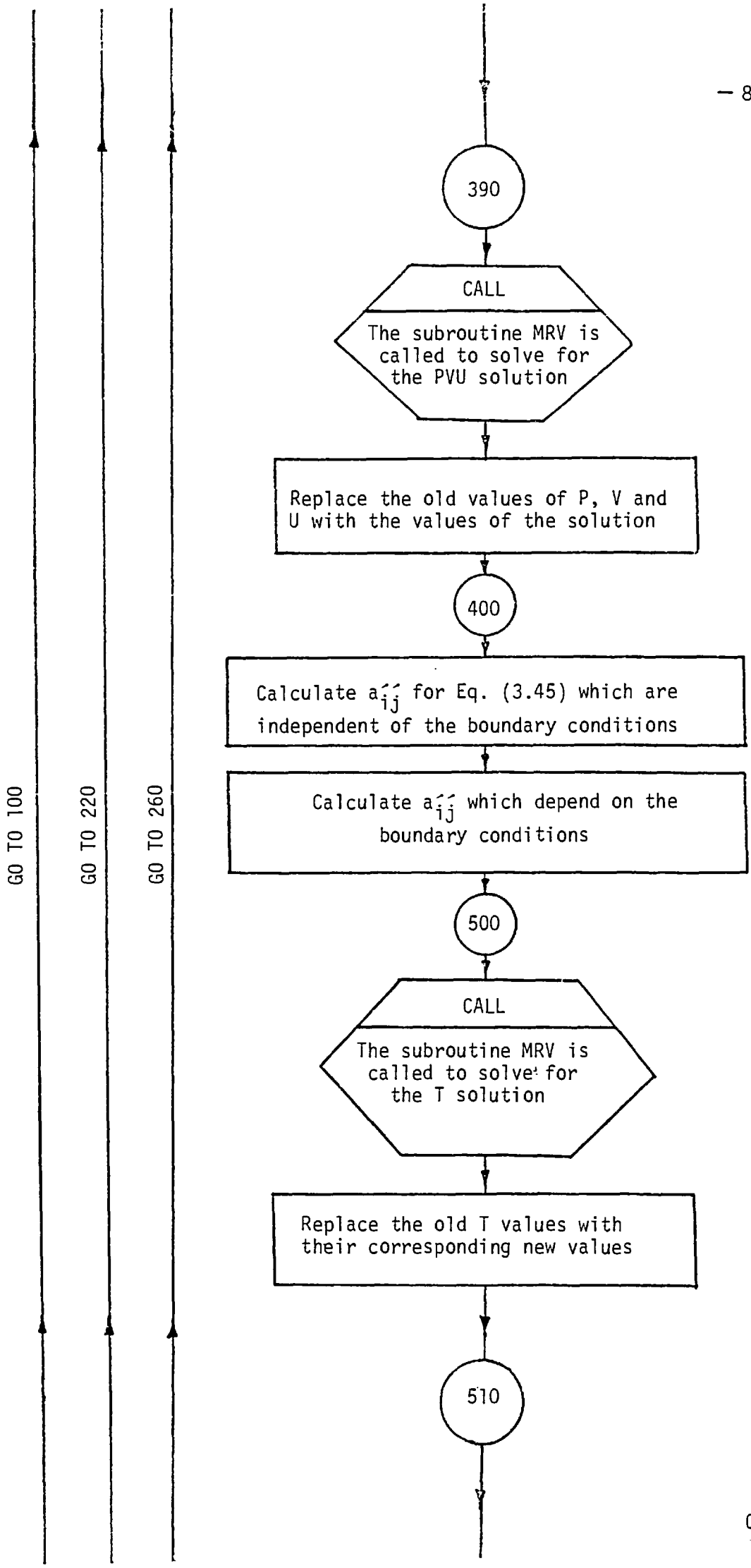
GO TO 100
GO TO 220
GO TO 260
390
CALL
The subroutine MRV is called to solve for the PVU solution
Replace the old values of P, V and U with the values of the solution
400
Calculate a'_{ij} for Eq. (3.45) which are independent of the boundary conditions
Calculate a''_{ij} which depend on the boundary conditions
500
CALL
The subroutine MRV is called to solve for the T solution
Replace the old T values with their corresponding new values
510

Contd.

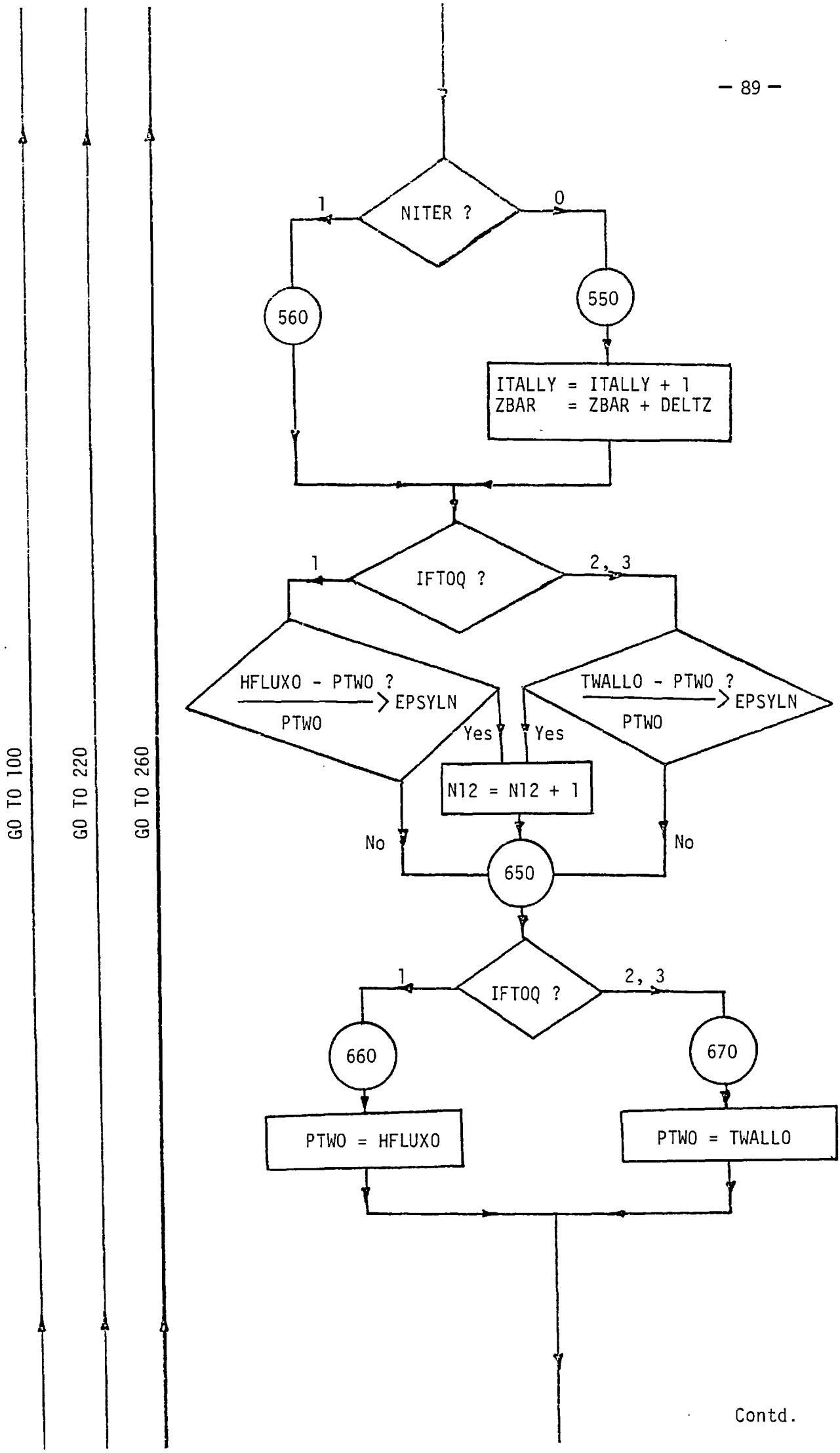
GO TO 100
GO TO 220
GO TO 260
NITER ?
1
0
560
550
ITALLY = ITALLY + 1
ZBAR = ZBAR + DELTZ
IFTOQ ?
1
2, 3
HFLUXO - PTWO ?
PTWO
EPSYLN
TWALLO - PTWO ?
PTWO
EPSYLN
Yes
Yes
N12 = N12 + 1
No
No
650
IFTOQ ?
1
2, 3
660
670
PTWO = HFLUXO
PTWO = TWALLO

Contd.

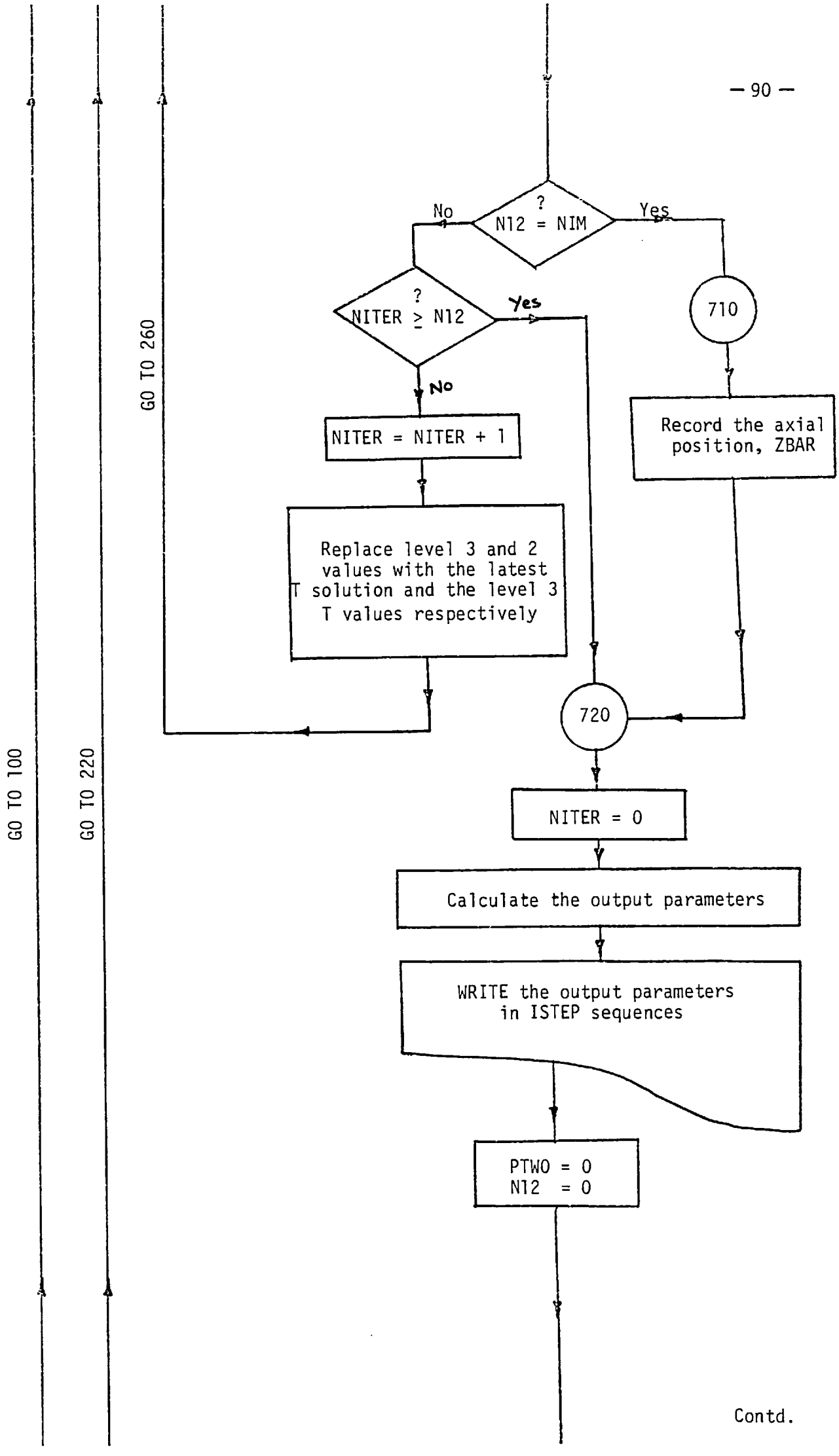
GO TO 100
GO TO 220
GO TO 260
? N12 = NIM
No
Yes
? NITER ≥ N12
Yes
No
710
NITER = NITER + 1
Record the axial position, ZBAR
Replace level 3 and 2 values with the latest T solution and the level 3 T values respectively
720
NITER = 0
Calculate the output parameters
WRITE the output parameters in ISTEP sequences
PTWO = 0
N12 = 0

Contd.

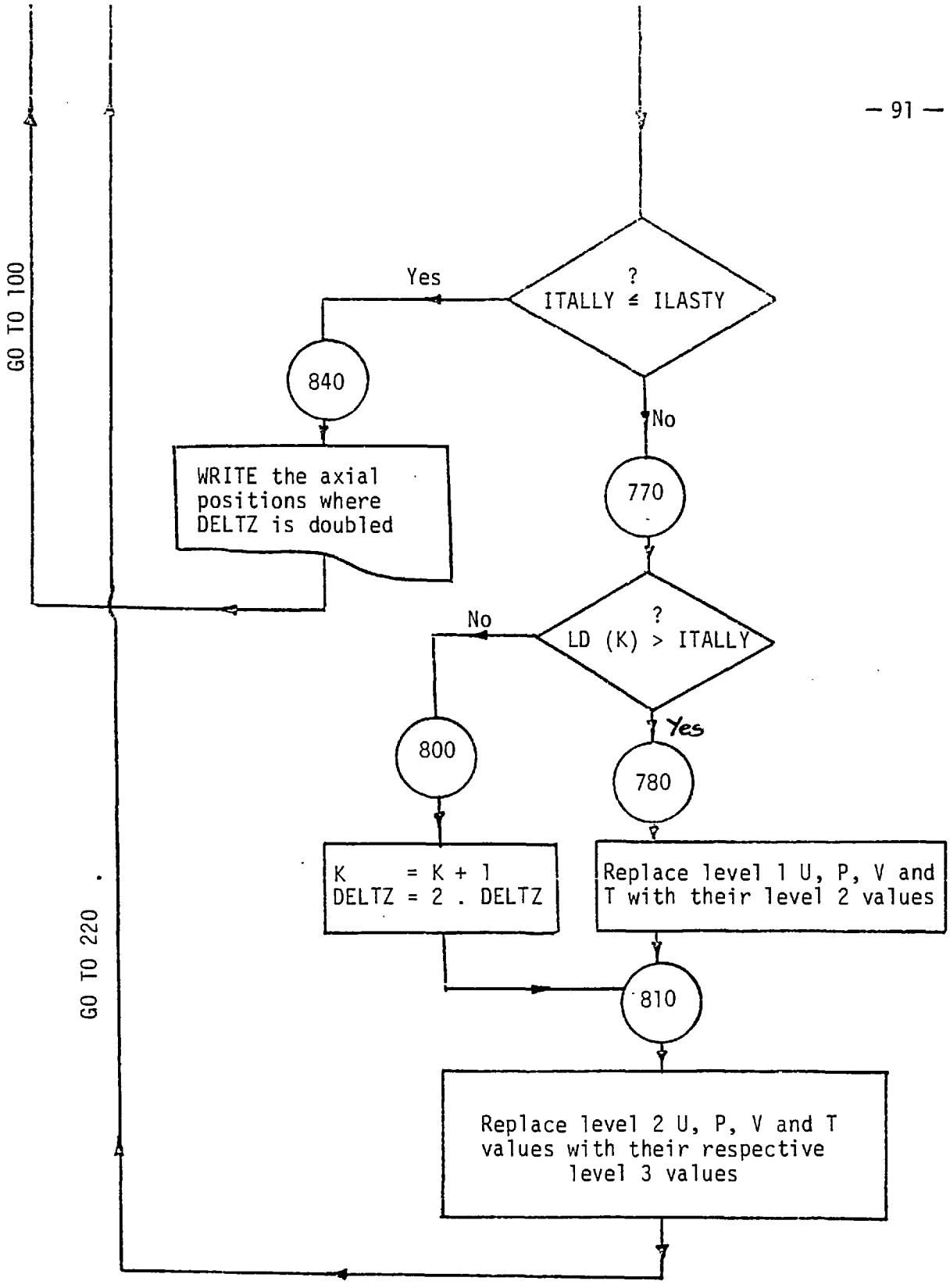
GO TO 100
Yes
? ITALLY ≤ ILASTY
840
No
WRITE the axial positions where DELTZ is doubled
770
No
? LD (K) > ITALLY
Yes
800
780
K = K + 1
DELTZ = 2 . DELTZ
Replace level 1 U, P, V and T with their level 2 values
810
Replace level 2 U, P, V and T values with their respective level 3 values
GO TO 220

CHAPTER 5

COMPUTER PREDICTIONS FOR ARBITRARY HEATED VERTICAL CHANNELS WITH FORCED OR MIXED-CONVECTIVE REGIMES

5.1 Introduction

In this chapter, attention is focused on the computer predictions for typical channels similar to that of the theoretical model mentioned in Chapter (3). Cases of both forced and mixed-convections are considered with the channel walls having symmetrical or asymmetrical heating. The density and the viscosity of water are assumed constant for the forced-convective cases while Equations (3.5a) - (3.6) are used to cater for their variations with temperature in the mixed-convective regimes.

In order to gain more confidence in the model, the computer predictions for several cases are compared with other available results. This is done as follows:-

(i) For the forced-convective cases, Kays (1966), among others, gives analytical solutions for a typical channel with both walls having identical (or non-identical) and uniform prescribed temperature or heat-flux. These results are accurately predicted by the computer program.

(ii) For the mixed-convective flows, experimental results of Vernier (1962) for a vertical channel with both walls having identical and uniform heat-fluxes, are compared with the computer predictions. These comparisons, executed for two examples, confirm the accuracy of the numerical approach of this thesis to be good.

Particular attention is paid to the cases where the profile of $\dot{q}_w''$ varies in a sinusoidal manner along the channel. Two models, each representing the "hot-channel" of a plate-type nuclear fuel element at different power levels, are solved by the computer program and their results are compared with each other. These calculations are compared with forced-convective cases to confirm that for forced-convective flow with a non-uniform $\dot{q}_w''$ profile, the parabolic U velocity profile will be established in the channel, together with a linear pressure-drop.

For asymmetrical heating cases, a further examination of the computer results, for the forced and the mixed-convective flows, is executed. This is done by "exchanging" the prescribed heating conditions of the two walls. The direct reflexion of this exchange on the predictions leads to the conclusion that they are not dependent on the choice of the heated wall.

A cross-checking was carried out by treating the t_w profile, obtained for a particular $\dot{q}_w''$ profile as data for a prescribed wall temperature case. Comparison between the $\dot{q}_w''$ profile obtained for the latter and the original $\dot{q}_w''$ profile reveals the fact that the predictions are reliable and accurate. This example may also be used to show that the numerical method of this thesis could also solve for the cases with a prescribed and non-uniform t_w profile.

5.2 Computer Predictions for Forced-Convective Heat Transfer in Vertical Channels

For this part, the typical channel of Fig. (5.1), with its walls having a uniform prescribed heating, is considered. Three types of heating are selected as follows:-

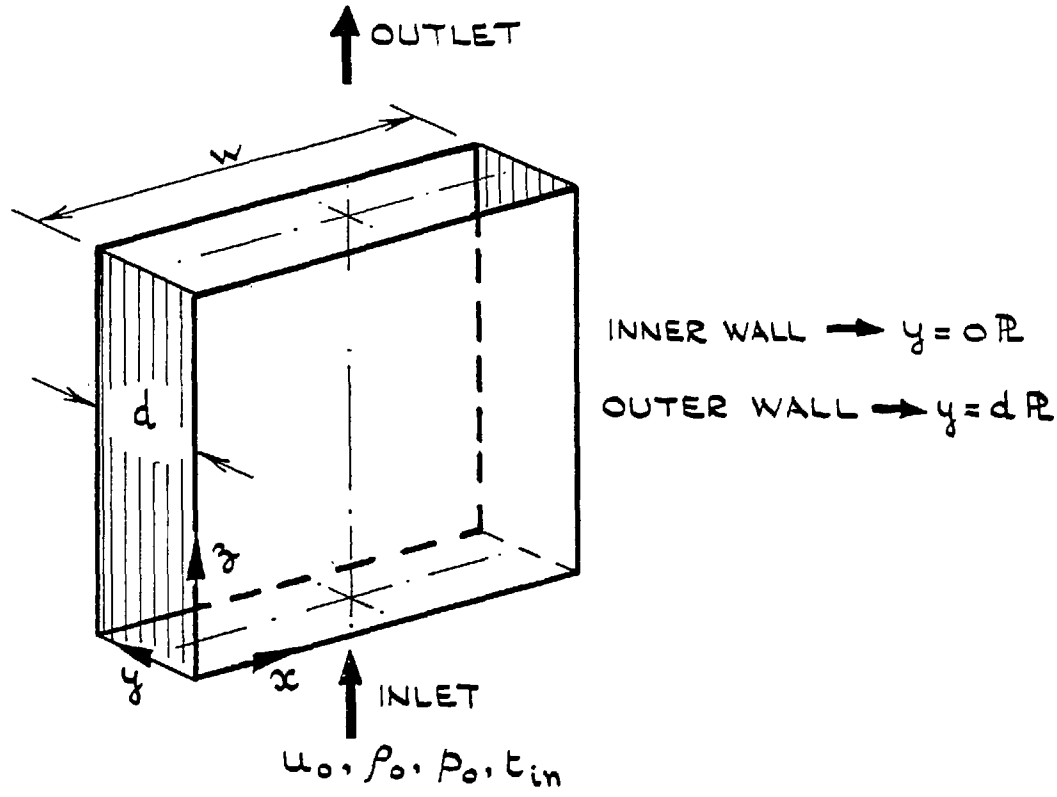

FIG.(5.1): THE TYPICAL CHANNEL.

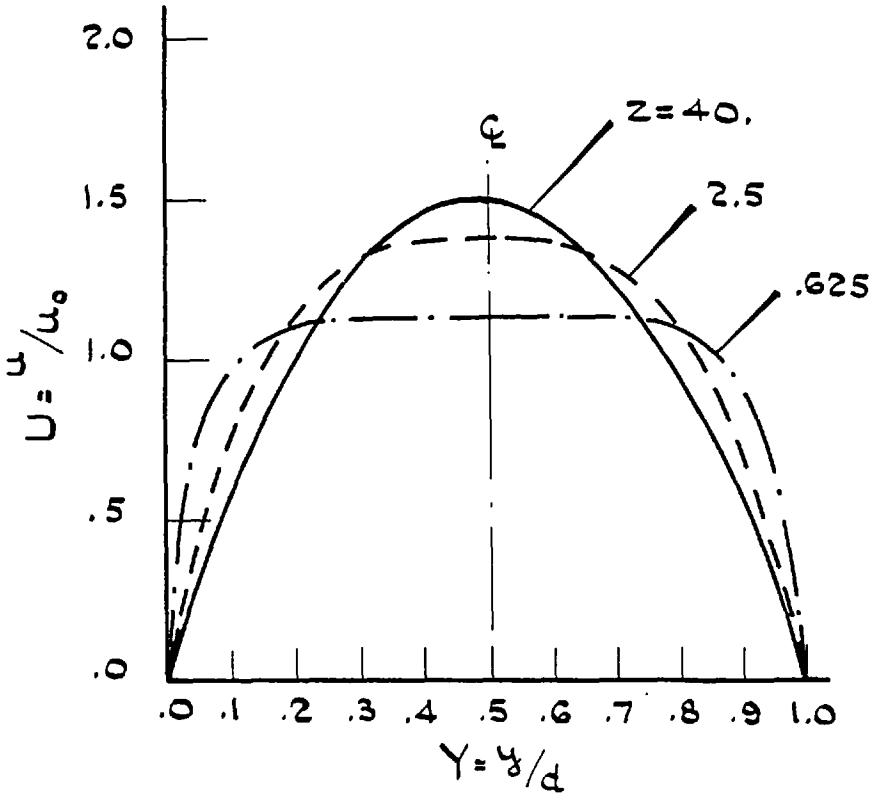

FIG.(5.2) HORIZONTAL DISTRIBUTION OF U AT DIFFERENT AXIAL POSITIONS.

(i) The walls having identical/non-identical prescribed heat-fluxes.

(ii) The walls having identical/non-identical prescribed temperatures.

(iii) Setting one wall to a prescribed temperature while the other one is thermally insulated.

The data of this channel is given in Table (5.1).

5.2.1 Computer Predictions for Prescribed Wall Heat-Flux Cases

These cases are referred to by their value of the parameter r_q, representing the ratio of the heat-fluxes on the two walls (i.e. $r_q = \dot{q}''_{wo}/\dot{q}''_{wi}$). Several cases of this type of heating with the identical and also non-identical wall heat-fluxes, $r_q = 1$ and $r_q < 1$ respectively, are solved for to obtain a general conclusion about the fully-developed specifications of the flow, i.e. the U_{ℓ} and Nu values, and their relationship with r_q.

(a) Uniform and Indentical Prescribed Wall Heat-Fluxes ($r_q = 1$)

The computer predictions for this case, which are identical for both walls, are classified in the following three ways:-

(a.1) Hydrodynamic Entry Length

Fig. (5.2) shows the development of the U velocity profile along the channel for $r_q = 1$. It is noted that the profile continues

TABLE (5.1) DATA FOR THE TYPICAL CHANNEL

Data \ Reduced Data	w/d	$Z_{max} = L/d$	$\dot{m}$ (gr/sec)	t_m (C^o)	Re	Re_D	Pr
d = 0.538 cm, w = 8.45 cm, L = 3.55 m $t_{in} = 5\ ^oC$, $u_o = 3.81$ cm/sec $\dot{q}''_w = 0.67$ (w/cm^2) → For r_q cases $t_w = 40\ ^oC$ → For r_t cases	15.7	660	17.32	19	208.15	416.3	6.82

to develop towards a parabolic shape as the fluid moves downstream. At Z = 40, the difference between the U values and their corresponding values for U = 6Y(1 - Y), which can be analytically obtained, are less than 1%. This length, which is to be referred to as the "hydrodynamic entry length", ZDU, may be expressed in relation with Re_D by the formula:-

$$ZDU = 0.0485\ Re_D$$

This relationship is checked with solutions for several other values of Re_D, leading to the conclusion that its coefficient is constant and does not depend on Re_D. Also, the relationship is in agreement with that suggested by Kays (1966): "A good approximate figure for the length of a conduit necessary for the development of the parabolic U velocity profile is: $ZDU = 0.05\ Re_D$".

Development of the U velocity profile towards the parabolic shape may also be noted from Figs. (5.3) - (5.4). On Fig. (5.3), development of the centreline velocity, U_{ℓ} towards its asymptotic value of $U_{\ell} = 1.5$ at the end of ZDU is shown. Here by use of a logarithmic abscissa, the development at the entry region is better represented. Also Fig. (5.4), which is the V velocity profile at Z = 20 (i.e. $\frac{1}{2}$ ZDU), confirms the horizontal movement of the fluid from the walls towards the centre of the channel. V values are:-

$V > 0$ for $\rightarrow 0 < Y < 0.5$

$V < 0$ for $\rightarrow 0.5 < Y < 1$

$V = 0$ for $\rightarrow Y = 0.5$

At axial positions larger than ZDU, the values of V are zero across the

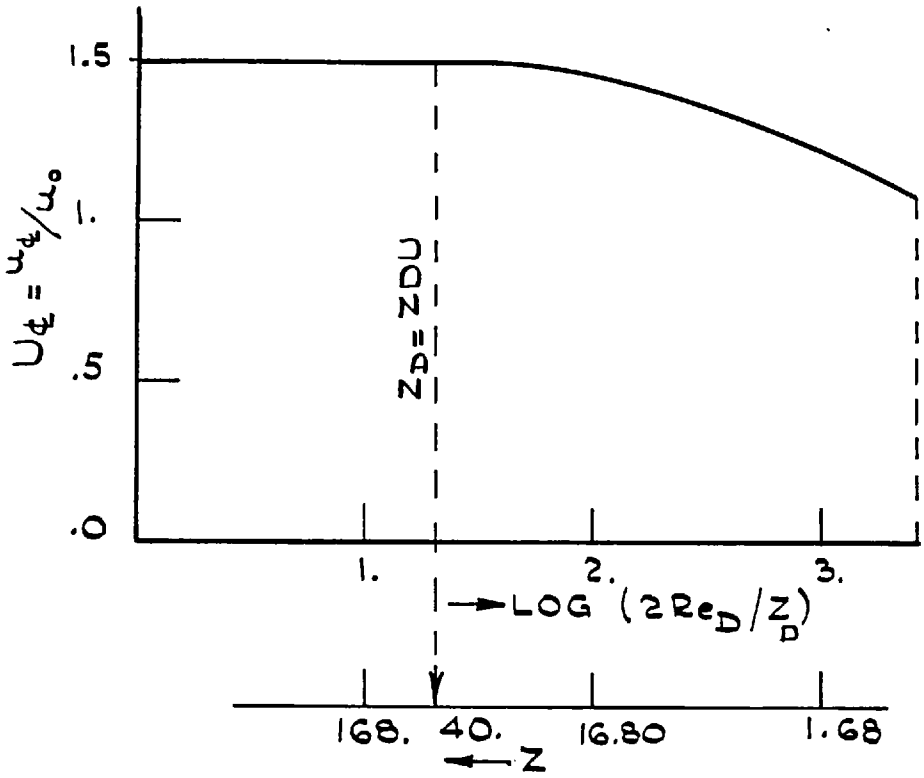

FIG. (5.3) AXIAL VARIATIONS OF U_ℓ ($Re_D = 416.3$)

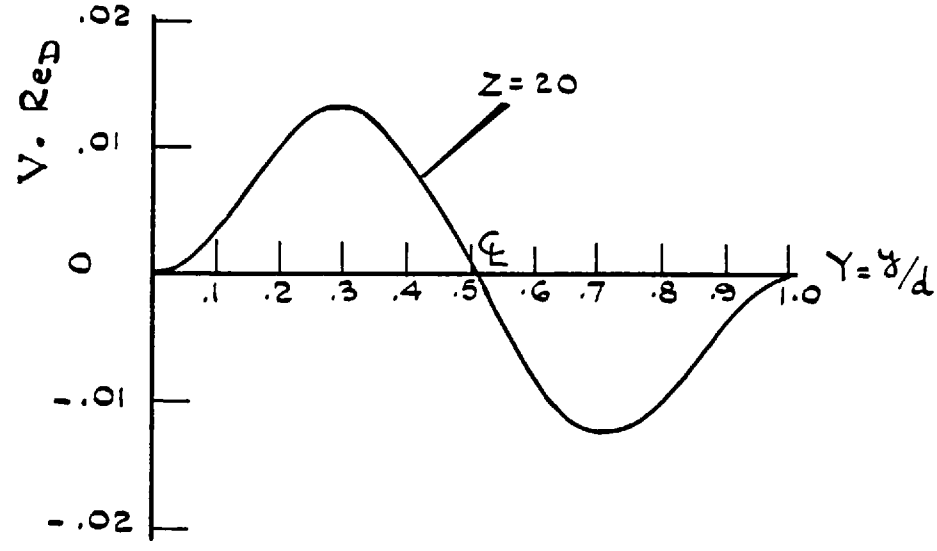

FIG. (5.4) HORIZONTAL DISTRIBUTION OF V AT THE AXIAL POSITION Z = 20 ($Re_D = 416.3$)

channel. This confirms the fact that once the hydrodynamic length is covered, there will be no further horizontal movement across the section. Consequently, the U profile does not change.

(a.2) Thermal Entry Length

Fig. (5.5) shows the temperature profile at different axial positions. Near the entry region (low Z values), the profile is very flat near the centre and sharp next to the walls, which leads to large Nusselt numbers.

As the fluid moves further downstream, the profile continues towards the establishment of its fully-developed shape. Because in general it is not possible to compare the continuously-developing t profiles, the fully-developed length, ZDT, is defined as that length in which the term $t_w - t_{\ell}$ does not change by more than 1% from its value $d/2$ upstream. This is a convenient definition for use with finite-difference methods. For the present problem at Z = 187.5 this criterion is satisfied. Application of several Reynolds and Prandtl numbers for the problem shows that ZDT is proportional to the product of these two numbers: $ZDT = 0.033\ Re_D\ .\ Pr.$

Fig. (5.6) shows axial variations of Nusselt number. This figure confirms that as a consequence of the establishment of the fully-developed temperature profile, the Nusselt number approaches its asymptotic value of Nu = 8.23 at the end of ZDT. Kays (1966) has analytically obtained the same value for Nusselt number and suggests that ZDT may be approximated by: $ZDT = 0.05\ Re_D\ .\ Pr.$

In the following table, the Nu values along the duct which were predicted by the present method are compared with those obtained by McCuen (1962) in a theoretical approach.

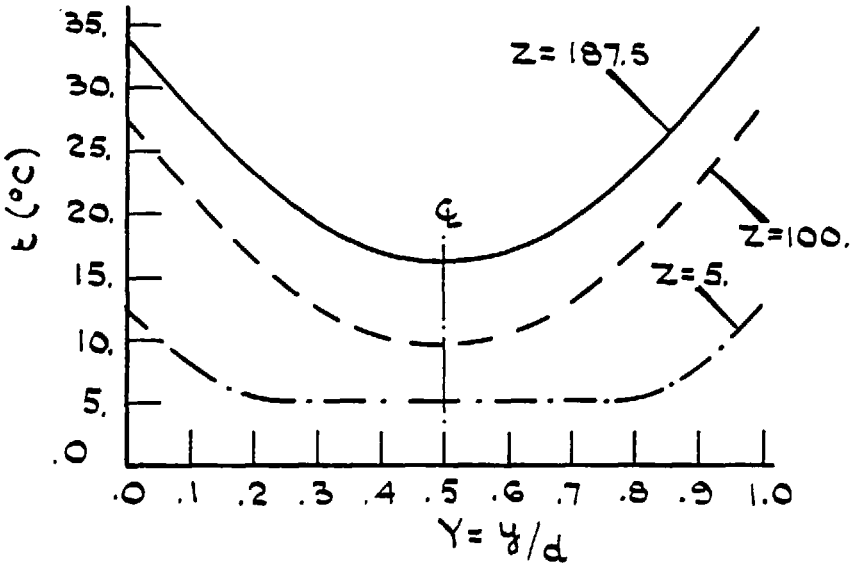

FIG. (5.5) HORIZONTAL TEMPERATURE DISTRIBUTION ALONG THE CHANNEL FOR $r_q = 1$ ($Re_D = 416.3$, $Pr = 6.82$).

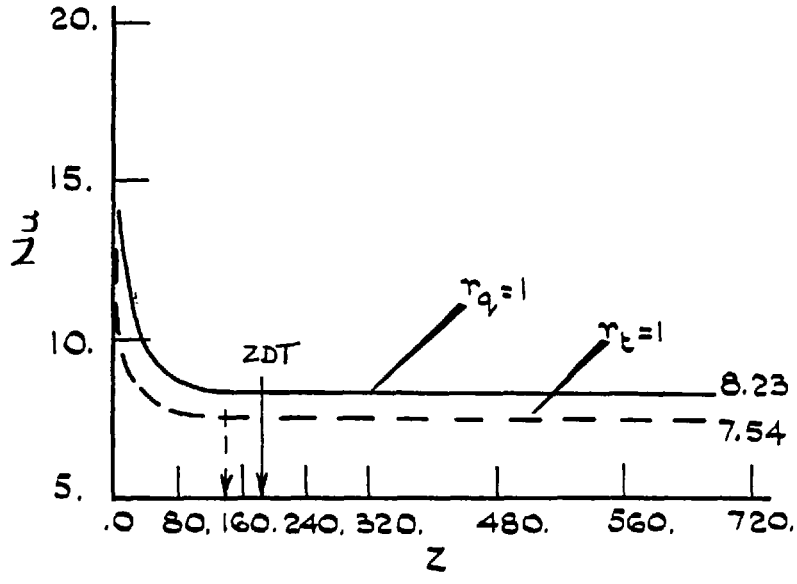

FIG.(5.6) AXIAL VARIATION OF NUSSELT NUMBER, Nu. ($Re_D = 416.3$, $Pr = 6.82$).

COMPARISON OF THE NUSSELT NUMBERS ALONG THE CHANNEL FOR UNIFORM AND EQUAL WALL HEAT-FLUXES ($r_q = 1$)

$Z_D/(Pr \cdot Re_D)$	McCuen (1962)	Present Method
0.0025	11.860	11.691
0.0100	8.803	8.771
0.0150	8.439	8.510
0.0250	8.263	8.269
0.0500	8.236	8.230
0.0750	8.235	8.230
0.1000	8.235	8.230
0.1250	8.235	8.230
0.1500	8.235	8.230
0.2500	8.235	8.230
0.5000	8.235	8.230

(a.3) The Pressure and the Shear Loss Factors (f_p and f_s)

Axial variations of these two parameters are shown on Fig. (5.7). Here, by employment of a logarithmic abscissa, the variations near the entry regions are clearer. According to this figure, f_p and f_s decrease as the fluid moves along the channel. At axial positions lower than ZDU, where changes in the U values are rather large, these two coefficients assume large values (as a consequence of the changes in the U profile). At the end of ZDU:-

$$f_p = f_s = 0.05765 = 24/Re_D$$

This relationship is the same as the one obtained by Knudson et al (1958) with an analytical approach, and suggests a linear pressure drop along the channel. It should be pointed out that equal values for the parameters f_p and f_s only occur when ρ and μ are constant because then the momentum and the energy equations, Equations (3.2) - (3.4), are not coupled.

(b) Uniform but Non-Identical Heat-Fluxes, $0 \leq r_q < 1$

Following the results for the symmetrical heating, $r_q = 1$, the channel with the data of Table (5.1) is to be solved for several values of the ratio r_q in order to generalize the results.

(b.1) The Computer Predictions for $r_q = 0$

One of the cases where the heating may be easily realised is the case where one of the channel walls is kept at a uniform and prescribed heat-flux while the other wall is thermally insulated. In

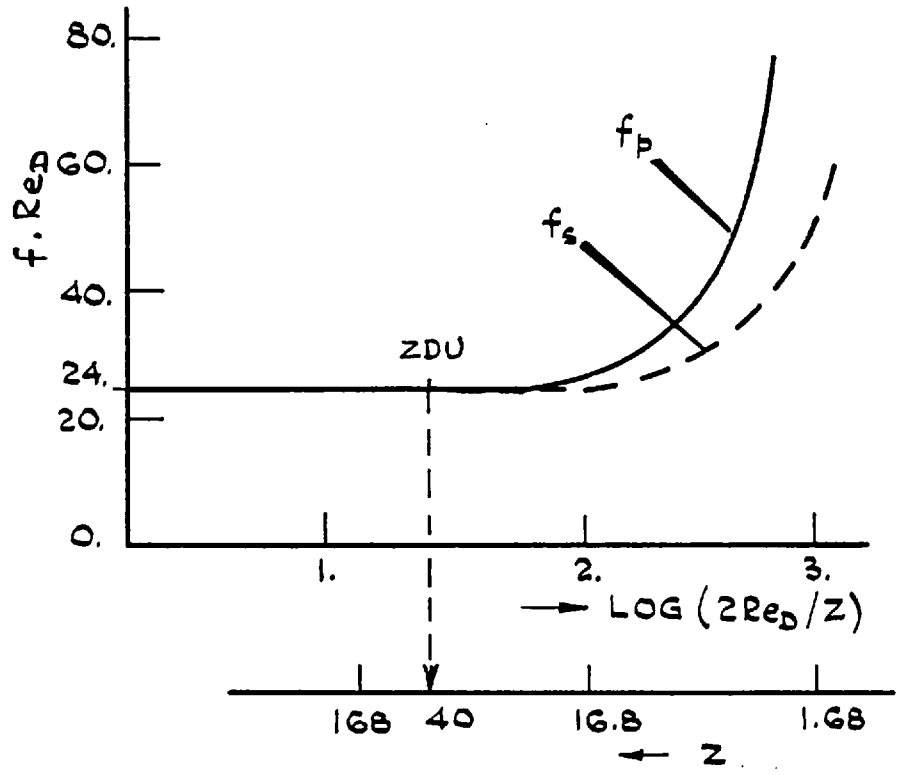

FIG. (5.7) AXIAL VARIATIONS OF THE PRESSURE AND THE SHEAR LOSS FACTORS, f_p AND f_s RESPECTIVELY.

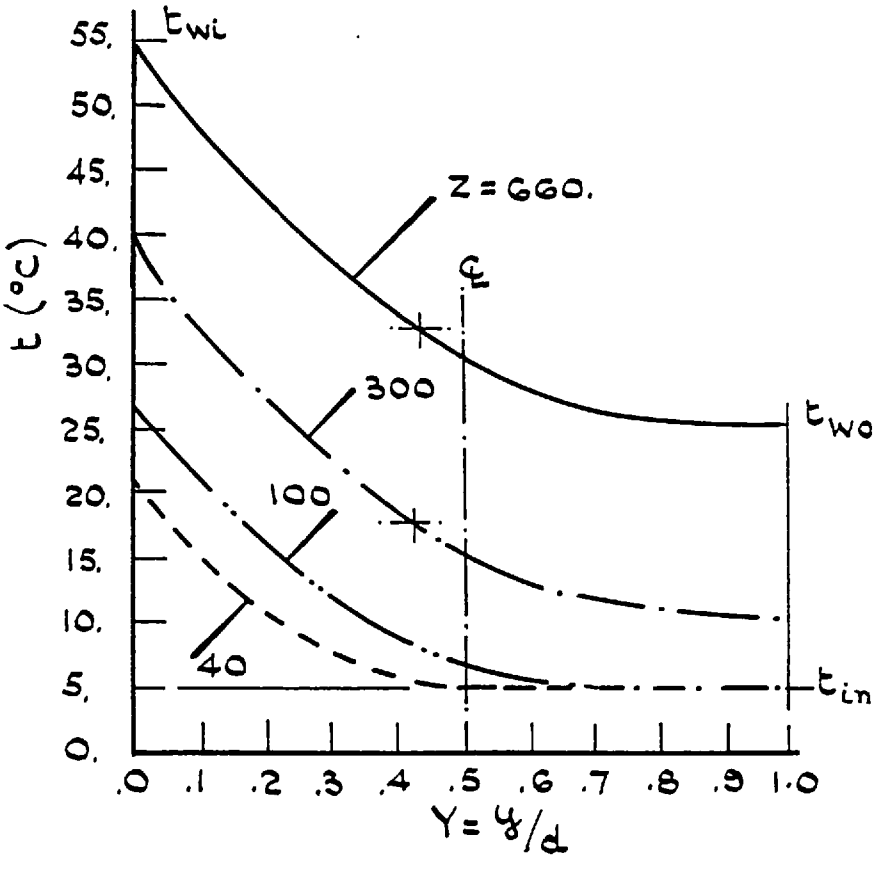

FIG. (5.8) HORIZONTAL TEMPERATURE DISTRIBUTION ALONG THE CHANNEL (FOR $r_q = 0$)

the following, the predictions are obtained for the case when $\dot{q}''' _{wi}$ = Const. and $\dot{q}''' _{wo}$ = 0.

(i) The U Velocity Profile

This profile is developed along the channel identical to Fig. (5.2) obtained for the symmetrical heating (r_q = 1). The parabolic profile is obtained at Z = 40 which may be expressed as: ZDU = 0.0485 . Re_D. It is noted that the same U velocity profile is obtained for both the r_q = 1 and r_q = 0 cases because for the forced-convection cases, the density and viscosity were assumed constant. As a consequence, the asymmetry in heating is not reflected in the U profile. However, the profile will differ when ρ and μ variations with temperature are considered. This is done when the same problem is solved for a mixed-convection regime.

(ii) The Temperature Profile

Fig. (5.8) shows the horizontal temperature distribution at different axial positions. Near the channel entry (low Z values), the profile is sharp near the wall which is heated, (Y = 0). This results in a large Nusselt number. As the fluid moves further downstream, the profile develops towards its fully-developed shape at Z = 660. From this axial position onwards, the profile remains unchanged and any further heating results in shifting the profile parallel to itself. Application of several Re_D's and Pr's confirm that the thermal entry length, ZDT for this case may be represented as:-

$$ZDT = 0.116\ Re_D\ .\ Pr$$

It is noted that for this case, the intersection of the line which represents t_{mean} with the temperature profile remains always between the centre of the channel and the wall which is heated (the so-called Inner-wall).

Establishment of the fully-developed temperature profile is reflected in the Nu_i profile. In Fig. (5.9), Nu_i starts from a large value near the entry to the channel and reduces gradually as water moves further downstream. At the end of the thermal entry length, ZDT, the Nu_i values approach to the ideal value of $Nu_i = 5.385$. This value is also obtained by Reynolds et al (1964). The table given in the next page shows comparison of the two results.

(iii) The Pressure and the Shear Loss Factors (f_s and f_p)

Development of these two parameters for this case is identical to that of the one previously mentioned ($r_q = 1$). Therefore, Fig. (5.7) may also be used for the asymmetrical heating ($r_q = 0$).

As will be mentioned, for the mixed-convection cases, the development of these two factors will differ when the variations of ρ and μ with temperature are considered.

5.2.2 General Discussion for the Prescribed $\dot{q}_w''$ Cases

This discussion is executed by solving the typical channel for several r_q values. In the first part of the following, the computer predictions are compared with their corresponding analytical results. In the second part, a general representation of the local Nu and t_w depending on the ratio r_q is given. This is followed by a search for a relationship between the thermal entry length, ZDT and the ratio r_q.

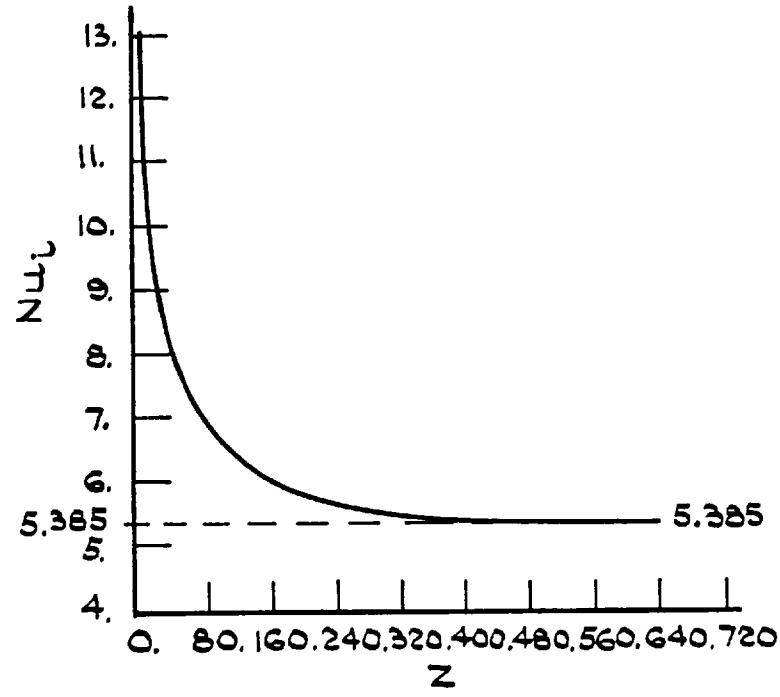

FIG.(5.9) AXIAL VARIATION OF Nui (FOR $r_q = 0$)

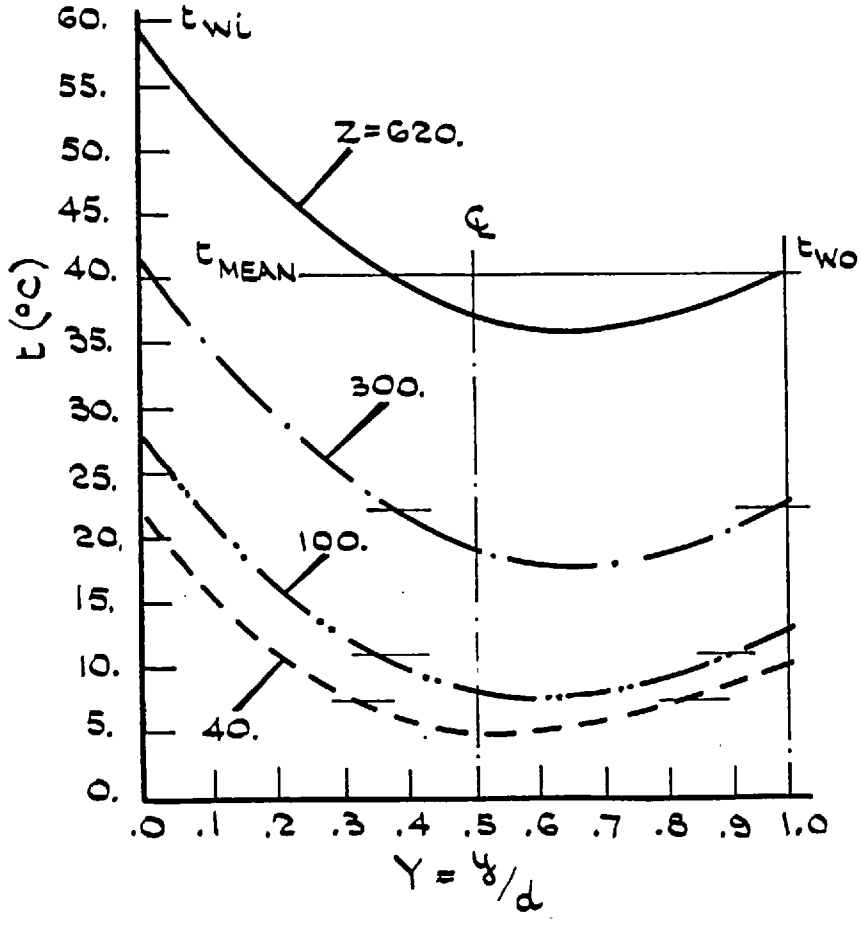

FIG.(5.10) HORIZONTAL TEMPERATURE DISTRIBUTION ALONG THE CHANNEL (FOR $r_q = .346$)

COMPARISON OF Nu_i VALUES

ALONG THE CHANNEL FOR $r_q = 0$

$Z_D/(Re_D \cdot Pr)$	Reynolds et al (1964)	Present Method
0.0010	15.56	15.950
0.0025	11.46	11.010
0.0050	9.20	8.960
0.0100	7.49	7.410
0.0250	6.09	6.122
0.0500	5.55	5.538
0.1000	5.40	5.392
0.2500	5.39	5.386
∞	5.39	5.385

(a) The Predictions for Several r_q Values

The predictions for the symmetric and the asymmetric cases previously mentioned: $r_q = 1$ and 0 respectively, showed that because of constant ρ and μ values, the U, f_p and f_s profiles are not affected by the type of heating on the channel walls. Therefore, the discussion was focused on the temperature and the Nusselt number profiles.

Examination of the temperature profiles, Figs. (5.5), (5.8) shows that throughout the channel, i.e. $0 < z \leq L$:-

$t_{mean} < t_{wo} \rightarrow$ For $r_q = 1$

$t_{mean} > t_{wo} \rightarrow$ For $r_q = 0$

Recalling the definition of Nu_o shows that the change of sign for the term $(t_{mean} - t_{wo})$ determines the behaviour of the Nu_o profile along the channel. If the difference becomes very small, the Nu_o value increases drastically. Moreover, for a particular value of the ratio $r_q : t_{wo} = t_{mean}$ (at the end of the thermal entry length). In this case, $Nu_o \rightarrow \infty$ and the problem must be regarded as a special case. Kays (1966) has proposed the following formula relating Nu_o at the end of ZDT with r_q:-

$$Nu_o = \frac{5.385}{1 - 0.346/r_q}$$

According to this formula:-

$Nu_o = 8.230$ for $r_q = 1$

$Nu_o = 5.385$ for $r_q = 0$

These results are the same as the predictions obtained earlier in this chapter. The "critical" r_q happens when:-

$$1 - 0.346/r_q = 0 \rightarrow r_q = 0.346$$

In order to examine this case, the typical channel of Table (5.1) is solved for this ratio.

(a.1) The Temperature Profile for $r_q = 0.346$

Fig. (5.10) shows horizontal temperature distribution at different axial positions. Horizontal lines on each profile represent the intersection of t_{mean} and the temperature profile at those axial positions. At Z = 620:-

$$t_{wo} - t_{mean} \cong 0.1\ ^{o}C\ ,\ Nu_i = 6.1146\ ,\ Nu_o = 383.88$$

This length may be represented in terms of the product $(Re_D \cdot Pr)$ as:-

$$ZDT = 0.1092\ Re_D \cdot Pr$$

The value $Nu_i = 6.1146$ reflects the establishment of the fully-developed temperature profile as shown on Fig. (5.11). This value may also be obtained by using, $r_q = 0.346$ in the formula:-

$$Nu_i = \frac{5.385}{1 - 0.346 r_q}$$

Axial variation of Nu_o is not monotonic. Fig. (5.12) shows

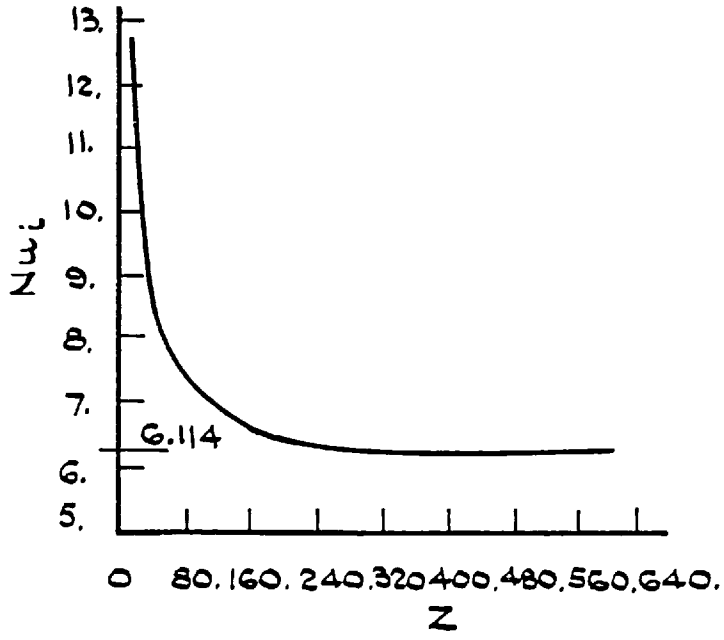

FIG. (5.11) AXIAL VARIATION OF Nu_i (FOR $r_q = .346$)

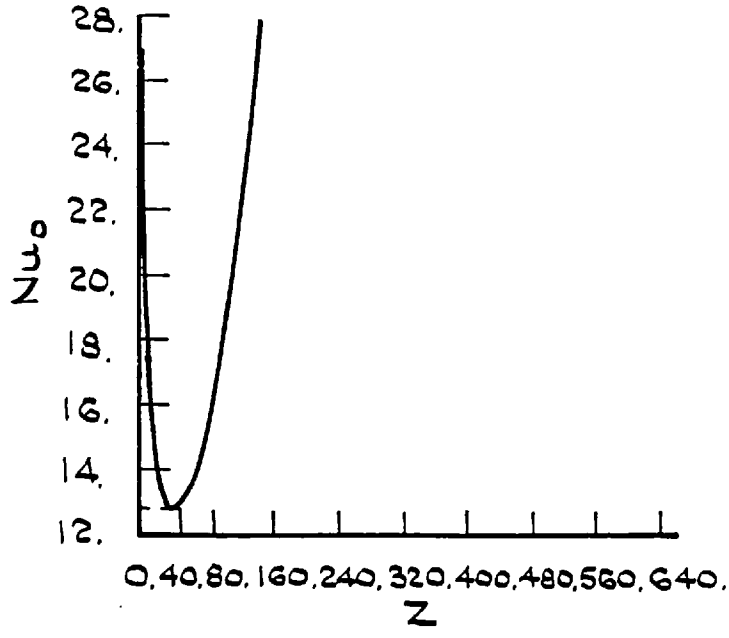

FIG. (5.12) AXIAL VARIATION OF Nu_o (FOR $r_q = .346$)

that it starts from a large value and continues to decrease. At Z = 40, (i.e. Z_D = ZDU), it goes through a minimum:-

$$Nu_{o.min} = 12.698$$

After this position, due to the ever-decreasing value of $(t_{wo} - t_{mean})$, Nu_o starts to increase rapidly. It assumes a large value near the ZDT position: $Z = 620 \rightarrow Nu_o = 383.88$.

It should be pointed out that the large Nu_o value does not invalidate the definition employed for it so long as the physical meaning of $t_{wo} = t_{mean}$ is understood.

(b) Relationship Between Specifications of the Flow and r_q

The temperature distribution along the Inner-Wall is shown on Fig. (5.13a) for various values of:-

$$r_q = \frac{\dot{q}''_{wo}}{\dot{q}''_{wi}}$$

Symmetrical heating corresponds to $r_q = 1$, whereas $r_q = 0$ represents the case for which the Outer-Wall is insulated. For $r_q = -1$ the heat addition at the Inner-Wall is equal to the heat extraction at the Outer-Wall. One may note that the length required to approach fully-developed conditions is greater for unsymmetric heating than for a symmetrical wall heat-flux. In order to formulate this

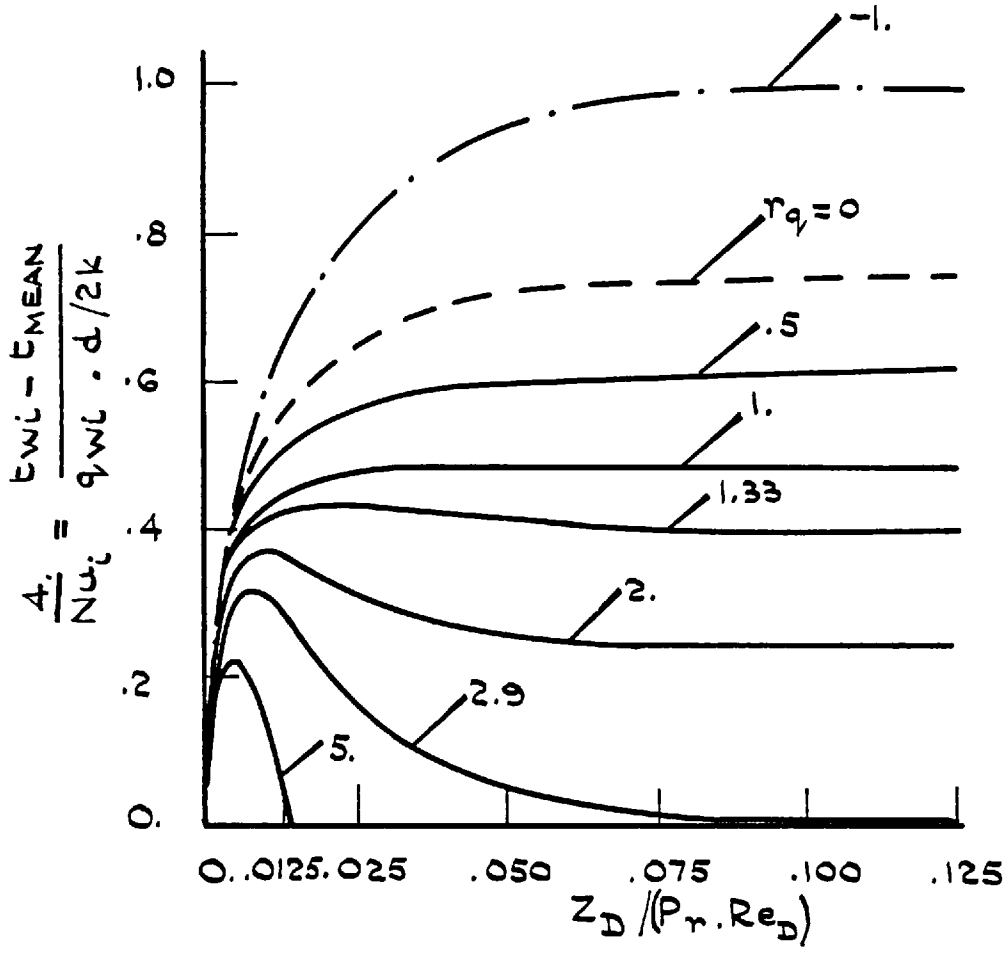

FIG.(5.13a) WALL TEMPERATURE FOR A CONSTANT HEAT-FLUX AT EACH WALL.

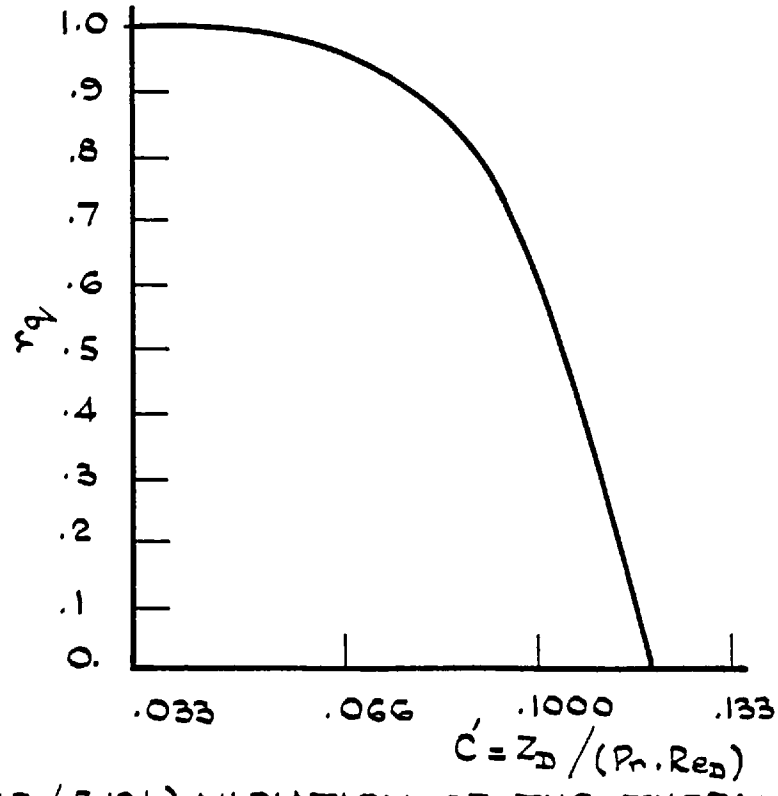

FIG.(5.13b) VARIATION OF THE THERMAL ENTRY LENGTH WITH THE RATIO r_q.

relationship, the following formula may be suggested:-

$$ZDT = C' \cdot Re_D \cdot Pr$$

where the constant C' is a function only of r_q. The suggestion is based on the following results which were obtained earlier in this chapter:-

$ZDT = 0.0330 \cdot R_D \cdot Pr \rightarrow$ For $r_q = 1.000$

$ZDT = 0.1092 \cdot Re_D \cdot Pr \rightarrow$ For $r_q = 0.346$.

$ZDT = 0.1160 \cdot Re_D \cdot Pr \rightarrow$ For $r_q = 0.000$

Variation of the constant C' against several r_q values is shown on Fig. (5.13b). It is noted that the variation is more apparent when:-

$0.9 \leq r_q \leq 1$

(c) Dependence of the Predictions on the Data

In order to confirm that the predictions were not dependent on the system of coordinates, or the values of heat-fluxes, two examinations were executed:-

(i) For the case with $r_q = 0$, the "Inner" and the "Outer" walls were exchanged and the problem was re-solved. The predictions, as expected, reflected the exchange directly (i.e. after the exchange, $Nu_i = 0$ and $Nu_o = 5.385$).

(ii) For the case with $r_q = 1$, the values of $\dot{q}''_{wi}$ and $\dot{q}''_{wo}$ were changed and the problem was re-solved. The predictions showed that the non-dimensional parameters; Nu, f_p, f_s together with ZDU and ZDT were repeated. This confirms that the predictions were independent of the $\dot{q}''_w$ values.

Table (5.2) summarizes the computer prediction for several r_q values.

5.2.3 Solution of the Prescribed t_w Cases

These cases, in comparison with those with prescribed $\dot{q}''_w$, may be regarded as the "reverse-problem". Their method of solution, as explained in Chapter (3), is essentially the same but with minor modifications to solve for this type of boundary condition. In the following, the computer predictions are obtained for several symmetrical

TABLE (5.2)

LOCAL NUSSELT NUMBER PREDICTIONS FOR SEVERAL PRESCRIBED WALL HEAT-FLUX CASES

Results / r_q	Nu_i	Nu_o	$C' = \frac{ZDT}{Pr \cdot Re_D}$
- 1.000	4.0000	4.000	0.12500
0.000	5.3850	0	0.11625
0.200	5.7850	- 7.666	0.11270
0.346	6.1146	383.884	0.10920
0.500	6.5128	16.767	0.10220
0.750	7.2710	9.824	0.09500
0.950	8.0240	8.374	0.07220
1.000	8.2340	8.183	0.03300

and asymmetrical heating cases of this category. The parameter r_t defined as:-

$$r_t = \frac{t_{wo} - t_{in}}{t_{wi} - t_{in}}$$

is used as the principal parameter by which these cases are to be referred.

(a) Uniform and Identical Wall Temperatures ($r_t = 1$)

The computer prediction for this type of heating is similar to the case with $r_q = 1$, (in terms of the establishment of the fully-developed U and T profiles, identical predictions for both of the channel walls, etc.) but is different for the values of some parameters. These results are explained in the following two points:-

(i) The U Velocity Profile and the f_p and f_s Values

The parabolic U velocity profile, $U = 6Y(1 - Y)$ shown on Fig. (5.2), is obtained at $Z = 40$. Similar to the r_q cases, this length may be expressed as:-

$$ZDU = 0.0485\ Re_D$$

Also, at the end of this hydrodynamic-entry-length, f_p and f_s assume their ideal value of: $f_p = f_s = 24/Re_D$ as shown on Fig. (5.7).

(ii) The Temperature Profile

As shown on Fig. (5.14), the temperature profile continues

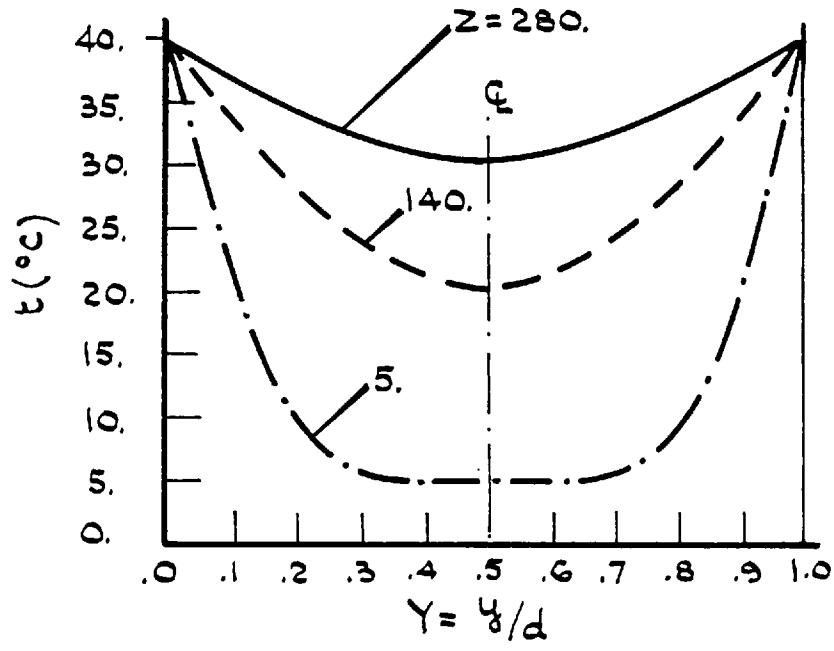

FIG(5.14) HORIZONTAL TEMPERATURE DISTRIBUTION ALONG THE CHANNEL (FOR $r_t = 1$)

towards a fully-developed shape. At Z = 140, the profile is approximately of a parabolic shape and satisfies the conditions for the fully-developed t profile. This situation is reflected in the value of Nu as shown on Fig. (5.6). According to this figure, Nu starts with a large value near the channel entry and approaches its fully-developed value of, Nu = 7.54 at Z = 140.

It should be pointed out that for this case (r_t = 1), at axial positions larger than the ZDT, the temperature profile changes slightly to cater for the heat input to the fluid (due to the ever-increasing value of t_{mean}). However, these changes appear in the temperature profile in such a way that the Nu value remains constant throughout.

In the table on the next page the Nu values along the duct which were predicted by the present method are compared with those obtained by McCuen (1962) in a theoretical approach.

(b) Non-Identical and Uniform r_t Cases ($0 \leq r_t < 1$)

In order to generalize the computer predictions for this type of heating, the typical channel of Table (5.1) is solved for several r_t values shown in Table (5.3). For all of these cases, a parabolic U profile, identical to Fig. (5.2) is obtained at Z = 40, i.e. ZDU = 0.0485 Re_D. Also, f_p and f_s values at the end of the ZDU are:-

$$f_p = f_s = 24/Re_D$$

Among the several r_t cases, the predictions for r_t = 0 and r_t = 0.486

COMPARISON OF THE NUSSELT NUMBERS ALONG THE CHANNEL FOR UNIFORM AND EQUAL WALL TEMPERATURES FOR $r_t = 1$

$Z_D/(Pr \cdot Re_D)$	McCuen (1962)	Present Method
0.0025	9.951	9.390
0.0100	7.741	7.728
0.0150	7.582	7.619
0.0250	7.543	7.541
0.0500	7.541	7.541
0.0750	7.541	7.540
0.1000	7.541	7.540
0.1250	7.541	7.540
0.1500	7.541	7.540
0.2500	7.541	7.540
0.5000	7.541	7.540

TABLE (5.3)

COMPUTER PREDICTIONS FOR THE PRESCRIBED WALL TEMPERATURE CASES AT Z = 660

Results / r_t	Nu_i	Nu_o	$\frac{Z_D}{Pr \cdot Re_D}$	Type of the Fully-Developed Temperature Profile
0.000	4.099	3.894	0.116	straight-line
0.200	4.146	3.839	0.116	straight-line
0.468	4.260	3.692	0.116	straight-line
0.657	4.430	3.426	0.116	straight-line
0.828	4.826	2.420	0.116	straight-line
1.000	7.541	7.540	0.025 *	parabolic

* At this position, a parabolic t profile is obtained

are discussed in the following:-

(b.1) The Temperature and the Nu Profiles (for $r_t = 0$)

This is the case when one wall is set at a prescribed temperature while the other one is kept at the fluid entrance temperature, t_{in}. The temperature profile at several axial positions is shown on Fig. (5.15). It is noted that far downstream, Z = 660, the profile turns into a straight-line drawn between the t_{wi} and the t_{wo}. This length is regarded as ZDT and may be expressed as:-

$$ZDT = 0.116\ Re_D \cdot Pr$$

The temperature profile does not change its straight-line shape at the axial positions larger than the ZDT. This is because, at these axial positions; $\dot{q}''_{wi} = -\dot{q}''_{wo}$. Therefore, t_{mean} is constant and the shape of the profile remains unchanged thereafter.

Fig. (5.16) shows axial variations of Nu_i and Nu_o for this case. According to this figure, Nu_i starts from a large value near the entrance to the channel and approaches its fully-developed value of: $Nu_i = Nu_o = 4$ at the end of the ZDT. These results confirm once again that for this case: $\dot{q}''_{wi} + \dot{q}''_{wo} = 0$ at the end of the ZDT. The Nusselt numbers just mentioned may be analytically obtained as follows:-

$$Nu_i = \frac{2d}{k} \cdot h_{wi} = \frac{2d}{k} \cdot \frac{\dot{q}''_{wi}}{t_{wi} - t_{mean}} = \frac{2d}{k} \cdot \frac{k \left|\frac{\partial t}{\partial y}\right|_{y=0}}{t_{wi} - t_{mean}}$$

As mentioned above, the fully-developed temperature profile for this case, ($r_t = 0$), is a straight line. Therefore:-

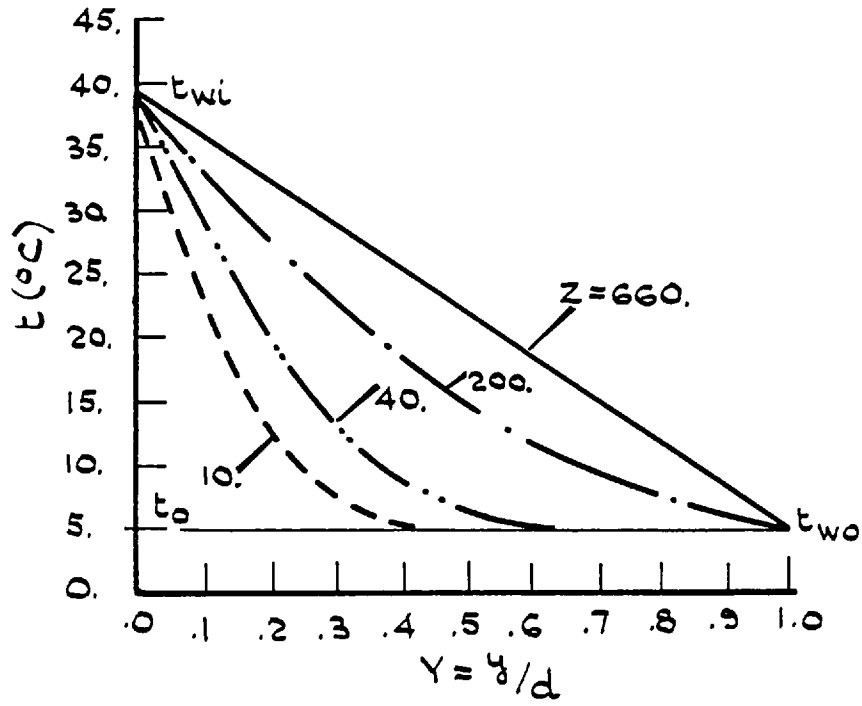

FIG. (5.15) HORIZONTAL TEMPERATURE DISTRIBUTION (FOR $r_t = 0$)

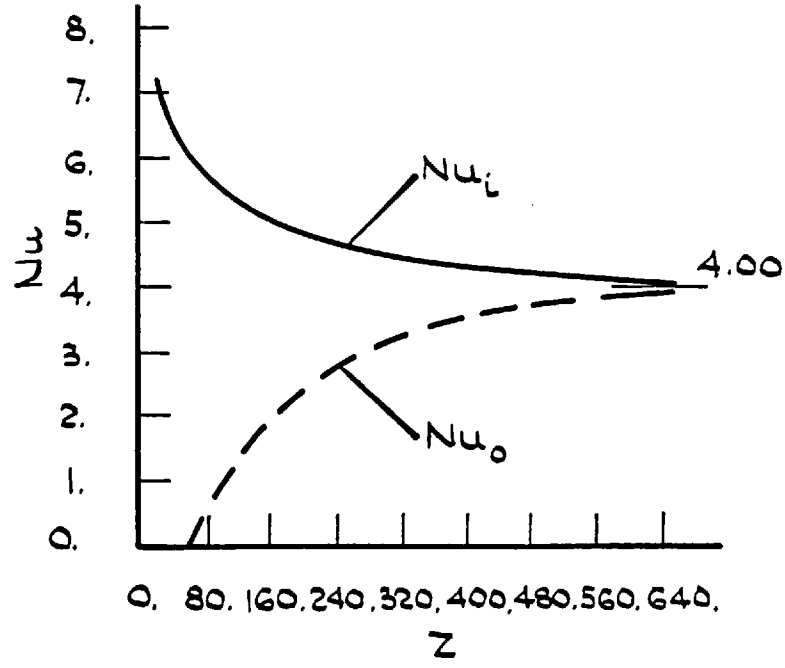

FIG. (5.16) AXIAL VARIATION OF Nu_i AND Nu_o (FOR $r_t = 0$)

$$\begin{cases} t_{mean} = (t_{wi} + t_{wo})/2 \\ \left.\frac{\partial t}{\partial y}\right|_{y=0} = (t_{wi} - t_{wo})/d \end{cases}$$

Combining these equations leads to:-

$$Nu_i = 4$$

(b.2) The Temperature and the Nu Profiles (for $r_t = 0.486$)

For this case, $t_{in} < t_{wo} < t_{wi}$, therefore, the situation is a mixture of the two previously mentioned cases, (i.e. $r_t = 1$ and 0 respectively).

Fig. (5.17) shows the development of the temperature profile towards its fully-developed shape. It is noted that the increase in the centreline temperature, t_{ℓ} is slowed down as the fluid approaches the axial position; Z = 160, where $t_{mean} = t_{wo}$. Thereafter, the temperature profile loses its semi-parabolic shape and develops towards the straight line drawn between t_{wi} and t_{wo}.

Axial variation of Nu_i is shown on Fig. (5.18). According to this figure, after the large value at the entrance region, Nu_i approaches its fully-developed value of $Nu_i = 4$. The continuous increase in the t_{mean} value does not seem to affect Nu_i significantly. On the contrary, Nu_o is very sensitive to the changes taking place in t_{mean} because:-

$$Nu_o \sim \dot{q}''' / (t_{wo} - t_{mean})$$

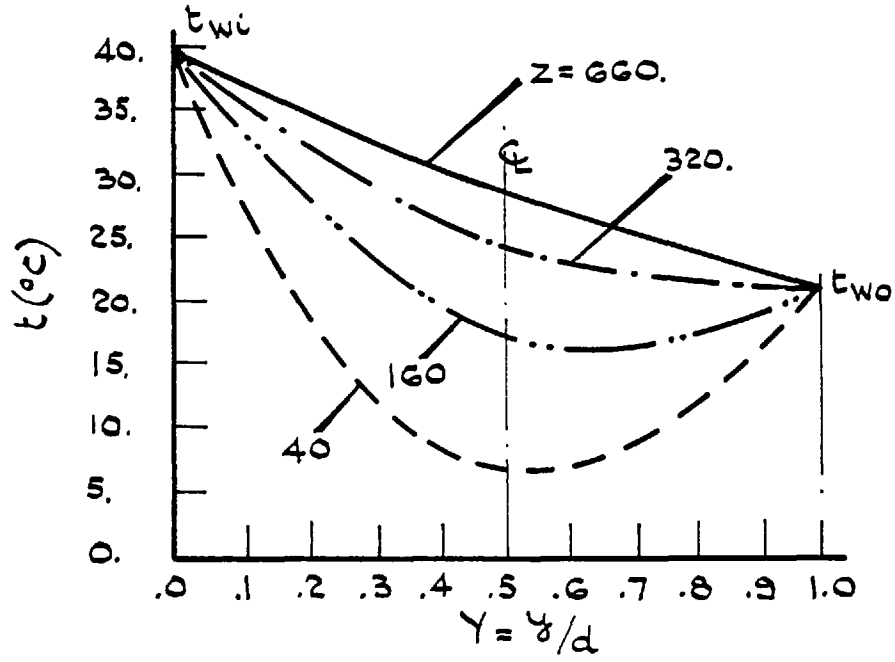

FIG(15.17) HORIZONTAL TEMPERATURE DISTRIBUTIONS ALONG THE CHANNEL (FOR $r_t = .468$)

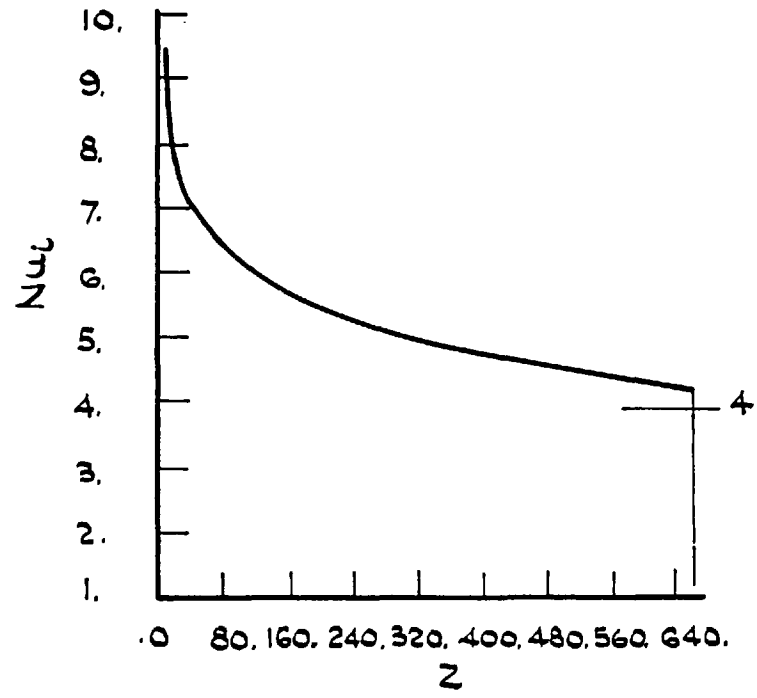

FIG.(5.18) AXIAL VARIATION OF Nu_i (FOR $r_t = .468$)

Fig. (5.19) shows Nu_o variations along the channel. It is noted that these variations take place in such a way as to keep the Nu_o profile somewhere between that of the two extreme cases of $r_t = 1$ and $r_t = 0$. Recalling:-

For $r_t = 1 \rightarrow Nu_o\Big|_{ZDT} = 7.54$

For $r_t = 0 \rightarrow Nu_o\Big|_{ZDT} = 4$

Therefore, Fig. (5.19) may be divided into two different regions:-

Region A, where : $t_{mean} < t_{wo} \rightarrow Z < 180$

Region B, where : $t_{mean} > t_{wo} \rightarrow Z > 180$

For the Region A, the temperature profile has the semi-parabolic shape shown on Fig. (5.17) and accordingly the Nu_o profile develops similarly to the symmetrical case of $r_t = 1$, shown as the dashed curve on Fig. (5.19). Near the axial position, Z = 180, the difference between the t_{wo} and the t_{mean} becomes very small and Nu_o assumes large values. This process does not invalidate the definition used for Nu_o when its physical reason, $t_{mean} = t_{wo}$, is understood.

For the Region B, Nu_o starts from large negative values. This happens because:-

$Z > 180 \rightarrow t_{mean} > t_{wo}$

But: $\dot{q}''_{wo} > 0$

Therefore:- $Nu_o \sim \dot{q}''_{wo}/(t_{wo} - t_{mean}) < 0$

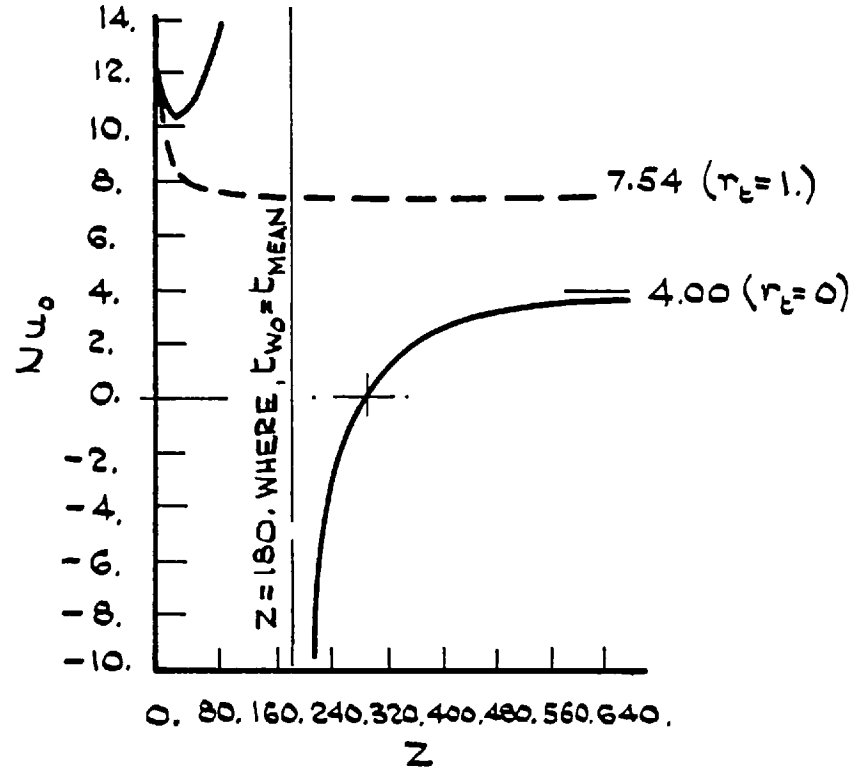

FIG (5.19) AXIAL VARIATION OF Nu_o (FOR $r_t = .468$)

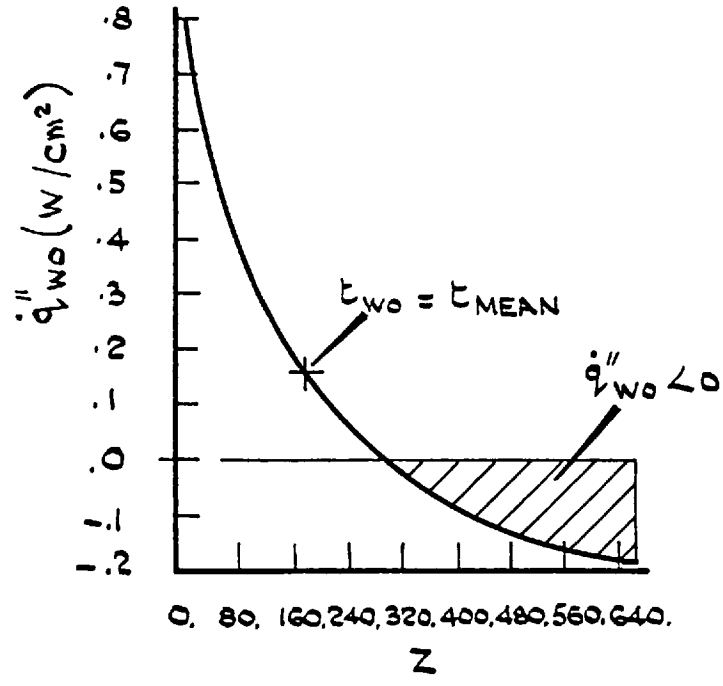

FIG(5.20) AXIAL VARIATION OF q''_{wo} (FOR $r_t = .468$)

At Z = 320, water layers near the "Outer" wall (Y = 1), assume temperature values very close to t_{wo}. Consequently:-

$$\dot{q}''_{wo} \cong 0 \rightarrow Nu_o \cong 0$$

In the axial positions where; Z > 320, the water temperature near the "Outer" wall becomes higher than that of the wall itself, so:-

$$\dot{q}''_{wo} < 0 \quad \text{and} \quad t_{wo} - t_{mean} < 0$$

leading to a positive value for Nu_o. From this axial position onwards, the temperature profile approaches the straight-line shape and, consequently, $Nu_o \rightarrow 4$. Despite the discontinuity in the Nu_o profile, the profile for the axial variations of $\dot{q}''_{wo}$, Fig. (5.20), is a monotonic curve.

From the foregoing discussion, it may be concluded that the criterion for the establishment of the fully-developed profile with the straight-line shape is that there should be $t_{mean} = t_{wo}$ at an axial position throughout the channel. This in turn forces the existence of a difference between the t_{wi} and the t_{wo} values because when they are equal (i.e. $r_t = 1$), there will always be a difference between the t_{mean} and the t_{wo} values. Therefore, only for the case with $r_t = 1$ there establishes a parabolic temperature profile, instead of the straight-line and $N_u = 7.54$ (instead of $Nu_i = 4$). Figs. (5.21) - (5.24) which respectively represent the profiles of the temperature, Nu_i, Nu_o and $\dot{q}''_{wo}$ along the channel for $r_t = 0.828$, also confirm these conclusions.

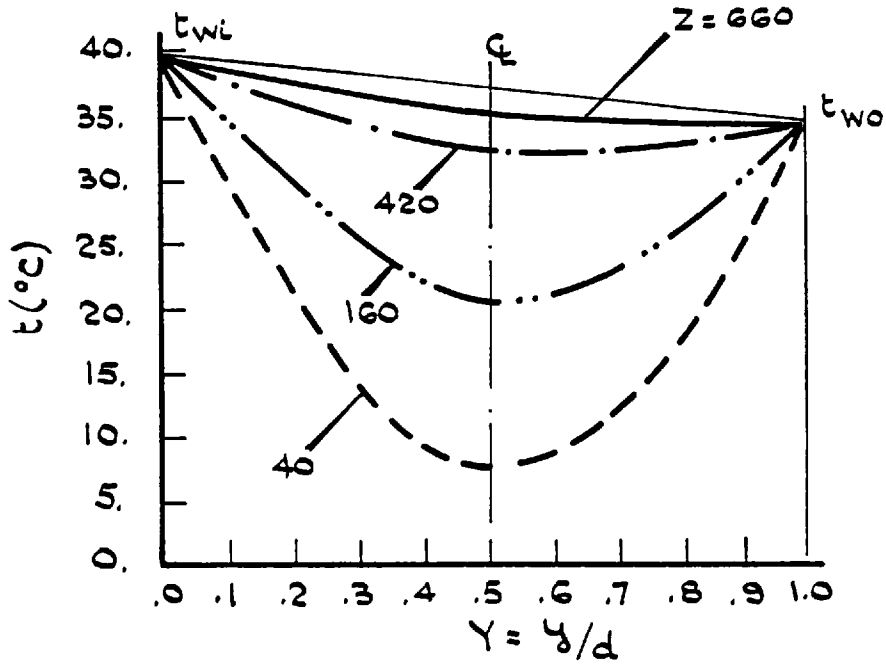

FIG (5:21) HORIZONTAL TEMPERATURE DISTRIBUTION (FOR $r_t = .828$)

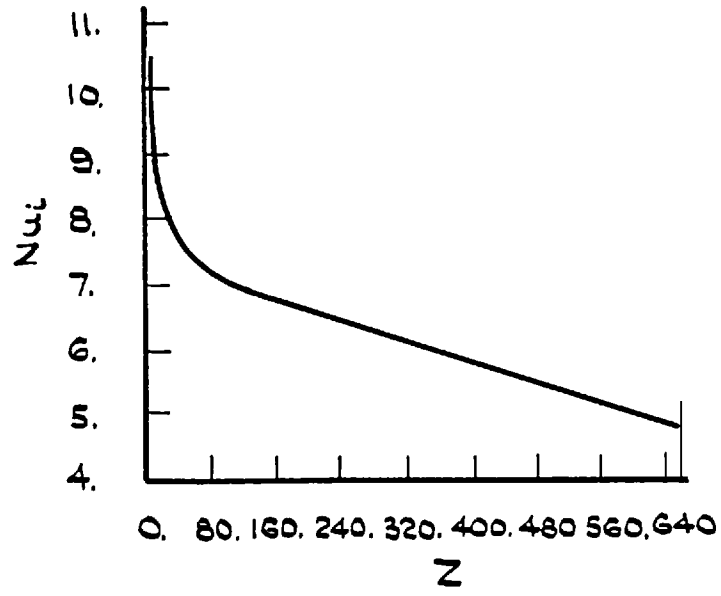

FIG(5:22) AXIAL VARIATION OF Nu_i (FOR $r_t = .828$)

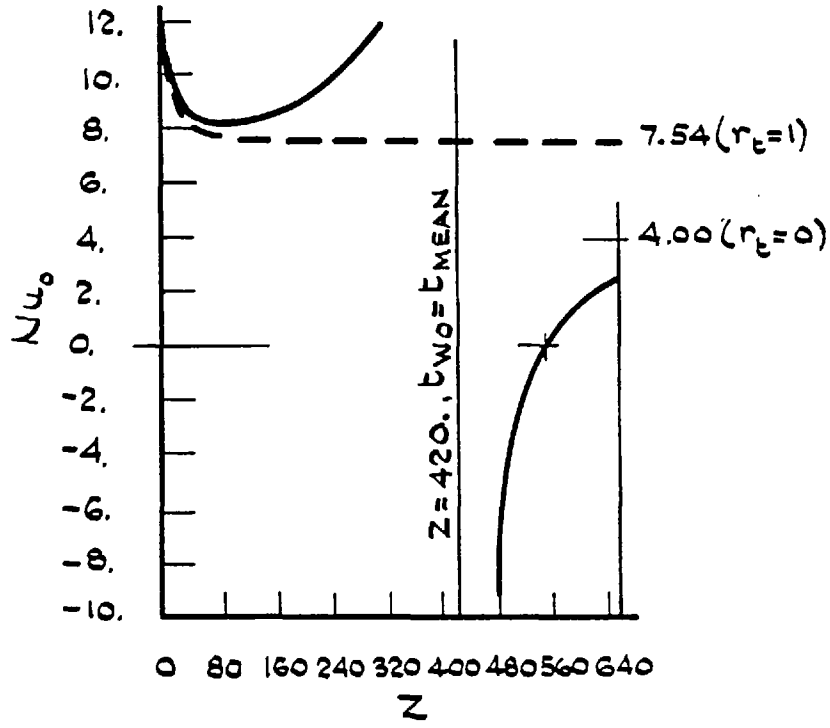

FIG (5.23) AXIAL VARIATION OF Nu_o
(FOR r_t = .828)

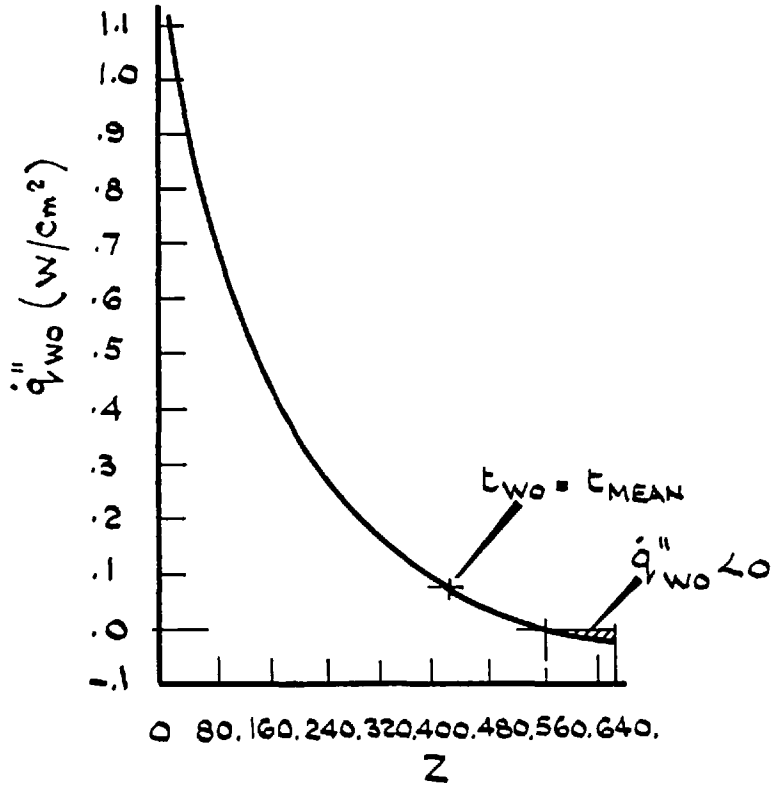

FIG(5.24) AXIAL VARIATION OF $\dot{q}''_{wo}$
(FOR r_t = .828)

(c) Dependence of the Computer Predictions of the Prescribed t_w Cases on the Data

Following the examinations for independence of the predictions for the prescribed $\dot{q}''_w$ cases from the system of coordinates and the value of the parameters involved, the following two tests are executed for the prescribed t_w cases:-

(i) For the case where $r_t = 0$, the "Inner" and the "Outer" walls were exchanged. A direct reflection of this exchange in the predictions for the problem confirmed that either of the walls may be used as the heated wall or the insulated wall.

(ii) For the case with $r_t = 1$, the values of the t_{wi} and the t_{wo} were changed and the problem was re-solved with the new data. The solution showed the same predictions for the non-dimensional parameters; Nu, f_p and f_s, together with the same constants in the ZDU and the ZDT formulae, and hence confirmed their independence from the data.

5.2.4 Solution for the Case With One Wall Set at a Prescribed Temperature While the Other Wall is Thermally Insulated

For this case, the typical channel of Table (5.1) is solved with the following boundary conditions:-

t_{wi} = Cte and $\dot{q}''_{wo} = 0$.

The method of solution, as executed in the DUCT computer program, is a combination of the prescribed wall heat-flux and temperature cases. It is based on the procedure by which t_{wo} is primarily calculated for the insulated wall. Then, the problem is treated as a prescribed wall temperature case and a solution is obtained. A current $\dot{q}''_{wo}$ is calculated from this solution and is compared with zero. If the $\dot{q}''_{w} \neq 0$, the procedure is repeated until the current $\dot{q}''_{wo}$ is satisfactorily close to zero. For the predictions mentioned here, the criterion is considered to be $Nu_o \leq .1$. The accuracy which results from this criterion has been sufficient to allow the duplication of the analytic results of, among others, Kays (1966).

The computer predictions are classified in the following two ways:-

(i) The U velocity profile is the same as that of the prescribed wall heat-flux or temperature cases shown on Fig. (5.2). According to this figure, the parabolic U profile of $U = 6Y(1 - Y)$ is established at $Z = 40$ which may be explained as:-

$$ZDU = 0.0485\ Re_D$$

Also, at the end of the ZDU, the pressure and the shear-loss factors assume their ideal values of $f_p = f_s = 24/Re_D$.

(ii) The temperature profile at several axial positions is shown on Fig. (5.25). It can be seen, with reference to this figure, that in the entrance region of the channel, t_{wo} does not rise significantly. It is after $Z = 120$ that it starts to increase more than that of smaller

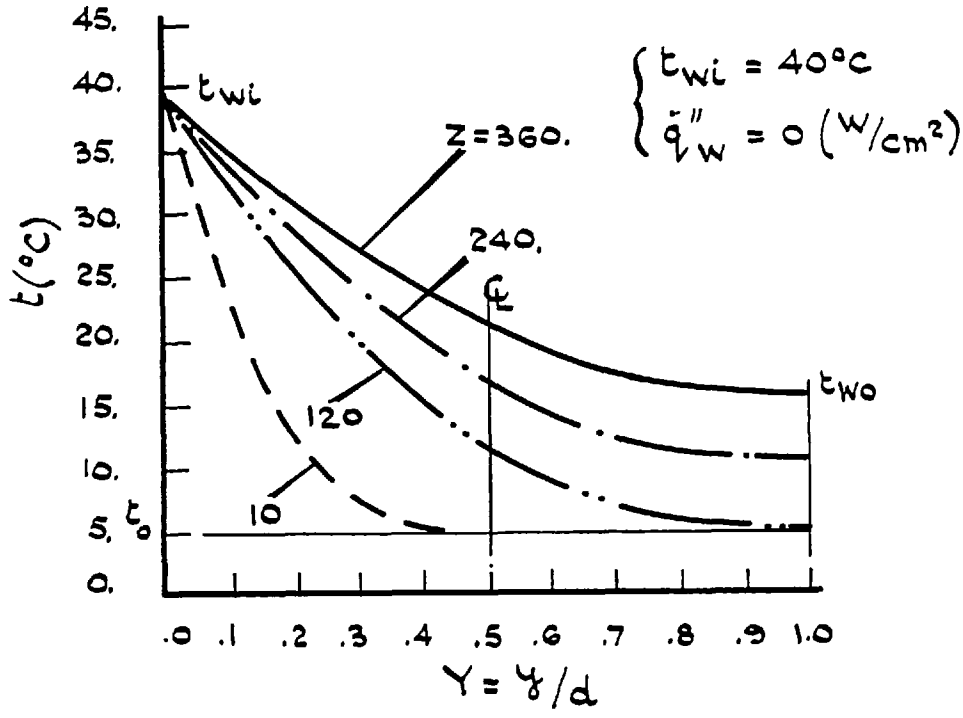

FIG(5.25) HORIZONTAL TEMPERATURE DISTRIBUTION ALONG THE CHANNEL

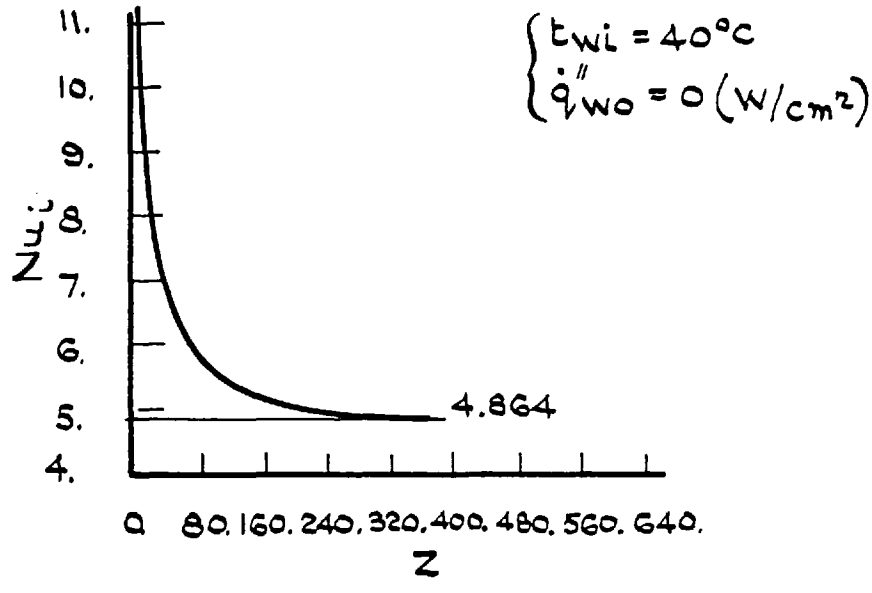

FIG(5.26) AXIAL VARIATION OF Nu_i

Z values. At Z = 360, the profile assumes its fully-developed form which is of a semi-parabolic shape (with having a slope near the "Inner" wall and being rather flat close to the "Outer" wall).

The above-mentioned variations in the temperature profile are also reflected in the Nu_i profile along the channel, Fig. (5.26). As shown on this figure, at the end of the thermal entry length, Nu_i approaches its fully-developed value, i.e.:-

$Z = 360 \rightarrow Nu_i = 4.864$ and $ZDT = 0.0634 \cdot Re_D \cdot Pr$

which are in accordance with the analytical results reported in Kays (1966).

5.2.5 General Conclusions for the Uniform Prescribed q''_w or t_w Profiles in the Forced-Convective Regimes

The main conclusions for the symmetrical and also the asymmetrical heating cases are:-

(1) There exists a hydrodynamic entry length, ZDU at the end of which the fully-developed U profile, $U = 6Y(1 - Y)$ is established. This length does not appear to be a function of the type of heating and only depends on the value of Re_D. Their relationship is found to be: $ZDU = 0.0485\ Re_D$.

The pressure drop is linear along the channel. As shown on Fig. (5.7), the pressure-loss factor, f_p and also the shear-loss factor f_s approach their ideal values at the end of the ZDU. These values are: $f_p = f_s = 24/Re_D$.

These results are in agreement with the analytical results of Knudson et al (1958).

(2) For the cases where $\dot{q}''_w$ is prescribed, the computer predictions for t_w or Nu values along the duct vary as shown on Fig. (5.13a). According to this figure, if the ratio r_q is known, the temperature and Nusselt number values on both walls along the duct can be determined. It could also be seen that there always exists a "thermal entry length", ZDT. This length is found to be a function of the product $(Re_D \cdot Pr)$ in the following form:-

$$ZDT = C' \cdot Re_D \cdot Pr$$

where the constant C is dependent on the ratio r_q as shown on Fig. (5.13b).

Analytical results which lead to the formula:-

$$Nu_o = 5.385/(1 - 0.346/r_q) \qquad \text{(Kays 1966)}$$

have been accurately obtained by the computer program, Figs. (5.5) - (5.13). Of special interest is when $r_q = 0.346$ for which $Nu_o\big|_{ZDT} = \infty$. The predictions for this case confirm that it does not invalidate the Nu_o definition so long as its physical meaning of $t_{mean} = t_{wo}$ is understood.

Table (5.2) summarises these predictions for several values of the ratio r_q. Values of Nu_i and Nu_o in this table are checked against the above-mentioned formula. The difference is less than 1% for Nu_i and 4% for Nu_o.

(3) In the cases where wall-temperatures are prescribed, it is concluded that the shape of the fully-developed temperature profile depends on the ratio of the wall-temperatures, r_t. Depending on this ratio, there are two possible shapes of the temperature profile:-

(i) Parabola, for $r_t = 1$. This type of profile is achieved at the end of the thermal entry length, ZDT where:-

$\dot{q}''_{wi} = \dot{q}''_{wo}$ and also, $Nu_i = Nu_o = 7.54$

(ii) Straight-line, for $0 \leq r_t < 1$. This profile is obtained by a straight line drawn between the t_{wi} and the t_{wo} as shown on Fig. (5.17). When this profile is established:-

$\dot{q}''_{wi} = - \dot{q}''_{wo} \rightarrow Nu_i = Nu_o = 4$

It should be pointed out that the fully-developed temperature profile will always be obtained if the channel is long enough. For the above-mentioned straight-line profile, ZDT is minimum when $r_t = 0$ and increases with it. For all of the r_t cases, the axial variation of Nu_i is a monotonic curve, Figs. (5.16), (5.18) and (5.22). Conversely, the Nu_o profile along the channel goes through a discontinuity, as shown on Figs. (5.19), (5.23). This is because for the cases where $0 \leq r_t < 1$ at an axial position inside the channel: $t_{wo} = t_{mean}$. This equilibrium forces a discontinuity in the Nu_o profile. However, the $\dot{q}''_{wo}$ profile for this case is monotonic, Figs. (5.20) and (5.24). Table (5.3) summarises the computer predictions for these prescribed wall-temperature cases.

(4) The computer predictions were also obtained for the case where one wall is set at a constant temperature while the other one is thermally insulated (i.e. t_{wi} = Cte. and $\dot{q}''_{wo} = 0$). For this type of heating also there exists a fully-developed temperature profile but with a semi-parabolic shape. It can be seen with reference to Fig. (5.25) that at the end of the ZDT for this case, Nu_i approaches its ideal value of $Nu_i = 4.864$, reported among others by Kays (1966). The criterion, $Nu_i \leq 0.1$ has been sufficient to reproduce the analytically obtained results for this case.

(5) To gain more confidence about the independence of the dimensionless predictions from the data and also from the system of coordinates, they have been re-examined. This is done according to the following two steps:-

(i) The predictions were repeated for several values of Re_D's and Pr's. They all agreed with their corresponding results previously mentioned in this chapter.

(ii) For the two cases, $r_q = 0$ and $r_t = 0$, a further checking is executed. This is done by exchanging the "Inner" and the "Outer" walls with each other. A direct reflection of this exchange in the predictions confirm that they do not depend on the choice of the coordinate system.

(6) Prescribed non-uniform $\dot{q}''_w$ or t_w profiles may be similarly

solved for. These predictions are to be reported together with their corresponding mixed-convection results later in this chapter, e.g. Fig. (5.42).

5.3 Mixed-Convection Heat Transfer

As mentioned in Chapters (2) - (3), in this mode of heat transfer, the effects of temperature on the density and the viscosity of the fluid should be considered. In the following, this point is taken into account for various types of heating. In so doing, the computer predictions are compared, for two cases of the identical and uniform prescribed wall heat-flux, with the experimental results of Vernier (1962). This is followed by the solution for the case, $r_q = 0$ where one wall is set at a uniform prescribed $\dot{q}''_w$ while the other one is thermally insulated.

Non-uniform prescribed $\dot{q}''_w$ or t_w profiles are also considered. An interesting and important application of the method introduced in this thesis is its ability to solve for the problems where $\dot{q}''_w$ varies in a specified manner along the channel. For this purpose, the computer predictions are obtained for two models of a nuclear fuel element where $\dot{q}''_w$ varies sinusoidally along the channel.

Also, non-uniform prescribed t_w profiles are investigated. This is done by using the t_w profile, which is obtained as the solution of a prescribed $\dot{q}''_w$ profile, as the data for a non-uniform prescribed t_w case. Comparison of the $\dot{q}''_w$ profile obtained for this case and the original $\dot{q}''_w$ profile is used for the following two conclusions:-

(i) The method of solution covers non-uniform prescribed t_w profiles also.

(ii) The comparison between the predicted $\dot{q}''_w$ profile by the solution and the original profile represents the accuracy of the predictions.

5.3.1 Comparison of the Computer Predictions and the Experimental Results for a Channel Having Identical and Uniform Prescribed Wall Heat-Fluxes

Vernier (1962) has investigated the convective heat transfer problem in a uniformly heated vertical channel with rectangular cross-section, Fig. (5.1). He focused his study on a set of wall heat-fluxes and aspect ratios. In the following, the computer predictions are obtained for two examples which Vernier studied and comparison is made between the predicted profiles of the U velocity and the temperature with his experimental results. Data for these examples are given in Table (5.4) and they are referred to as Example No. 1 and Example No. 2 respectively.

Figs. (5.27) - (5.32) show the predictions obtained based on these data. (The full-line on these figures represent the computer predictions while the dots show Vernier's experimental results). Also, the system of coordinates used for the computer predictions are at the right hand side of the graphs and those of Vernier on the left.

(a) Comparisons for Example No. 1

These comparisons are made for the corresponding U velocity and the temperature profiles at the exit of the channel (i.e. $Z = Z_{max}$ or $z = L$). The Nusselt number, Nu is also compared at different axial positions along the channel.

TABLE (5.4) DATA FOR THE TWO EXAMPLES

Reduced Data / Data	w/d	Z_{max}	$\dot{Q}_{tot}$ (w)	$\dot{m}$ (gr/sec)	Δt_{tot} (C^o)	t_m (C^o)	t_{out} (C^o)	Re	Re_o	Re_m	Re_D	Gr_D	Gr_D/Re_D^2	Pr
Example No. 1 u_o = 5.34 cm/sec, w = 7 cm, d = 0.91 cm, t_{in} = 17.3 ^oC, L = 70 cm, $\dot{q}''_w$ = 1.498(w/cm^2)	7.692	76.92	1468	33.93	10.32	22.46	27.62	495.0	456.0	518.8	990.0	5.05×10^6	5.149	6.763
Example No. 2 u_o = 4.2 cm/sec, $\dot{q}''_w$ = 1.057 (w/cm^2), t_{in} = 17.5 ^oC. The rest the same as for Example No. 1	7.692	76.92	1036	26.68	9.26	22.13	26.76	390.8	356.5	397.0	781.6	3.56×10^6	5.830	6.763

(a.1) The U Velocity Profile

Fig. (5.27) shows this profile at the exit of the channel ($Z = Z_{max} = 76.92$). The figure suggests that the present theoretical method represents a significant improvement over that of Vernier. In both of them, there is a peak velocity somewhere between the centre of the channel and the wall. This comparison proves that when variation of ρ and μ with temperature are also considered, the U velocity profile develops continuously and the ideal parabolic profile will not be produced. This is because the water at the centre is denser than that at the same horizontal positions near the wall. Also, because of heat gain from the walls, the water temperature varies from one section to another. This is followed by changes in ρ and μ and, consequently, the U velocity and the temperature profiles cannot reach their fully-developed shapes and will continue to change.

As shown on Fig. (5.27), the computer predictions are lower near the walls and higher at the centre of the channel. At the peak position:-

$$Y = 1/8 \rightarrow \begin{cases} U_p = 1.333 \text{ (c.f. } U_{p.experiment} = 1.395) \\ \Delta U_p = 4.6\% \end{cases}$$

and at the centre of the channel:-

$$Y = 1/2 \rightarrow \begin{cases} U_{\ell} = 0.771 \text{ (c.f. } U_{\ell.experiment} = 0.684) \\ \Delta U_{\ell} = 11.2\% \end{cases}$$

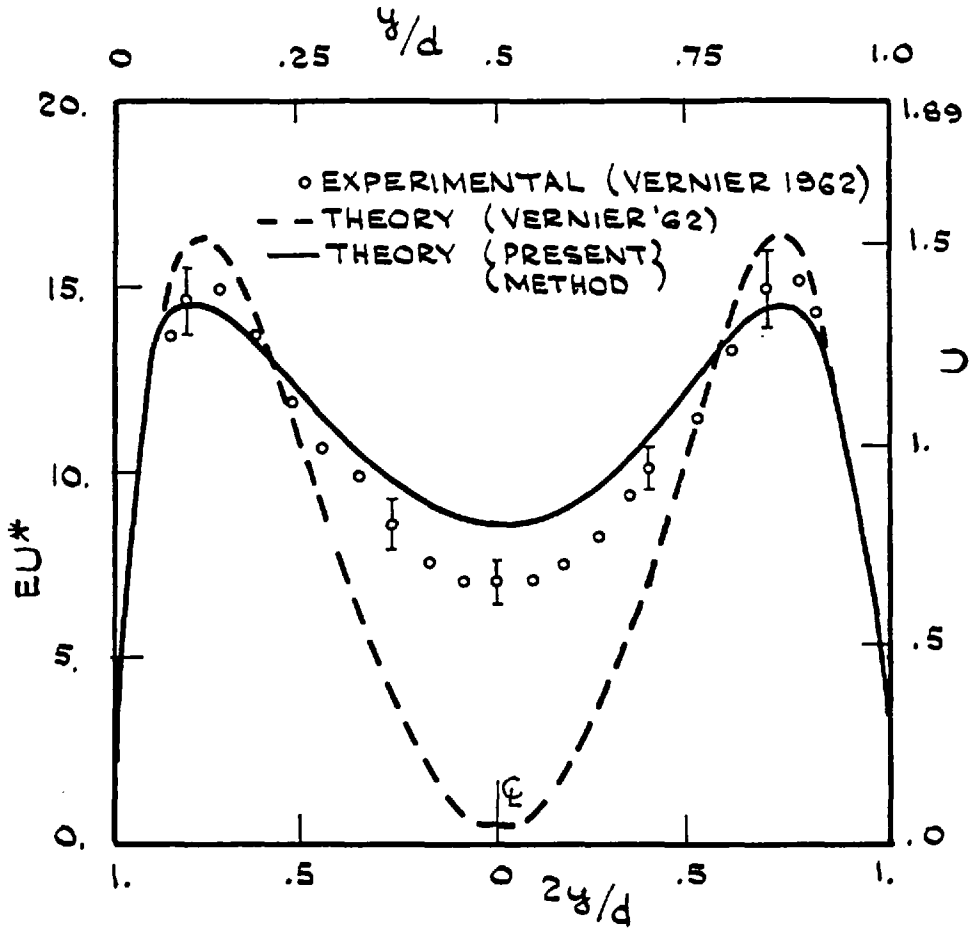

FIG (5.27) THE U VELOCITY PROFILE AT THE EXIT (EXAMPLE · Nº 1)

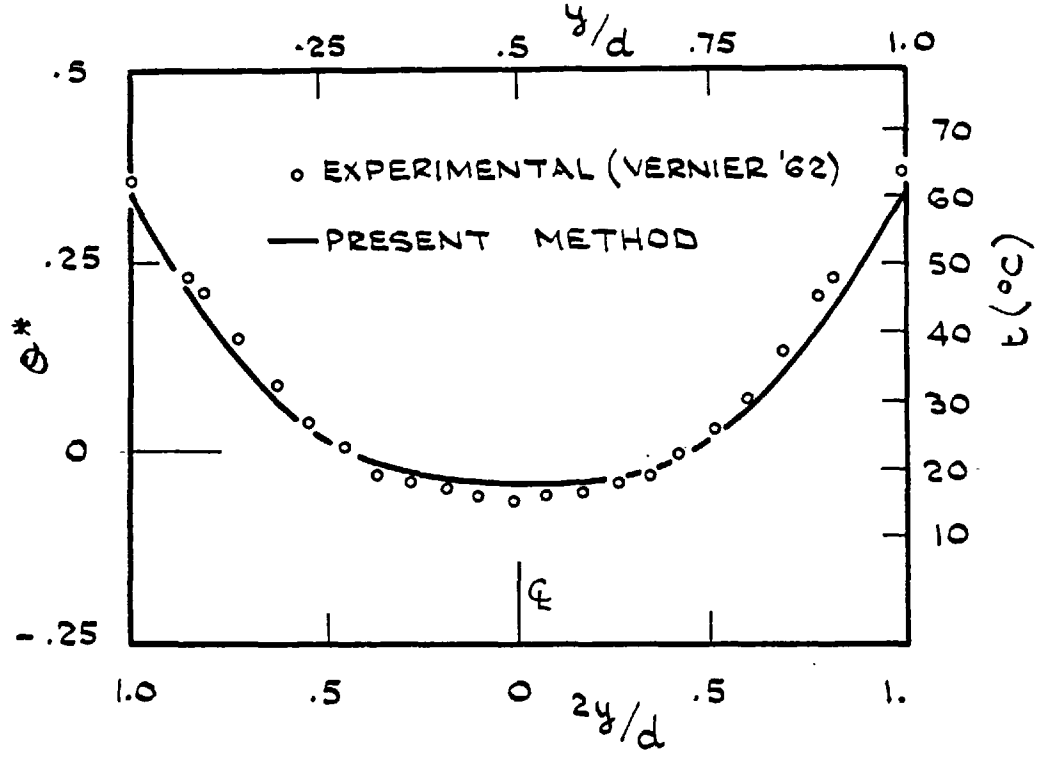

FIG (5.28) HORIZONTAL TEMPERATURUE DISTRIBUTION AT THE EXIT (EXAMPLE Nº 1.)

It should be noted that because of the low values of U in these comparisons, percentage calculations may not be quite representative of the differences. Also, the experimental results were obtained by using a pitot tube and their accuracy is reported to be within 6 to 7%. The computer predictions represent a significant improvement on Vernier's own theoretical results.

(a.2) The Temperature Profile

Fig. (5.28) shows the predicted and also the measured water temperature distribution across the channel at the exit (i.e. $Z = Z_{max} = 76.92$). The differences are:-

At the wall, $t_w = 59.5\ ^{o}C$ (c.f. $t_{w.experiment} = 63\ ^{o}C$)
$(Y = 0 \text{ or } 1)^{\rightarrow}$

Also:-

At the centre of the channel, $(Y = \frac{1}{2})^{\rightarrow}$ $t_{\ell} = 18.2\ ^{o}C$ (c.f. $t_{\ell.experiment} = 17.5\ ^{o}C$)

It is noted that Vernier's experimental results are reported to be accurate within 0.2 to 0.8 ^{o}C. Vernier's own theoretical results are too close to the computer predictions to be shown separately.

(a.3) Nusselt number, Nu

Fig. (5.29) shows the axial variation of the Nusselt number, Nu. Comparison of the predicted and the measured values shows a good agreement, the difference being less than 3%.

(b) Comparisons for Example No. 2

Example No. 2 is the same as the afore-mentioned Example No. 1, except for the changes mentioned in the first column of Table (5.4). In the following, the comparisons are explained.

(b.1) The U Velocity Profile

Fig. (5.30) shows this profile at the end of the channel and as with the example No. 1, the shape of the profile for both results is similar, but the computer predictions are higher in the centre and lower near the wall. At the centre:-

$$Y = \frac{1}{2} \rightarrow U_{\ell} = 0.763 \quad (\text{c.f. } U_{\ell,\ \text{experiment}} = 0.610)$$

At the peak position:-

$$Y = 0.15 \rightarrow U_{p} = 1.335 \quad (\text{c.f. } U_{p.\text{experiment}} = 1.423)$$

These differences might be less regarding the fact that Vernier's results are reported to be accurate to 6 - 7%. As with Example No. 1, the computer predictions represent a significant improvement on Vernier's own theoretical results.

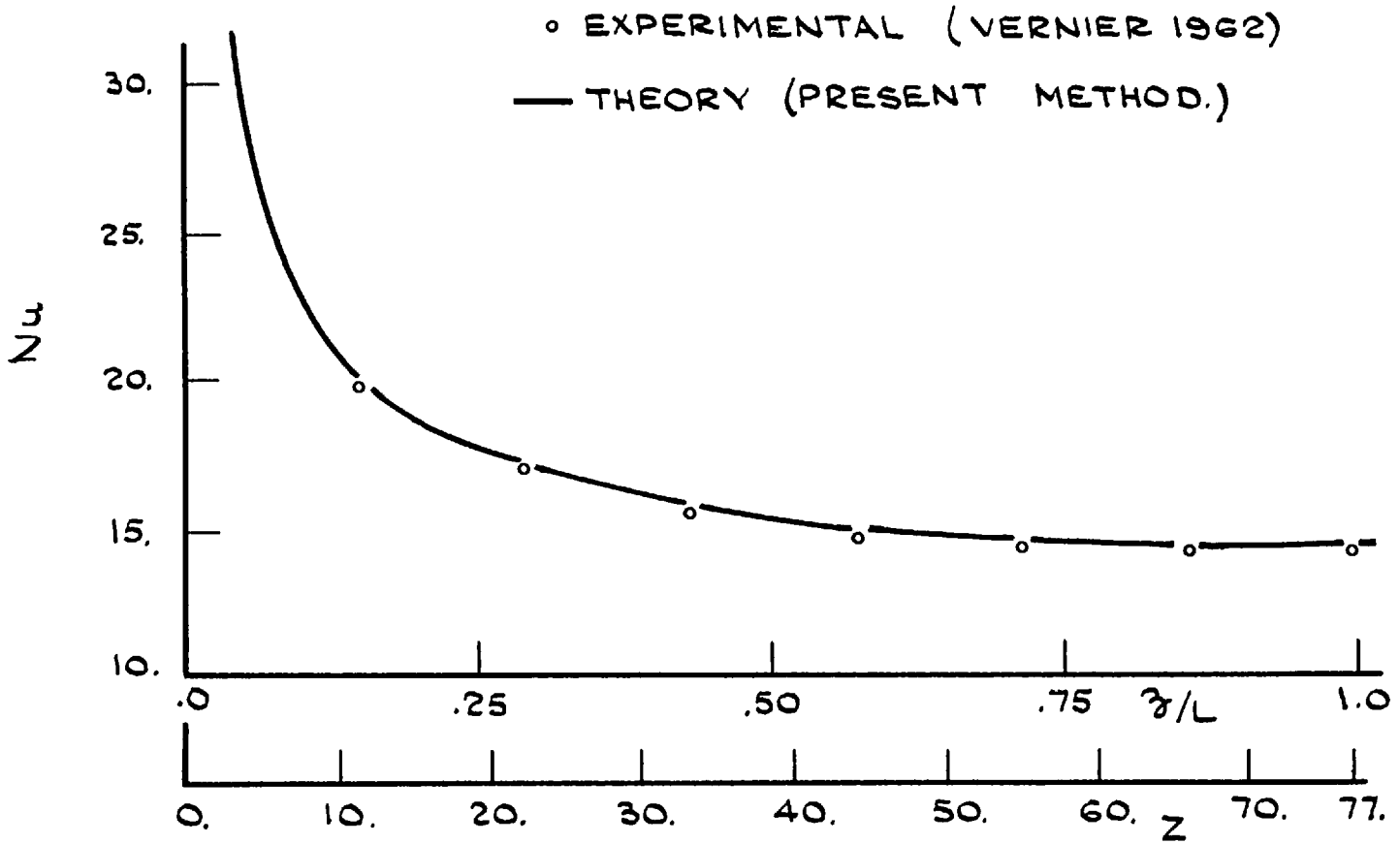

FIG (5.29) Nu VARIATIONS ALONG THE CHANNEL (EXAMPLE Nº 1)

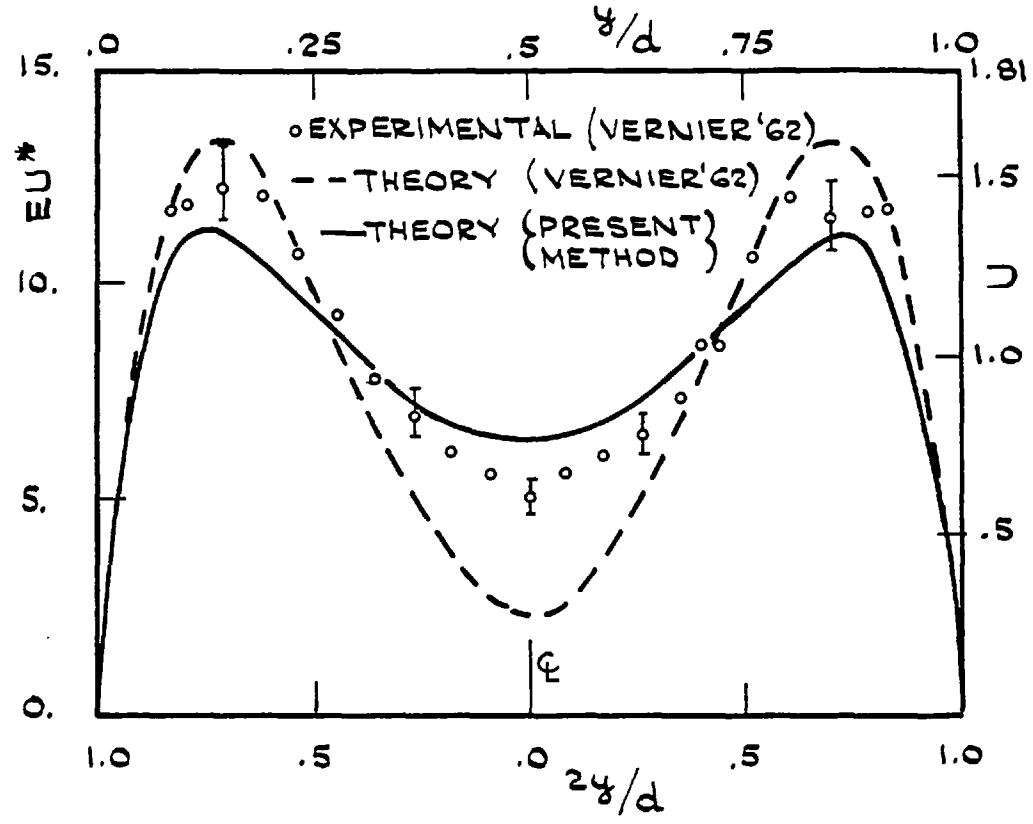

FIG(5.30) THE U VELOCITY PROFILE AT THE EXIT (EXAMPLE NO.2.)

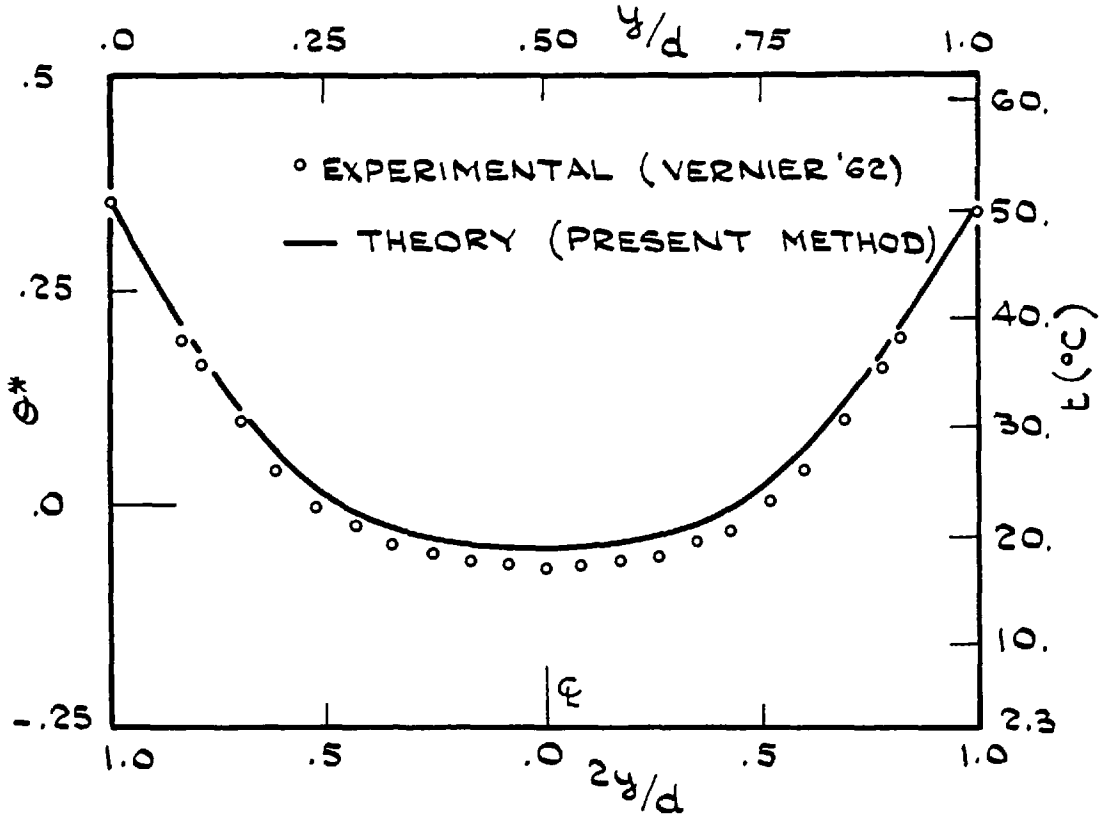

FIG(5.31) HORIZONTAL TEMPERATURE DISTRIBUTION AT THE EXIT. (EXAMPLE NO.2.)

(b.2) The Temperature Profile

Fig. (5.31) shows this profile at the exit of the channel. Here, as for Example No. 1, the overall shape of the profile is the same for both the predicted and the measured temperatures. However, there are some differences:-

For $Y = \frac{1}{2} \rightarrow t_{\ell} = 18.6\ ^{o}C$ (c.f. t_{ℓ}. experiment $= 17.8\ ^{o}C$)

and for $Y = 0$ or $1 \rightarrow t_{w} = 50.5\ ^{o}C$ (c.f. $t_{w.experiment} = 50.45\ ^{o}C$)

It is noted that the experimental results are reported to be accurate to 0.2 - 0.8 ^{o}C.

(b.3) Nusselt Number, Nu

Fig. (5.32) represents axial variations of the Nusselt number, Nu. The accuracy of the computer predictions seem to be good with the differences being less than 2%.

5.3.2 The Computer Predictions for the Case (with $r_q = 0$)

As mentioned for the forced-convective flows, this type of heat transfer is realised when; $\dot{q}''_{wi} = Cte.$ while $\dot{q}''_{wo} = 0$ · The predictions show that for the mixed-convective regimes, where variations of ρ and μ with temperature are considered, the velocity and the temperature profiles continue to develop and do not assume the fully-developed shapes. Because of the asymmetric type of heating, the U velocity and the temperature profiles are essentially asymmetric also. These profiles, obtained for the typical channel of Table (5.1), with extention of the length, are discussed in the following.

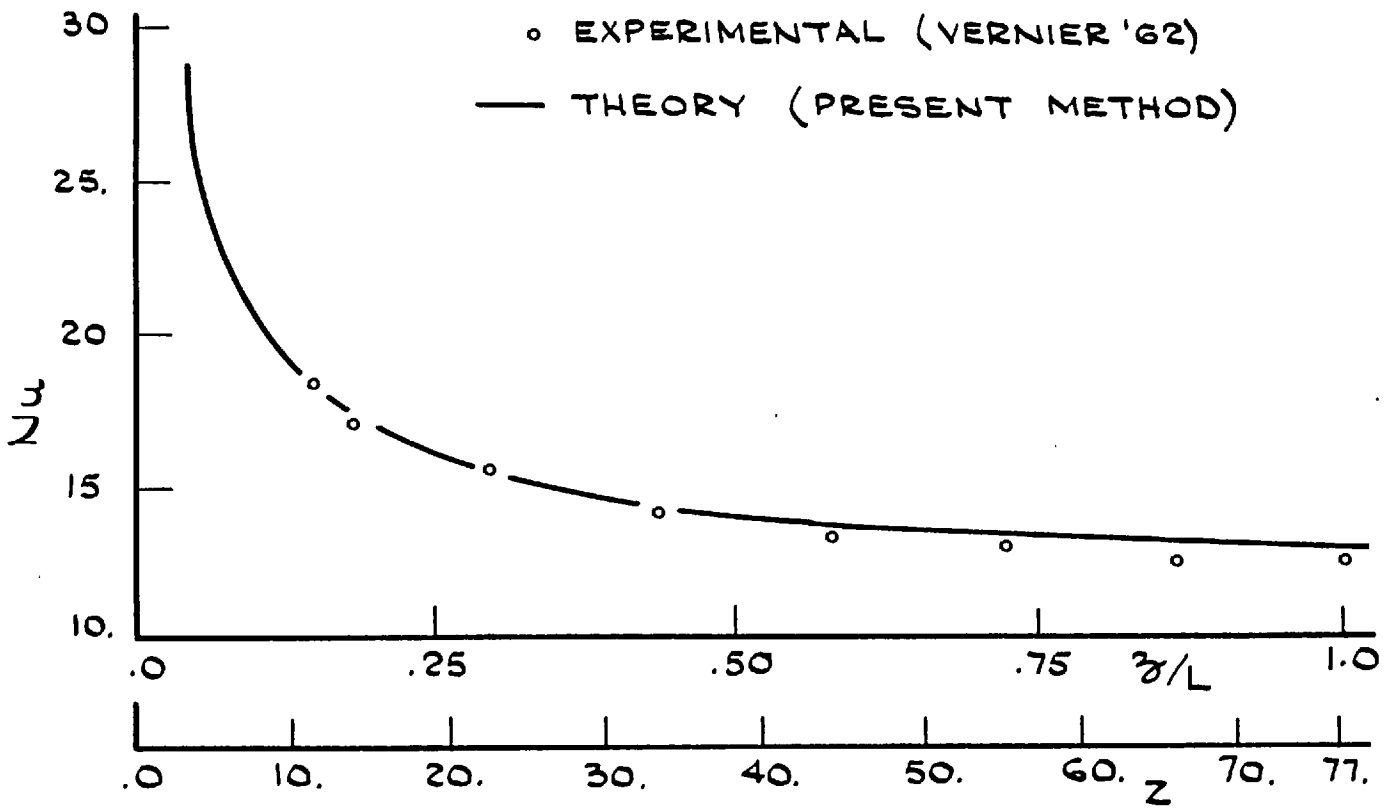

FIG(5.32) VARIATIONS OF Nu ALONG THE CHANNEL (EXAMPLE NO.2.)

(i) The U Velocity Profile

Fig. (5.33) shows the U profile at two axial positions along the channel (at Z = 355, 715 respectively). For comparison, the predictions of the corresponding case with symmetrical heating are also given. It is noted that near the heated-wall, the U values for the asymmetric heating are considerably higher than the symmetric case. This is attributed to the ρ and μ reductions there. It is interesting to note that as shown on Fig. (8.34) the effects of the variations of the density, ρ are more significant than those for viscosity, μ. For the area near the insulated wall, a similar argument describes the low U values there. These results are in agreement with those of Savkar (1970) for a similar case.

(ii) The Temperature Profile

Fig. (5.34) shows the temperature profiles at two axial positions (Z = 355, 715 respectively) for this case, (r_q = 0) together with those of its corresponding symmetrical case, (r_q = 1). As expected the profile continues to develop along the channel and there is no sign of its approach to a fully-developed shape. For the same axial position, the t_{wi} value is lower for the asymmetric case. This difference increases as the fluid continues to move downstream. There exists a similar situation for t_{wo}.

In order to represent the above-mentioned differences more clearly, axial variations of Nu_i for both of the cases are plotted on Fig. (5.35). According to this figure, Nu_i for the asymmetric case is lower throughout the channel, compared to the symmetric predictions. The forced-convection results are also represented to show the natural-convection effects on the Nu_i values. The larger Nu_i values, for both

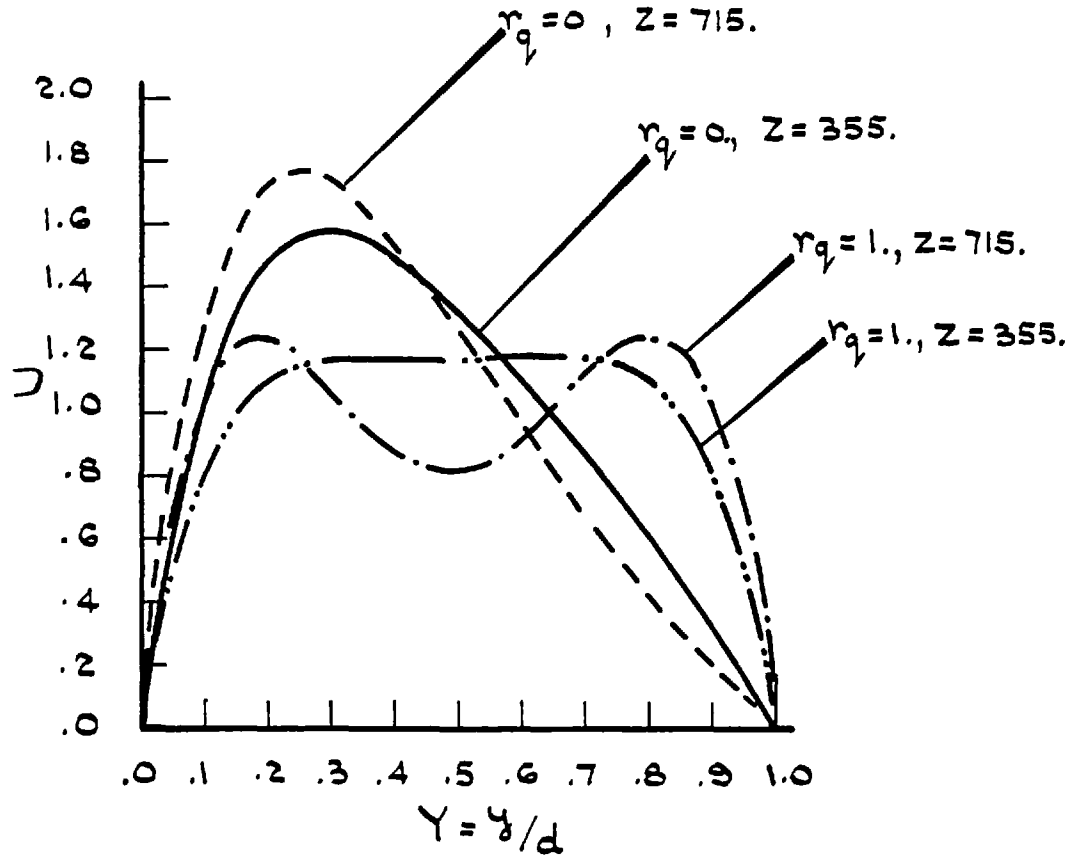

FIG(5.33) THE U VELOCITY PROFILES ALONG THE CHANNEL.

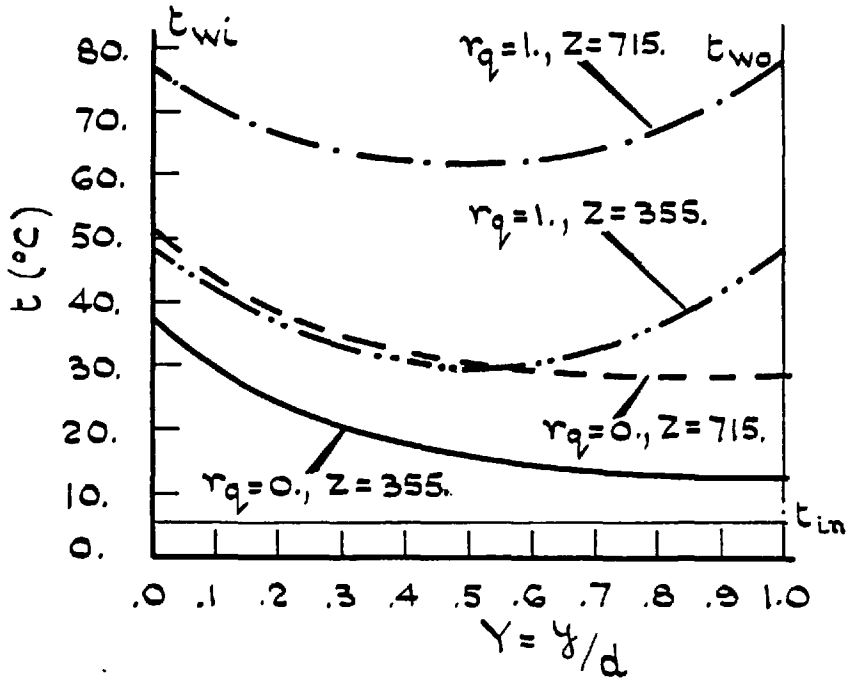

FIG(5.34) HORIZONTAL TEMPERATURE PROFILES ALONG THE CHANNEL.

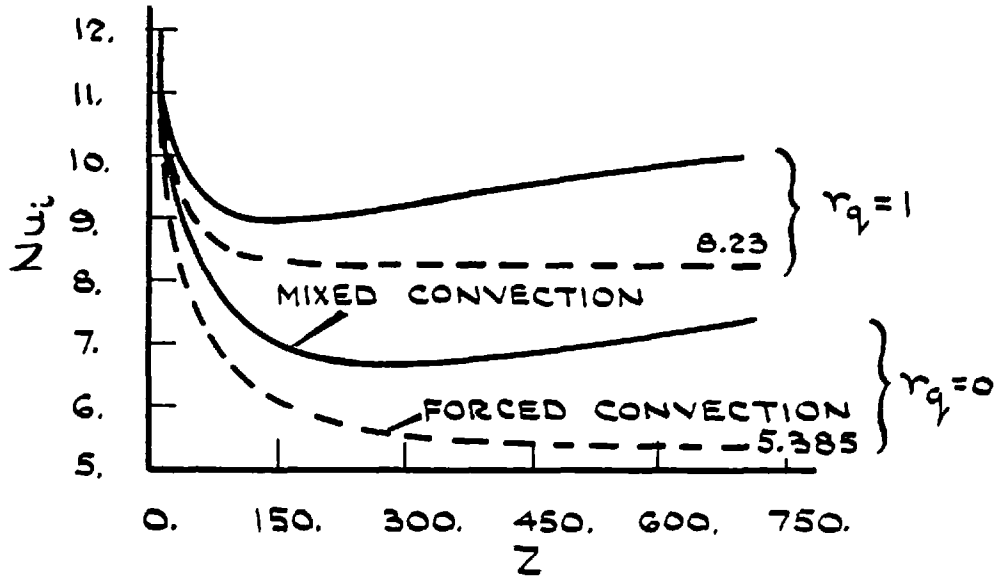

FIG(5.35) AXIAL VARIATIONS OF THE NUSSELT NUMBER, Nu_i IN THE MIXED AND THE FORCED CONVECTION REGIMES.

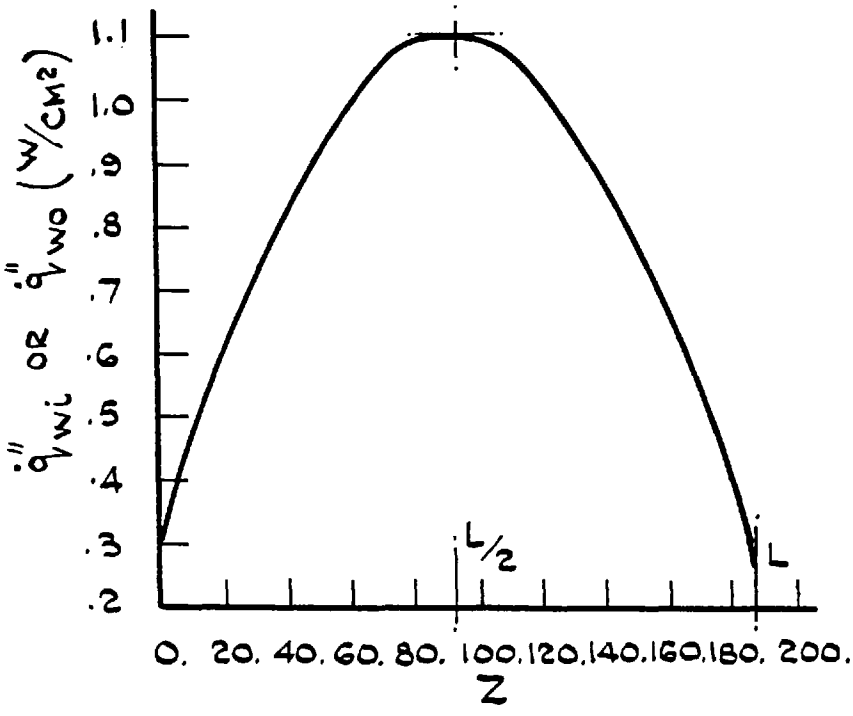

FIG(5.36) AXIAL VARIATIONS OF WALL HEAT-FLUX FOR THE 650 W MODEL.

of the cases, (r_q = 0 and 1 respectively), compared to their corresponding forced-convective values, confirm that the natural-convection effects significantly improve the heat-transfer rate in the channel. They also suggest that if the heat-transfer calculations for these two types of heating are based on the fully-developed Nu_i values, they will be subject to errors which will be bigger for longer channels.

(iii) The predictions for the case with r_q = 0 do not depend on the choice of the heated-wall. This is confirmed by the exchange of the boundary conditions between the two walls, which was directly reflected in the predictions (i.e. after the exchange of the data between the walls, their predictions were also exchanged).

5.3.3 The Predictions for Sinusoidally Heated Flat Ducts

An interesting and important application of the solution technique developed in this thesis is to problems where $\dot{q}''_w$ varies in a specified manner along the channel. For this purpose, the computer predictions are obtained for two models of a nuclear fuel element where $\dot{q}''_w$ varies sinusoidally along the cooling channel.

These two models are chosen to simulate the hot-channel in the core of the University of London Reactor, (ULR) at two different power levels (108.5 KW and 325 KW respectively). The general configuration of these models is the same as that of Fig. (5.1) and their numerical data are given in Table (5.5). For convenience, they are referred to as 650 W and 1950 W Models, these being their total heat rates.

Heat fluxes prescribed on the walls of these models are considered to vary according to the formulae:-

TABLE (5.5) DATA FOR THE TWO MODELS

Reduced Data / Model	w/d	Z_{max}	$\dot{Q}$ (w)	Δt_{tot} (C^o)	t_m (C^o)	Re	Re_o	Re_{mD}	Re_D	Gr_D	Gr_D/Re_D^2	Pr	P_o
650 W Model t_{in} = 30 ^oC, w = 6.5 cm, d = 0.32 cm, L = 60 cm, u_o = 4.06 cm/sec	20.3	187.5	650	18.7	39.35	131.3	159.8	382.6	262.6	1.39×10^5	2.020	6.503	0
1950 W Model u_o = 7.38 cm/sec. The rest as for the 650 W Model	20.3	187.5	1950	30.55	45.28	238.5	281.7	727.3	477.0	4.83×10^5	2.124	6.426	0

$$\begin{cases} \dot{q}''_{wi}(z) = \dfrac{\dot{Q}_{tot} \cdot \beta}{W \cdot L} \cdot \cos\left(\pi \dfrac{z}{L} - \dfrac{\pi}{2} \cdot \dfrac{L}{L}\right) \\ \dot{q}''_{wo}(z) = \dot{q}''_{wi}(z) \end{cases}$$

These profiles are obtained based on the typical flux curve provided by the ULR . The procedure to approximate the flux curve, leading to the above-mentioned sinusoidal functions for $\dot{q}''_{wi}(z)$ and $\dot{q}''_{wo}(z)$, is explained in Chapter (6). Application of the data of the two models into the above-mentioned sinusoidal $\dot{q}''_{w}$ profile leads to:-

For the 650W Model : $\dot{q}''_{wi}(z) = 1.104 \cos(0.043z - 1.291)$

For the 1950W Model : $\dot{q}''_{wi}(z) = 3.312 \cos(0.043z - 1.291)$

where z is measured in (cm) and $\dot{q}''_{w}$ in (w/cm^2) respectively and for both of them; $\dot{q}''_{wo}(z) = \dot{q}''_{wi}(z)$.

The computer predictions for these two models are given in the following two sections (a) and (b).

(a) Results for the 650 W Model

(a.1) The Wall Heat-Flux Profile

Fig. (5.36) shows the $\dot{q}''_{w}$ profile which is used for the numerical integration in the DUCT computer program. The negligible difference between the computed and the actual heat-input values along the channel confirms that the accuracy of the predictions is good.

(a.2) The Velocity Profiles

Fig. (5.37) shows the development of the U profile along

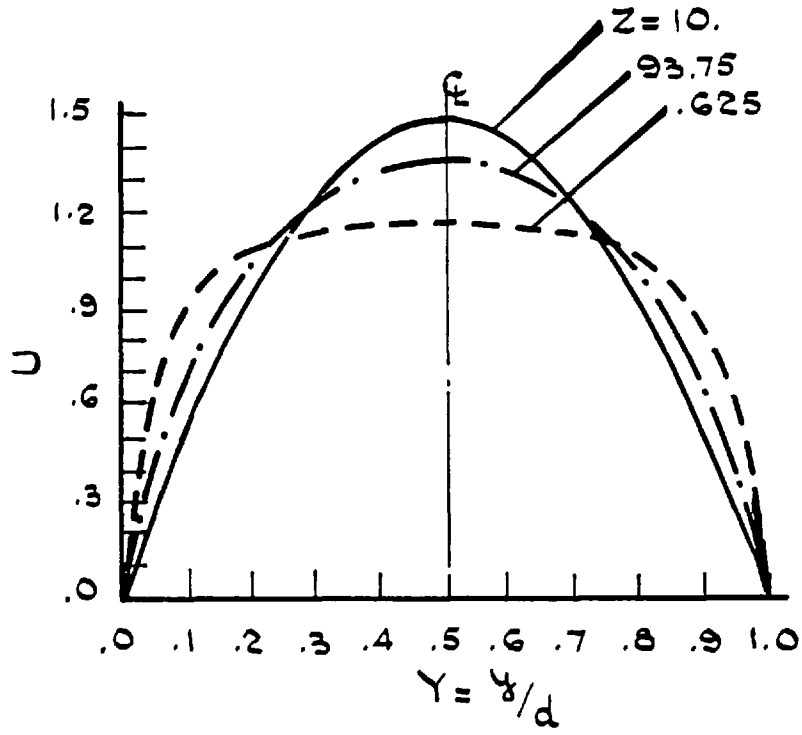

FIG (5.37) HORIZONTAL DISTRIBUTION OF U AT DIFFERENT AXIAL POSITIONS.

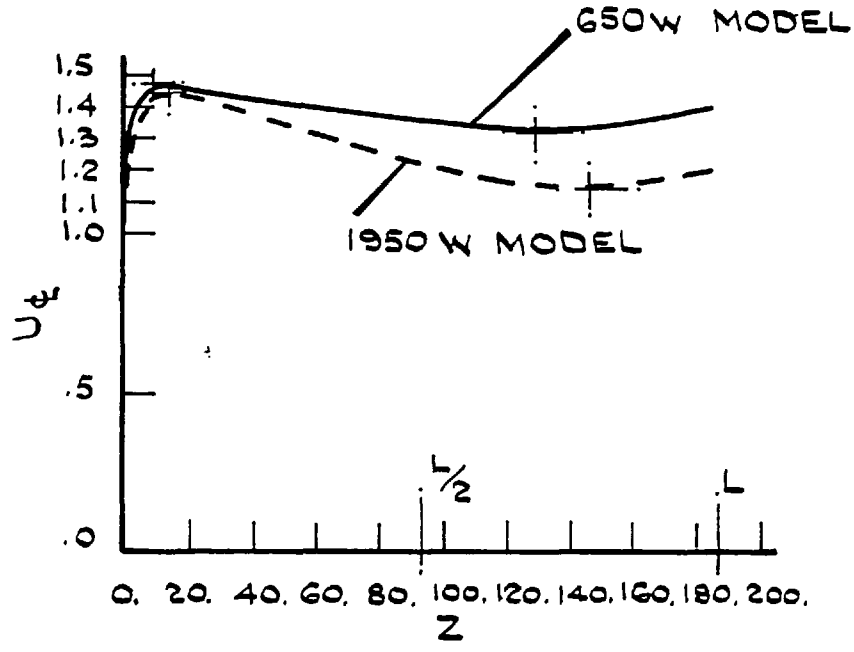

FIG (5.38) AXIAL DEVELOPMENT OF $U_{\mathfrak{C}}$ FOR THE TWO MODELS.

the channel. According to this figure, the uniform profile at the entry gradually develops towards the parabolic shape obtained for the forced-convection cases. At Z = 10, the U_{ℓ} reaches its peak value (U_{ℓ} = 1.476), but later, in contrast with the forced-convection cases, the profile develops towards a more flat shape. This is because of the natural-convection effects under which the resistance against the movement of the fluid becomes increasingly lower near the walls and higher in the centre. Halfway through the channel, U_{ℓ} is still decreasing, (Z = 93.75, U_{ℓ} = 1.354). After this axial position, because of the sinusoidal shape of $\dot{q}''_w$, the heat addition to the fluid reduces, which leads to slower rate of ρ value reductions. At Z = 130, where U_{ℓ} = 1.337, the flattening process of the U profile comes to an end and it starts to assume a more parabolic shape. Comparatively low rates of heat-input in this area are responsible for this change in the trend. At the exit of the channel, the profile is still not parabolic, (Z = 187.5, U_{ℓ} = 1.40).

The development of the U velocity profile may best be shown by Fig. (5.38) showing axial variations of U_{ℓ}.

The movement of the fluid across the channel, as mentioned for the U profile, may also be confirmed by examining the V profile at two axial position, (e.g. Z = 50, 150 respectively). These positions are chosen to represent axial positions below and above Z = 130 (where the flattening process of the U profile stops). On Fig. (5.39), the signs of the V values confirm the movement of the water layers from the centre towards the walls of the channel. These signs change at Z = 150, where the movement takes place in the opposite direction. Naturally, the V values represent the rate at which the fluid moves across the channel.

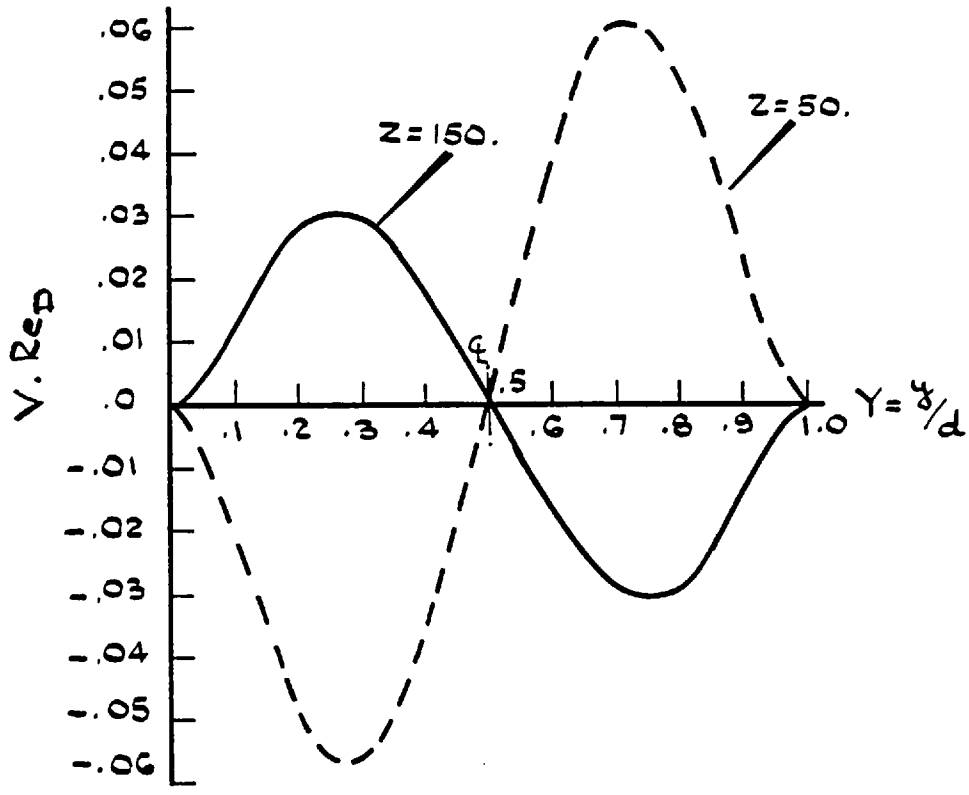

FIG (5.39) HORIZONTAL DISTRIBUTION OF V AT TWO DIFFERENT AXIAL LEVELS (G50 W MODEL)

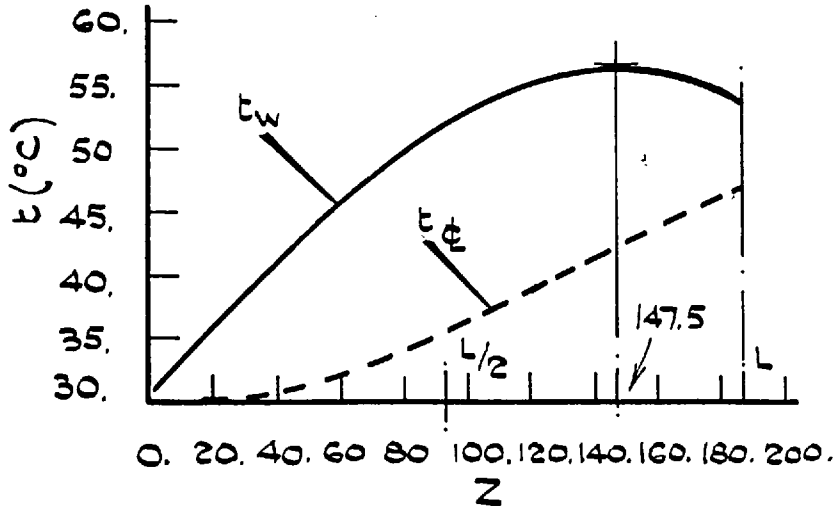

FIG (5.40) AXIAL VARIATIONS OF THE WALL AND THE CENTRELINE TEMPERATURES (FOR THE G50 W MODEL)

(a.3) The Temperature Profiles

Axial variations of t_w and horizontal distribution of the temperature are predicted by the computer program and are represented by Figs. (5.40) - (5.41) respectively.

According to Fig. (5.40), t_w values increase as the fluid moves downstream. Its peak value, $t_w = 56.4\ ^oC$ occurs at Z = 147.5 which is beyond the middle of the channel.

The reason is that after $\dot{q}''_w$ has its peak in the middle of the channel and starts to decrease, the effects of this decrease on the fluid are felt some distance along the channel. It may be suggested that there is a "phase-lag" between the $\dot{q}''_w$ and the t_w profiles. This is in agreement with the results of the well-known Ginn's equation.

Fig. (5.41) shows the fluid temperature distribution across the channel at different axial positions. It is noted that near the entry to the channel, the profile is rather flat at the centre and sharp near the walls. This trend continues up to the axial position where $t_{w_{max}}$ occurs, (i.e. Z = 147.5). Beyond this point, because of the reduction in t_w, a higher proportion of the heat-input is absorbed by water layers near the centre. This in turn brings about a higher rate of increase in $t_{\underline{\ell}}$ values than before and, consequently, near the end of the channel, the temperature profile becomes more flat, (Z = 187.5, $t_{\underline{\ell}} = 46.7\ ^oC$). Fig. (5.40) shows $t_{\underline{\ell}}$ variations along the channel.

(a.4) The Nu Profile

Fig. (5.42) shows axial variations of the Nusselt number, Nu. For the axial positions before the middle of the channel, i.e. Z < 93.75, where the heat-flux is increasing in the direction of the flow, the Nu values always exceed their asymptotic value of 8.23

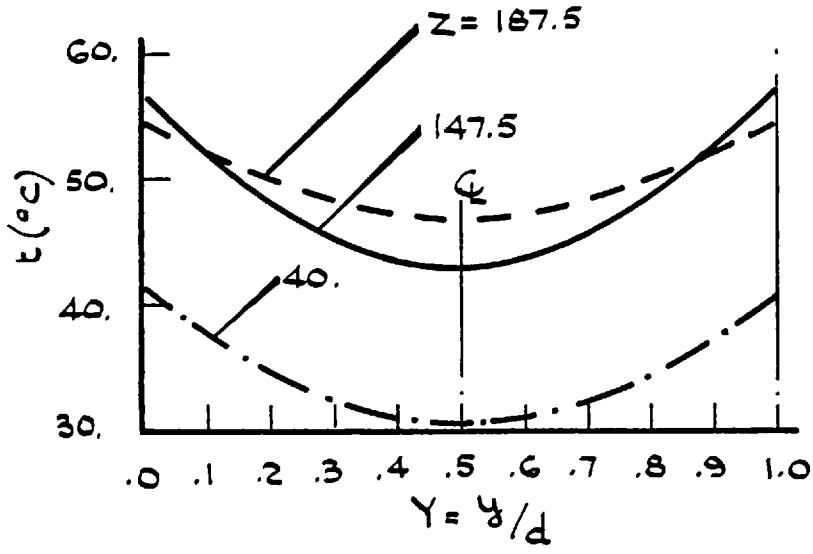

FIG (5.41) HORIZONTAL TEMPERATURE DISTRIBUTION AT DIFFERENT AXIAL LEVELS (FOR THE 650.W MODEL)

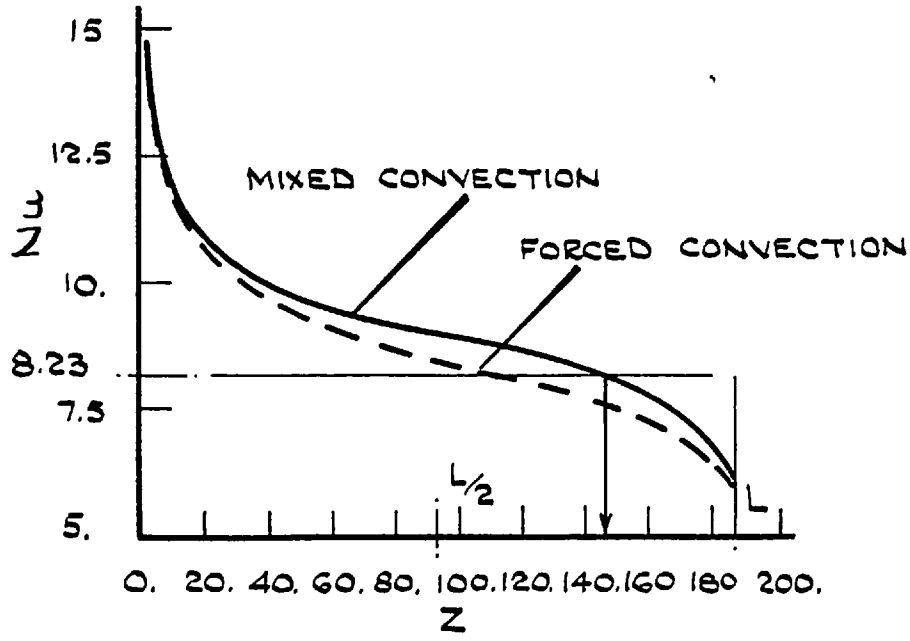

FIG. (5.42) AXIAL VARIATION OF THE NUSSELT NUMBER (FOR THE 650.W MODEL)

pertaining to the case of uniform wall heat-flux. In the region beyond Z = 140 (i.e. z/L = 0.746), characterised by an axial decrease of heat-flux, the Nu values start to fall below the asymptotic value and at the end of the channel, Nu = 6.05 · This may also be noted by examining the horizontal temperature profile, Fig. (5.41). For the region beyond Z = 140, the increase in t_{ℓ} values becomes significant. This process forces the profile to assume a more flat shape. These predictions for Nu are in agreement with those of Nijsing et al (1973), who obtained a similar Nu profile for sinusoidal heating along a round tube.

(a.5) The Pressure Profiles

Pressure distributions across the channel at three different axial positions are shown on Fig. (5.43). The pressure is less near the walls than at the centre and the shape of these profiles is inverted with respect to that of the temperature profiles across the section, Fig. (5.41).

Fig. (5.44) shows the axial variation of the integrated pressure, p_{mean}, which is calculated based on the formula:-

$$p_{mean} \cdot w \cdot d = \int_{o}^{d} p \cdot w \cdot dy$$

The profile is nearly linear and as a consequence, the pressure loss factor, f_p is nearly constant. The predictions show that:-

$$f_p = - \frac{dp_{mean}}{dZ} = 0.075 \quad (\text{c.f. } f_{p.ideal} = \frac{24}{Re_{mD}} = 0.0627)$$

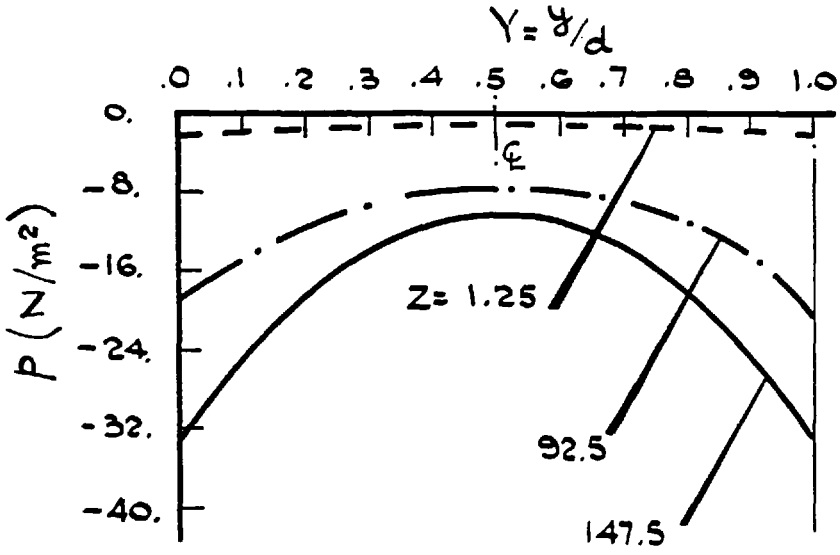

FIG (5.43) HORIZONTAL PRESSURE DISTRIBUTION AT DIFFERENT AXIAL LEVELS (FOR THE 650W MODEL).

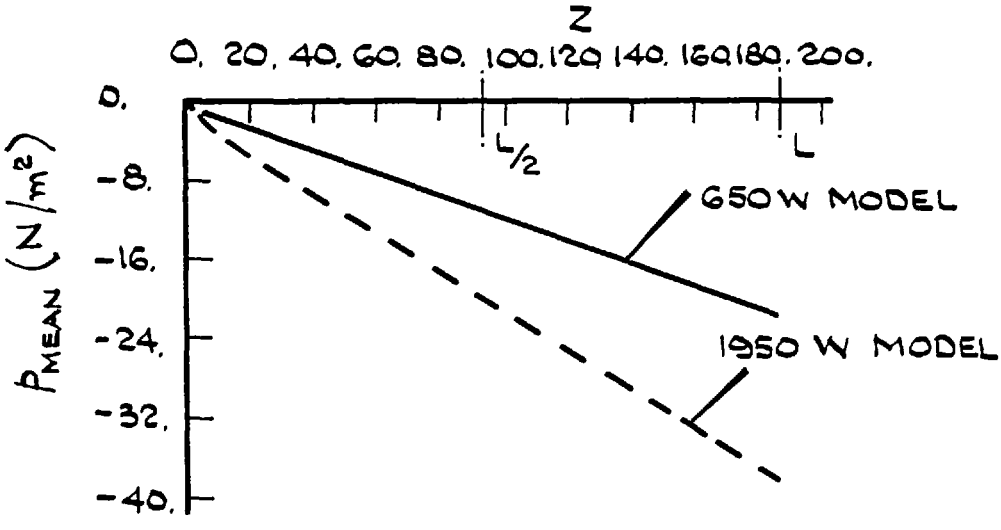

FIG. (5.44.) AXIAL VARIATIONS OF P_{MEAN} FOR BOTH OF THE MODELS.

The difference between the predicted and the ideal values of f_p depends on the total heat-input to the model through the U velocity profile, Fig. (5.37). In other words, the difference is reduced as the U profile gets closer to the parabolic shape. This difference also suggests that the calculations, based on the $f_{p.ideal}$, underestimate the values of pressure drop.

For the mixed-convection cases, it is always useful to predict the extra pressure needed at the entry to the channel. This is done by predicting at each axial position the difference between the "friction" and the "buoyancy" pressure terms, where the "buoyancy" term is in turn the difference between the static pressure drop which actually occurs with the heated fluid, and the static pressure drop which occurs in the channel if the fluid density remained at its entrance value, i.e.:-

$$p_{o(Extra)} = \int_{o}^{z} \{\rho_{mean}\,(\delta) - \rho_o\} \cdot g \cdot d\delta - \Delta p_f\,(z)$$

Therefore, this variable represents the extra pressure necessary to force the fluid through the channel and must be zero for the pure natural-convection cases. Fig. (5.45) shows the axial variation of $p_{o(Extra)}$. This figure suggests that the heat transfer mode in the model is not a pure-natural convection because the $p_{o(Extra)}$ is positive at the end of the channel.

The magnitude of the "buoyancy" and the "friction" terms in the above-mentioned formula are compared on Fig. (5.46). This figure shows axial variation of the index representing the ratio of the two terms at each axial position, i.e.:-

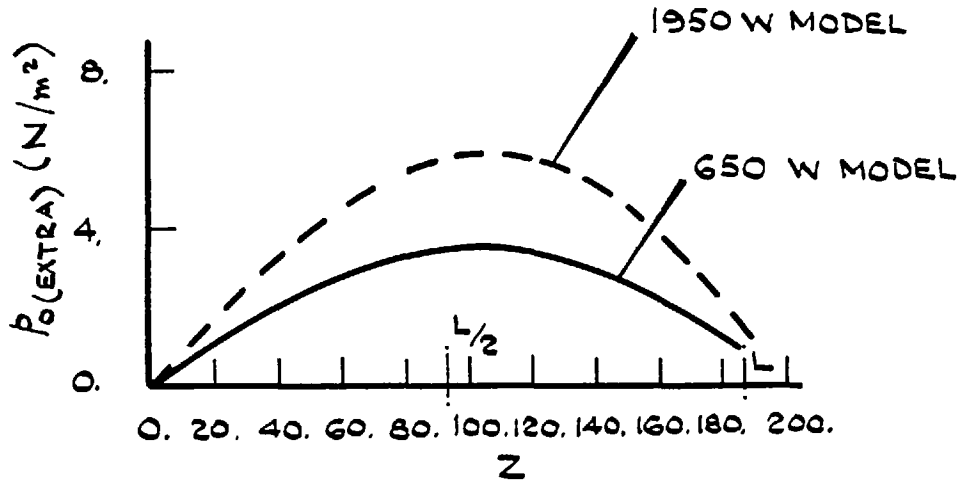

FIG (5.45) AXIAL VARIATIONS OF $p_{o(EXTRA)}$

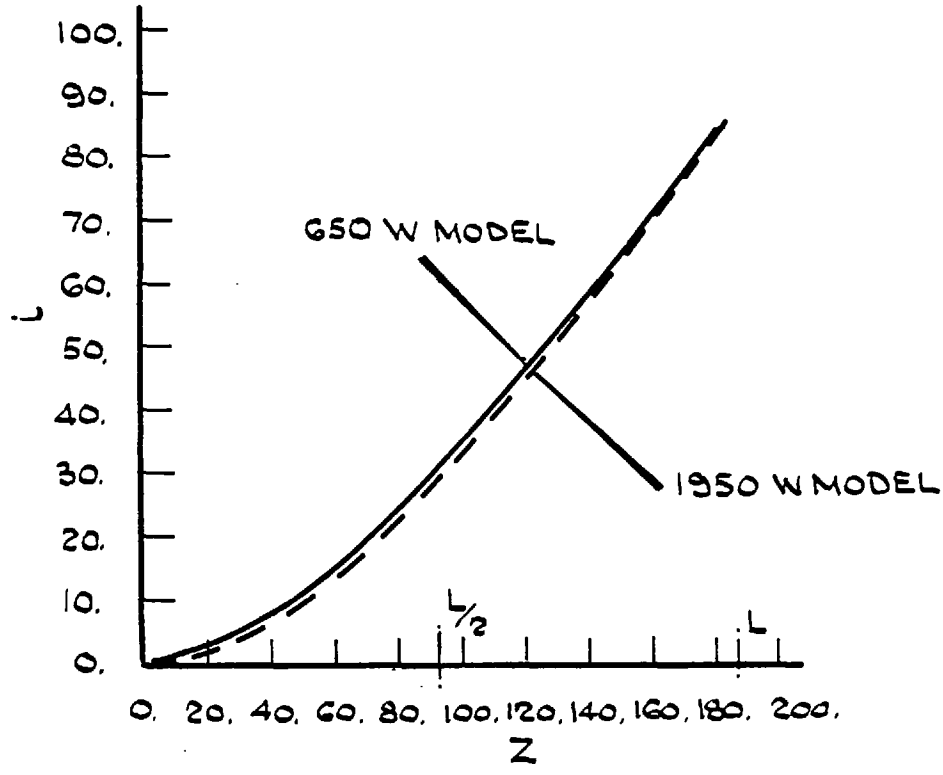

FIG (5.46) AXIAL VARIATIONS OF THE MIXED-CONVECTION INDEX, L.

$$i = \frac{\int_0^z \{\rho_{mean}\ (\delta) - \rho_o\} \cdot g \cdot d\delta}{\Delta p_f\ (z)} \times 100$$

Therefore:-

For pure natural-convection $i = 100$

For pure forced-convection $i = 0$

For the 650 W Model, this index at the end of the channel is; $i = 88.8$.

(b) Results for the 1950 W Model

The computer predictions for this model are represented by Figs. (5.47) - (5.49). For comparison, the predictions of the 650 W Model are also shown on these figures.

(b.1) The U Velocity Profile

For this Model, the U profile develops along the channel in a similar manner to that of the 650 W Model, Fig. (5.37). The only differences being in the axial positions where the maximum and the minimum values of U_{ℓ} occur, i.e.:-

$U_{\ell}{}_{.Max} = 1.447$, at $Z = 15$ (c.f. $U_{\ell}{}_{.Max} = 1.476$, at $Z = 10$)

$U_{\ell}{}_{.min} = 1.153$, at $Z = 147.5$ (c.f. $U_{\ell}{}_{.min} = 1.337$, at $Z = 130$)

Axial variations of U_{ℓ} for this model are also shown on Fig. (5.38). It is noted from this figure that for the present model, the effects

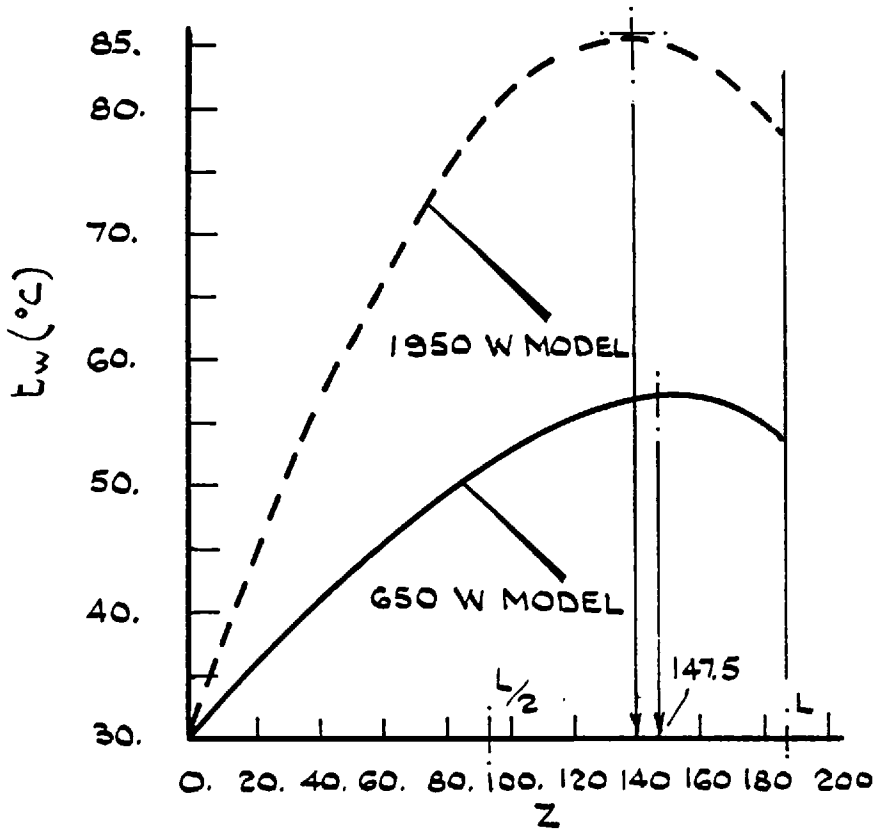

FIG (5.47) AXIAL VARIATIONS OF WALL TEMPERATURE.

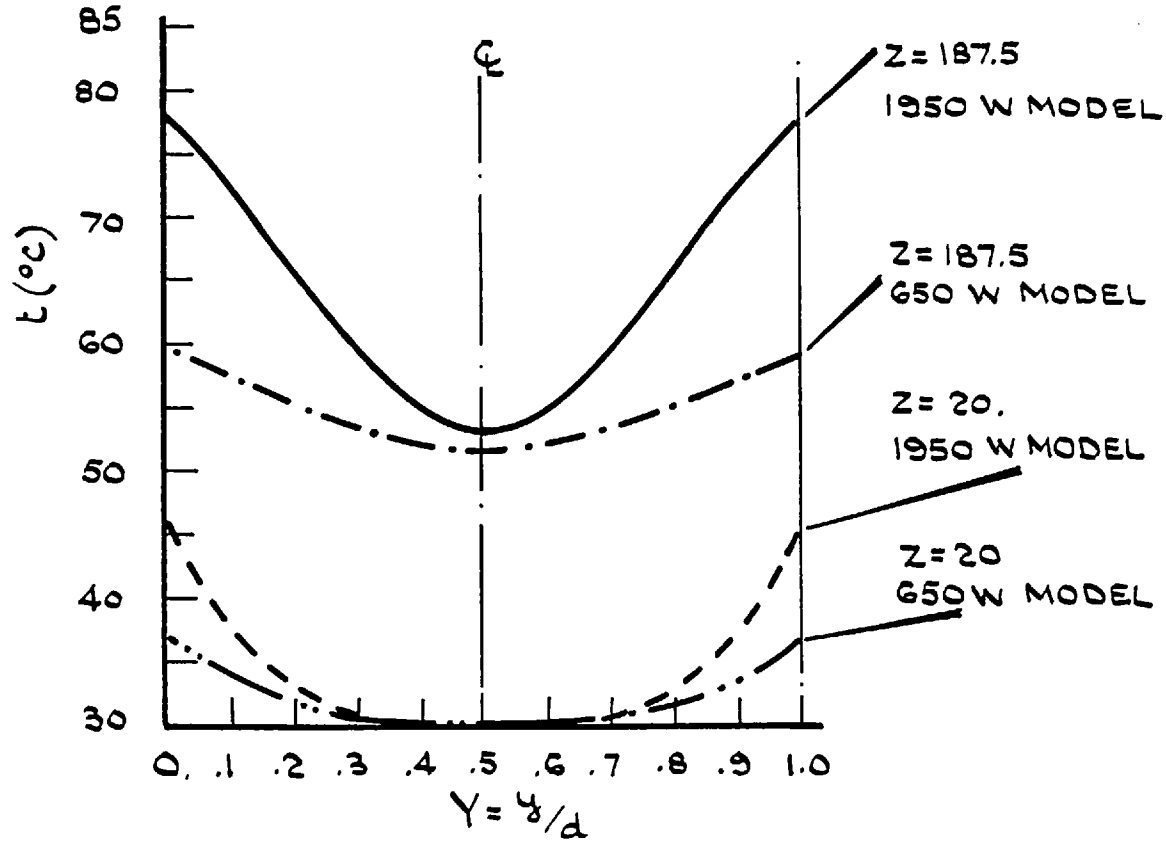

FIG (5.48) HORIZONTAL TEMPERATURE DISTRIBUTION AT TWO AXIAL LEVELS FOR THE TWO MODELS.

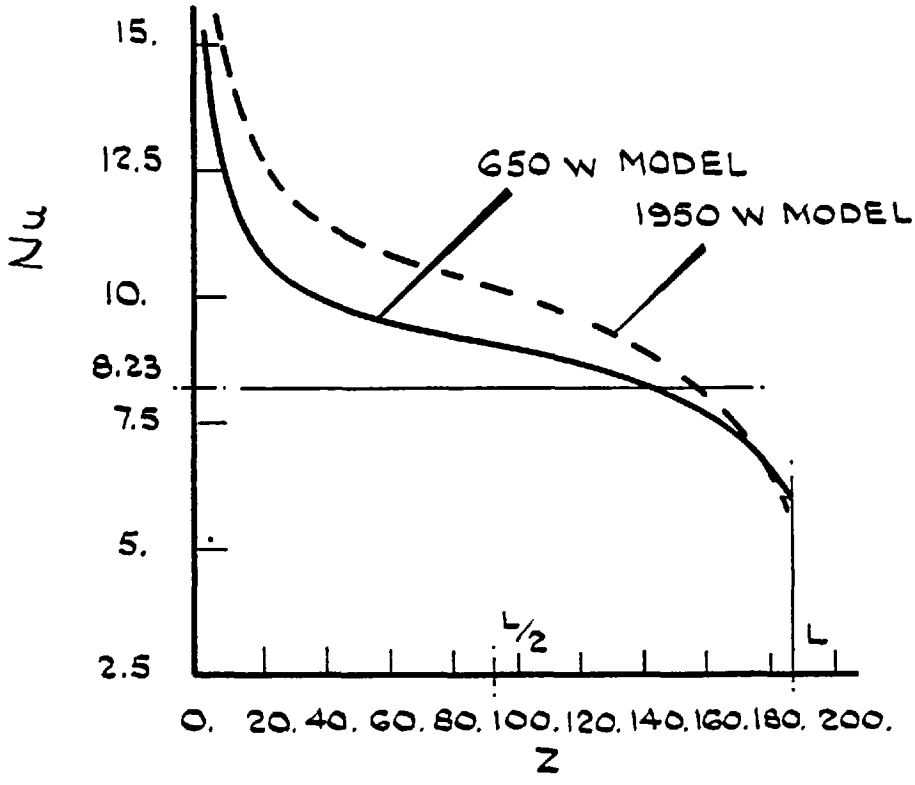

FIG. (5.49) AXIAL VARIATIONS OF THE NUSSELT NUMBER FOR BOTH OF THE MODELS.

of "natural-convection" in distorting the U profile are stronger (U_{ℓ}'s are less than those of the 650 W Model at the same axial positions). This is because of higher density reductions resulting from a higher temperature rise throughout the channel (30.55 ^{o}C for the present model c.f. 18.7 ^{o}C for the 650 W Model).

(b.2) The Temperature Profiles

Fig. (5.47) shows the wall temperature for both of the models. It is noted that $t_{w.Max}$ for the 1950 W Model is much higher than that of the 650 W Model, and occurs at a shorter axial distance:-

$t_{w.Max}$ = 86 ^{o}C at Z = 140 (c.f. $t_{w.Max}$ = 56.4 ^{o}C at Z = 147.5)

On Fig. (5.48), horizontal temperature distributions for the two models are shown. According to this figure, there is a higher gradient near the wall for the present model. This results in a higher Nusselt number as shown on Fig. (5.49).

(b.3) Comparisons of the Nusselt Number for the Two Models

Fig. (5.49) represents the axial variations of Nusselt number for both of the models. It is noted that Nu values for the present model are higher throughout the channel. However, near the exit, this is not the case. The reason is thought to be that for the present model, $t_{w.Max}$ occurs at a smaller Z value, Fig. (5.47). Therefore, in the cooling process of the heated walls, there seems to be more time (distance) for t_w to decrease, as compared to the 650 W Model. This leads to a lower rate of heat transfer and, consequently, lower Nu values near the exit. As for the 650 W Model, these results

are in agreement with those of Nijsing et al (1973).

(b.4) The Pressure Profiles

Fig. (5.44) shows the axial variations of the integrated pressure, p_{mean}. It is noted that the profile is nearly linear with a bigger slope than that of the 650 W Model. The higher Reynolds number of the present model is responsible for that, (238.5 c.f. 131.3). The pressure loss factor is:-

$$f_p = -\frac{dp_{mean}}{dZ} = 0.038 \text{ (c.f. } f_{p.ideal} = \frac{24}{Re_{mD}} = 0.033)$$

On Fig. (5.45) is shown the extra needed entrance pressure, $p_{o(Extra)}$ for the two models. According to this figure, $p_{o(Extra)}$ for the present model is positive at the end of the channel (similar to the 650 W Model).

It is important to notice that when the mixed-convection index, i is plotted against the axial coordinate, Z the curve is nearly the same, (strictly speaking slightly less), as that of the 650 W Model, Fig. (5.46). This curve shows that despite the differences in data, as far as the relative magnitude of the "buoyancy" and the "friction" pressures are concerned, the two models are the same, (e.g. at the exit, i = 88.80 for both of the models).

This was to be expected because according to Burholt (1974), the data for these two models were obtained based on assuming a constant f_p and equalizing the frictional and the buoyancy pressure terms at the end of the channel. Moreover, according to an order of magnitude analysis, the dominant parameter for the mixed-convection problems is Gr_D/Re_D^2 which for the two models is:-

$Gr_D/Re_D^2 = 2.020$ For the 650 W Model, Table (5.5).

$Gr_D/Re_D^2 = 2.124$ For the 1950 W Model, Table (5.5).

The closeness of the parameter for the two models suggest that the "degree" of mixed-convection for both of them is the same. On the other hand, by recalling the definition of i (i.e. ratio of the buoyancy and the frictional pressure terms), it is concluded that the index i and the parameter Gr_D/Re_D^2 have the same physical meaning but with different scales. Therefore, the profile for i throughout the channel must be nearly the same for both of the models because their Gr_D/Re_D^2 parameter is nearly the same, Fig. (5.46).

5.3.4 Effects of Reynolds Number, Parabolic U_o Profile, and Asymmetric Heating on the Predictions for the Two Models

In order to generalize the results of the 650 W and 1950 W model to cover a wider variety of cases, three following cases were considered:-

(i) The 650 W Model is re-solved for two Re's, (one below and one above what is given in Table (5.5) i.e. Re = 100, 200 c.f. Re = 131.3).

(ii) A parabolic U_o profile, instead of the uniform one, is used for the solution of the 650 W Model.

(iii) Asymmetric heating is exerted on the 1950 W Model

by assuming that one of its walls is being thermally insulated.

In the following, the results for these cases are discussed.

5.3.4.1 Effects of Reynolds Number

These effects are most significant on the pressure and its related parameters. Fig. (5.50) shows that the axial variation profile of $p_{o(Extra)}$ is in the same direction as Reynolds number. For the mixed-convection index, i the effects are considerable, Fig. (5.51). To give an example, the i values at the middle of the channel are:-

i = 32 → (For the 650 W Model , Re = 131.3)

i = 13 → (For the 650 W Model but Re = 200)

i = 52 → (For the 650 W Model but Re = 100)

The physical explanation of these changes is that by applying a higher Re, which means a higher mass flow rate, the temperature rise throughout the channel is reduced. As a result, the "buoyancy" term of the pressure is also lowered, leading to lower i and higher $p_{o(Extra)}$ values. By the same argument, it is concluded that lowering the Reynolds number boosts i values and reduces $p_{o(Extra)}$ for the channel.

When Re is changed, the wall temperature and the U velocity profiles along the channel, retain their overall shape. However, changes do take place in the magnitude and the axial position of their peaks and troughs. These are shown in the table given on the next page.

According to this table, when Re is decreased, $t_{w.Max}$ increases and occurs at a larger axial distance. Moreover, because

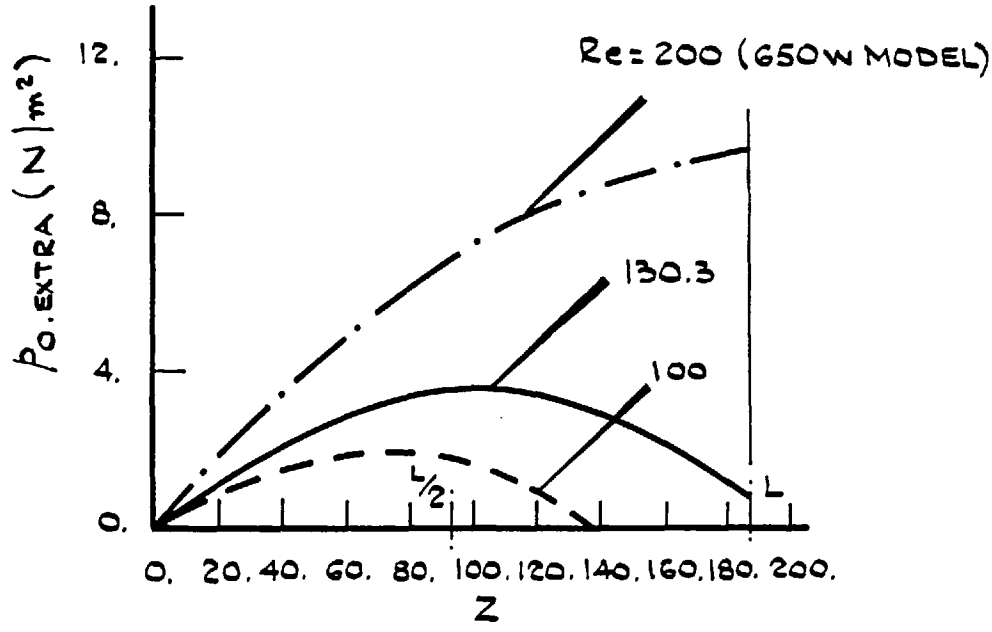

FIG(5.50) AXIAL VARIATIONS OF $P_{o(EXTRA)}$ WITH SEVERAL Re's FOR THE 650W MODEL.

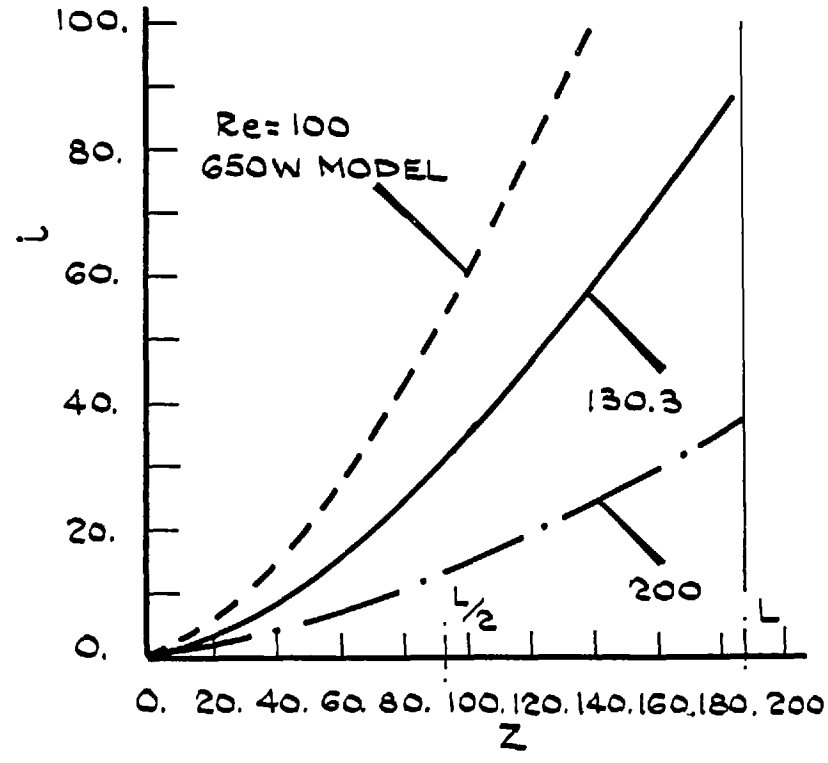

FIG(5.51) EFFECTS OF REYNOLDS NUMBER ON THE MIXED-CONVECTION INDEX L

EFFECT OF REYNOLDS NUMBER ON THE COMPUTER PREDICTIONS

Re	$t_{w.Max}$ (^oC) / Z	$U_{\ell.Max}$ / Z	$U_{\ell.min}$ / Z
100.0	61.1 / 157.5	1.474 / 7.5	1.281 / 132.5
131.3 *	56.4 / 147.5	1.476 / 10.0	1.337 / 130.0
200.0	51.32 / 140.0	1.477 / 15.0	1.390 / 127.5

* The 650 W Model

U_{ℓ} VALUES ALONG THE CHANNEL

Z	Uniform U_o Profile $U_o = 1$	Parabolic U_o Profile $U_o = 6Y(1 - Y)$
0.00	1.000	1.500
1.25	1.284	1.498
2.50	1.399	1.495
5.00	1.460	1.489
10.00	1.476	1.479
15.00	1.469	1.470
20.00	1.461	1.461
25.00	1.452	1.452
100.00	1.349	1.349
187.50	1.399	1.399

of the increase in the temperature rise throughout the channel, the natural-convection effects are amplified and, consequently, the shape of the U velocity profile will be more distorted.

5.3.4.2 Effects of the Parabolic U_o Profile

So far, a uniform U_o profile is assumed for all of the cases. In order to generalize the results to cover also the non-uniform U_o profile, the 650 W Model mentioned in (5.3.3), is re-solved with this additional assumption. In the table, given on the previous page it is shown how a parabolic U_o profile might affect the predictions.

According to this table, only at the entrance region, i.e. $Z < 20$, do there exist any differences, and these gradually diminish along the channel. Other parameters, namely, t_w, Nu, follow the same path. Therefore, it is concluded that the effects of the parabolic U_o profile are limited to the entrance region of the channel.

5.3.4.3 Effects of Asymmetric Heating on the Computer Predictions of the 1950 W Model

The problem of heat transfer in a flat duct in the case of asymmetrical one-sided heating is relatively rare in the literature. Following the results of the asymmetric heating for prescribed and uniform $\dot{q}''_w$ in (5.2.1) and (5.2.4) it is intended to extend the result to cover non-uniform $\dot{q}''_w$ profiles also. This is done by re-solving the afore-mentioned 1950 W Model assuming that one of its walls is thermally insulated, i.e.:-

$$\begin{cases} \dot{q}''_{wi} = 3.312 \text{ Cos } (0.043z - 1.291) \\ \dot{q}''_{wo} = 0 \end{cases}$$

where $\dot{q}''_w$ and z are measured in (w/cm^2) and (cm) respectively.

Fig. (5.52) shows the U velocity profile at the exit of the channel for this case. According to this figure, the profile is also non-symmetric and the U values near the heated wall are comparatively large. This is attributed to the fact that at this region, the reduction in μ value is more significant than in the rest of the cross-section. The reduction is followed by a lower resistance to the flow which leads to the large magnitudes of U. For comparison, the corresponding U profile for the 1950 W Model (symmetrical heating) is also given.

The axial variation of Nu_i also reflects the effects of the asymmetric heating. According to Fig. (5.53), Nu_i values are less, compared to their corresponding values obtained for the 1950 W Model, throughout the channel. It is only near the exit of the channel, where Nu_i values fall below 5.385 (which was obtained for the asymmetric but uniform heating of a forced-convective regime).

Other variables, such as t_w and i, are also affected. On the heated-wall:-

$$t_{w_{i.Max}} = 80\ ^{o}C \text{ at } Z = 135$$

(c.f. $t_{w_{i.Max}} = 86\ ^{o}C$ at $Z = 140$ for symmetrical heating)

while the insulated-wall's temperature changes are not significant. As for the mixed-convection index, i the effects are substantial, Fig. (5.54). This is due to the reduction of the total heat-input by half. As a result, at the exit of the channel:-

$i = 40$ (c.f. $i = 88.8$ for the 1950 W Model)

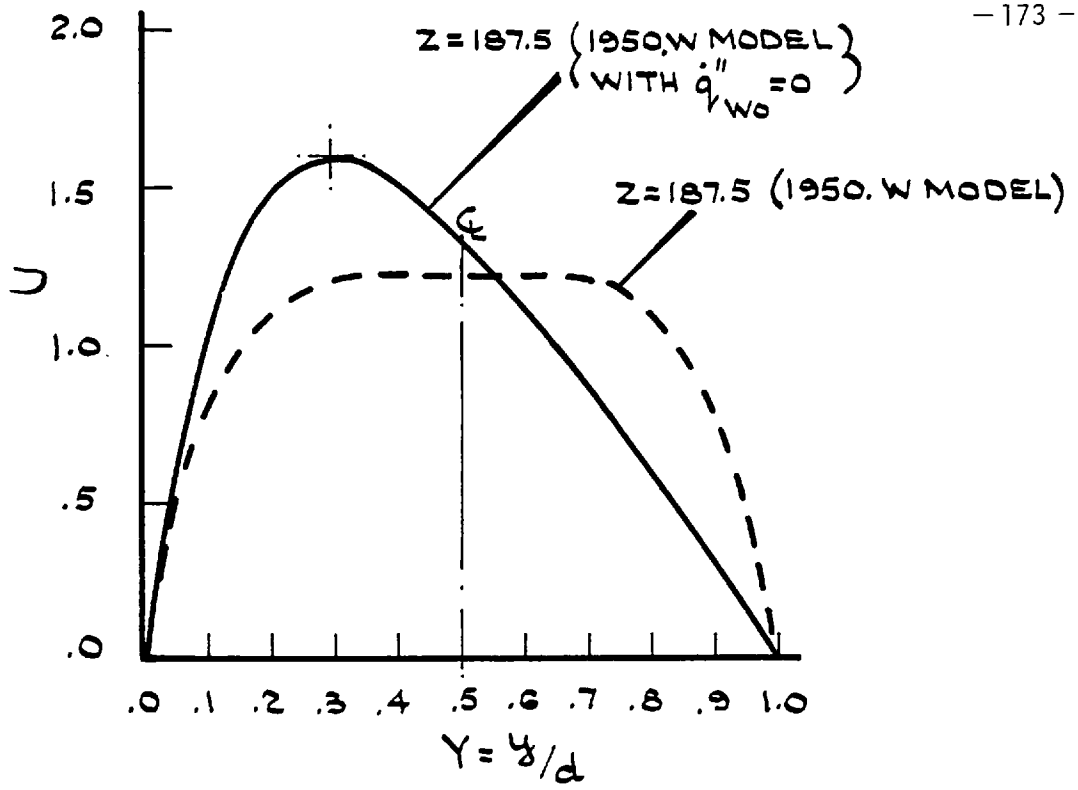

FIG(5.52) THE U PROFILE AT THE EXIT OF THE CHANNEL FOR THE SYMMETRICAL AND THE ASYMMETRICAL HEATING.

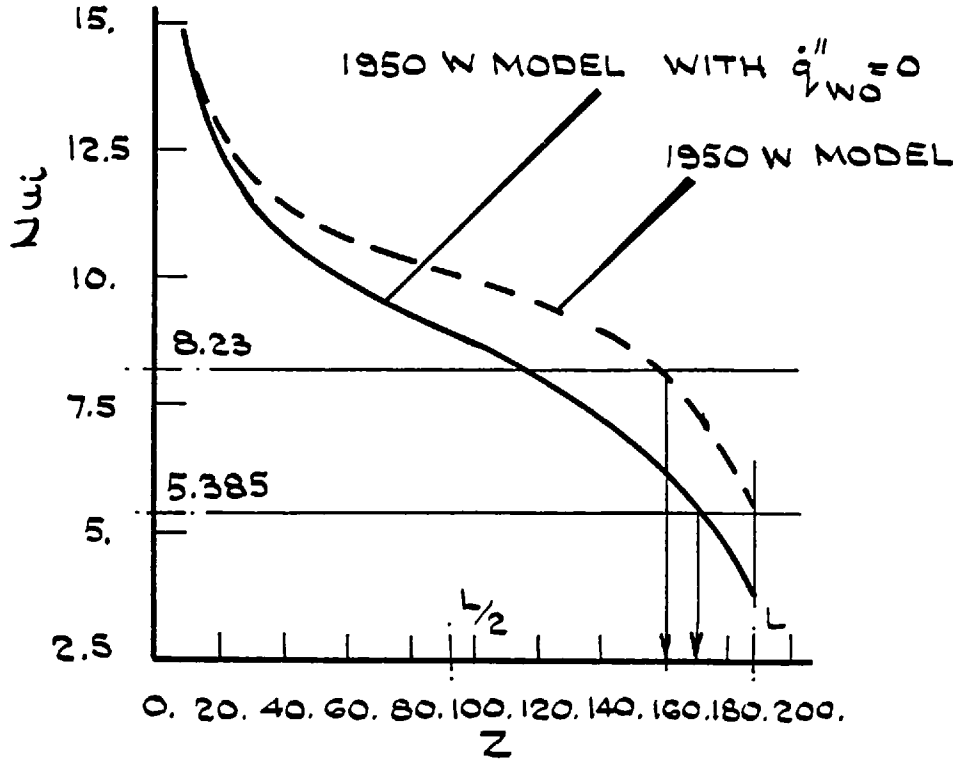

FIG(5.53) AXIAL VARIATIONS OF Nu_i FOR THE SYMMETRICAL AND THE ASYMMETRICAL HEATING.

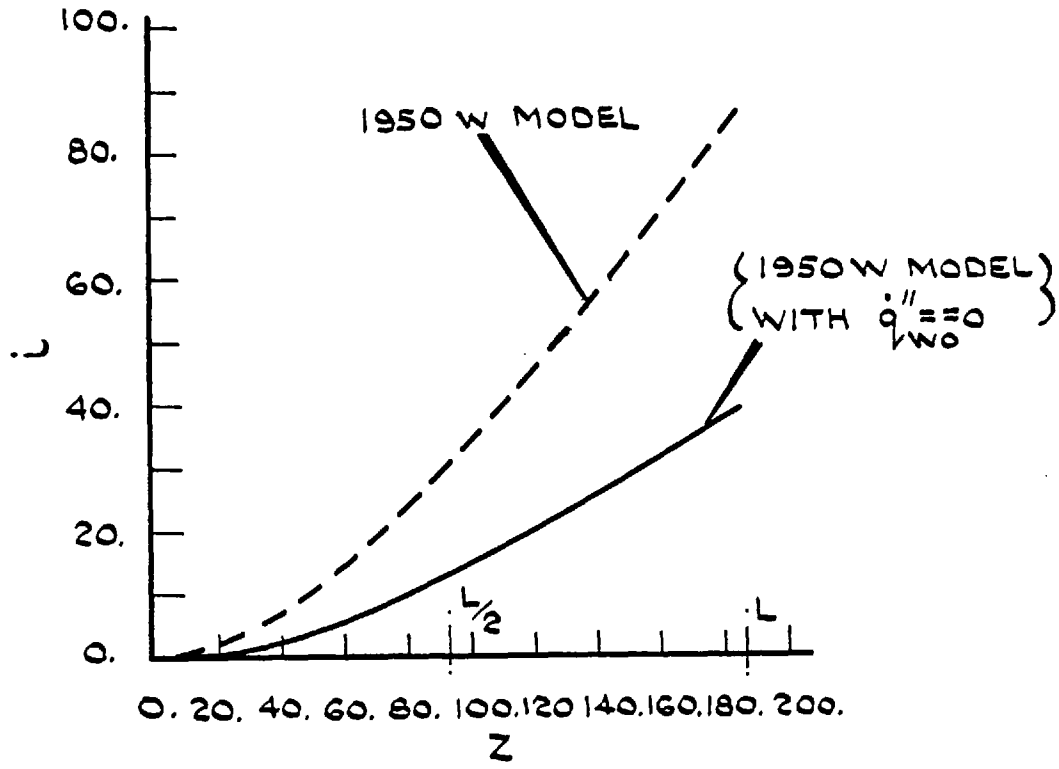

FIG(5.54) AXIAL VARIATIONS OF THE MIXED-CONVECTION INDEX i, FOR THE SYMMETRICAL AND THE ASYMMETRICAL HEATING.

5.3.5 The Main Conclusions for Mixed-Convection Heat Transfer in Channels With Prescribed $\dot{q}''_w$ Profiles

The following conclusions are obtained for three types of heating , namely: uniform, sinusoidal and asymmetrical.

(i) Uniform Prescribed $\dot{q}''_w$

1. Computer predictions for the U profile, at the exit of two typical channels, are in agreement with what was experimentally obtained by Vernier (1962). Quantitatively, the predicted U values are slightly higher in the centre of the channels and lower near the walls, Figs. (5.27), (5.30). For both of the examples, the computer predictions show a significant improvement on Vernier's own theoretical results.

2. The temperature profiles at the exit of the channels also agree with their corresponding experimental results. However, the predictions seem to be slightly higher near the central region, Figs. (5.28), (5.31).

3. Nusselt numbers, predicted at different axial positions, are within 3% of their corresponding experimental values, Figs. (5.29), (5.32).

4. The computer program may be equally used to solve also for asymmetric heating cases. Predictions for a typical channel with one wall heated while the other wall is thermally insulated show that the U profile will be also non-symmetrical, Fig. (5.33). The U values are higher near the heated-wall. Nusselt numbers throughout the channel

are higher than their corresponding values obtained for the forced-convective regimes, Fig. (5.35). These results are in agreement with those of Savkar (1970).

(ii) Sinusoidal Prescribed $\dot{q}''_w$

Two channels of the same geometry were considered. These two were chosen to model the "hot-channel" in the core of the University of London Reactor (ULR) at two different power levels (108.5 KW and 325 KW respectively). These models are referred to as 650 W and 1950 W models, after their total heat ratings.

Comparison of the predictions for these two models shows that:-

1. The U velocity profiles, which continuously develop along the channel, are rather flat. Particularly, there is no sign of an inflexion in these profiles, Fig. (5.37). Therefore, for the two models, the possibility of transition into an unstable-flow is not predicted.

2. In the 1950 W Model, the maximum wall temperature is higher than the 650 W Model and occurs at a shorter axial distance, Fig. (5.47).

3. For the 1950 W Model, Nu is generally bigger than that of the 650 W Model, Fig. (5.49). However, for both of them, in axial positions before the middle of the channel, where the heat-flux is increasing in the direction of the flow, the Nu values always exceed their asymptotic value of 8.23 pertaining to the case of uniform $\dot{q}''_w$. In the regions beyond z/L = 0.75, characterised by an axial decrease of $\dot{q}''_w$, the Nu values start to fall below the asymptotic value and at the end of the channel, Nu = 5.67 and 6.05 for the two models respectively.

The sharper-falling trend for the 1950 W Model is thought to be due to the fact that its $t_{w.Max}$ occurs at a shorter distance.

These results are in general agreement with those obtained by Nijsing et al (1973) for sinusoidal heating in a round tube.

5. The axial variation of p_{mean} for both of the models is nearly linear, Fig. (5.44). But their pressure loss factors are higher than the ideal value of $24/Re_{mD}$ which is traditionally used for these types of problems. These predictions suggest that the results of the calculations based on the ideal f_p are underestimates.

The relative importance of the "buoyancy" and the "frictional" pressure terms is quantified by defining the mixed-convection index, i. The index varies between 100 and 0 for the pure-natural convection and pure-forced convections respectively. Fig. (5.46) shows that this index is very close for both of the models throughout the channel. At the exit, the condition i = 88.8 suggests that some extra pressure, equal to the value shown on Fig. (5.45), is needed to force the fluid in both of the models.

It is also seen, that the index i, and the parameter Gr_D/Re_D^2, have the same physical meaning but with two different scales.

6. Effects of a parabolic U_o profile, instead of the universally assumed uniform profile, are limited to the entrance region and do not affect the overall predictions.

7. Re-solving the 650 W Model for two other Reynolds numbers, one below and one above the original Re, shows that when Re is decreased:-

(a) Natural-convection effects become more significant, and, consequently, the U velocity profile is more distorted.

(b) The mixed-convection index, i increases drastically, Fig. (5.50).

(c) $t_{w.Max}$ increases and occurs at a larger axial distance.

These trends are reversed for an increase in the Reynolds number.

(iii) Asymmetrical Heating

This part of the study is based on the computer predictions for two typical channels which both have one thermally insulated wall, while the other wall is set at a uniform/sinusoidal prescribed heat-flux. The main conclusions are:-

1. The U velocity profile will be non-symmetrical with comparatively large U values near the heated-wall, see Figs. (5.33) and (5.52) for the uniform and the sinusoidal heating cases respectively. As the fluid moves further downstream, the asymmetry of the profile will be amplified, Fig. (5.33). These results are in good agreement with those of Savkar (1970).

2. Throughout the channel, the Nu values for the heated-wall are lower than their corresponding values with symmetrical heating, see

Figs. (5.35) and (5.53) for the above-mentioned two examples.

3. In the two examples, the exchange of the heated and the insulated walls reflect directly on their results (error < 2%). This shows that the computer predictions do not depend on the choice of the heated-wall. In other words, the predictions are independent of the system of coordinates chosen for the solution.

5.4 Mixed-Convection in Vertical Channels Having Prescribed Wall Temperature Profiles

As discussed in Chapter (3), the solution technique can also solve for the cases with prescribed wall temperature. Of particular interest are those cases with non-uniform t_w profiles. For this purpose, a typical channel with the data of Table (5.6) is solved for with the t_w profile shown on Fig. (5.55). This profile is specially chosen because it is obtained as the solution of a uniform $\dot{q}''_w$ case. Therefore, ideally the heat-fluxes which will be obtained as the solution of the present case, will be constant throughout the channel and also be equal to the $\dot{q}''_w$ value which is used in the prescribed $\dot{q}''_w$ case.

It is noted that the results of this part of the study serve as a cross-checking of the solution technique developed for the present thesis.

5.4.1 Computer Predictions for the Prescribed t_w Profile

Fig. (5.56) shows axial variation of the $\dot{q}''_{wi}$ or $\dot{q}''_{wo}$ predicted by the program. It is noted that the profiles are nearly a straight line parallel to the abscissa. This confirms that the accuracy of the solution technique is good. However, at the entrance region

TABLE (5.6) DATA FOR THE PRESCRIBED WALL-TEMPERATURE CASE

Data \ Reduced Data	w/d	Z_{max}	$\dot{Q}_{tot}$ (w)	$\dot{m}$ (gr/sec)	Δt_{tot} (C^o)	t_m (C^o)	t_{out} (C^o)	Re	Re_{mD}	Re_D	Gr_D	Gr_D/Re_D^2	Pr
t_{in} = 21.1 ^oC, d = 0.538 cm, w = 8.45 cm, L = 200 cm, u_o = 7.62 cm/sec, $\dot{q}''_w$ = 1.34 (w/cm^2)	15.70	371.75	4529	33.14	32.76	37.48	53.86	419.7	1158	839.4	1.24×10^6	1.75	6.503

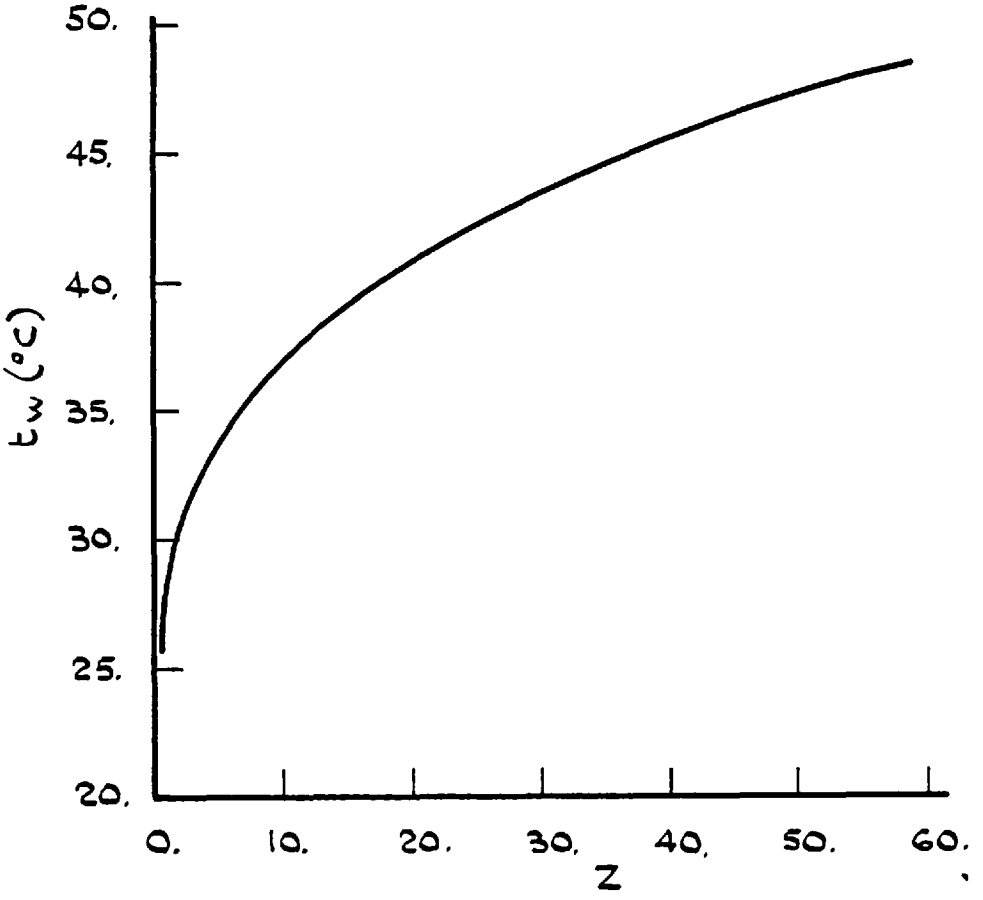

FIG (5.55) AXIAL VARIATION OF THE t_w PROFILE USED FOR THE CROSS CHECKING.

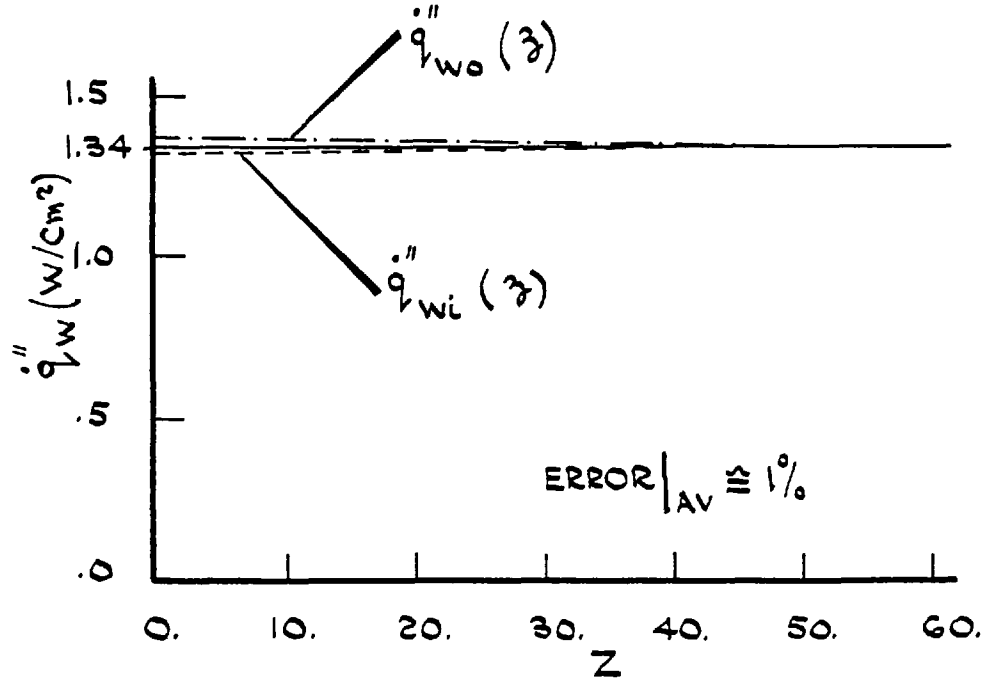

FIG (5.56) THE UNIFORM $\dot{q}''$ AND IT'S RECALCULATED VALUES ON THE TWO CHANNEL WALLS.

there are small differences, (e.g. at Z = 10. Error $\cong$ 1%).

Based on the comparison of the assumed and the obtained wall heat-flux values, it is concluded that the solution technique produces reliable and accurate predictions for both prescribed $\dot{q}''_w$ or t_w cases.

Also, the reproduction of the results is extended to the other parameters such as: U, V, P, Nu and the mixed-convection index, i.

CHAPTER 6

EXPERIMENTAL STUDY - DESCRIPTION OF THE MIXED-CONVECTION APPARATUS

6.1 The Purpose of the Experimental Study

Very little data, or in some cases none, are available about mixed-convection heat transfer in vertical channels with arbitrarily heated walls. The development of boilers, transformers, turbines and low-power nuclear reactors has amplified attention towards a thorough study of this problem. The purpose of this test-rig is to investigate such a problem with special reference to the cases where the channel walls bear identical sinusoidal prescribed heat-fluxes and prove their present theoretical predictions. The two special features of the rig are:-

(i) Heating plates with sinusoidal heat-flux profile.

(ii) Controllable pressure at the channel entrance.

6.2 Description of the Test-Rig

The general arrangement of the test-rig is shown on Fig. (6.1) and also on the Photos. (1) - (3). According to this figure, the rig may be divided into two main parts, namely, the four tanks and the test-section. In what follows, these two main parts, as well as their function in the rig, are described.

6.2.1 The Four Tanks

These tanks are located in different parts of the rig and are named according to their function as follows:-

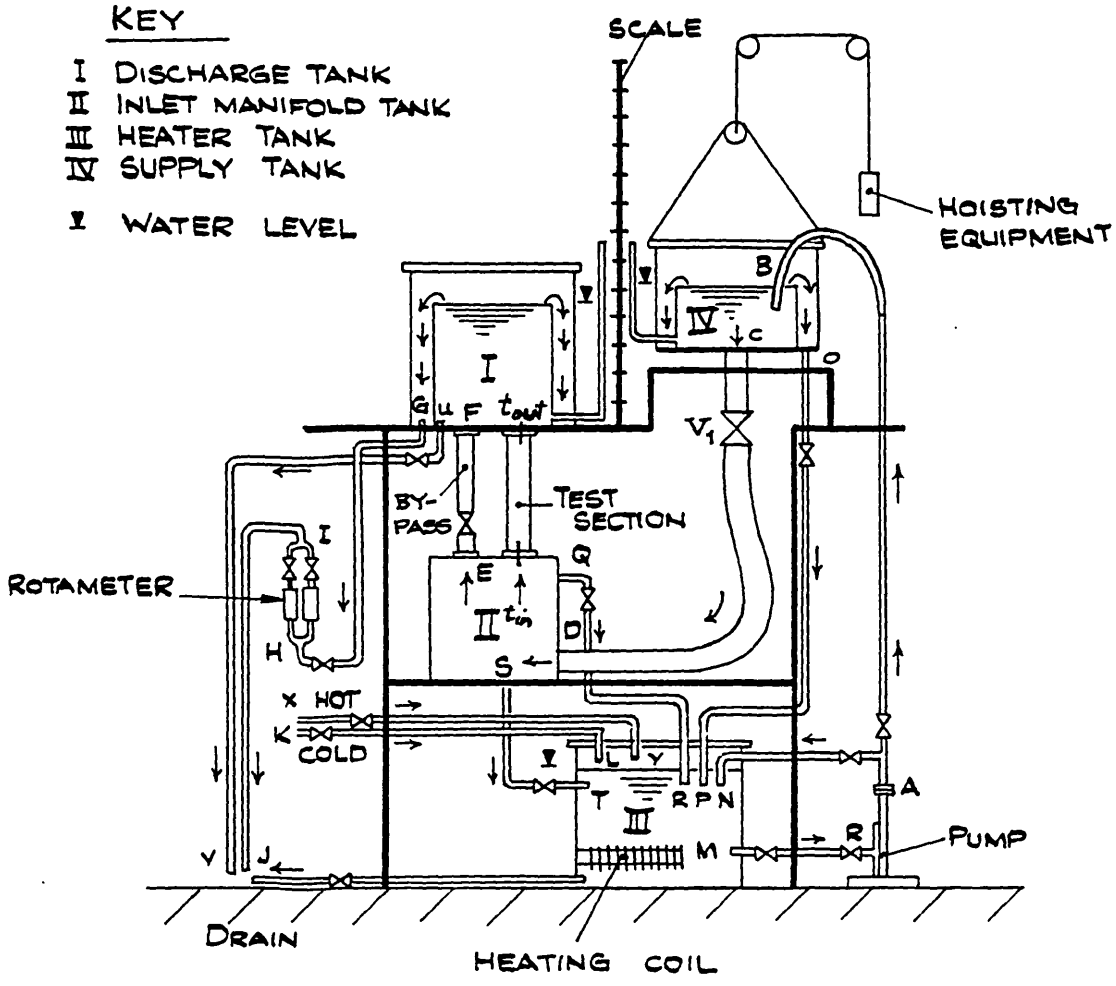

FIG. (6·1): GENERAL ARRANGEMENT OF THE TEST RIG.

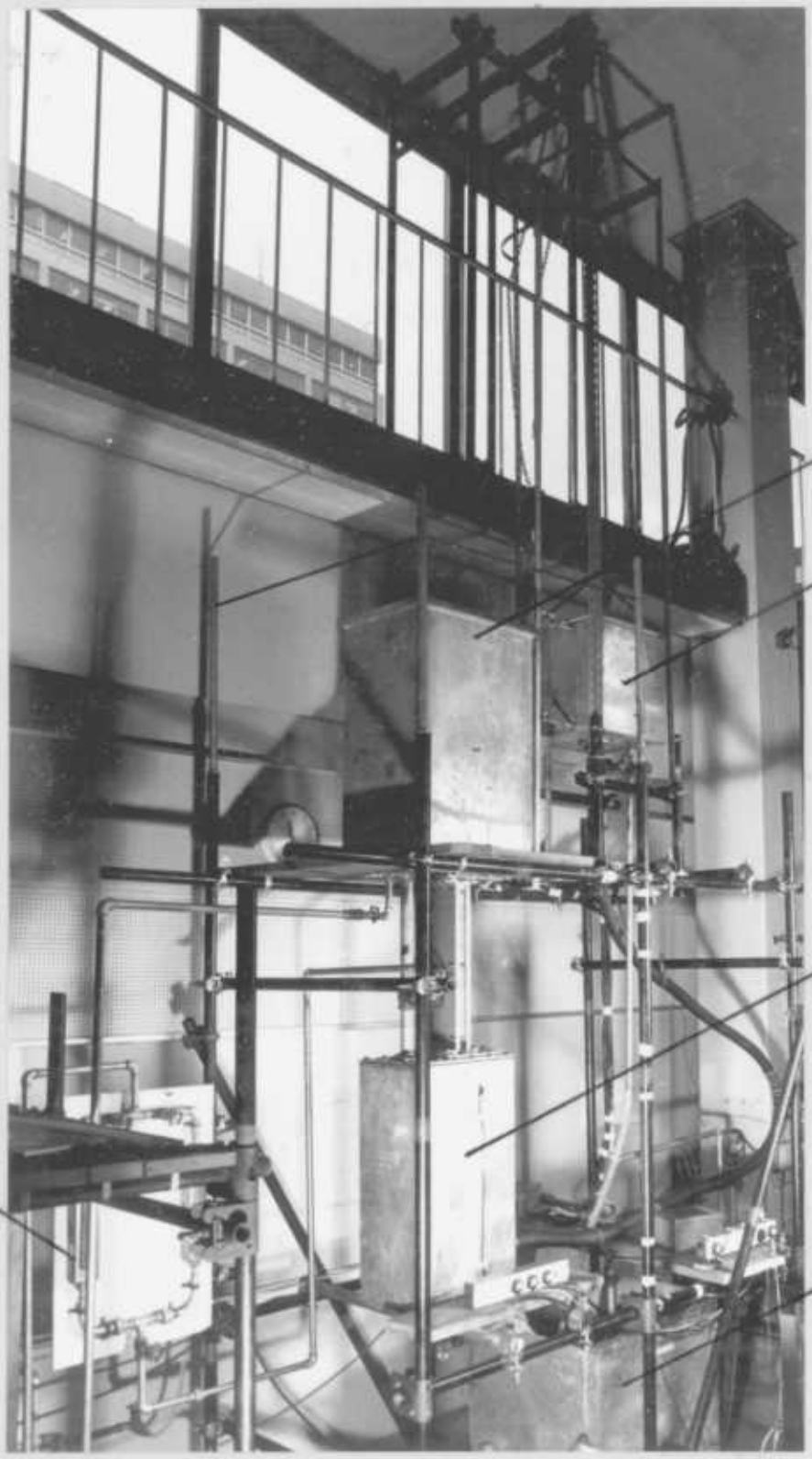

Photo. (1) Front view of the test-rig

Photo. (1) Front view of the test-rig

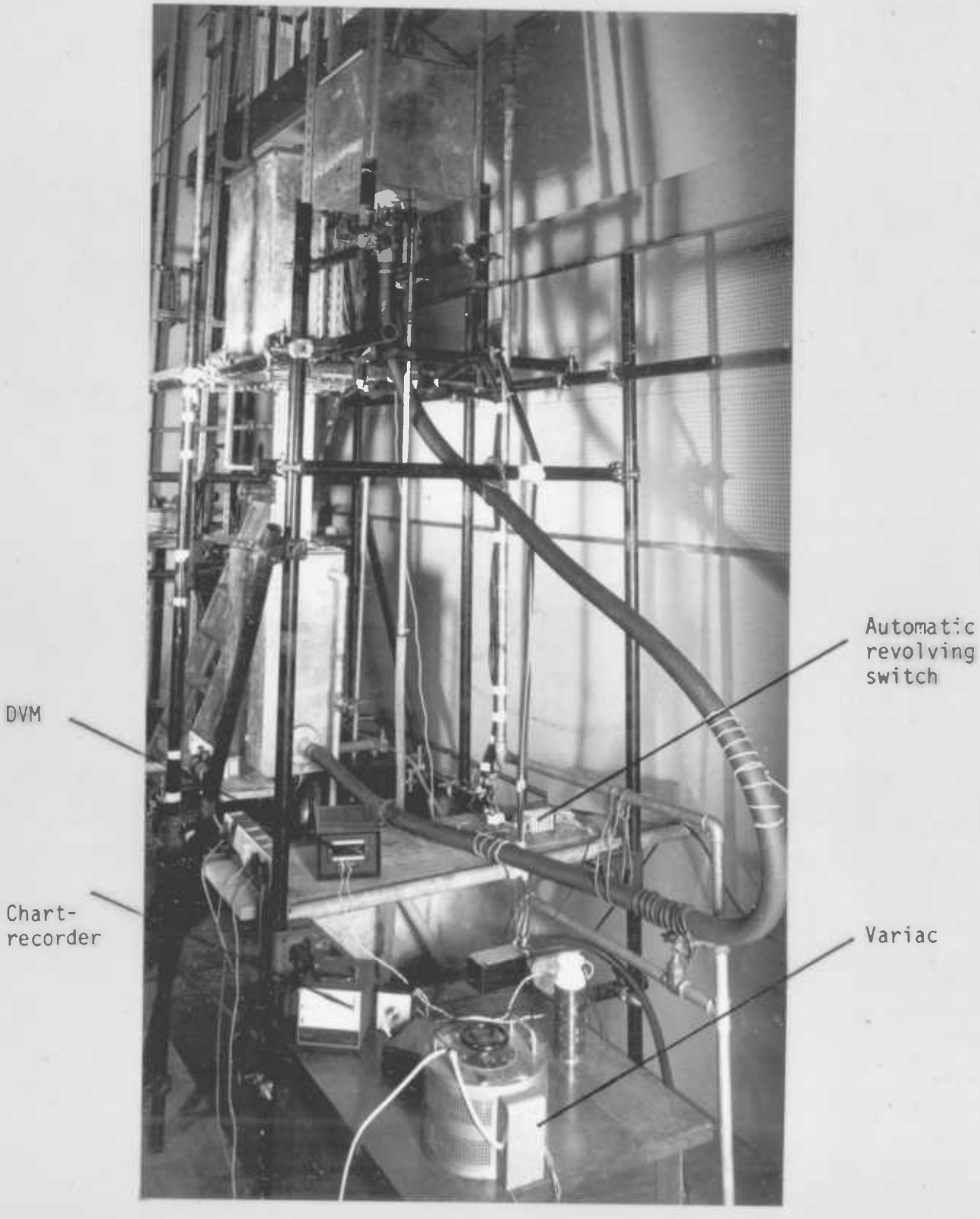

Photo. (2) Side view of the test-rig

Photo. (2) Side view of the test-rig

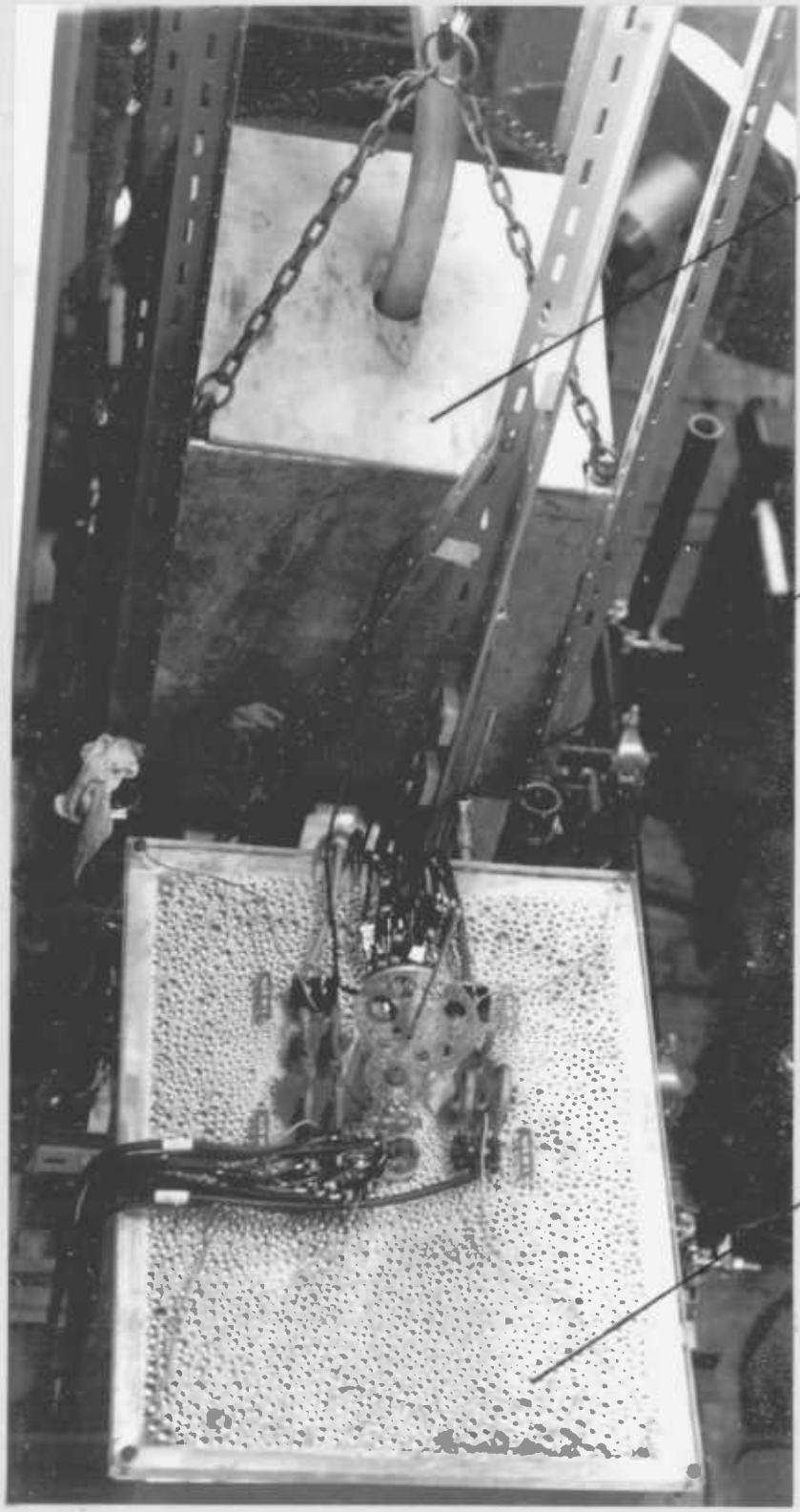

Photo. (3) Top view of the test-rig

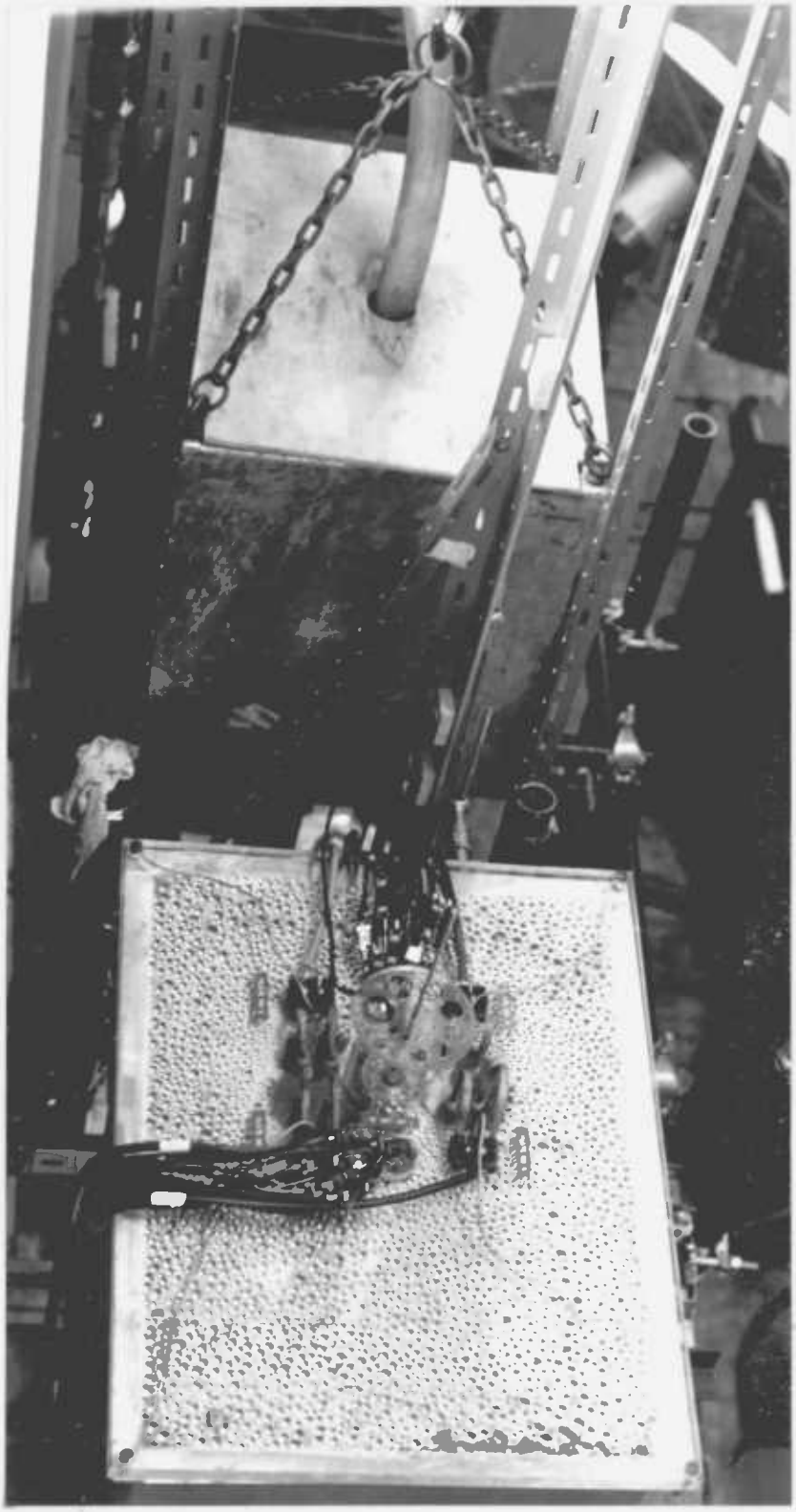

Photo. (3) Top view of the test-rig

(a) Heater Tank (Tank III)

Here, tap water is collected and warmed up to a preselected temperature, t_1, by two heating-coils (5 KW each). A hot-water line is also connected to this tank which facilitates the warming up of the water to the desired temperature. When drainage takes place, this tank is used for collecting the water from various parts of the test-rig. For a detailed drawing see Fig. (6. 2).

(b) Supply Tank (Tank IV)

This is a small constant-level tank. Its duty is to supply the test-section with a constant but controllable inlet pressure. The water level in this tank may be read against a scale by means of a glass pipe connected to the inner part of the tank.

In order to vary the inlet pressure at the test-section, this tank is vertically movable by means of the hoisting equipment also shown on Fig. (6.1). A detailed drawing of this tank is given in Fig. (6. 2).

(c) Inlet Manifold Tank (Tank II)

This tank is where water arrives from the Supply Tank and, subsequently, flows into the test-section. The large flexible pipe 'CD' (2" diameter), provided with the regulating valve V_1, connects these two tanks together. The top of this tank is covered by a special plate which also serves as the foundation of the test-section and the by-pass pipe, Fig. (6.3). A detailed drawing of this tank is given in Fig. (6.4).

(d) Discharge Tank (Tank I)

This is a constant-level tank and is connected to the exit

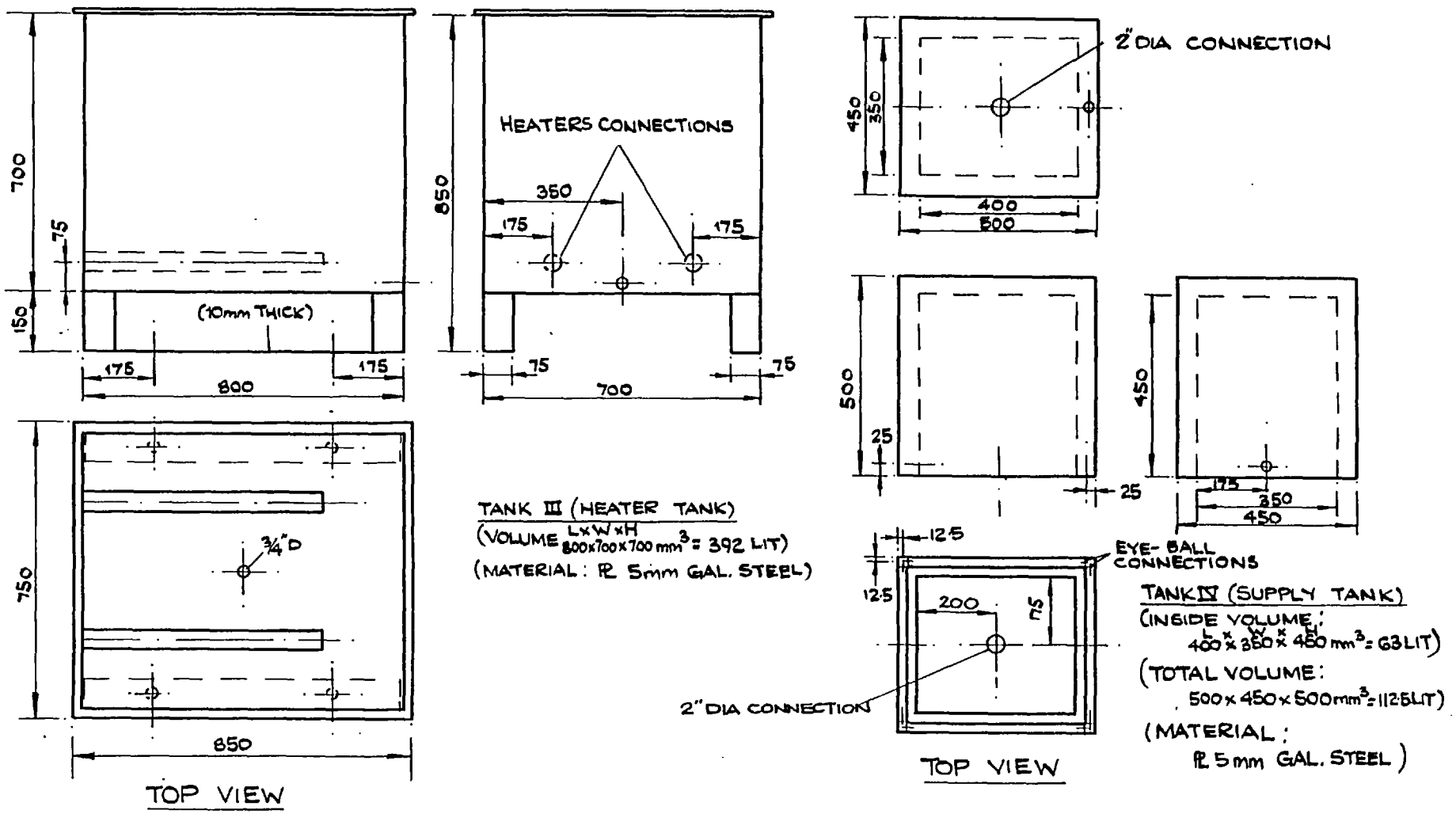

FIG.(6.2): THE 'HEATER' AND THE 'SUPPLY' TANKS.

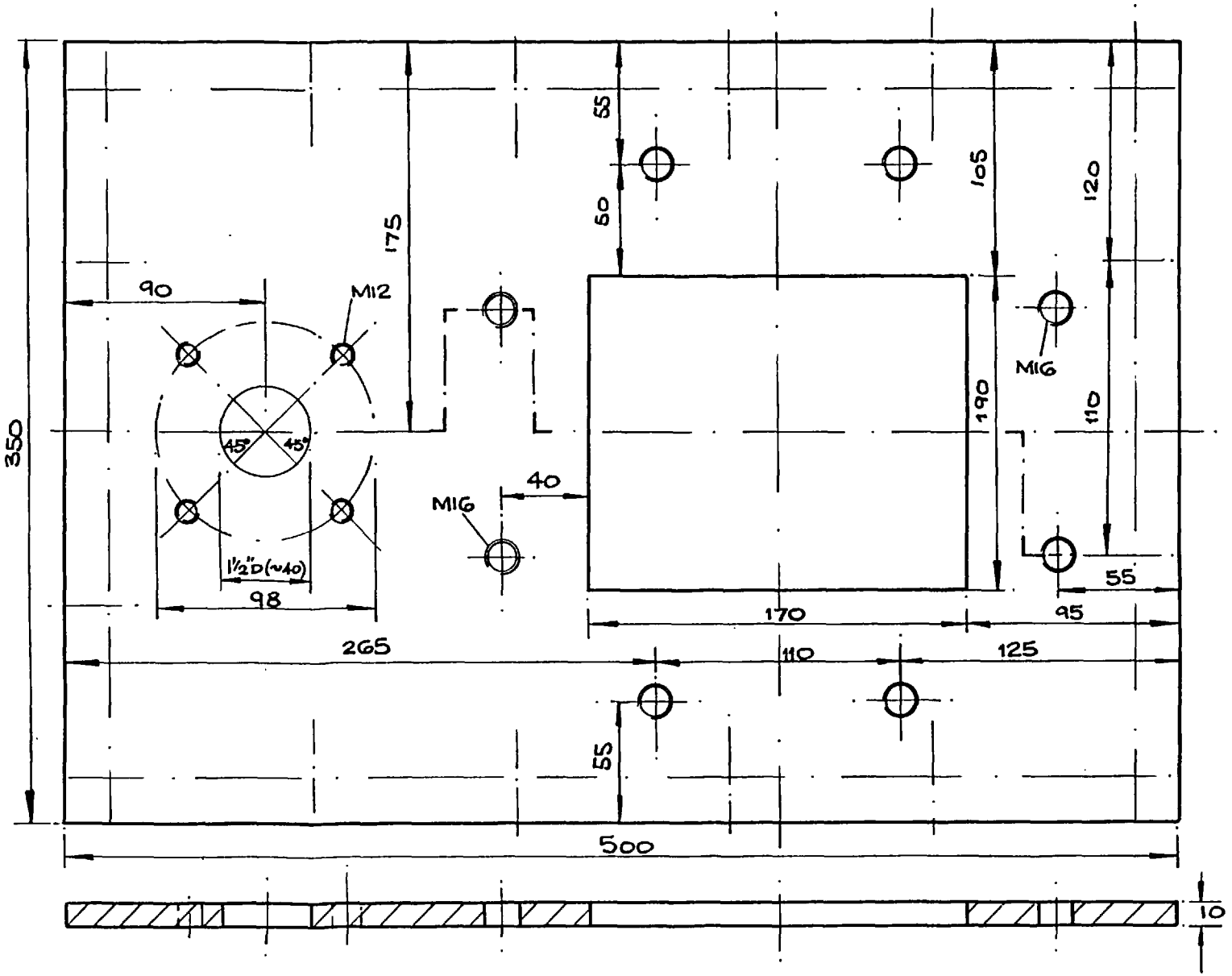

FIG. (6.3): FOUNDATION PLATE OF THE TEST SECTION.

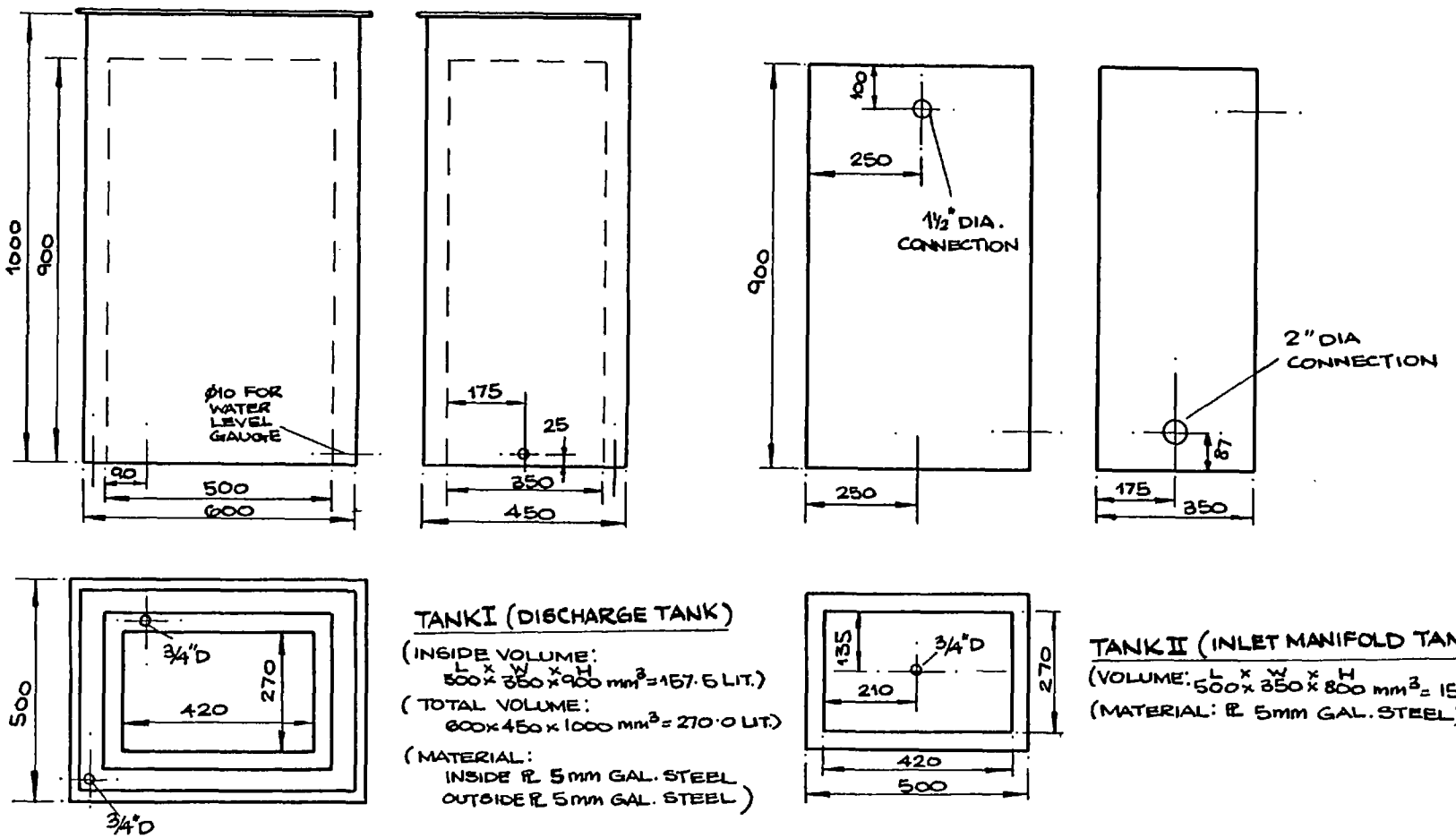

FIG.(6.4): THE 'INLET MANIFOLD' AND THE 'DISCHARGE' TANKS.

of the test-section and the by-pass pipe by a special plate. The tank is covered by a perspex plate shown on Photos. (3), (6a) - (6b). This plate is used as the base for the electrical connections of the test-section heaters (simulating plates) and also holds the cold-end-junction of their thermocouples. A spherical bearing, which is placed at the centreline of the perspex plate, holds a vertical probe designed to measure water temperatures along the test-section. A detailed drawing of this tank is given in Fig. (6.4).

6.2.2 Test-Section

As shown on Figs. (6.5a) - (6.5b), the test-section contains four heating plates. These plates with the four side walls make three similar channels in the middle and two narrow channels at the sides. The central channel is referred to as the "test-channel" of the rig while the rest of the channels are for simulation purposes. The heating plates are held in the grooves which are cut in the narrow side-walls, Fig. (6.6). A pair of bolts fix the side walls together to form the test-section.

Two special plates, shown on Fig. (6.7), were bolted to the top and the bottom of the test-section, to fix it to the Inlet Manifold and the Discharge tanks shown on Figs. (6.8) - (6.9). In order to prevent heat dissipation from the sides of the test-section, it is wrapped by several folds of Fibre-Glass insulation, Fig. (6.5b).

When the test-rig is operating, all of the four heating plates are heated, but temperature measurements are only executed in the test-channel. These measurements include measuring the wall temperature t_w and the temperature at the centre of the test-channel, t_{ℓ}, along the channel.

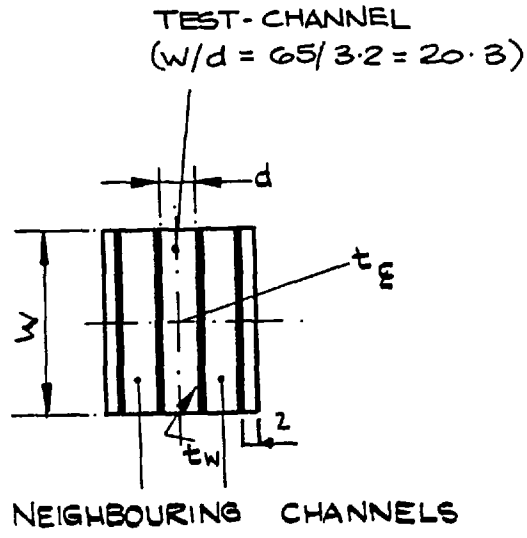

FIG. (6.5 a): SCHEME OF THE TEST-SECTION.

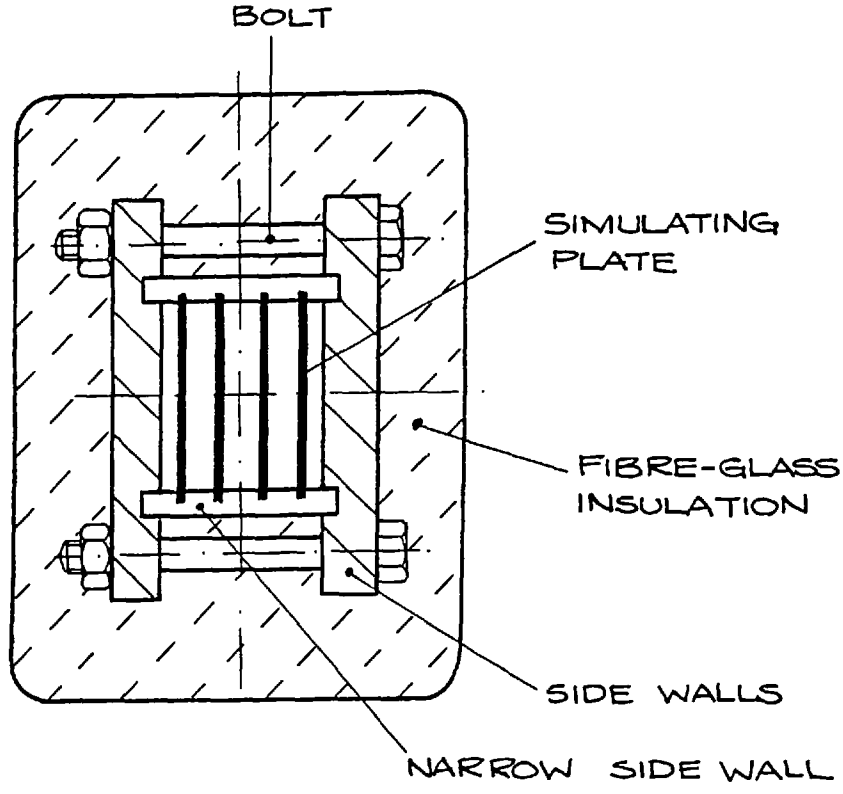

FIG. (6.5 b): TEST SECTION.

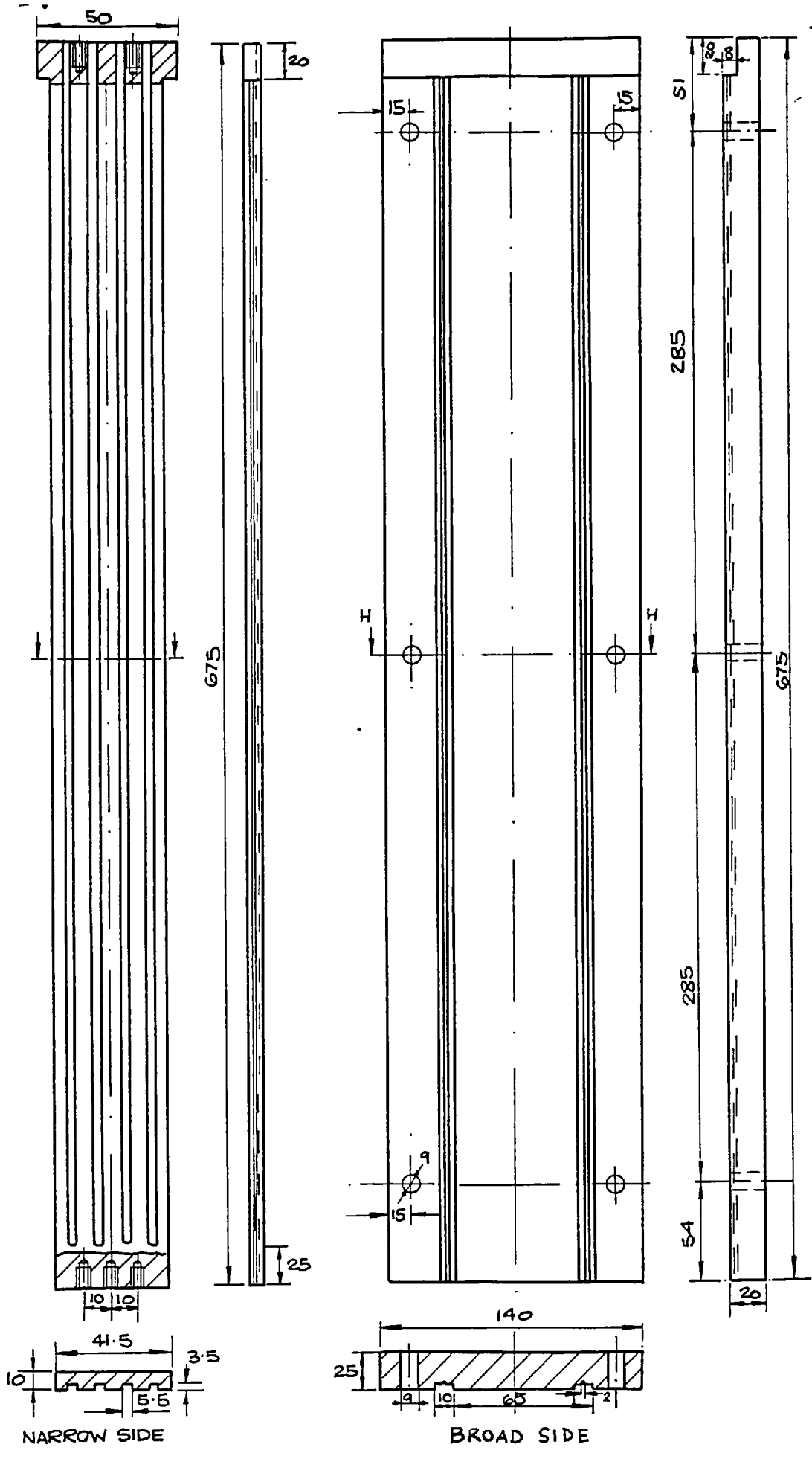

FIG.(6.6): SIDE WALLS OF THE TEST SECTION

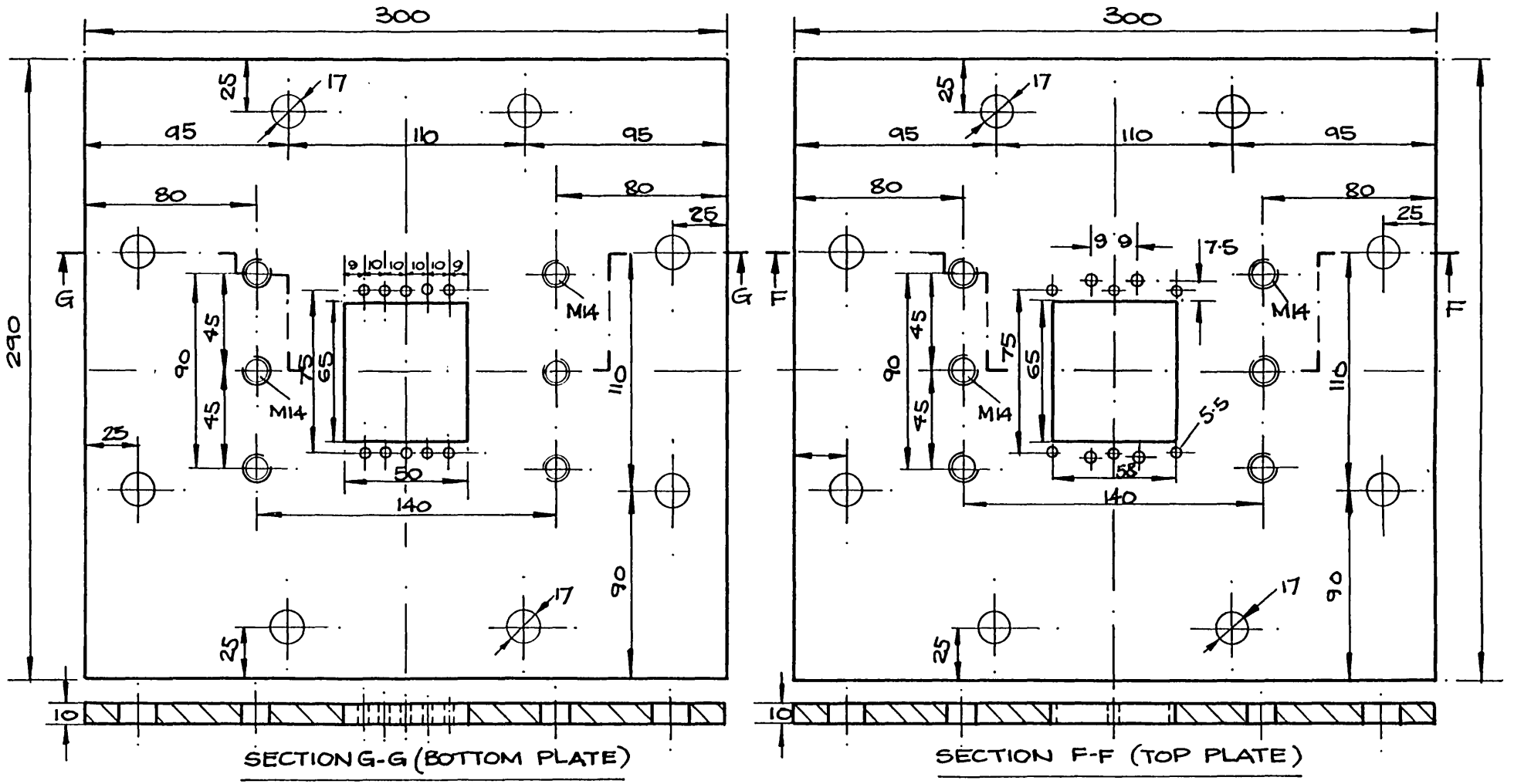

FIG. (6.7): BASE PLATES OF THE TEST-SECTION.

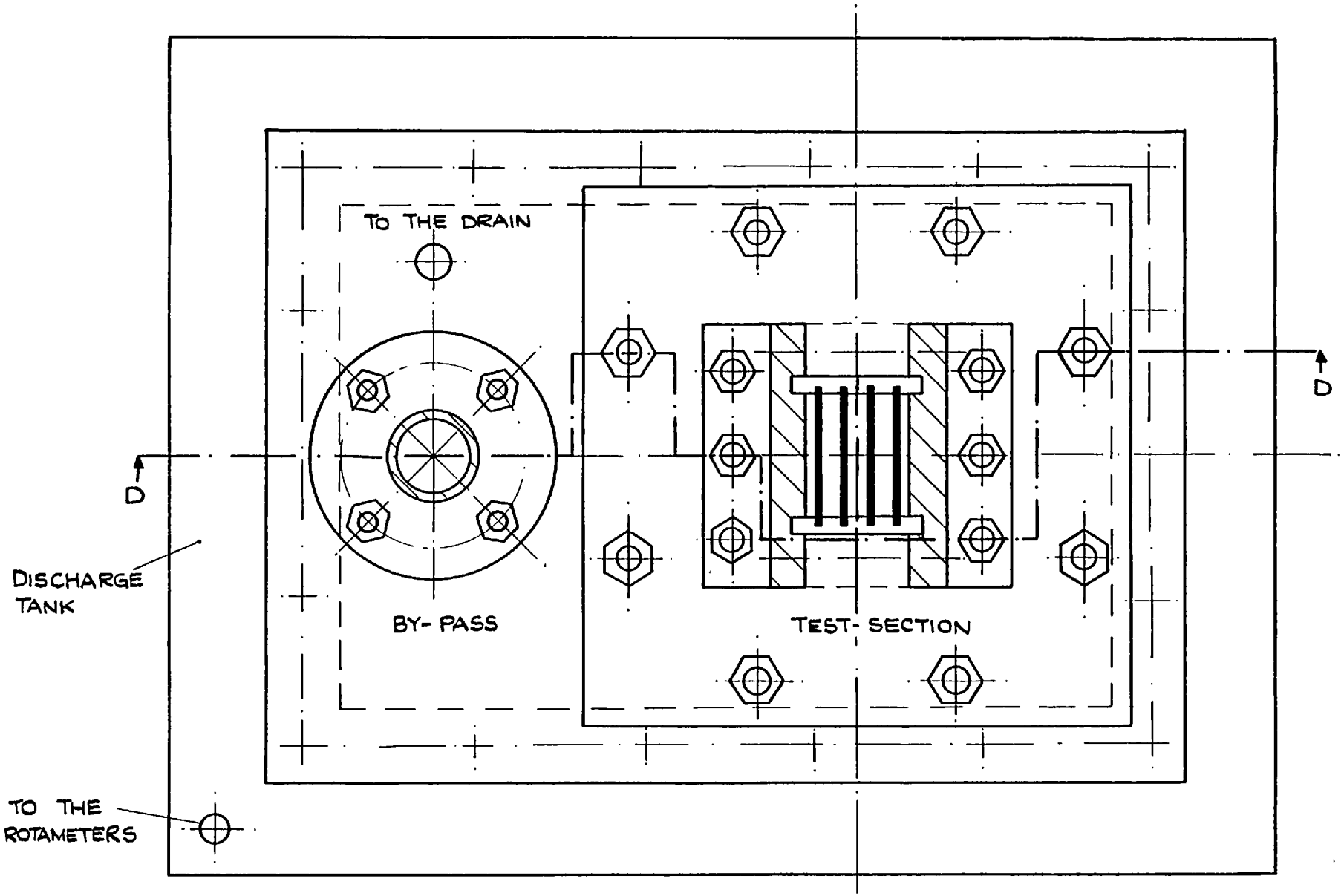

FIG.(6.8): TEST-SECTION AND THE BY-PASS PIPE CONNECTIONS TO THE DISCHARGE TANK (PLAN VIEW).

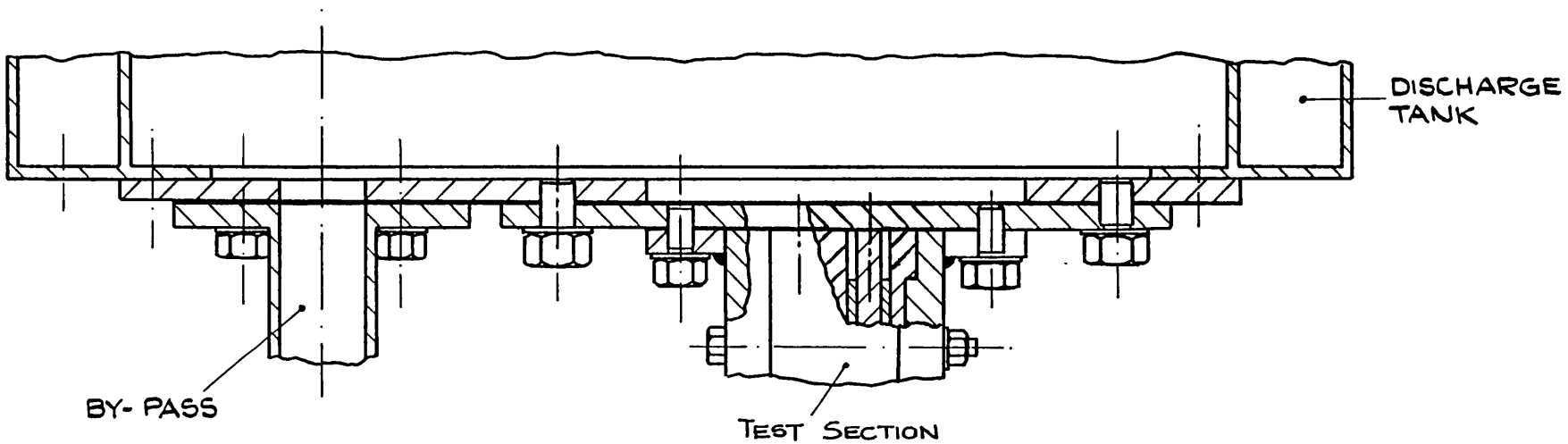

FIG. (6.9): CONNECTION OF THE TEST-SECTION AND THE BY-PASS TO THE 'DISCHARGE' TANK. (VERTICAL VIEW).

Photo. (4) shows the test-section and the by-pass pipe parallel to it. Also on this photograph is shown the probes measuring water temperature at the entrance and the exit of the channel.

For practical application of the results, the dimensions of the test-channel are designed to be the same as those of the "hot-channel" of a plate-type fuel element in the core of a nuclear reactor. For the experimental results, to be given in Chapter (7), fuel plates of the Mark 2 element of the University of London Reactor (ULR), are simulated to serve as the heaters in the test-channel. In what follows the simulation technique is explained.

6.2.3 The Simulating Heaters

A typical ULR fuel plate is shown on Fig. (6.10). According to this figure, the fuel covers an area of 600 x 60 mm^2 of the plate. Axial variations of the heat-flux on the fuel plates has never been measured but results are available from a similar reactor (MERLIN) shown on Fig. (6.11). It is noted on this figure that the profile is almost of a sinusoidal shape (apart from the distortions at the two far-ends caused by the reflector effects). In conclusion, a sinusoidal heat distribution in the following form is considered:-

$$\dot{q}'' = \dot{q}''_{max} \cdot \sin \frac{\pi z}{L'}$$

Therefore, the heat-flux profile between the points A and B is chosen to represent the actual heat-flux profile of the fuel plate.

Fig. (6.12a) shows the actual and the sinusoidal profiles. It is noted that the actual values are slightly higher in the first half of the channel and are lower in the second half. Therefore,

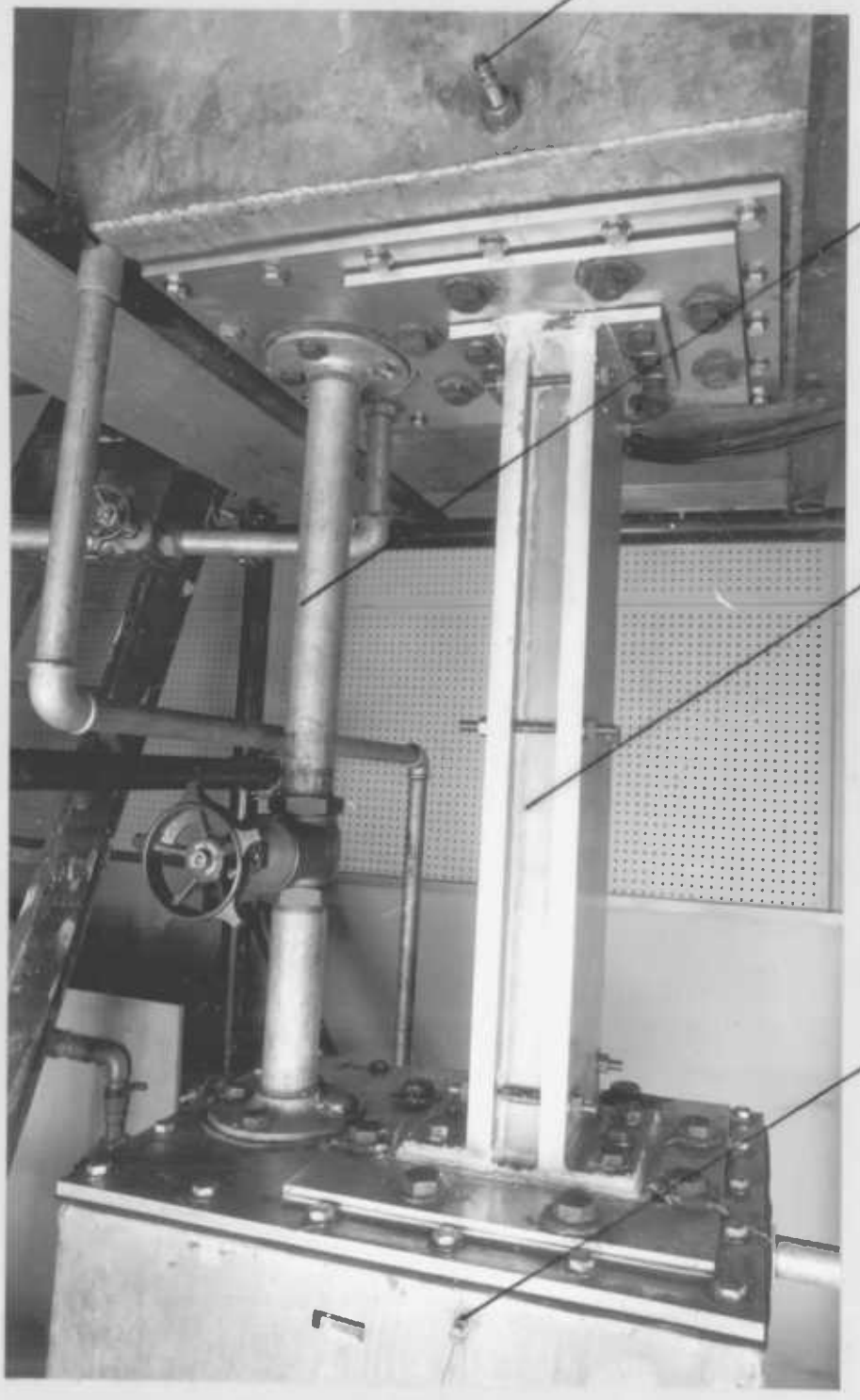

Photo. (4) Test-section and the by-pass pipe

Photo. (4) Test-section and the by-pass pipe

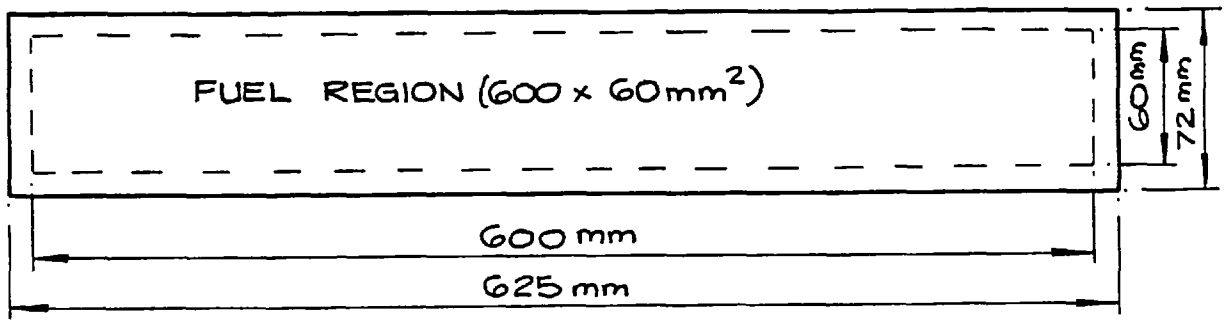

FIG.(6.10): A TYPICAL ULR FUEL PLATE.

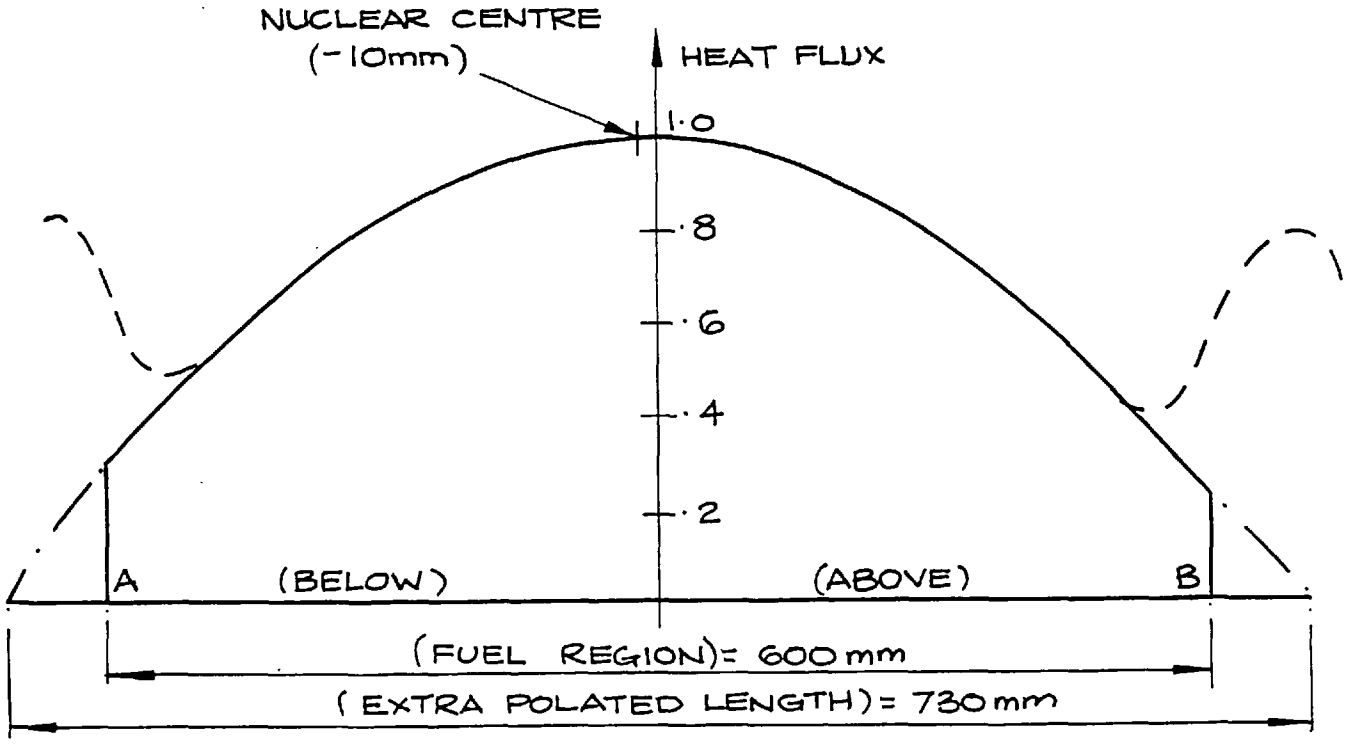

FIG. (6.11): HEAT-FLUX PROFILE ALONG THE FUEL PLATES.

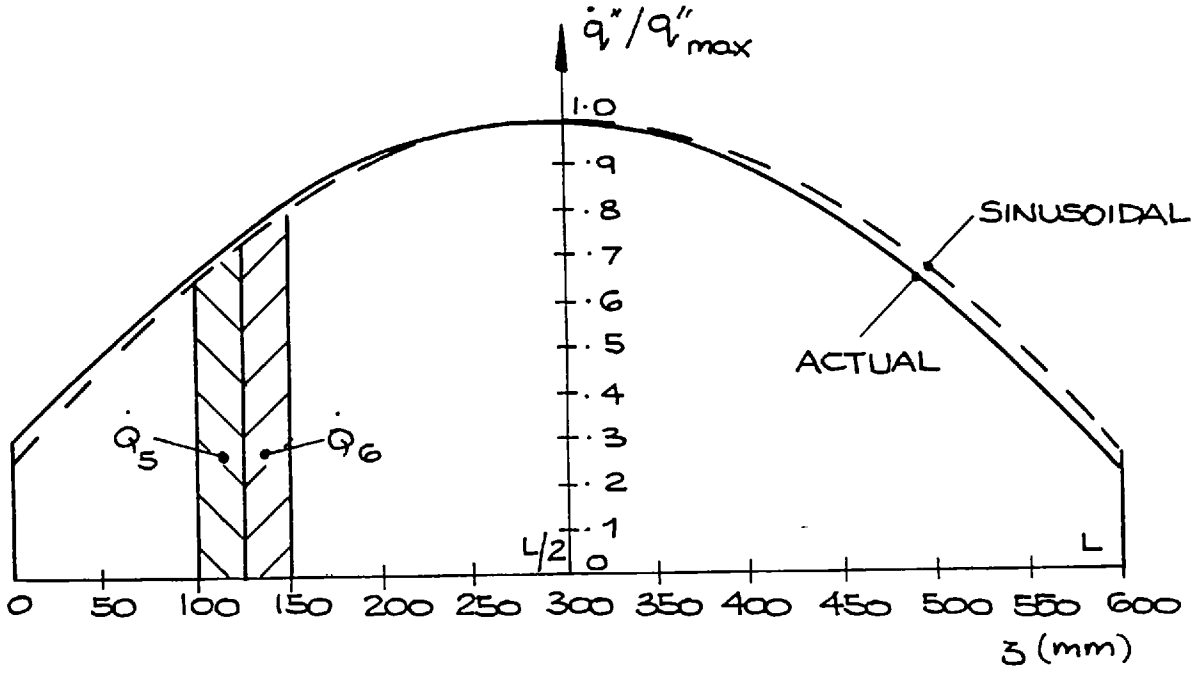

FIG. (6.12a): AXIAL VARIATION OF THE ACTUAL AND THE SINUSOIDAL HEAT-FLUX.

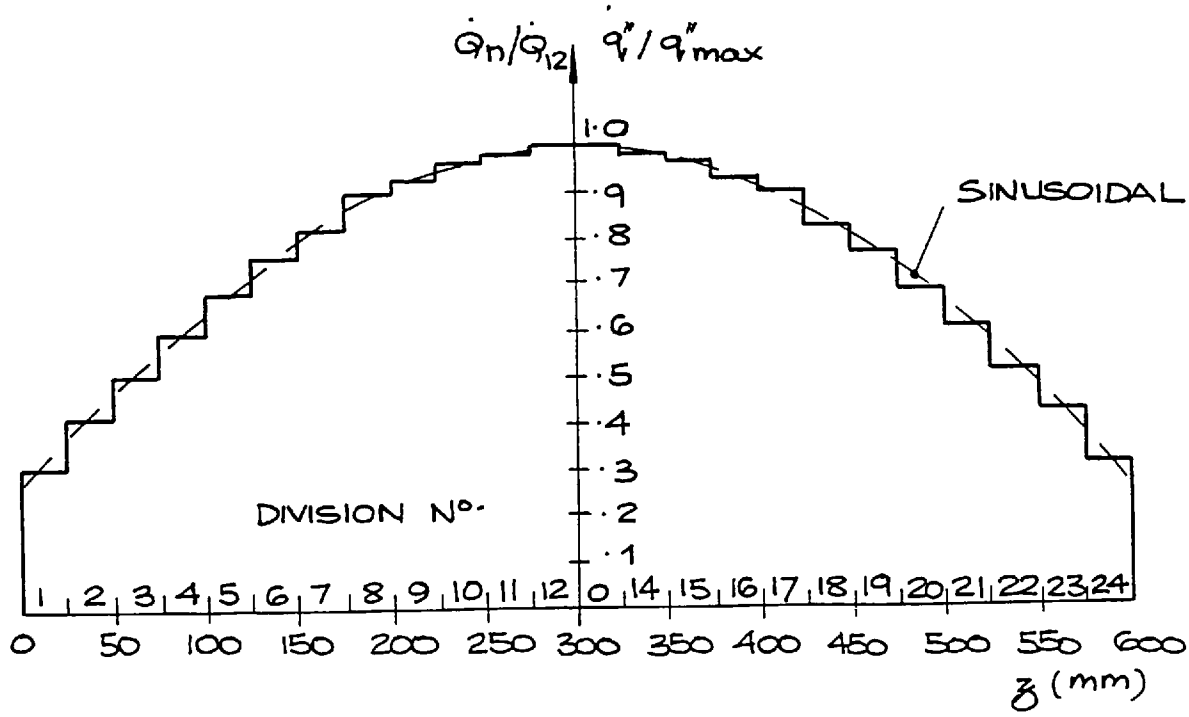

FIG. (6.12b): HEATING RATE OF THE 24 DIVISIONS USED FOR THE SIMULATION TECHNIQUE.

although the overall difference between the two profiles is negligible, there exist some differences at the two far-ends. The differences may be quantified in terms of the two ratios: $\dot{q}''_{w.Max}/\dot{q}''_{w.av}$ and $\dot{q}''_{w.min}/\dot{q}''_{w.av}$. For the sinusoidal approximation, these ratios are 1.343 and 0.37 respectively, while on the actual profile, they are 1.315 and 0.393 for the first half and 1.390 and 0.335 for the second half. For the actual profile as a whole:-

$\dot{q}''_{w.Max}/\dot{q}''_{w.av}$ = 1.355 (c.f. 1.343 from the sinusoidal profile)

$\dot{q}''_{w.min}/\dot{q}''_{w.av}$ = 0.365 (c.f. 0.370 from the sinusoidal profile)

From the foregoing discussion, it is concluded that the actual profile can be approximated with only small errors at the far-ends. The question which follows this approximation is: "what method of heating should be adopted to produce the sinusoidal profile along the channel?"

As discussed in the literature survey, Chapter (2), there exist two basic methods:-

(i) Sinusoidal heat-flux production by means of an electrically heated plate of variable thickness. This method is attempted by Dijkman (1969) and later by Muzzy et al (1974).

(ii) Sinusoidal heat production by means of wrapping an electrical resistor with a variable pitch over a plate. This method is attempted by Petrovichev (1960) and recently by Reisman et al (1977).

If the sizes of the simulating plates are to be kept the same as those of the fuel plates, i.e. 625 x 72 mm^2, Fig. (6.10), application of the variable thickness method involves the longitudinal tapering of a very thin plate from the far ends towards the middle. This process leads to some technical problems, also observed by Dijkman (1969), and proves to be costly also (see Appendix II). Therefore, the second method is attempted.

In the execution of the variable-pitch method of simulation, the heat-flux profile is divided into 24 divisions each 25 mm long, Fig. (6.12b). Then the sinusoidal profile is integrated for each of the divisions to determine the fraction of the total heat which each one of them should produce; $\dot{Q}_n$. The first three columns of Table (6.1) show $\dot{Q}_n$ values for a typical plate (with $\dot{Q}_{tot}$ = 975 W). Column 6 of this table shows the electrical resistances for every division if the electric resistor bears the current of I = 13.25 A. Fig. (6.12b) shows the result of this method of simulation. On this figure, the abscissa shows the division numbers as well as their distances along the plate, while the ordinate shows the ratio $\dot{Q}_n/\dot{Q}_{12}$. Also on Fig. (6.12b) is shown the sinusoidal heat-flux profile for comparison. It is noted that the differences virtually disappear near the middle of the channel.

Having established the heating requirements of the simulating heaters, the heating element, as shown on Fig. (6.13), is designed. The element is assembled by wrapping a Nickel-Chrome (NICHROME) heating tape around two layers of a special material industrially called FILAMIC. This cardboard-type material conducts heat but is an electrical insulator. As shown on Fig. (6.13), the pitch of the heating tape gradually decreases to produce the $\dot{Q}_n$ values of Table (6.1). The specifications of the tape, (4.76 x 0.36 mm^2 and 0.75 Ω/m),

TABLE (6.1) CALCULATIONS FOR A SIMULATING PLATE

($\dot{Q}_{tot}$ = 975 W, I = 13.25 A, ρ' = 0.75 Ω/m)

Division No. n	Distance z (mm)	Heating Rate $\dot{Q}_n$ (w)	$\dot{Q}_n/\dot{Q}_1$	$\dot{Q}_n/\dot{Q}_{12}$	Resistance R' (Ω)	Tape Length (mm)
1	25	17.0	1.000	0.309	0.0968	129.0
2	50	23.0	1.352	0.418	0.1310	174.6
3	75	28.0	1.647	0.509	0.1595	212.6
4	100	33.0	1.941	0.600	0.1880	250.7
5	125	37.5	2.205	0.682	0.2136	285.0
6	150	42.0	2.470	0.764	0.2392	319.0
7	175	45.0	2.647	0.818	0.2563	341.7
8	200	49.5	2.912	0.900	0.2820	376.0
9	225	51.0	3.000	0.927	0.2905	387.3
10	250	53.0	3.118	0.963	0.3019	402.5
11	275	54.0	3.176	0.981	0.3076	410.1
12	300	55.0	3.235	1.000	0.3133	417.8

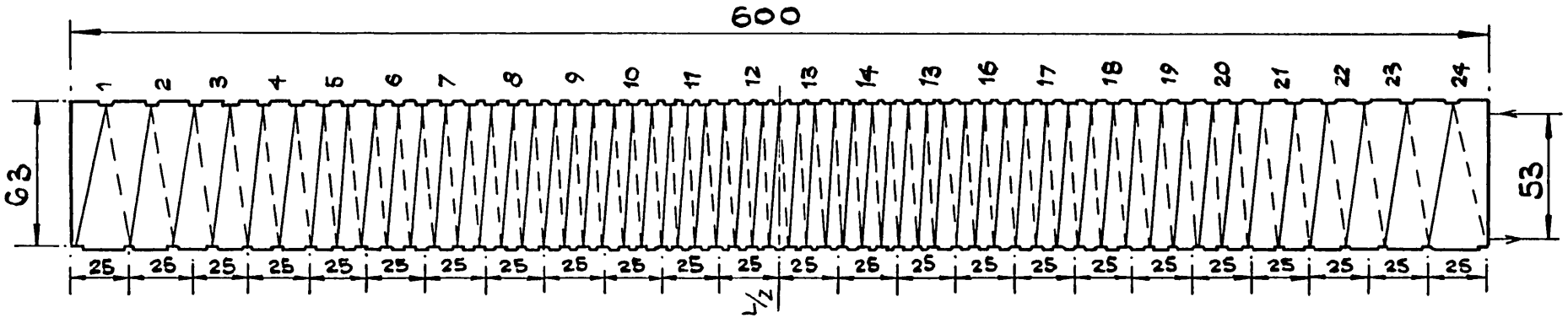

FIG. (6.13) : THE FILAMIC PLATES WRAPPED WITH NICHROME TAPE (HEATING ELEMENT)

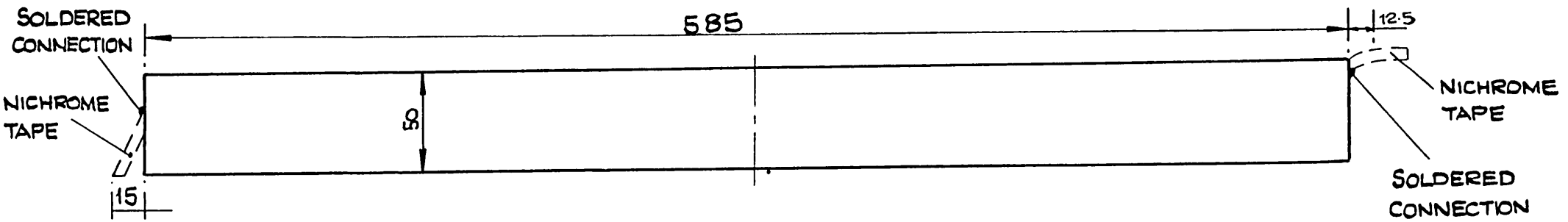

FIG. (6.14) : THE COPPER PLATE.

made by British Driver-Harris, permit the required heat production along the heating element by almost 2 turns of it round the FILAMIC plate near the far-ends (for $\dot{Q}_1$ or $\dot{Q}_{24}$) which gradually increases to 6.5 turns at the middle (for $\dot{Q}_{12}$ or $\dot{Q}_{13}$). In order to have both of the electrical terminals at one end of the heating element, a copper plate, as shown on Fig. (6.14), is placed between the two FILAMIC layers. The copper plate connects one of the electrical terminals to the other end of the element where the wrapping starts. Employment of copper assures a good contact there, together with a negligible heat dissipation.

The simulating plate is designed as shown on Fig. (6.15). In addition to the heating element above-mentioned, it contains two stainless-steel plates, one thicker than the other. The thicker plate accommodates twelve thermocouples embodied in it for measuring the surface temperature, t_w of the simulating plate at different axial positions (see Fig. (6.16) for their positions). A simulating plate is assembled by covering the heating-element with two thin layers of FILAMIC. Then the thin stainless steel plate, which is tray-shaped, accommodates the element. Assembling is completed by welding the two stainless steel plates together along three sides. The fourth side of the plate is filled with silicon-rubber and gives passage to the cold-end-junctions of the thermocouples and also the electric terminals of the NICHROME tape.

The test-section with the simulating heaters are also shown on Photos. (5a) - (5b).

6.2.4 Water Circuit

As shown on Fig. (6.1), water is pumped from the Heater Tank

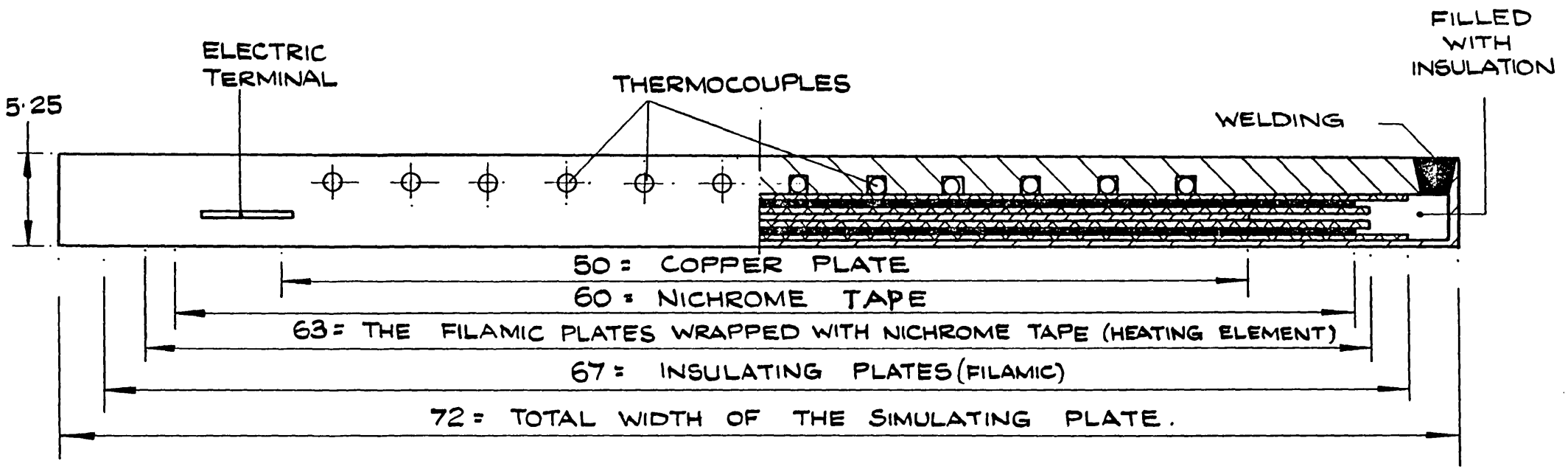

FIG. (6.15) : CROSS SECTION OF THE SIMULATING PLATE.

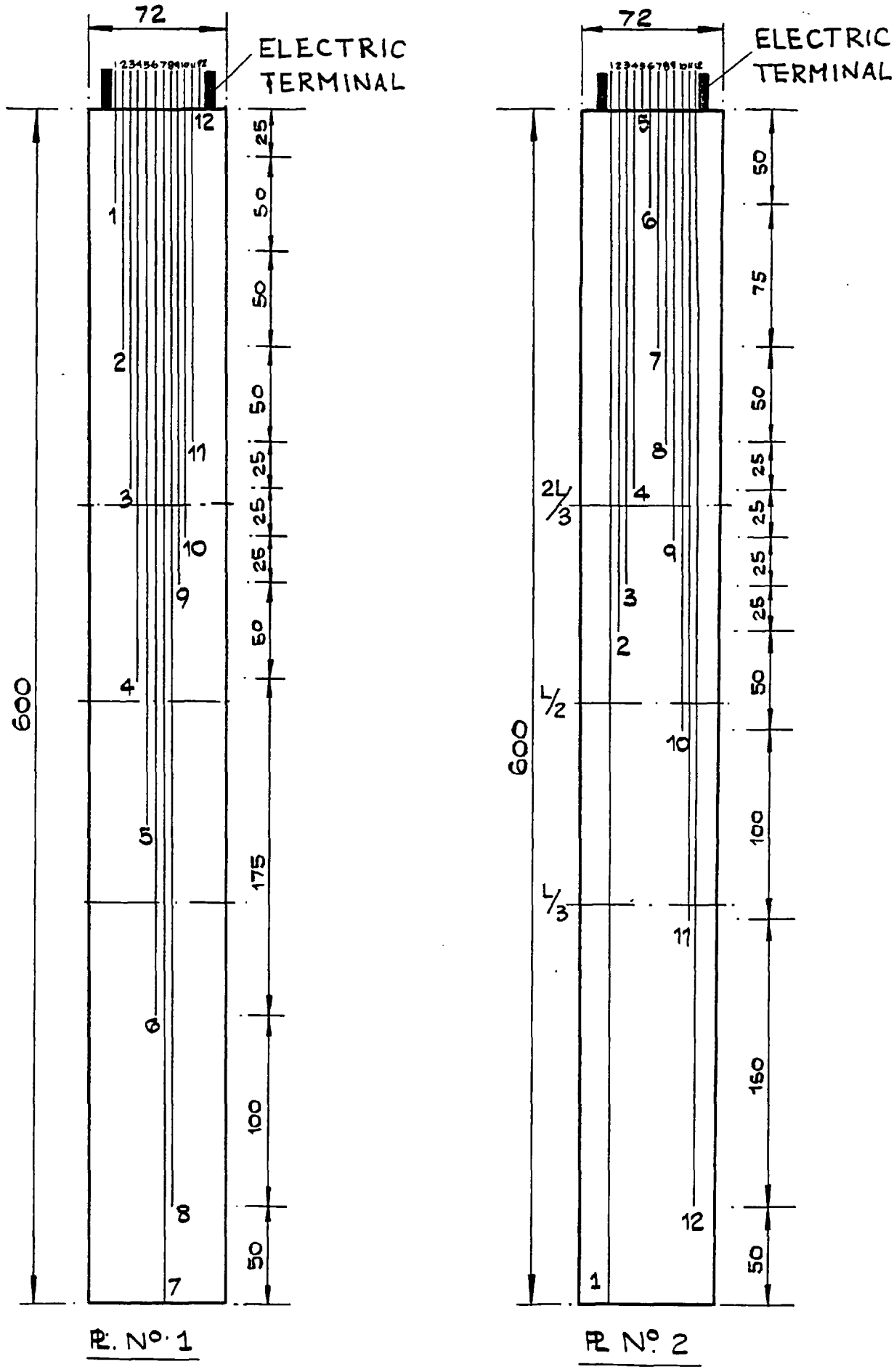

FIG. (6.16): THERMOCOUPLE ARRANGEMENTS OF THE SIMULATING PLATES.

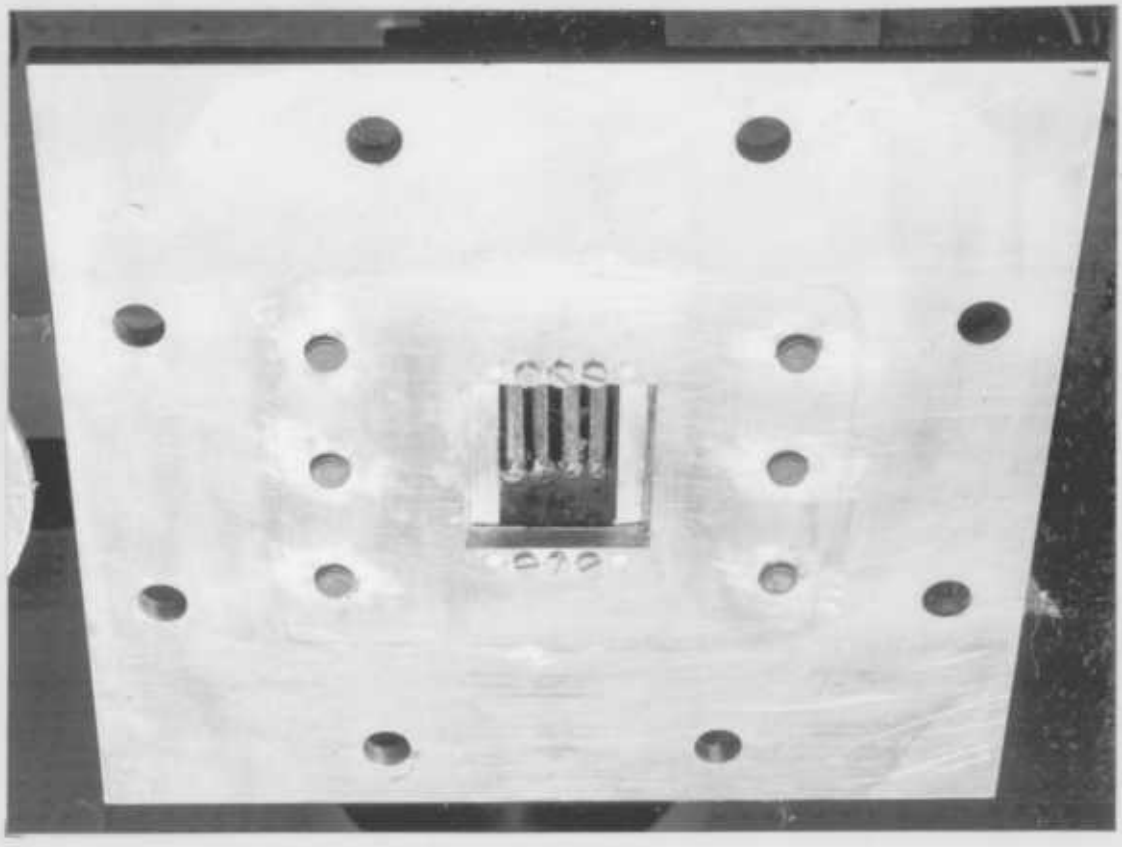

Photo. (5a) Test-section and its base plate

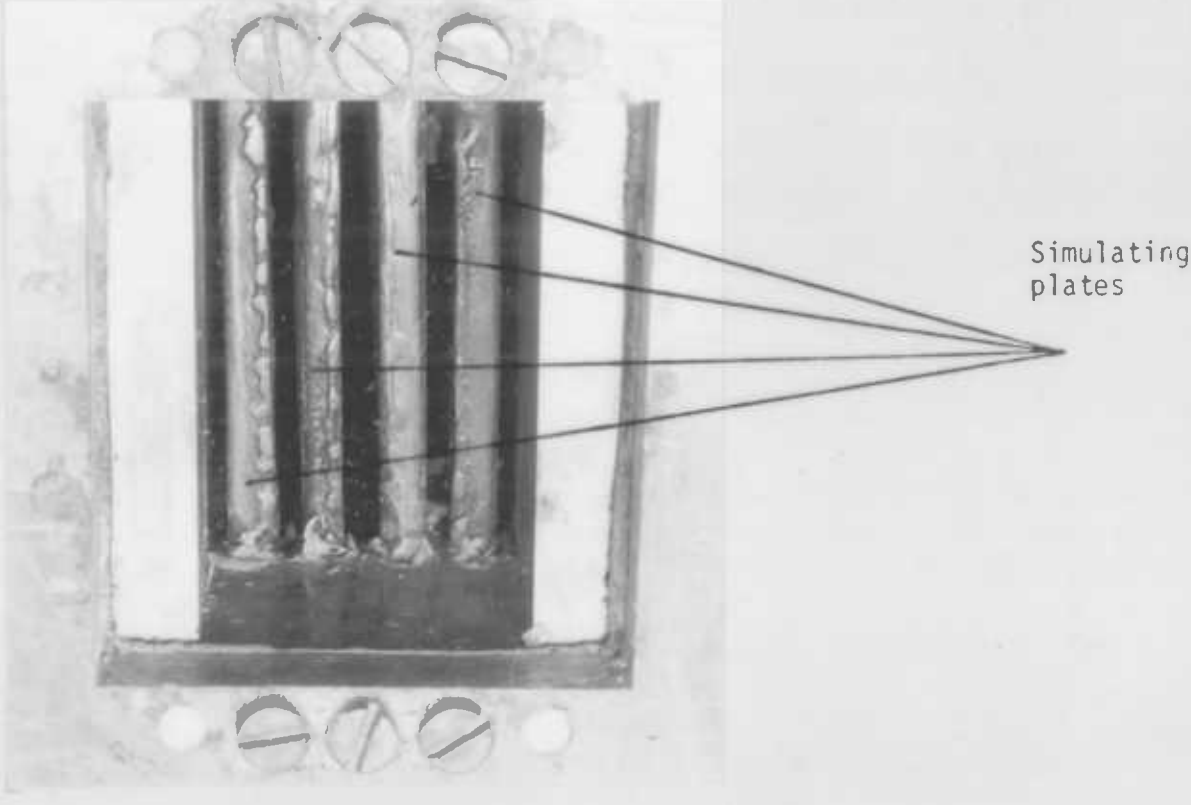

Photo. (5b) Test-channel and its neighbouring channels

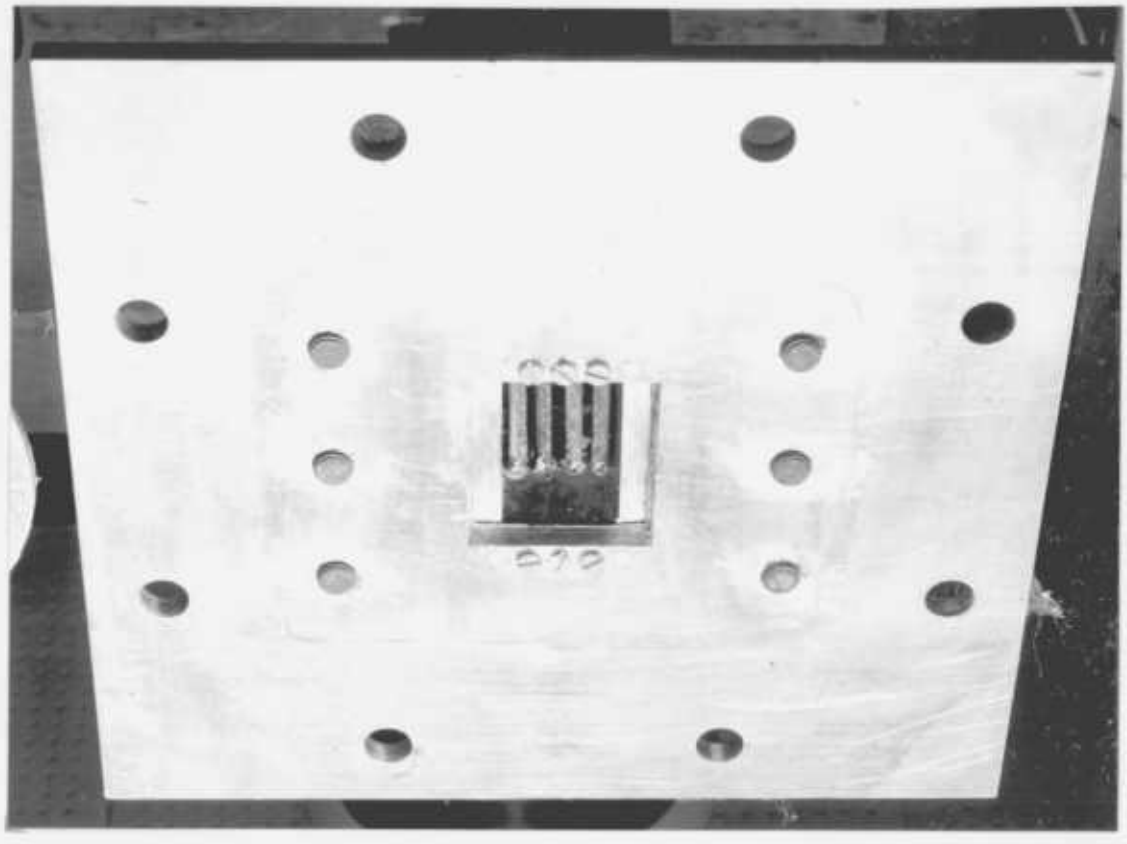

Photo. (5a) Test-section and its base plate

Photo. (5b) Test-channel and its neighbouring channels

to the Supply Tank via the partly flexible pipe 'AB'. From this tank, water flows to the Inlet Manifold Tank via the large flexible pipe 'CD'. The regulating valve V_1 provided in this pipeline controls the flow throughout the circuit. Water enters the test-section from the Inlet Manifold Tank and is discharged at the end of this section to the Discharge Tank. Water overflowing from the inner to the outer shell of this tank is collected and directed through the rotameters via the pipeline G-J. The water cycle finishes at the draining point 'J' and starts by pumping from the Heater Tank to the Supply Tank. Water gauges connected to the inner shell of the Supply and Discharge tanks show the difference between their water levels. This is interpreted as an indicator of the inlet pressure of the test-channel; p_o. This pressure is zero when the Supply Tank is seated on its foundation. Therefore, the test-rig is suitable for studying both the natural and the mixed convection cases. Drain lines 'ST' and 'UV' and also the overflow line 'QR' provide the water circuit with a quick drainage system.

The by-pass pipe is used as an alternative water passage when the test-section is not in the circuit. However, during experiments it was fully closed.

The water circuit may also be followed on Photo. (1).

6.2.5 Electrical Circuit

The four heater plates of the test-section are fed by a system of two transformers. Fig. (6.17) shows this electrical circuit which is controlled by a Variac placed at the Main connections of the transformer R_1. Because of the high current required by the heaters, (40 - 53A), and also the relatively higher power needed for all of the heaters, (2.6 to 3.9 KW), the transformers are connected in series. For

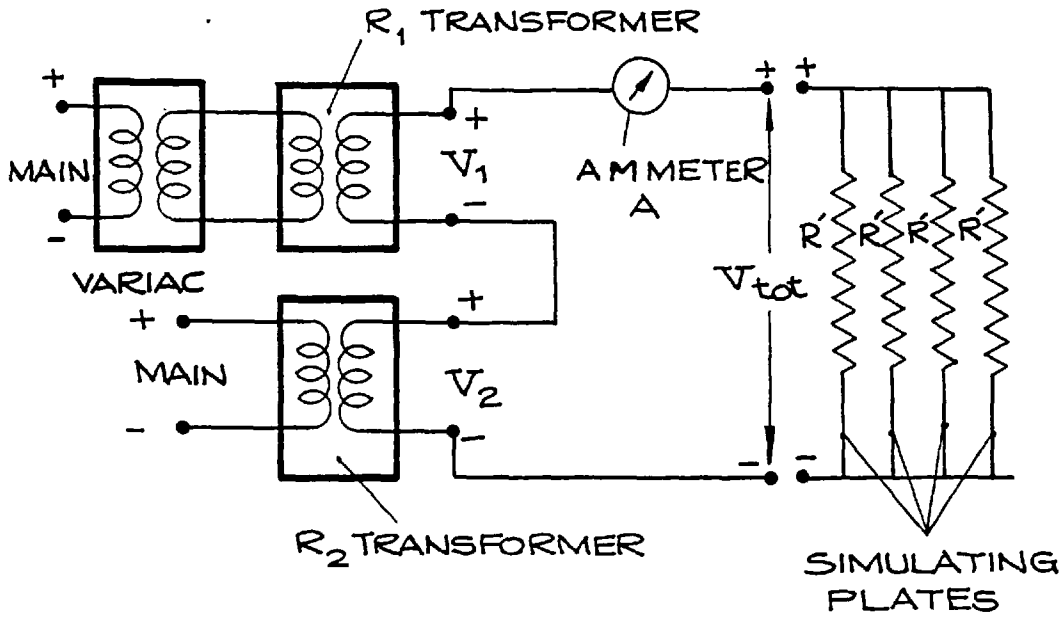

FIG. (6.17) : ELECTRICAL CIRCUIT

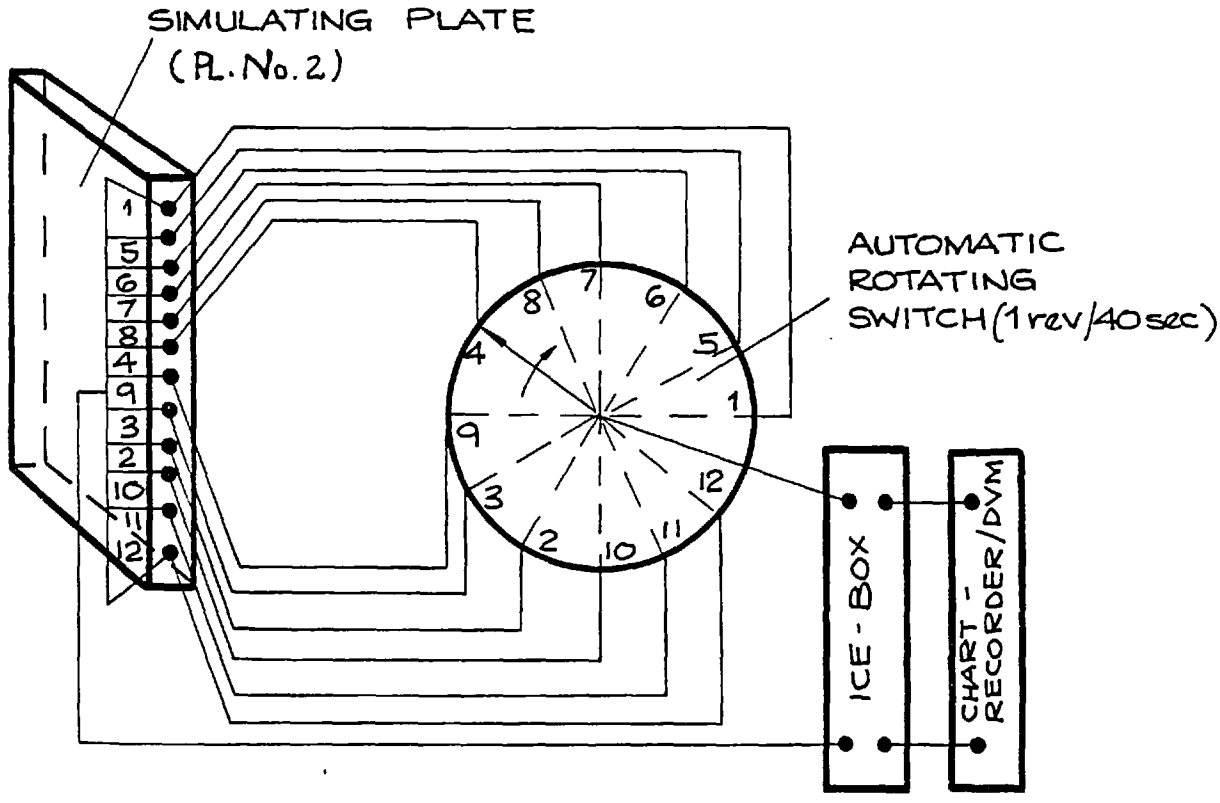

FIG. (6.18): TEMPERATURE RECORDING CIRCUIT OF THE SIMULATING PLATES.

the experiments reported in Chapter (7) of this thesis, the ratios R_1 and R_2 are 5 and 8 respectively. This gives the circuit, when connected to 240 V Main, the capability of providing the heaters with 30 to 76 Volts. The four heaters of the test-channel are positioned in parallel when they are connected to the V_{tot} shown on Fig. (6.17). This connection is also shown on Photos. (6a) - (6b). The leads of the electrical terminals of the heaters are covered by silicon-rubber sleeving when they pass through the Discharge Tank. The total current passing through the test-section heaters, I_{tot} is measured by the ammeter 'A' in the electrical circuit, ($I = \frac{1}{4} I_{tot}$).

6.2.6 Measurements For Each Experiment

For each experiment, the level-difference between the Supply and the Discharge tanks, $\Delta h'$ and the total heat in the test-channel, $\dot{Q}_{tot}$ were kept at prescribed values while water flow rate, $\dot{m}_c$ and various temperatures at the test-section were measured. The parameters involved in each test are determined as follows:-

(1) The inlet pressure at the test-section, p_o is determined by the difference between the water levels of the "Supply" and the "Discharge" tanks.

(2) The power input to each simulating plate, $\dot{Q}_{tot}$ is calculated according to the formula: $\dot{Q}_{tot} = I^2.R'$.

(3) The water flow rate, $\dot{m}_c$ is read by the rotameters provided in the water circuit. This reading is confirmed by collecting the drained water from the rotameters in a graded container for a specific period of time. The flow through the test-channel, $\dot{m}_{t.c}$, shown on Fig. (6.5a) is considered to be $\frac{1}{4}$ of the total flow, $\dot{m}_c$. It is noted

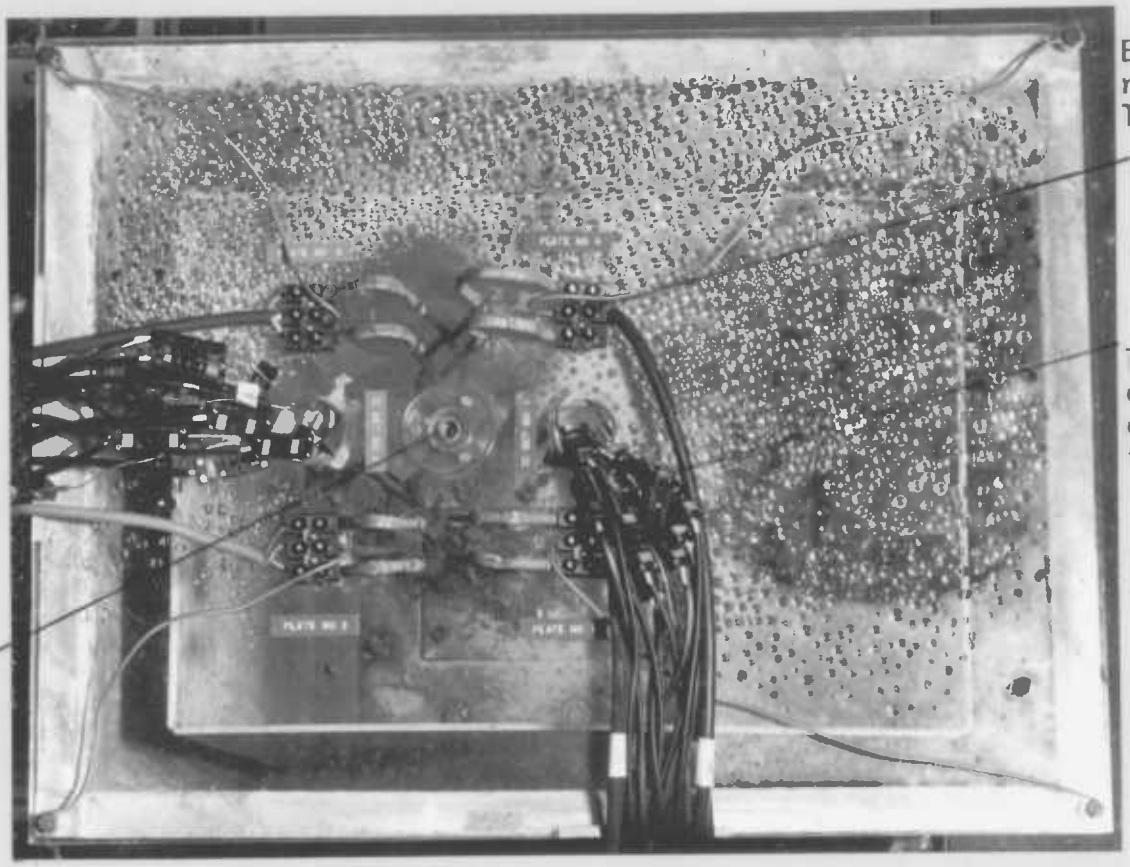

Photo. (6a) The perspex cover of the Discharge Tank

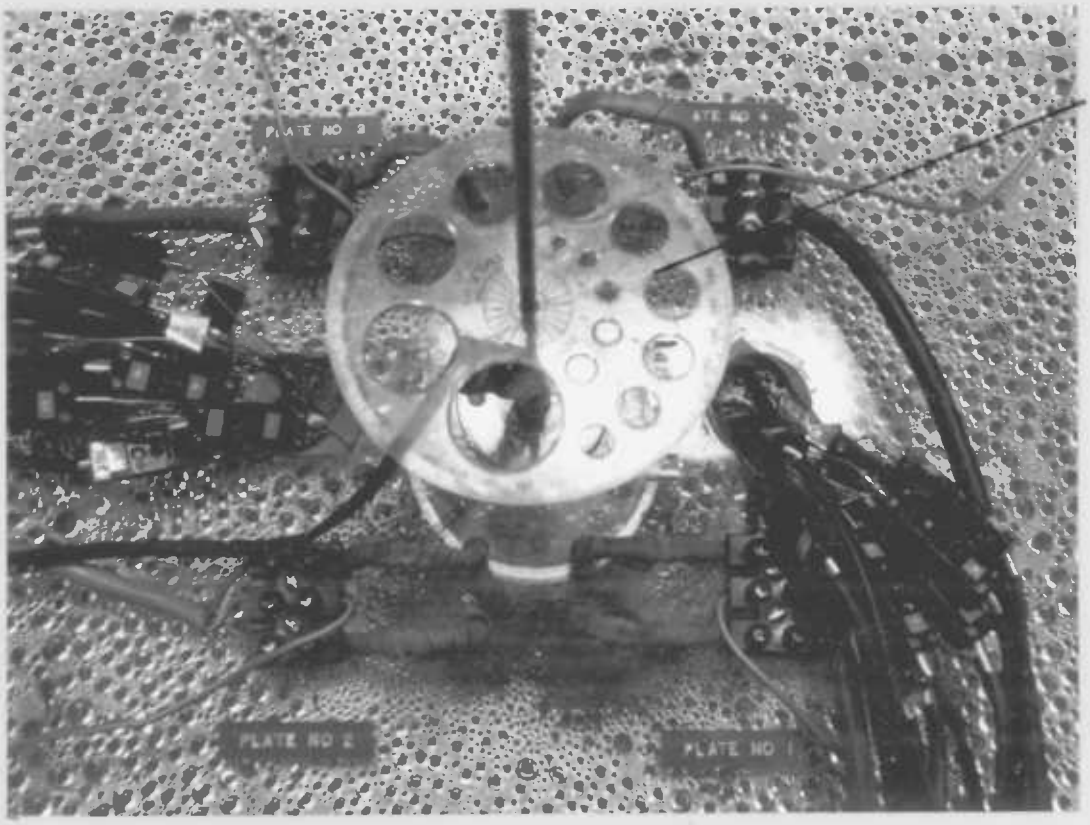

Photo. (6b) The perspex cover of the Discharge Tank with the vertical probe

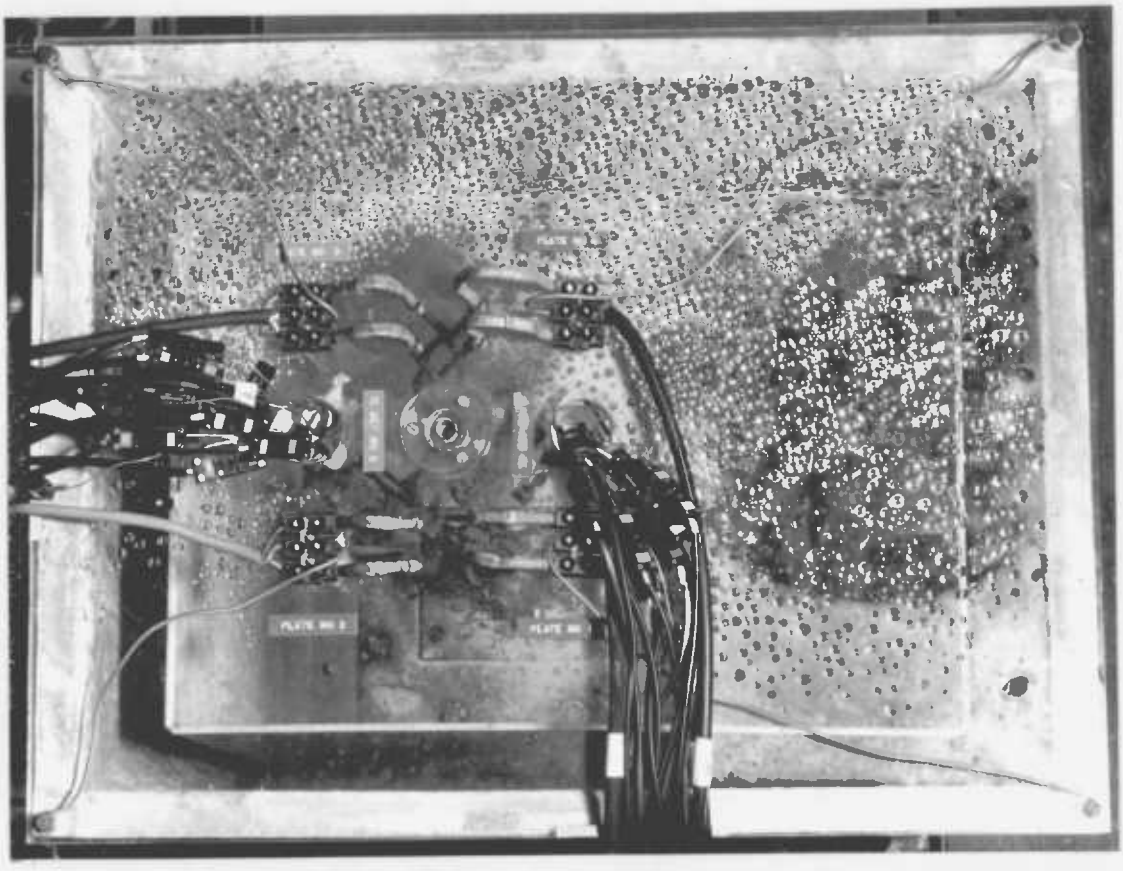

Photo. (6a) The perspex cover of the Discharge Tank

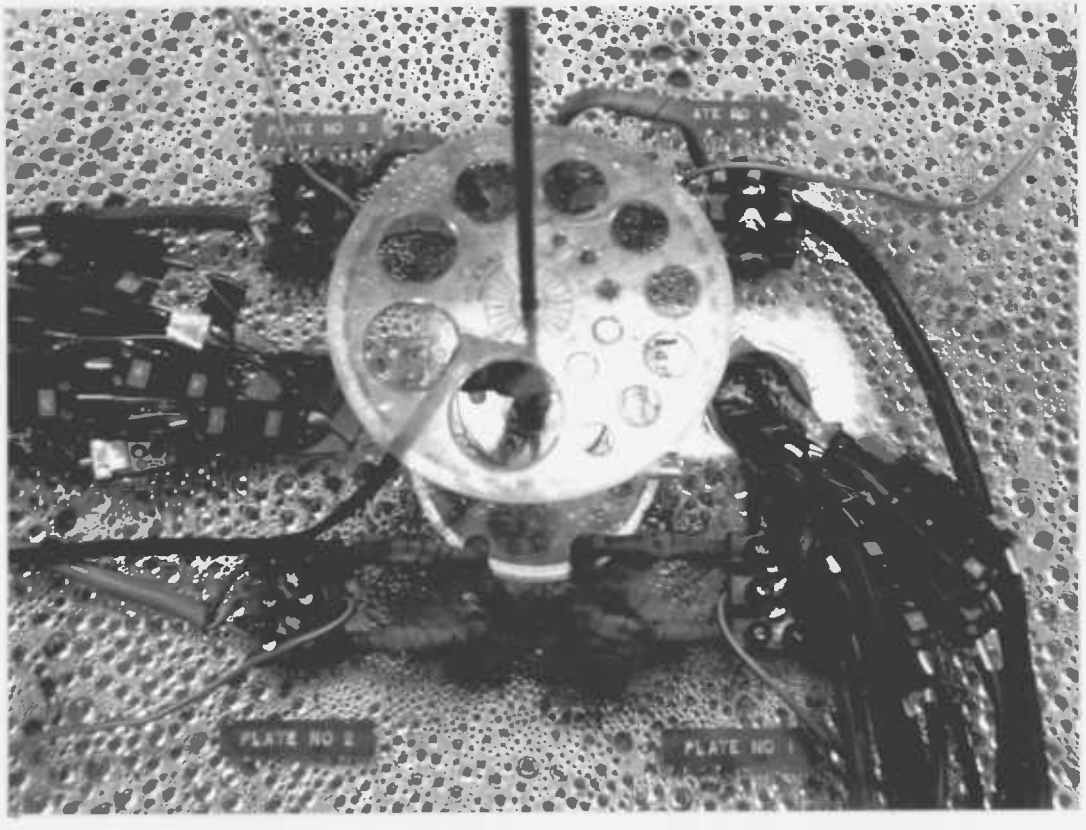

Photo. (6b) The perspex cover of the Discharge Tank with the vertical probe

that $\dot{m}_{t.c}$ which is estimated as such is subject to some underestimation - order of 10% - and the error could have been avoided by setting up a single rectangular channel rather than the sub-assembly fuel plates, Fig. (6.5a). For the present study, however, the need for representing the fuel elements in ULR core has led to the choice of the latter.

(4) The temperature is measured in different parts of the water circuit. Iron-Constantan thermocouples were used for these measurements and their signals were read by DVM/Chart-recorder.

In addition to the test-section, the temperature is also measured at the three following parts of the circuit:-

(i) In the Heater Tank, by a thermocouple positioned near the bottom of the tank.

(ii) At the inlet to the test-section, by the probe shown on Photo. (4). The probe contains a thermocouple positioned in a thin hypodermic tube and is placed near the top of the Inlet Manifold Tank.

(iii) At the exit of the test-section, by the horizontal probe shown on Photos. (4) and (8). The probe is positioned near the bottom of the Discharge Tank and exposes its thermocouple above the exit of the test-channel. A more accurate measurement of the t_{out} was executed by means of the vertical probe, Photo. (7), which could travel over the exit of the channel.

6.2.7 Temperature Measurements for the Test-Channel

Provisions were made to measure the temperature on the walls and also at the centre of the test-channel, t_w and t_ℓ, shown on Fig. (6.5a). The temperature on the walls of the channel is measured by thermocouples embodied in the walls as shown in Fig. (6.16). The

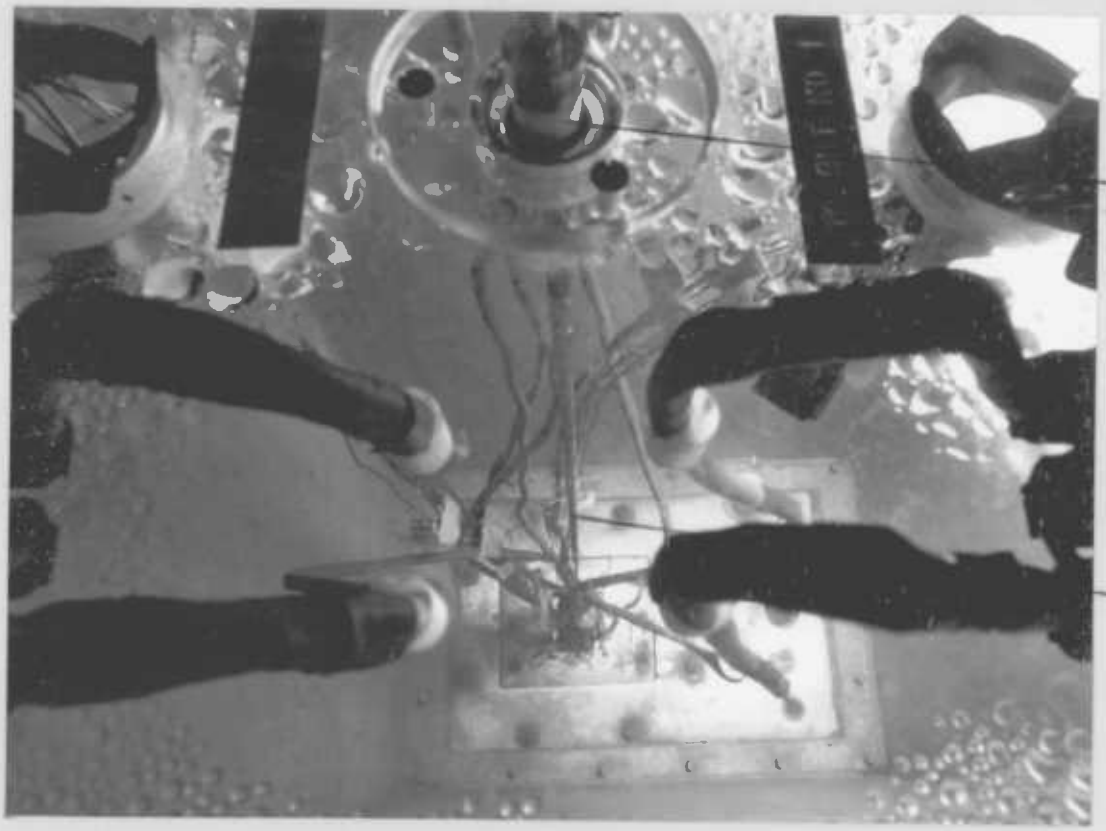

Photo. (7) The vertical probe for t_{ℓ} measurement and its holding arrangement on the perspex plate

Photo. (8) The horizontal probe measuring water temperature at the exit of the test-channel

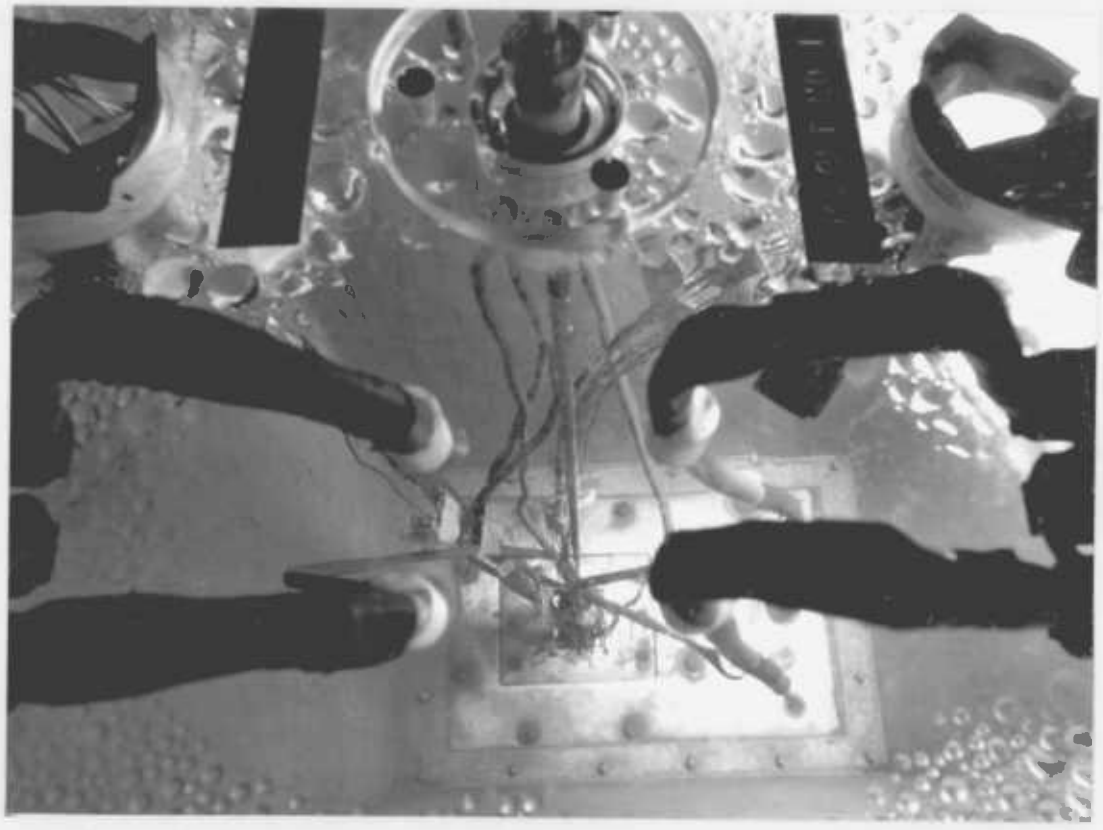

Photo. (7) The vertical probe for t_ℓ measurement and its holding arrangement on the perspex plate

Photo. (8) The horizontal probe measuring water temperature at the exit of the test-channel

centreline temperature is measured by a vertical probe travelling along the channel, Photo. (7). In the following, these two measurements are discussed in detail.

(i) Wall Temperature Measurement

The wall temperature on the broad-sides of the test-channel is measured by means of the twelve thermocouples embodied in the walls according to two-dimensional patterns shown on Fig. (6.16). The patterns were designed to reveal information about the temperature distributions across and along the channel. These two plates, which are used in the simulating heaters and make the broad-sides of the test-channel, were named PL. No. 1 and PL. No. 2 according to their temperature measuring patterns. The signal of their thermocouples is sent via a rotating switch (1 rev/40 sec) to a chart-recorder, Fig. (6.18) and Photo. (2). By this method, axial variations of the t_w profile in the channel are recorded every 40 seconds. For higher accuracy, and confirmation of the temperature recordings, the signals are also read by a Digital Volt Meter, DVM (accurate up to 0.2 ^{o}C).

(ii) Centreline Temperature Measurement

In order to obtain axial variations of the centreline temperature, t_{ℓ} a vertical probe, shown on Photo. (7), has been designed. The probe is made of a thermocouple placed inside two hypodermic tubes. The smaller tube, OD = 2 mm , is chosen to be small enough to move along the test-channel (d = 3.2 mm),Fig. (6.5a). The large tube, OD = 4.76 mm , is to fit into a spherical bearing located in the perspex cover of the Discharge Tank, Photo. (6a). This tube is marked at 24 equal distances representing different

longitudinal positions inside the test-channel.

Because of the rather large length of this probe, it is very difficult to have it ideally straight. Therefore, although the probe holder in the perspex plate is designed to position it at the centre of the test-channel, it is not quite possible to measure $t_{\underline{\ell}}$ relying only on this fact. Moreover, for the present arrangement of the test-section, its solid sides do not permit observation of the position of the probe inside the test-channel.

To make sure that at every axial position the probe is placed at the centre of the channel, it is noted that if the simulating heaters of the test-channel are equally heated, then the minimum coolant temperature occurs at the centre of the channel. This gives a practical solution to the uncertainties about the position of the tip of the probe because at every axial position, the probe could be turned around until the minimum value is read (by the recorder DVM). This minimum is regarded as the $t_{\underline{\ell}}$ value at that axial position.

A circular plate, graded on the circumference, is placed at the end of the vertical probe, Photo. (6b), which facilitates the finding of the next centreline position when a $t_{\underline{\ell}}$ recording is completed.

CHAPTER 7

EXPERIMENTAL RESULTS AND COMPARISON WITH THEORY

7.1 Introduction

In this chapter, the results of several tests which have been carried out on the test-rig, described in Chapter (6), are discussed. These consist of several mixed-convection cases as well as a natural-convection case.

For each case, a comparison is made between the experimental results and their corresponding theoretical predictions which are obtained by the computer program DUCT, explained in Chapter (4).

In order to facilitate the discussion of the results for the above-mentioned cases, a plan is proposed at the end of this chapter. Here, every case is represented by two dimensionless numbers related to it, namely, Re_D and Gr_D. The plan has the advantage of showing the boundaries of the forced, natural, and mixed-convections within the range of the two numbers considered for the tests.

Results of a pressure-loss test for different water flow rates in the water circuit of the test-rig, Fig. (6.1), are shown at the end of this chapter.

7.2 Mixed-Convection Tests

One of the objectives of the test-rig has been to study axial variations of temperature at the wall and also at the centre of the flat duct with large aspect ratio, when its broad-sides are heated according to a sinusoidal law, Fig. (6.5a), under various mixed-convection regimes. The study compares several of these cases, assuming given total heat input, $\dot{Q}_{tot}$ and inlet pressure p_o. In what follows, the t_w and the t_{ℓ} profiles are obtained for these cases.

According to dimensional analysis, two dimensionless numbers, Re_D and Gr_D may represent each of the above-mentioned cases. The Reynolds number is selected to signify the effects of the forced-convection while Gr_D is representative of the natural-convection effects. Also, by an order- of-magnitude analysis, these two numbers may be combined into a parameter which represents the effects of both of them together. As mentioned in Chapter (5), this parameter is Gr_D/Re_D^2 and represents the relative importance of the "buoyancy" and "viscous" forces together. Table (7.1) summarises the data of the tests conducted for this chapter. According to this table, the first two tests have the same $\dot{Q}_{tot}$ but differ in p_o. The second test is executed in order to study the effects of gradually moving from one mixed-convection case towards another which displays stronger effects of forced-convection. In the third and the fourth tests, the total power input, $\dot{Q}_{tot}$ has been set at lower values than that of the first test while keeping the t_m nearly the same. This allows us to assume the same water properties for all of the tests in the theoretical predictions.

7.2.1 Procedure of the Experiments

Results for the mixed-convection tests, mentioned in Table (7.1), were obtained by taking the following steps for each of the tests:-

(1) The test rig, Fig. (6.1) was filled with water at the preselected temperature t_1.

(2) The Supply Tank was raised to the height where its level-difference with the Discharge Tank was:- $\Delta h' = 20$ cm

TABLE (7.1) DATA FOR THE MIXED-CONVECTION TESTS (SEE TABLE (5.5) FOR GEOMETRICAL DATA)

Reduced data / Test No.	$\dot{Q}_{tot}$ (w)	$\dot{q}''_{w.av}$ (w/cm^2)	$\dot{m}_c$ (gr/sec)	t_m (^oC)	p_o (cm H_2O)	Re_D	Gr_D	Gr_D/Re_D^2
1	975.0	1.2	43.3	40.76	33.3	341.4	2.219×10^5	1.903
2	975.0	1.2	66.7	36.96	80.0	525.6	1.943×10^5	0.703
3	812.5	1.0	40.0	39.71	27.6	315.3	1.749×10^5	1.760
4	650.0	0.8	33.3	39.33	20.0	262.6	1.387×10^5	2.012

(3) After shutting the by-pass pipe, the water flow rate, $\dot{m}_c$ was regulated by the valve V_1 to be:-

$\dot{m}_c$ = 33.3 gr/sec (2 lit/min on the Rotameters)

(4) The Supply Tank was raised to provide the test-section with the prescribed mass flow rate, $\dot{m}_c$ and its corresponding inlet pressure, p_o.

(5) Power was connected to the electrical terminals of the simulating plates.

(6) After 30 minutes, the first set of the t_w and the t_{ℓ} profiles were recorded. The next readings were executed at 15 minute intervals.

(7) For the tests where an increase in the p_o value was to be studied, e.g. the second test in Table (7.1), the following step was also needed.

After the recording of the t_w and the t_{ℓ} profiles for the first test, the Supply Tank was gradually raised to the height required by the second test. Naturally, this was followed by a gradual increase in the $\dot{m}_c$ value leading to reductions in the t_w and the t_{ℓ} values.

7.2.2 Results for the First Test (Re_D = 341.4, Gr_D/Re_D^2 = 1.903)

Fig. (7.1) shows the axial variation of t_w recorded for this

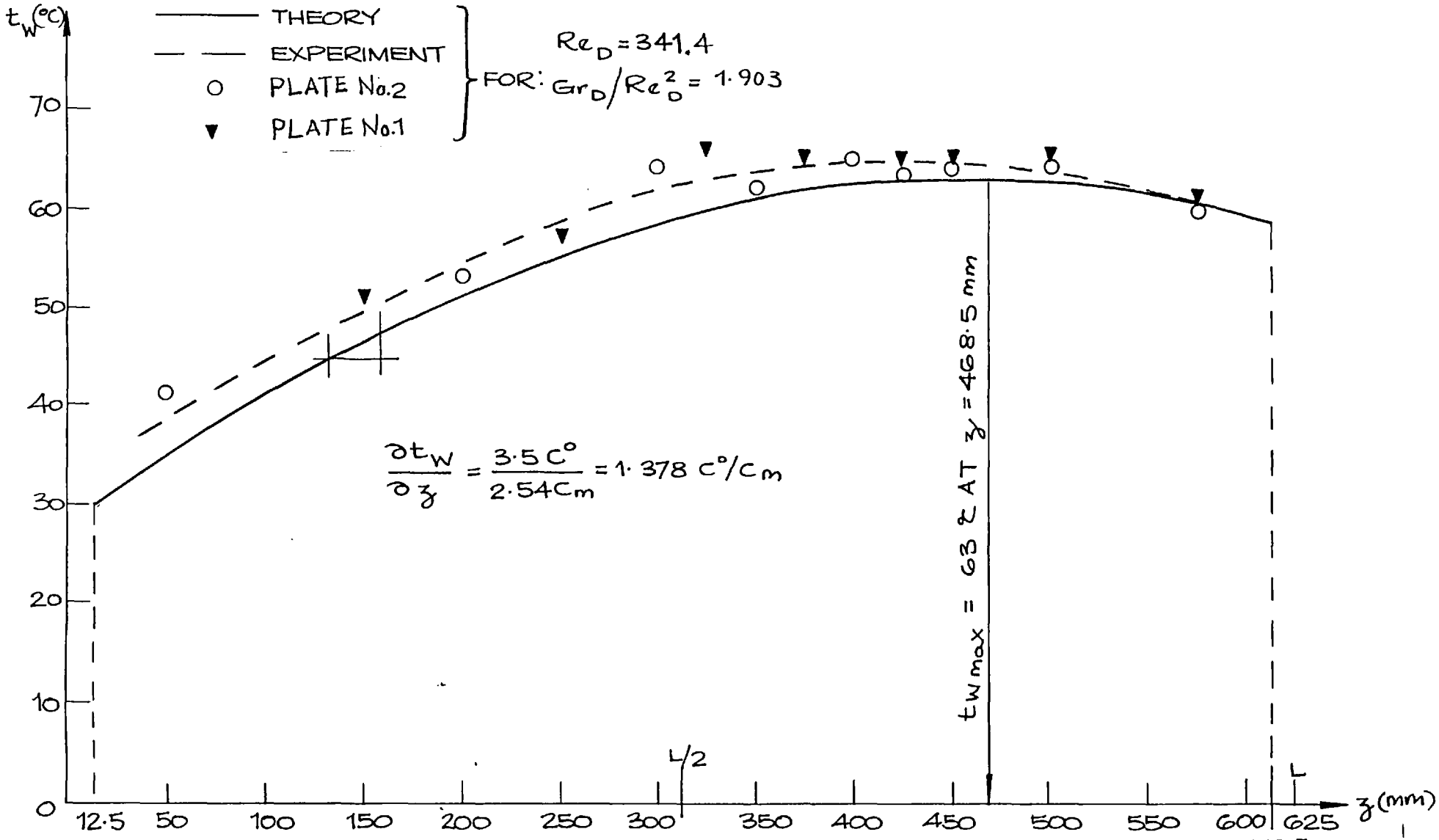

FIG. (7.1): EXPERIMENTAL AND THEORETICAL WALL TEMPERATURE DISTRIBUTIONS ALONG THE CHANNEL.

case. The profile was obtained by the recordings of the twelve thermocouples embodied in each side of the test-channel, Fig. (6.16). It is recalled from Chapter (6) that these thermocouples were positioned according to a two-dimensional pattern. The simulating plates are referred to as Plate No. 1 and Plate No. 2 according to their thermocouple patterns. The different symbols used in Fig. (7.1) for the reading of the two plates facilitate distinguishing their results. Table (7.2) shows the positions of the thermocouples in the two simulating plates.

On Fig. (7.1) the dotted curve represents a curve-fit between the temperature reading of the two plates. Having only one sign at a position shows either that there has been only one reading for that position or that the t_w recording for both of the plates has been the same.

Theoretical predictions for the t_w profile along the test-channel are also shown on this figure (full-line). A comparison between these two curves suggest that qualitatively both of them are the same, i.e. the overall shape is the same and there exists a maximum value for the t_w at an axial position in the second half of the channel. However, the $t_{w.max}$ appears to be higher on the experimental curve and occurs at a shorter distance from the channel entry.

Also, the experimental curve shows higher temperatures for the positions situated before the maximum. The reason for this may be due to a "longitudinal" conduction of heat which takes place along the channel, $\dot{q}''_{cd}$ (z) shown on Fig. (7.2). This conduction is due to the existence of a temperature gradient along the channel. In order to

TABLE (7.2)

SUMMARISING THE THERMOCOUPLE PATTERNS OF THE TWO SIMULATING PLATES (SHOWN ON FIG. (6.9))

PL . No. 1

T/C. No	z/L	x/w
7	0.000	0.461
8	0.080	0.400
6	0.240	0.523
5	0.400	0.585
4	0.520	0.638
9	0.600	0.330
10	0.640	0.277
3	0.680	0.715
11	0.720	0.215
2	0.800	0.769
1	0.920	0.830
12	0.984	0.153

PL . No. 2

T/C. No	z/L	x/w
1	0.000	0.830
12	0.080	0.161
11	0.320	0.215
10	0.480	0.277
2	0.560	0.777
3	0.600	0.707
9	0.640	0.346
4	0.680	0.654
8	0.720	0.408
7	0.800	0.800
6	0.920	0.523
5	0.984	0.585

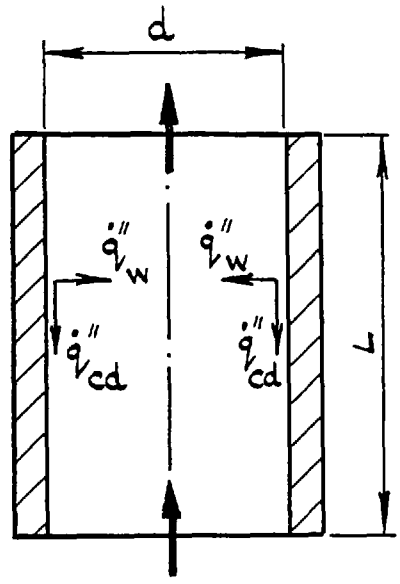

FIG.(7.2): THE LONGITUDINAL AND THE NORMAL WALL HEAT-FLUXES.

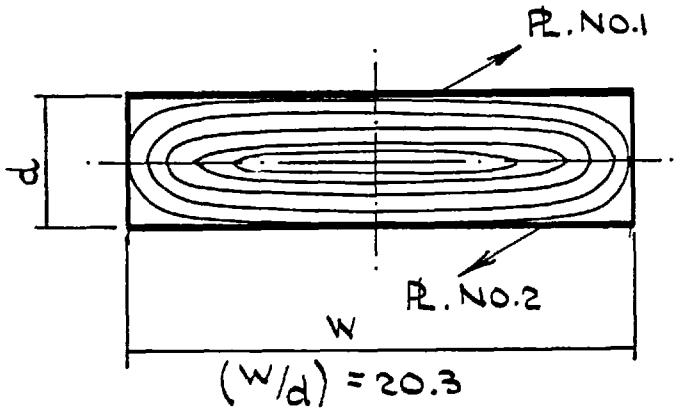

FIG.(7.3): THE CORNER EFFECTS IN THE RECTANGULAR CROSS SECTION.

obtain a measure of the value of this conduction, the ratio of the net heat conduction $\dot{Q}_{cd}$ - which is proportional to $\partial^2 t_w/\partial z^2$ - to the total generated heat of a strip of a finite length $\dot{Q}_z$, is calculated. For a strip near the entrance of the channel, this ratio is found to be 0.0018, while for a similar strip located at the vicinity of the axial position where $t_{w_{max}}$ occurs, the ratio is 0.003. Therefore, in both of the cases, the value of $\dot{Q}_{cd}$ is less than or equal to 0.3% of $\dot{Q}_z$.

Existence of the longitudinal conduction is also noted by other workers, namely, Petrovichev (1960) and McCuen (1962). It is recalled from the literature survey, Chapter (2), that in Petrovichev's experiment, a round tube was heated according to a sinusoidal law by winding an electric heater (with a variable pitch) around it. In order to reduce the axial heat-losses, he divided the tube into twelve parts by circular grooves.

In McCuen's experiment, a vertical flat duct was heated in the broad-sides by dividing it to twenty four divisions each heated by water at different temperatures. Each of the divisions was thermally insulated from its neighbouring divisions by a thin layer of an insulator. By this method, he assumes that during operation the divisions may be maintained at different temperatures without the possible axial heat-losses between the divisions.

In the entrance region, there exists a difference between the experimental and the theoretical values of t_w. This may be explained by considering that there exists a finite heat-flux at this region but a near zero temperature difference between the coolant and the wall. The convective heat transfer coefficient h would theoretically

be nearly infinite. However, because of axial heat conduction through the wall (or through a nuclear fuel element) toward the entrance, the wall temperature actually rises above the temperature of the coolant and the heat transfer coefficient, though large, is finite.

Fig. (7.1) also shows that the t_w values experimentally obtained for Plate No. 1 are higher than those of Plate No. 2 at the same axial positions. This suggests that there is a temperature profile across the simulating plates. From Table (7.2), it is noted that there exists two different thermocouple patterns on these plates. In these patterns, some thermocouples are placed at the same axial positions on the two plates (e.g. T/C no. 3 of PL. No. 1 and T/C no. 4 of PL. No. 2) but they differ in their distances across the plates (x/w = 0.715 and 0.654 respectively). As shown on Fig. (7.1), the reading for the former is higher than that of the latter. This may be explained by considering that because of the rectangular shape of the cross-section, the velocity of the coolant particles near the corners is less than at the centre. Therefore, the cooling process is rather poor near the corners leading to higher t_w values. Following this argument it may be concluded that because the thermocouples embodied in PL. No. 1 are nearer to the corners of the cross-section than those of PL. No. 2, they measure higher t_w values at the same axial positions, Fig. (7.3).

Existence of the temperature profile across the plates was also noted by Savino et al (1964) in their study of convective heat transfer in rectangular channels. Although they were only concerned with a uniform $\dot{q}_w''$, they also concluded that because of the poor convection in the corners and along the narrow sides of a rectangular channel, the peak temperature at every axial position occurs at the

corners.

The above-mentioned discussion suggests that the assumption of a uniform wall temperature across the plates employed in the theoretical model is not strictly correct.

Fig. (7.4) shows axial variations of the temperature at the centre of the channel, t_{ℓ}. According to this figure, the shapes of the experimental and the theoretical curves are the same. However, the experimental values seem to be slightly higher all along the channel. The differences are higher near the entrance and decrease further downstream. The same argument as what is used for the t_w profile, Fig. (7.1), may be used to explain these differences.

7.2.3 Results for the Second Test (Re_D = 525.6, Gr_D/Re_D^2 = 0.703)

In the theoretical model, the predictions for t_w and t_{ℓ} were obtained by considering the effects of the natural and the forced-convection regimes together. Consequently, the predictions were affected by the degree to which the problem was close to these two regimes. In this part of the thesis, it is intended to study the effects of increasing the degree by which the problem depends on the forced-convection type of condition.

The study is based on the t_w and the t_{ℓ} profiles obtained after raising the Supply Tank of Fig. (6.1) to a higher level than that required by the first mixed-convection test mentioned above. The increase in the level-difference between the Supply and the Discharge tanks affects p_o directly and leads to an increase in the water flow rate, $\dot{m}_c$. Results for this case, reported as Test No. 2 in Table (7.1) were obtained following this procedure, i.e. by gradually

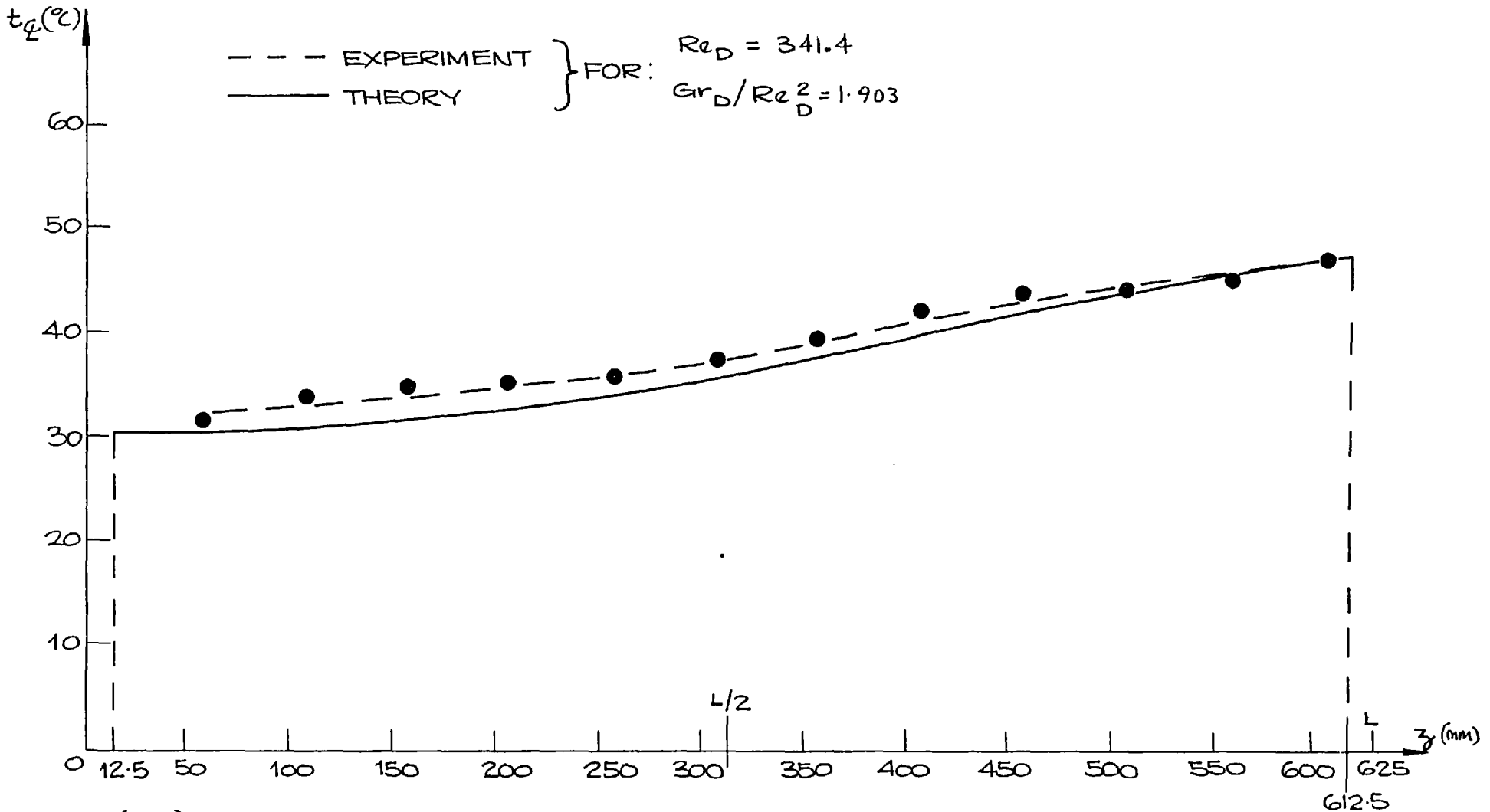

FIG. (7.4): EXPERIMENTAL AND THEORETICAL CENTRE-LINE TEMPERATURE DISTRIBUTIONS ALONG THE CHANNEL.

raising the Supply Tank to a higher level (80 cm level-difference c.f. 33.3 cm for the first test). Figs. (7.5) - (7.6) show the t_w and the t_{ℓ} profiles experimentally obtained for this test together with their corresponding computer predictions. The results show the same trend as that of the first test although the differences are slightly lower. This may be attributed to a lower water temperature rise throughout the test-channel.

In order to facilitate the comparison of the t_w profiles for the first and the second tests, they are both shown on Fig. (7.7). It is noted on this figure how the increase in the p_o value is followed by a reduction in the t_w values throughout the channel. The reduction is smaller at the entrance region of the channel and gradually increases along the channel. Also, $t_{w.Max}$ occurs at a shorter axial distance from the channel entry. The reason may be as follows.

As mentioned earlier, Chapter (5), in the sinusoidal heating case, there exists a "lag" between the axial positions where $\dot{q}''_{w.Max}$ and $t_{w.Max}$ occur. This is due to the fact that the reduction in the $\dot{q}''_w$ values after the middle of the channel is not immediately reflected by the coolant and its adjustment takes some distance along the channel. Therefore, the $t_{w.Max}$ occurs further than the middle of the channel. The difference between the axial positions where $t_{w.Max}$ and $\dot{q}''_{w.Max}$ occur may be lowered by increasing the speed of the heat recovery from the channel walls, i.e. increasing the water mass flow rate, $\dot{m}_c$. In the second test, the gradual increase in the p_o value directly leads to an increase in $\dot{m}_c$ which in turn shortens the axial distance needed for the $t_{w.Max}$ to occur.

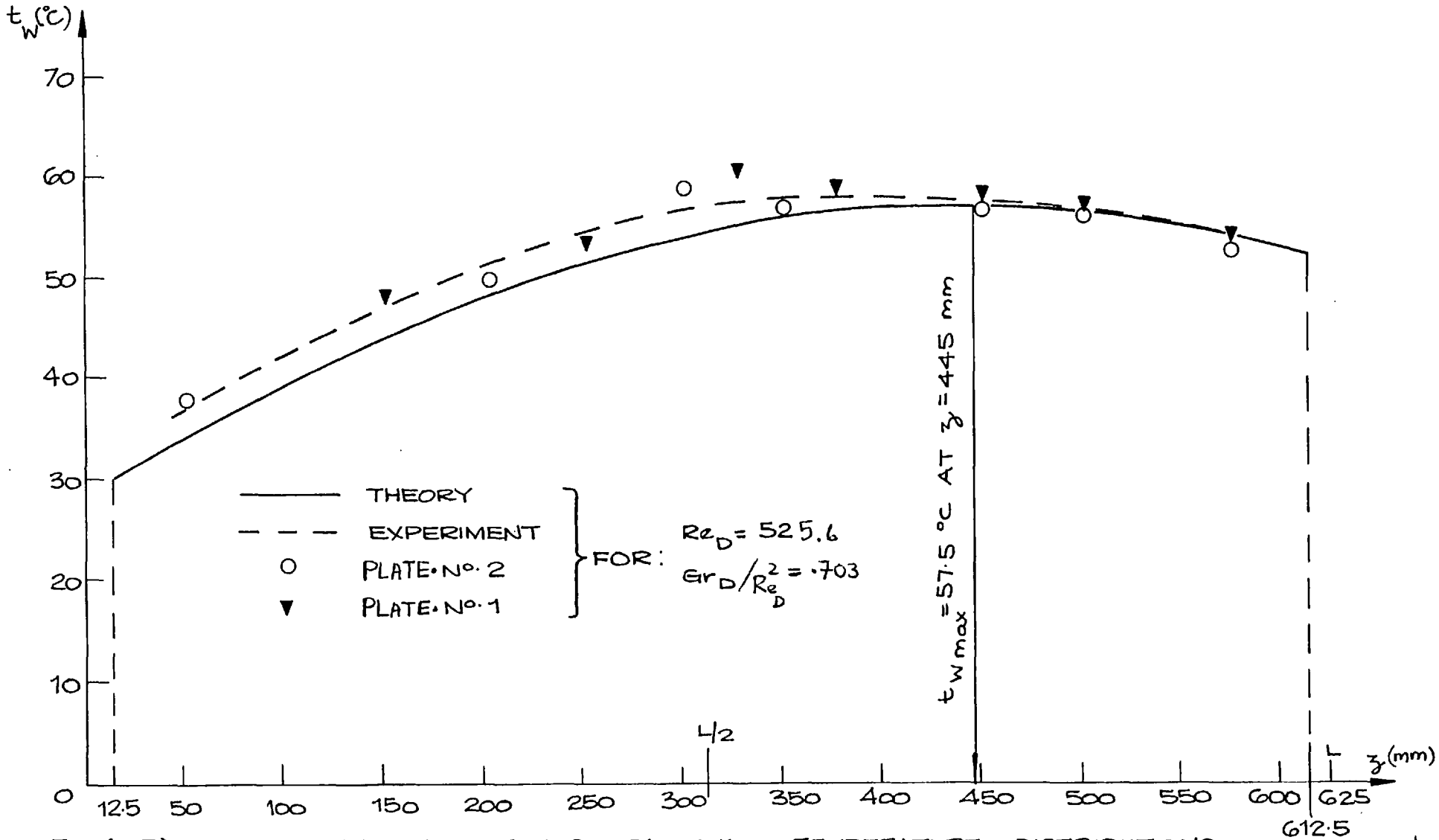

FIG.(7.5): EXPERIMENTAL AND THEORETICAL WALL TEMPERATURE DISTRIBUTIONS ALONG THE CHANNEL.

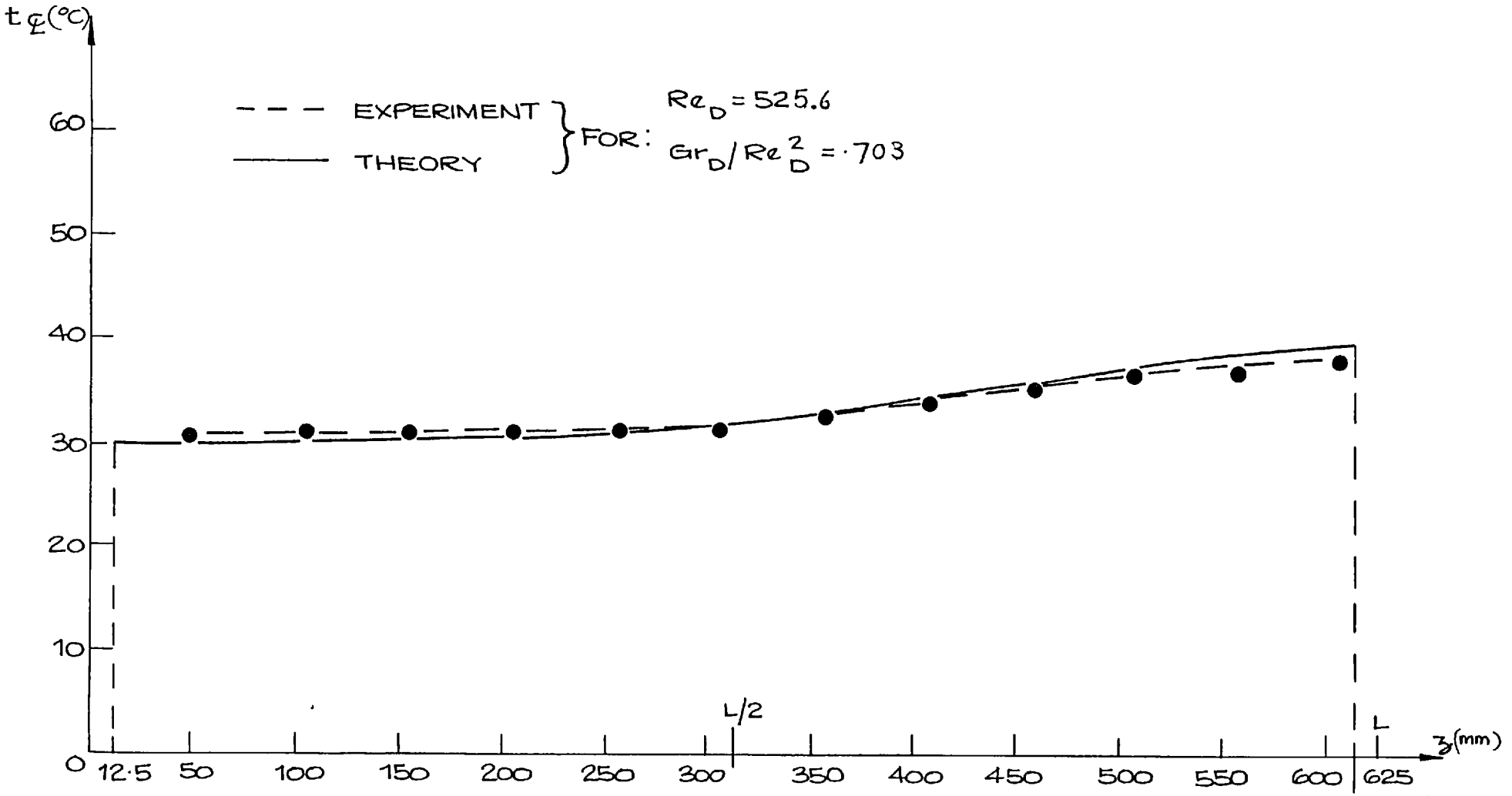

FIG. (7.6): EXPERIMENTAL AND THEORETICAL CENTRE-LINE TEMPERATURE DISTRIBUTIONS ALONG THE CHANNEL.

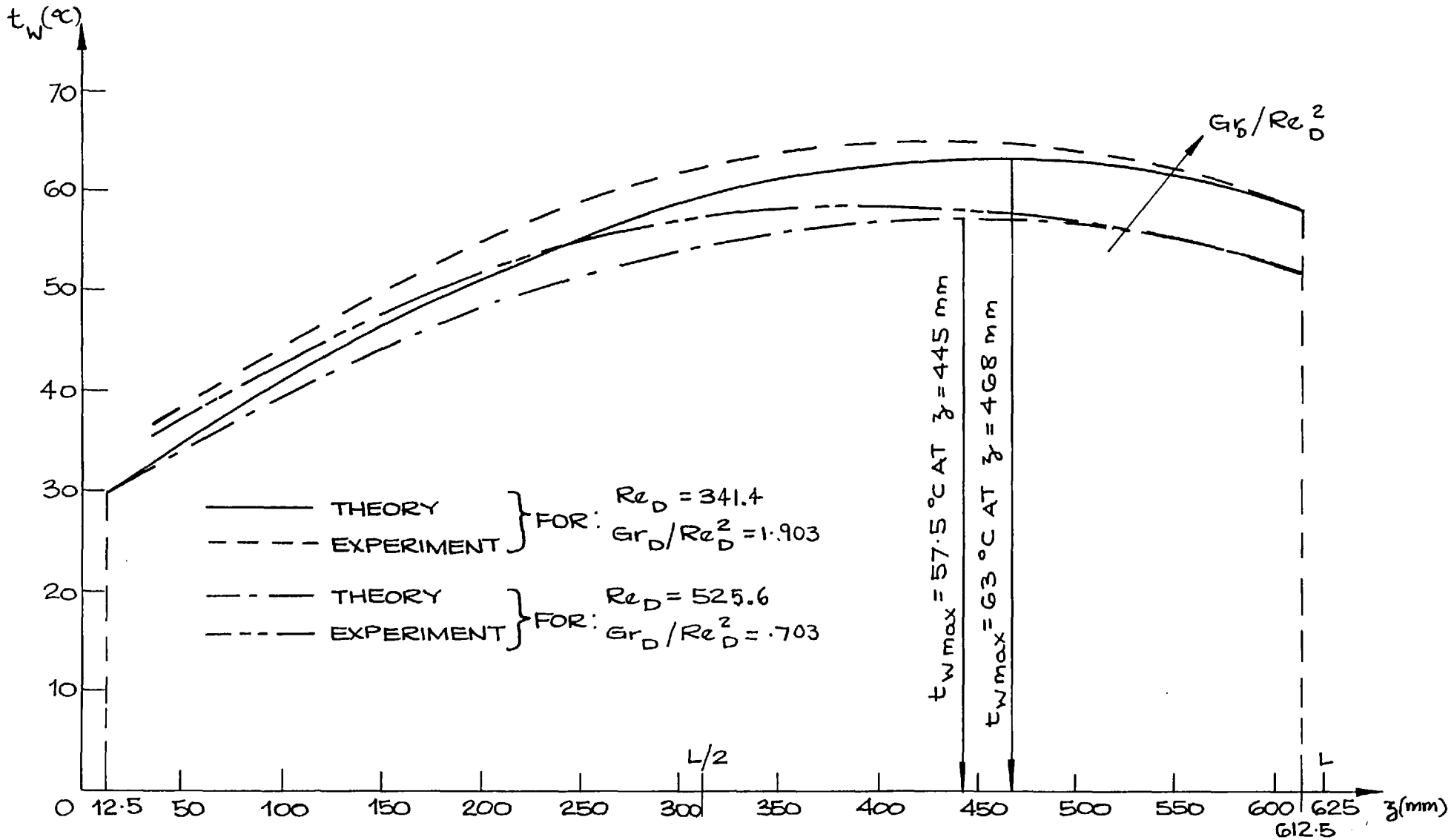

FIG.(7·7): COMPARISON OF THE WALL TEMPERATURE DISTRIBUTIONS FOR TWO CASES.

7.2.4 Results for the Third and the Fourth Typical Tests (Re_D = 315.26, Gr_D/Re_D^2 = 1.76 and Re_D = 262.6, Gr_D/Re_D^2 = 2.01)

In order to confirm the experimental results obtained for the first two tests mentioned in Table (7.1), similar tests were carried out for two other cases which differ in the $\dot{Q}_{tot}$ and the p_o values.

As shown on Table (7.1), for the third and the fourth tests the $\dot{Q}_{tot}$ value is lower than the first test (16.3% and 33.3% respectively) while the t_m value is very close. The experimental results for the t_w and the t_{ℓ} profiles compare favourably with corresponding computer predictions; similar to those of the first test, although the differences seem to be slightly lower, Figs. (7.8) - (7.11).

7.3 Natural-Convection Test

The problem of natural-convection in a vertical heating channel is one of the many problems which are presented in the sphere of natural-convection. The term "natural-convection" is used here for heat transfer in the test-channel when the pressure gain due to buoyancy of the coolant (water) equals the total pressure drop throughout the channel. This definition is employed in the computer program to calculate the water flow rate, $\dot{m}_c$ which corresponds to a total heat rate, $\dot{Q}_{tot}$ for this type of regime in the test-channel.

In performing an experimental test for natural-convection on the test-rig, Fig. (6.1), the pressure loss in the water circuit other than the test-section should also be considered. (These losses have so far been neglected because of their comparatively small values in regard to the level-difference of the Supply and the Discharge tanks). To account for these, the following method has been used:-

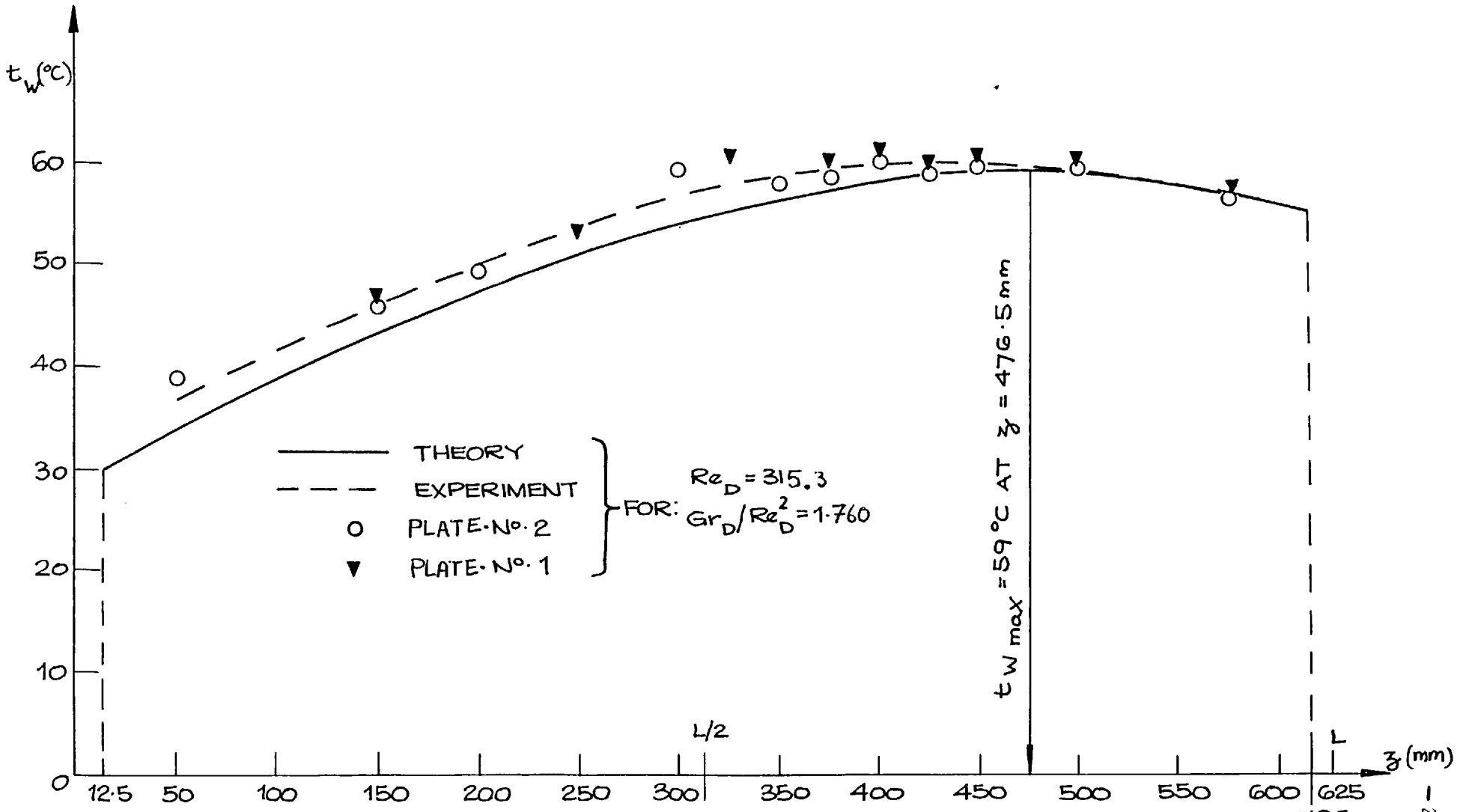

FIG. (7.8): EXPERIMENTAL AND THEORETICAL WALL TEMPERATURE DISTRIBUTIONS ALONG THE CHANNEL.

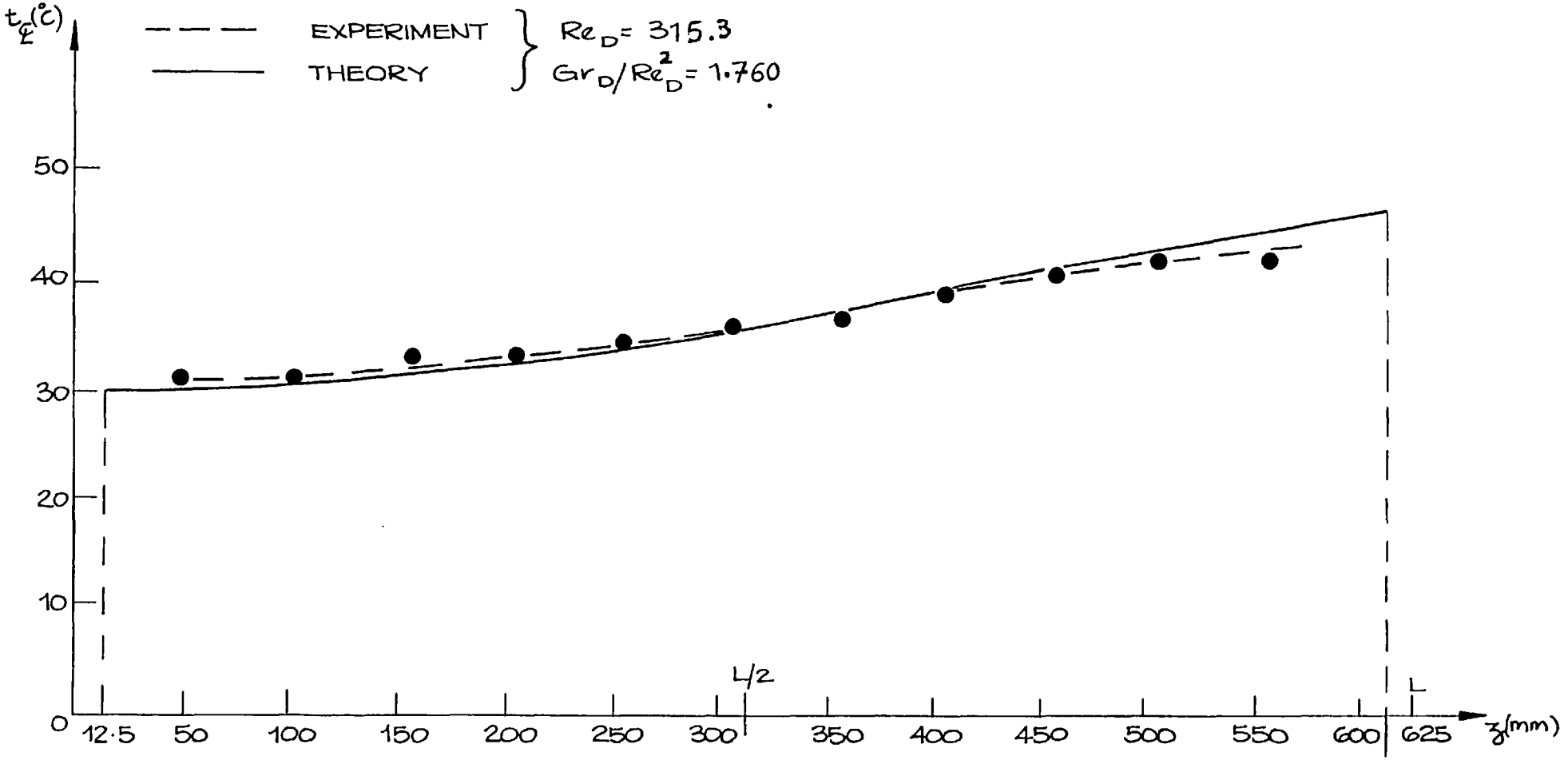

FIG. (7.9) : EXPERIMENTAL AND THEORETICAL CENTRE-LINE TEMPERATURE DISTRIBUTIONS ALONG THE CHANNEL.

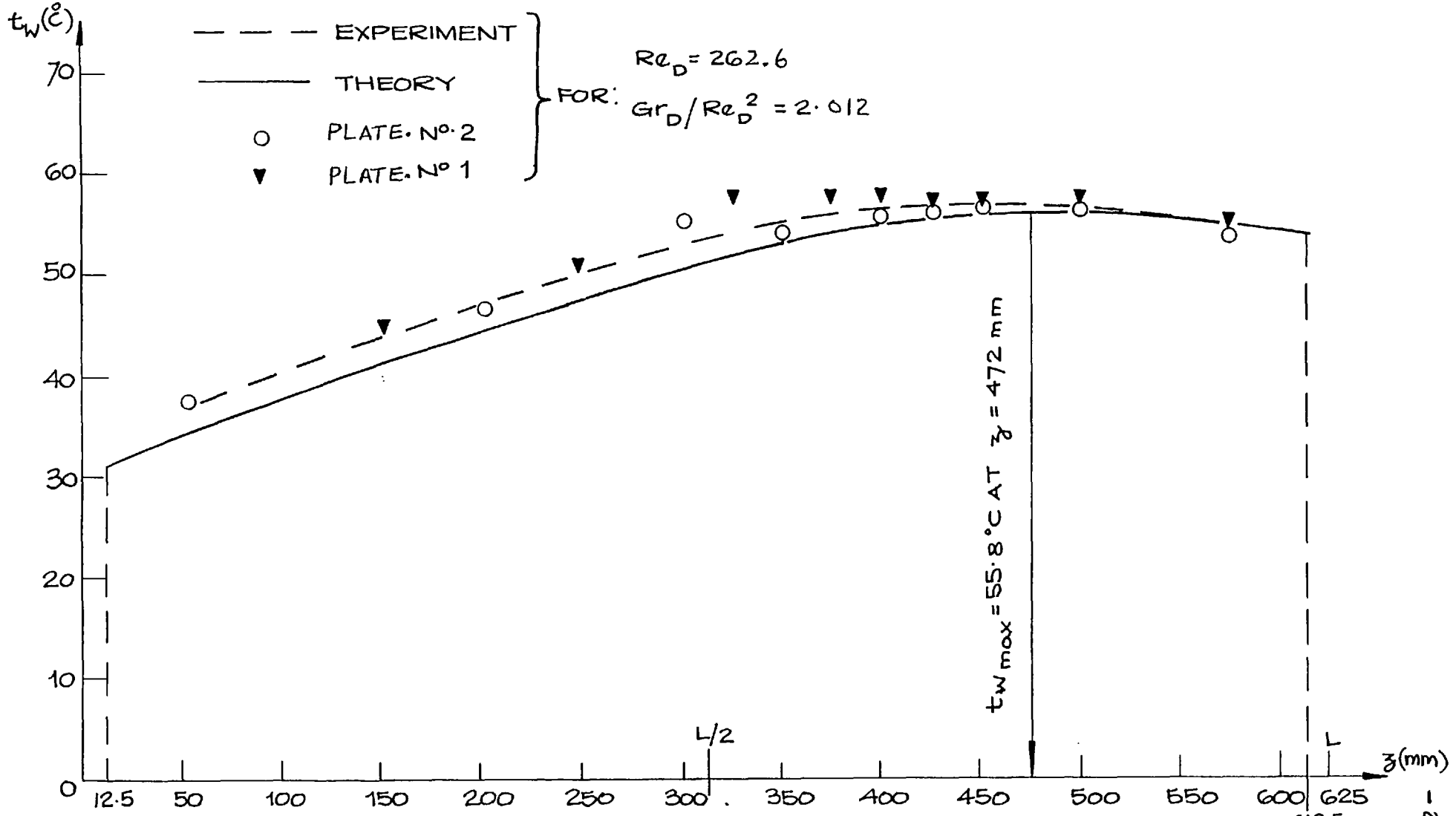

FIG. (7.10): EXPERIMENTAL AND THEORETICAL CENTRE-LINE TEMPERATURE DISTRIBUTIONS ALONG THE CHANNEL.

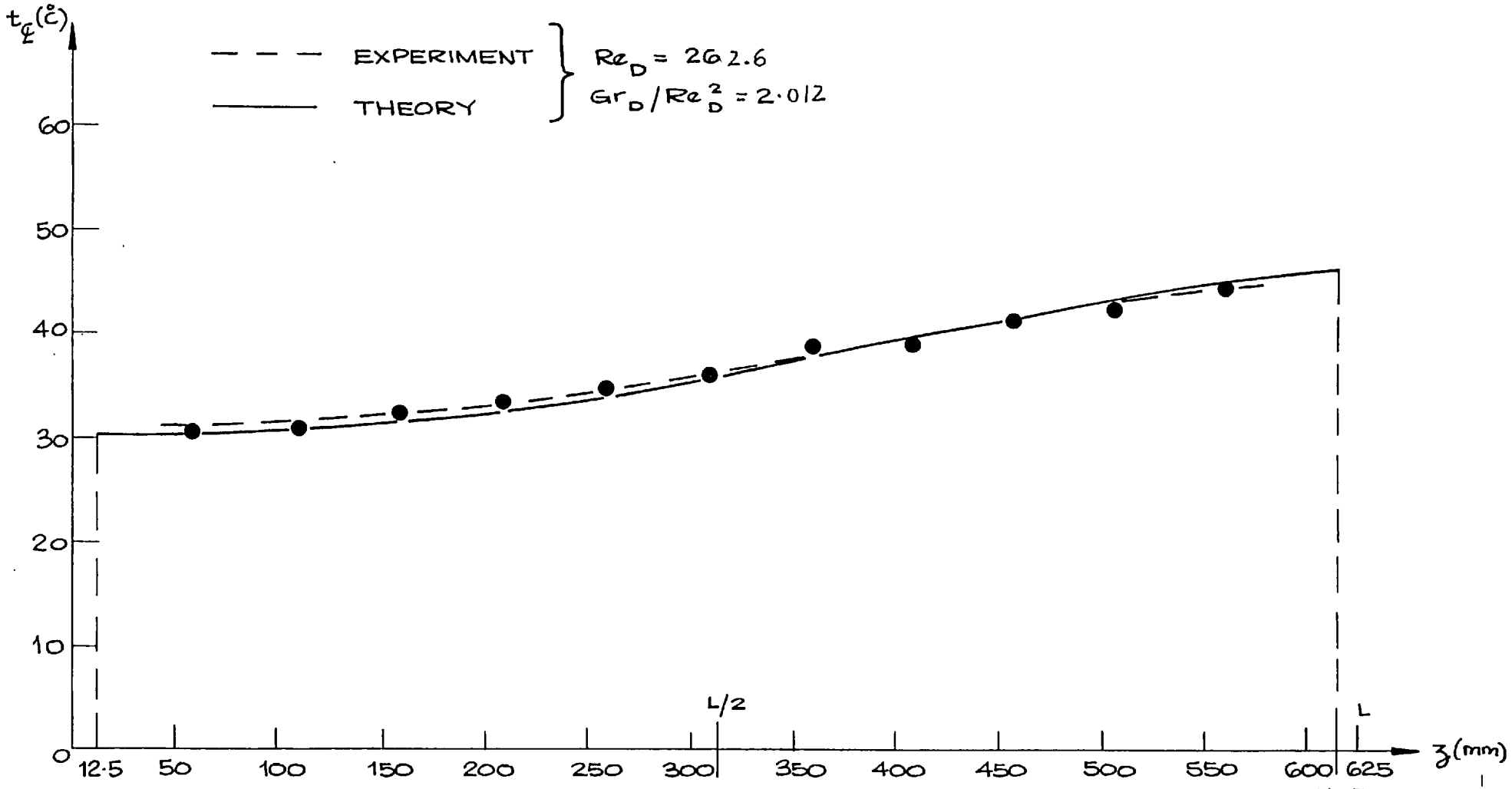

FIG. (7·11) : EXPERIMENTAL AND THEORETICAL CENTRE-LINE TEMPERATURE DISTRIBUTIONS ALONG THE CHANNEL.

(1) The ideal flow rate, $\dot{m}_c$ for a given total heat $\dot{Q}_{tot}$ is determined by the computer program.

(2) Total pressure loss throughout the water circuit is measured; Δp_{tot}.

(3) Total pressure gain in the test-channel for the $\dot{m}_c$ and the $\dot{Q}_{tot}$ is calculated; Δp_{gain}.

(4) The extra level-difference needed between the Supply and the Discharge tanks is therefore:-

$$\Delta h'_e = \Delta p_{tot} - \Delta p_{gain}$$

Table (7.3) shows the pertinent data for the natural-convection test (Test 5).

To gain more confidence about this method of experiment, several tests were carried out for the same $\dot{Q}_{tot}$ but with lower $\Delta h'_e$ values. They all caused less water flow rates than the above-mentioned ideal value of $\dot{m}_c$ (therefore the results obtained following the above-mentioned four steps seem to be the closest possible results to the real results in the circumstances) but, in fact, the error between the real and the ideal $\dot{m}_c$ values was within the range of the systematic error of the Rotameters (1.67 gr/sec).

Fig. (7.12) shows axial variation of t_w for the natural-convection test. A comparison between the experimental and the theoretical predictions on this figure demonstrates that they are qualitatively the same. However, as for the mixed-convection tests,

TABLE (7.3) DATA FOR THE NATURAL-CONVECTION TEST (SEE TABLE (5.6) FOR GEOMETRICAL DATA)

Reduced data / Test No.	$\dot{Q}_{tot}$ (w)	$\dot{q}''_{w.av}$ (w/cm^2)	$\dot{m}_c$ (gr/sec)	t_m (^oC)	p_o (cm H_2O)	Re_D	Gr_D	Gr_D/Re_D^2
5	975.0	1.2	39.2	42.00	0	307.7	2.216×10^5	2.340

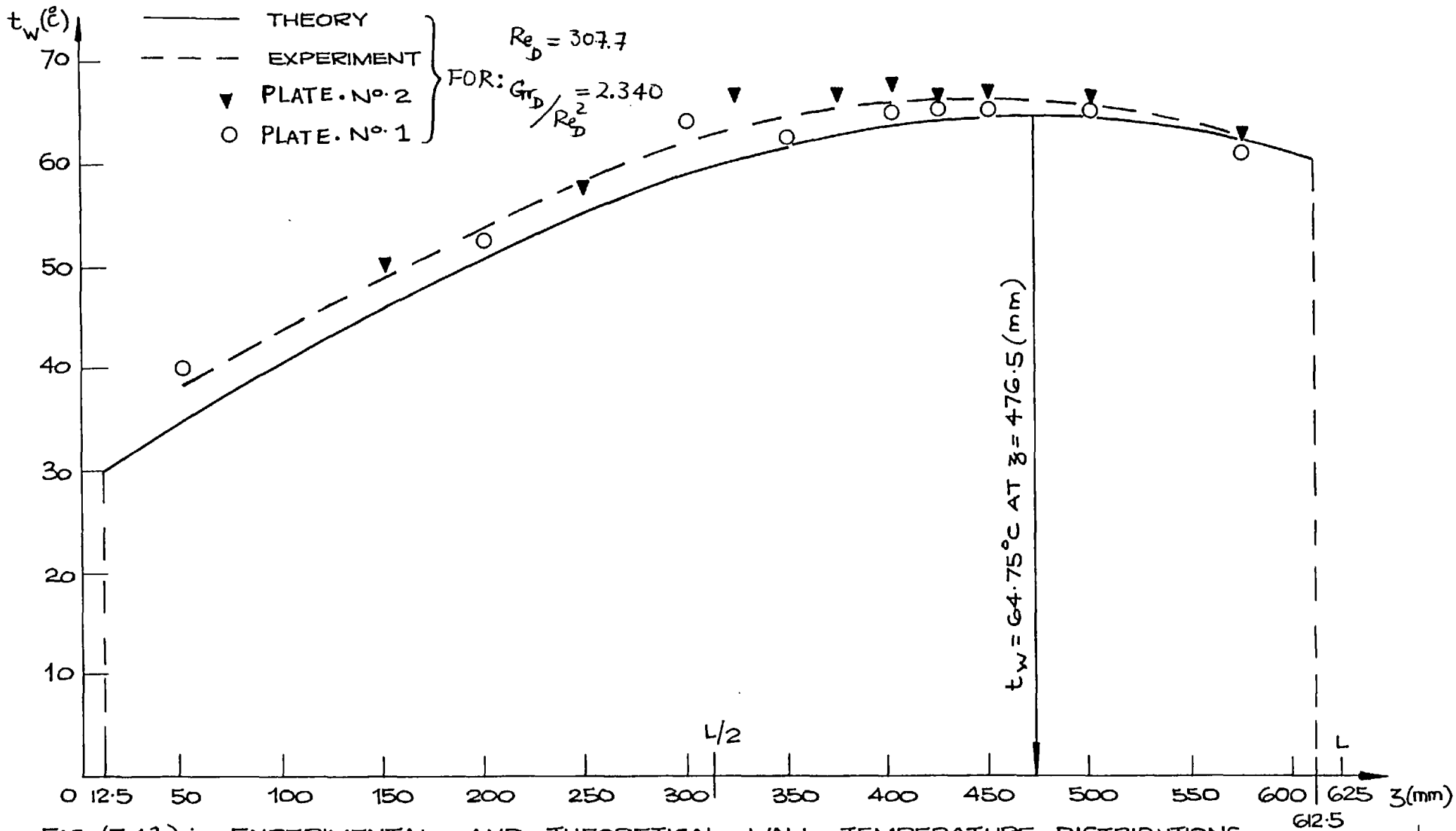

FIG. (7.12): EXPERIMENTAL AND THEORETICAL WALL TEMPERATURE DISTRIBUTIONS ALONG THE CHANNEL.

Tests 1 - 4 in Table (7.1), there are differences between the two curves. These differences reduce near the $t_{w.Max}$ position and confirm the effects of the "longitudinal heat-conduction", $\dot{q}''_{c\,d}$ mentioned earlier in this chapter.

This test also confirms the existence of a temperature profile across the simulating plates, since higher wall temperatures were recorded for PL. No. 1 than PL. No. 2 at the same axial positions. (It is recalled that in the former plate, the thermocouples are positioned nearer the corners of the channel, Table (7.2).

Fig. (7.13) shows the t_{ℓ} profile along the test-channel. Here, quite a good agreement exists between the experimental and the theoretical values near the entry of the channel. Further downstream, however, experimental values seem to be higher. This is thought to be because of some small recirculations taking place there.

7.4 General Representation of the Natural and the Mixed-Convection Tests

Following the comparison of the theoretical and the experimental profiles of t_w and t_{ℓ} for several cases of natural and the mixed-convections, Tables (7.1), (7.3), a trial is made to represent all of them in a general plan.

Fig. (7.14) shows the proposed plan with Re_D and Gr_D numbers on the ordinate and the abscissa axes respectively. The plan is divided to three distinct regions for the forced, the mixed, and the natural-convection regimes. The boundary between the forced and the mixed-convection regions is made by the curve representing $Gr_D/Re_D^2 = 1$. This is because, as mentioned in Chapter (2), when this relationship is satisfied, neither the forced nor the natural-convection effects dominate. Naturally above this curve, where $Gr_D/Re_D^2 < 1$, the forced-convection effects dominate.

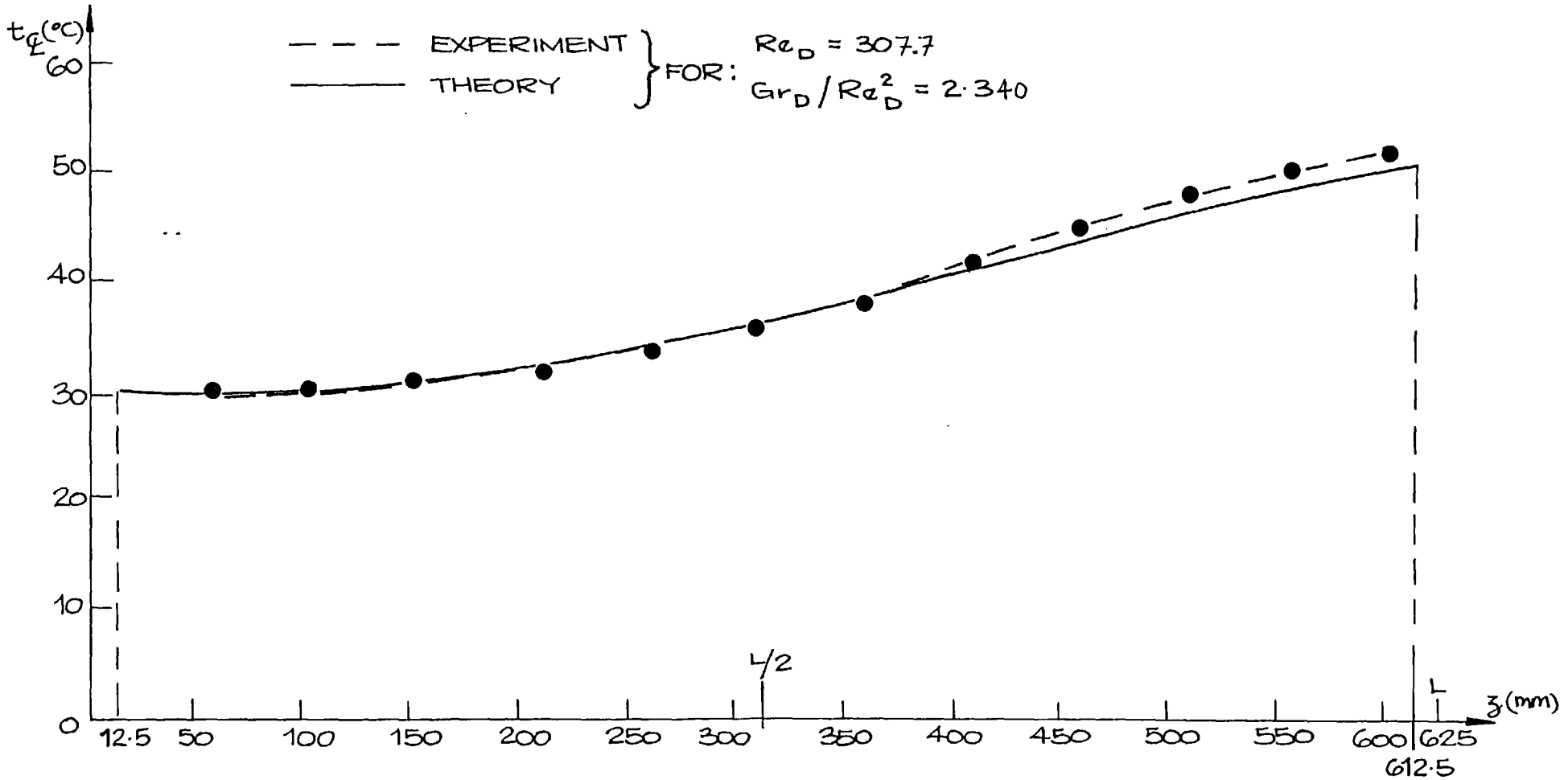

FIG. (7.13): EXPERIMENTAL AND THEORETICAL CENTRE-LINE TEMPERATURE DISTRIBUTIONS ALONG THE CHANNEL.

TEST Nº	Gr_D / Re_D^2
2	0.703
3	1.760
1	1.903
4	2.012
5	2.340

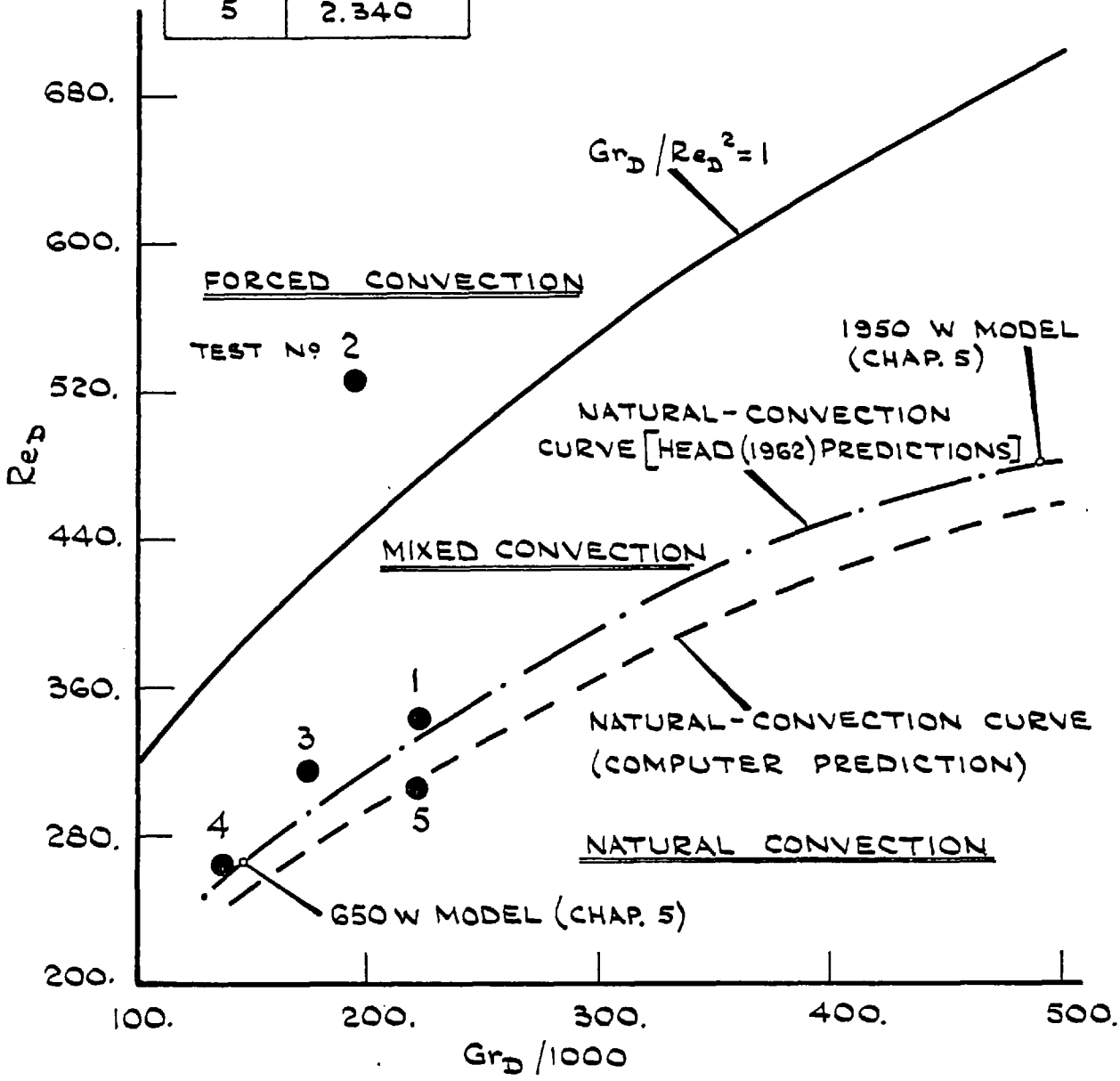

FIG (7.14): THE PLAN REPRESENTING THE EXPERIMENTAL TESTS AND THE COMPUTER PREDICTIONS.

Conversely, for the points located below that curve, $Gr_D/Re_D^2 > 1$, the natural-convection effects do prevail and they become stronger the larger the ratio becomes. The region below the curve for $Gr_D/Re_D^2 = 1$ is, therefore, representative of the cases where the forced and the natural-convection effects are combined together, i.e. mixed-convection region. For the points far below the $Gr_D/Re_D^2 = 1$ curve, the natural-convection effects dominate the situation to the degree that the forced-convection effects can be ignored, i.e. the natural-convection region. The boundary between the natural and the mixed-convection regions is shown by the dotted curve on the figure. This curve is predicted by the computer program DUCT for several natural-convection cases with the data of the test-channel mentioned in Chapter (6).

The five experimental tests reported in this chapter are shown on this plan. It is noted that one test (Test 2) is placed in the forced-convection region, three tests (Tests 3, 1 and 4) are in the mixed-convection region and one test (Test 5), in the natural-convection region. The sequence of the position of these points is according to their Gr_D/Re_D^2 value, see Table (7.1) which confirms the relevance of the choice of this parameter in representing the mixed-convection cases in general, and the two extreme cases of it, i.e. the forced and the natural-convection regimes, in particular.

Also on this plan is shown the natural-convection curve which will be obtained following the method of Head (1962). On this curve the two models considered in Chapter (5) (the 650 W and the 1950 W models) are also shown.

7.5 Frictional Characteristics of the Water Circuit of the Test-Rig

In order to study the pressure losses which occur in the

water circuit for the range of water flow rates mentioned in Table (7.1), i.e. 33.3 to 66.6(gr/sec), a graph presented on Fig. (7.15) was experimentally obtained. The graph (dotted-line) which represents $\dot{m}_c$ against the level-difference between the Supply and the Discharge tanks, $\Delta h'$ is the result of several tests executed in the absence of the power input to the test-section heaters. The following three steps were taken to obtain the data for this graph:-

(1) The Supply Tank was raised to the height where its level-difference with the Discharge Tank was:-

$\Delta h' = 20$ cm

(2) The water flow rate, $\dot{m}_c$ was then regulated by the valve V_I of Fig. (6.1) to be:-

$\dot{m}_c = 33.3$ gr/sec (i.e. 2 lit/min on the Rotameter's scale)

(3) The Supply Tank level was adjusted to obtain the required water flow rate, $\dot{m}_c$.

Results of these tests together with the results which were obtained by the relationship:-

$\dot{m}_c \sim \sqrt{\Delta h'}$

are shown on Fig. (7.15). It can be seen that $\dot{m}_c$ varies as would be expected since the resistance in the water circuit is partly laminar and partly due to constrictions.

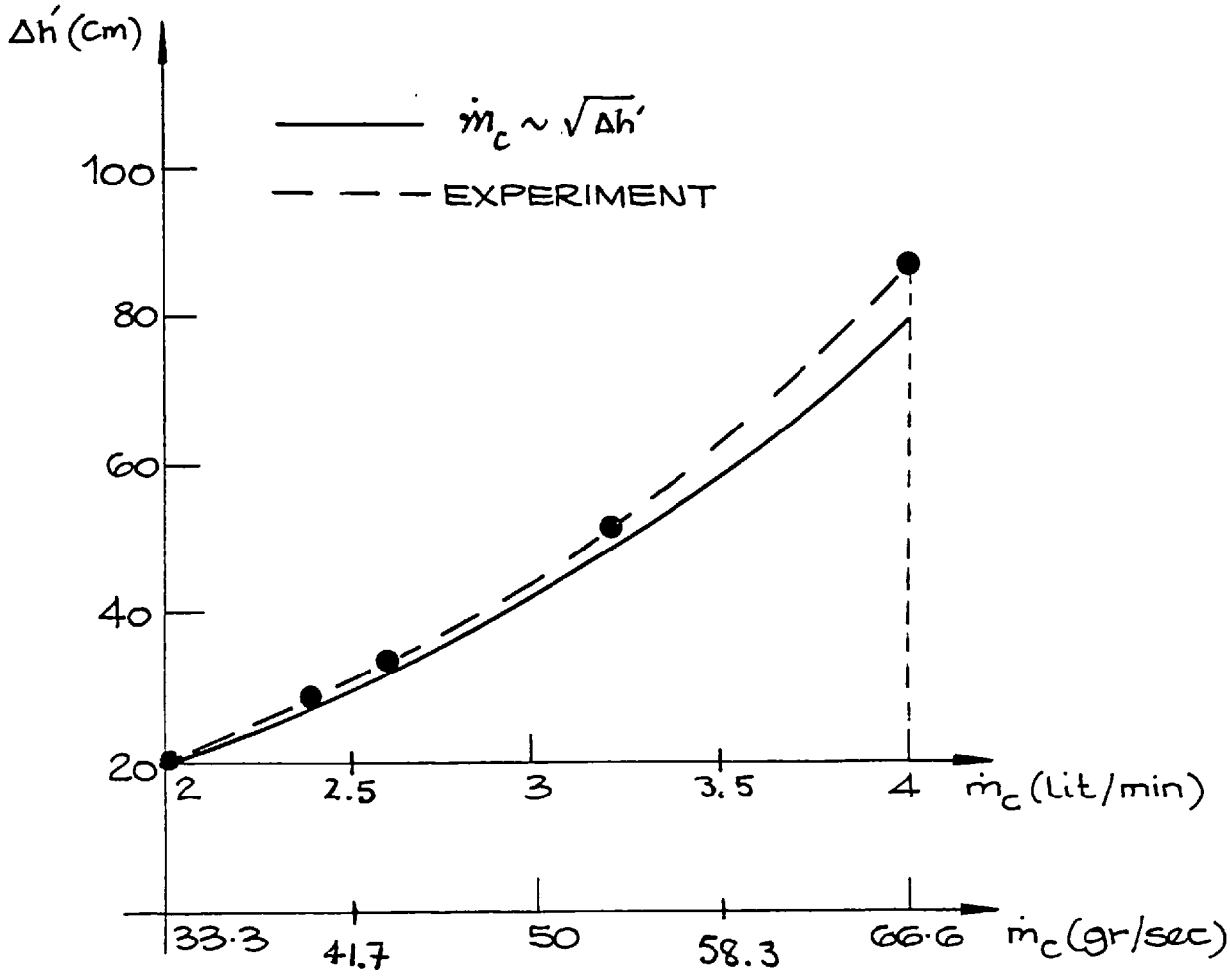

FIG. (7.15): FRICTIONAL CHARACTERISTICS OF THE WATER CIRCUIT.

7.6 The Effect of the Inlet Temperature, t_{in} on the t_w and the t_{ℓ} Profiles

Some of the mixed-convection tests mentioned in Table (7.1) were once more tested but with a higher water inlet temperature t_{in} into the test-section. The result has been an upward shift for the t_w and the t_{ℓ} profiles along the channel. The shift was equal to the difference between the water inlet temperatures for the two corresponding tests. This result is used for the "correction" of the experimental values of the t_w and the t_{ℓ} profiles when the t_{in} has slightly changed during a test.

7.7 Conclusions

The main conclusion is that simulation of a sinusoidal heat-flux by dividing it into a number of strips with gradually increasing heat rating is a viable possibility. This method is confirmed by the experiments reported in this chapter, Table (7.1), to be successful in dealing with both the mixed and the natural-convection regimes. The average error for wall temperature is of the order of 10%.

It is also concluded that although the test-section is covered by the Fibre-Glass insulation, there is a slight heat-loss. This is incorporated in the computer predictions obtained for each of the tests.

A general plan, in the form of the graphical representation of the Reynolds number, Re_D against the Grashof number, Gr_D could represent the results of each of the tests, Fig. (7.14). Two curves acting as the forced and the natural-convection boundaries divide the plan into three regions, namely, the forced, the mixed and the free-convection regions. The first curve represents the relationship

$Gr_D/Re_D^2 = 1$ while the second one shows the computer predictions for the natural-convection regimes. The parameter Gr_D/Re_D^2 is the dominant parameter in regard to the position of the different tests in the plan. This is confirmed by the five typical tests conducted for this chapter which fall into one of the three regions according to their value of the parameter Gr_D/Re_D^2. On the plan is also shown the natural-convection curve based on the calculations in which the average pressure drop is equalized with the average pressure gain in the test-section, Head (1962), leading to some over-estimation of the mass flow rate, $\dot{m}_c$.

Specific conclusions for the mixed-convection and also for the natural-convection are described in the following:-

(a) For Mixed-Convection

Comparison between the experimental and the theoretical predictions of the t_w and the t_{ℓ} profiles for the four typical tests of Table (7.1) shows that:-

(a.1) The shape of the t_w profile is the same for the experiment and the theory, Figs. (7.1) and (7.7). For both of them, there exists a $t_{w,Max}$ at an axial position downstream from the middle of the channel. However, before that position, the experimental values are higher. Also the $t_{w,Max}$ predicted by the computer program is lower and occurs further from the channel entry. These are thought to be due to the existence of a longitudinal heat-conduction, $\dot{q}''_{cd}$ along the channel in addition to the normal $\dot{q}''_w$ which

is convected to the coolant water, Fig. (7.2). The ratio of the net heat conduction $\dot{Q}_{cd}$, which is proportional to $\partial^2 t_w/\partial z^2$, to the total heat generation in a typical finite strip along the channel, $\dot{Q}_z$ is at the order of 0.003.

Two other workers, Petrovichev (1960) and McCuen (1962) have also observed such a heat conduction and attempted to reduce it by various means (the former divided the test tube with a number of circular grooves, while the latter insulated each division along the channel using an insulation layer).

At the entrance region of the test-channel, the experimental t_w values are higher. This is because the heat transfer coefficient, which is theoretically infinite, in practice, is finite but with a large value. The reason for this is that the axial conduction through the wall toward the entrance, raises the wall temperature above the entrance temperature t_{in} of the coolant leading to a large heat transfer coefficient but not an infinite one.

The assumption of a uniform temperature profile across the channel has also been investigated. Based on the experimental temperature recordings of the two simulating plates of the channel, it is concluded that this assumption is not strictly correct. (The temperature readings for the PL. No. 1, whose thermocouples are nearer to the corners of the channel,are higher than those of the PL. No. 2 for the same axial positions, see Table (7.2) and also Fig. (7.1). Existence of a temperature profile across the channel was

also noted by Savino et al (1964) and small coolant velocities at the corners, leading to a poor convection of heat in these areas, are believed to be responsible.

(a.2) The effect of a stronger degree of forced-convection in the flow has been studied. This was done by gradually increasing p_o in a typical mixed-convection test, Test 1, Table (7.1), while keeping $\dot{Q}_{tot}$ unchanged. The effect has been an immediate increase in $\dot{m}_c$ followed by a reduction in the t_w and the t_{ℓ} values along the channel. These temperature drops increase along the channel, Fig. (7. 7). Also the axial length where the $t_{w.Max}$ occurs shortens and gets closer to the middle of the test-channel.

(a.3) Comparison of the experimental and the theoretical predictions of the t_{ℓ} profile along the channel shows a good agreement, see Fig. (7.4). However, the experimental values are slightly higher near the entrance region and are lower for the axial positions beyond the middle of the channel. As for the difference between the t_w profiles, the existence of the longitudinal heat-flux $\dot{q}''_{cd}$ and also the finite value of h at the entry to the channel are thought to be the causes.

(b) For Natural-Convection

It is concluded that in addition to the pressure drop in the test-channel, Δp_{ts} there exists an external pressure drop in the water circuit, Δp_e. This extra pressure drop, which has been neglected in

the mixed-convection tests, in comparison with their p_o value, Table (7.1), is caused mainly by the flow of water through the connecting pipe between the Supply and the Discharge tanks, Fig. (6.1). The practical solution is to compensate the Δp_e by an extra level-difference between the two tanks as described in Section (7.3).

Figs. (7.12) - (7.13) show the t_w and the t_{ℓ} profiles for this case. Comparison of the theoretical and the experimental values of these profiles lead to the following conclusions which are similar to those of the mixed-convection tests:-

(i) There exists a longitudinal heat-conduction along the channel, $\dot{q}''_{cd}$. The effect of this is higher experimental t_w values before the $t_{w.Max}$ position.

(ii) The heat transfer coefficient in the entry to the channel has a large value but it is not infinite (as the ideal theoretical analysis requires). This is thought to be the reason why the experimental t_w values are higher in this region.

(iii) Because of the low coolant velocities near the corners of the cross-section, heat transfer is rather poor in these areas. This is confirmed by higher t_w readings for RL. No. 1 whose thermocouples are nearer to the corners of the channel, Fig. (7.12), Fig. (6.16) and Table (7.2).

(iv) There is a good agreement between the theoretical

and the experimental profiles of t_{ℓ} at the entrance region of the test-channel. However, at the axial positions near the end of the channel, the experimental values are slightly higher. This may be attributed to some small recirculation taking place near the exit of the channel, Fig. (7.13).

(c) The effect of raising the inlet water temperature, t_{in} is a parallel shift for the t_w and the t_{ℓ} profiles, equal to the amount of the increase in the t_{in} value. This conclusion has been used to correct the thermocouple readings for the tests where t_{in} was slightly lower or higher than its prescribed value.

(d) Pressure losses in the water circuit were studied by obtaining an experimental curve for $\dot{m}_c$ values against the level-difference in the Supply and the Discharge tanks $\Delta h'$, Fig. (7.15). According to this figure, there exists a difference between the experimental and the ideal values for $\Delta h'$ which increases with higher water flow rates, $\dot{m}_c$.

CHAPTER 8

APPLICATION OF THE PRESENT METHOD OF SOLUTION TO CIRCULAR CHANNELS

8.1 Introduction

In this chapter, it is intended to extend the present method, introduced in Chapter (3), to solve for vertical round tubes.

As mentioned in the literature survey, Chapter (2), the mixed-convection problem in round tubes with uniformly prescribed wall heat-flux or temperature has been tackled by, among others, Lawrence et al (1966) and later by Collins (1971) - (1975). Lawrence's measurements for the centreline velocity and the temperature profiles along a round tube agreed favourably with his theoretical results. However, the significant shortcoming of these works is that they have only dealt with the uniform wall conditions and, consequently, some important practical examples, where $\dot{q}''_w$ or t_w varies along the channel in a specified manner, are left out. One of these cases, which is of special interest in nuclear reactors, is the case where wall heat-flux varies in a sinusoidal manner along the tube. In view of the fact that the present method can solve for arbitrary wall conditions, it is decided to extend its application to solve for round tubes too.

For the execution of the method, the computer program CIRCLE is developed which predicts the axial and the radial distributions of the velocities, temperatures and pressures for the forced and the mixed-convection regimes with arbitrary wall conditions. For uniform heating, the program is, to some extent, similar to the two programs developed by Lawrence (1965) and Collins (1971) respectively.

As an example, the predictions are obtained for a certain

set of uniform and sinusoidal heating cases according to the general formula:-

$$\dot{q}''_w(z) = \dot{q}''_{wo}\left(b + c \cdot \sin\frac{\pi z}{L}\right)$$

Examination of these predictions showed a marked effect of natural-convection on the U velocity profile which distorts its fully-developed parabolic shape and, in certain cases, brought about an inflexion. In view of this, the possibility of the transition into an unstable flow in the tube is studied. This is based on the transition-parameter introduced by Lawrence et al (1966) which depends on the shape of the continuously developing U profile and also on the Reynolds number of the flow.

The effects of the entrance conditions on the computer predictions are also examined. These consist of obtaining solutions for several Reynolds numbers and also for the parabolic entrance velocity profile.

As for the rectangular cross-section, Chapter (5), a cross-checking of the computer predictions is made. This is done by treating the t_w profile, obtained for a sinusoidal $\dot{q}''_w$ profile, as data for a prescribed t_w case. A comparison between the $\dot{q}''_w$ profile obtained for the latter and the original sinusoidal $\dot{q}''_w$ profile adds to the confidence about the present method of solution for round tubes.

Published results of Hsu (1965) and Nijsing et al (1973), in the form of the axial distribution of the Nusselt number for prescribed sinusoidal $\dot{q}''_w$ profiles for certain cases, are to be reproduced in this chapter to point out that their results are only applicable for the forced-convection regimes and that the contribution of the viscosity and

the density variations in the mixed-convection regimes should not be ignored.

8.2 Formulation of the Problem

8.2.1 Equations

The problem to be considered is that of flow in vertical round tubes with prescribed wall conditions. A two-dimensional model, with axial and radial coordinates, as shown in Fig. (8.1), is considered.

The following equations, as also mentioned in Lawrence et al (1966), Kays (1966) and Collins (1971), represent the mass (continuity), momentum (Navier-Stokes) and the energy equation for the model:-

$$\frac{\partial u}{\partial z} + \frac{\partial v}{\partial r'} + \frac{v}{r'} = 0 \tag{8.1}$$

$$\rho \left(u \frac{\partial u}{\partial z} + v \frac{\partial v}{\partial r'}\right) = - \frac{\partial p}{\partial z} - S \cdot \rho \cdot g + \mu \left(\frac{\partial^2 u}{\partial z^2} + \frac{1}{r'} \cdot \frac{\partial v}{\partial r'} + \frac{\partial^2 v}{\partial r'^2}\right) +$$

$$+ 2 \frac{\partial \mu}{\partial z} \cdot \frac{\partial u}{\partial z} + \frac{\partial \mu}{\partial r'} \left(\frac{\partial u}{\partial r'} + \frac{\partial v}{\partial z}\right) \tag{8.2}$$

$$\rho \left(u \frac{\partial v}{\partial z} + v \frac{\partial v}{\partial r'}\right) = - \frac{\partial p}{\partial r'} + \mu \left(\frac{\partial^2 v}{\partial r'^2} + \frac{1}{r'} \cdot \frac{\partial v}{\partial r'} - \frac{v}{r'^2} + \frac{\partial^2 v}{\partial z^2}\right) +$$

$$+ 2 \frac{\partial \mu}{\partial r'} \cdot \frac{\partial v}{\partial r'} + \frac{\partial \mu}{\partial z} \left(\frac{\partial v}{\partial z} + \frac{\partial u}{\partial r'}\right) \tag{8.3}$$

$$u \frac{\partial t}{\partial z} + v \frac{\partial t}{\partial r'} = \frac{k}{\rho \cdot C_p} \left(\frac{\partial^2 t}{\partial z^2} + \frac{1}{r'} \cdot \frac{\partial t}{\partial r'} + \frac{\partial^2 t}{\partial r'^2}\right) \tag{8.4}$$

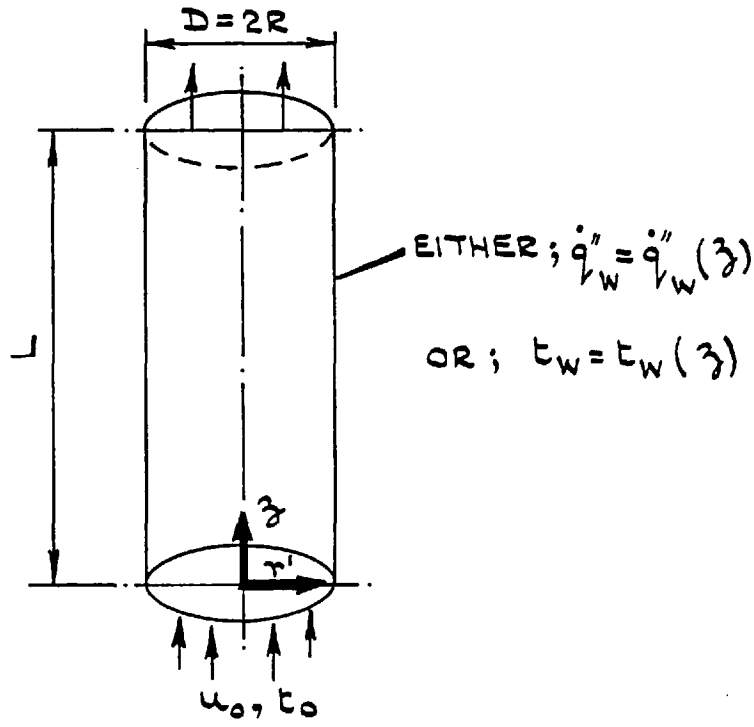

FIG(8.1) THE THEORETICAL MODEL.

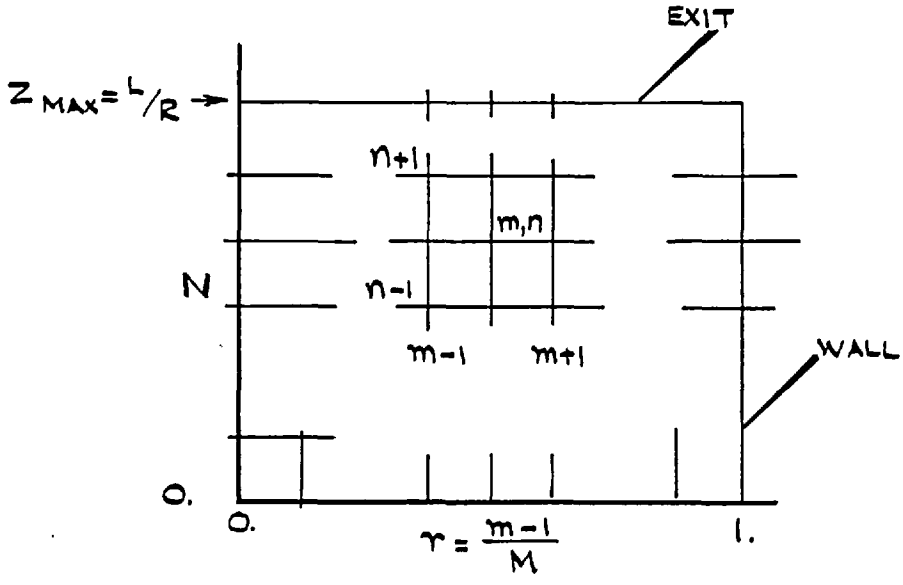

FIG(8.2) THE GRID FOR THE FINITE-DIFFERENCE METHOD.

The assumptions in these equations are:-

(a) The flow is steady and laminar.

(b) The flow is axially symmetric. This is also true about the prescribed heat-flux or temperature at the wall.

(c) Viscous energy dissipation is negligible.

(d) C_p and k are constant.

(e) ρ is constant except in the buoyancy term of Equation (8.2). (This assumption is justified when the effect of the density variation with temperature in this term is compared with the other terms).

As for the rectangular cross-section, the buoyancy term in Equation (8.2) will represent the natural-convection effects in the vertical flow when S = + 1 (upward flow), or S = - 1 (downward flow). These effects are assumed absent for the forced-convection regime in any orientation, and for the adiabatic flow, i.e. S = 0.

The variations of the viscosity and the density with temperature may be represented by several correlations depending on the working fluid. As mentioned in Chapter (3), the following two correlations approximate accurately the functional relationship of μ and ρ with temperature:-

$$\frac{\mu}{\mu_B} = \left(\frac{t + C_1}{C_2}\right)^{- C_3} \qquad (8.5)$$

$$\frac{\rho}{\rho_B} = C_4 - C_5 \cdot t + C_6 \cdot t^2 \qquad (8.6)$$

Numerical values of the constants C_1 - C_6 and the comparison of these approximations with the actual values of μ and ρ are shown in Tables (3.1) - (3.2).

The mass conservation equation may also be written in the following integral form:-

$$u_o \cdot \pi R^2 = \int_o^R u \cdot 2\pi r' \cdot dr' \qquad (8.7)$$

In the numerical analysis which will follow, Equation (8.7) is used as part of the analysis, rather than as a mass check balance. This guarantees mass conservation at each axial step.

The wall thermal boundary condition is prescribed either as heat-flux or temperature, i.e:-

$$\dot{q}''_w = \dot{q}''_w (z) \qquad (8.8)$$

or:-

$$t_w = t_w (z) \qquad (8.9)$$

where these functions are given as data for each case.

The overall energy balance, over an infinitesimal length, Δz can be written:-

$$\pi R^2 \cdot \rho \cdot u_o \cdot C_p \cdot \Delta t_{mean} = 2\pi R \cdot \int_{z_1}^{z_2} \dot{q}''_w(z) \cdot dz \qquad (8.10)$$

where Δt_{mean} is the increase in the mixed-mean temperature at the axial position and is defined as:-

$$t_{mean} = \frac{\int_o^R \cdot \rho \cdot u \cdot t \cdot r' \cdot dr'}{\int_o^R \rho \cdot u \cdot r' \cdot dr'} \qquad (8.11)$$

and:-

$$\Delta t_{mean} = t_{mean}\Big|_{z_2} - t_{mean}\Big|_{z_1} \qquad (8.12)$$

8.2.2 The Boundary Conditions

These may be classified in the four following sets:-

(a) Entrance conditions, i.e. $z = 0$, $0 \leq r' \leq R$

$$u = u_o \quad , \quad v = 0 \quad , \quad p = p_o \quad , \quad t = t_{in}$$

(b) At the tube axis, i.e. $z > 0$, $r' = 0$

$$\frac{\partial u}{\partial r'} = 0 \quad , \quad v = 0 \quad , \quad \frac{\partial t}{\partial r'} = 0 \quad , \quad \frac{\partial p}{\partial r'} = 0$$

(c) The wall flow conditions, i.e. $z > 0$, $r' = R$

$$u = 0 \quad , \quad v = 0$$

(d) The wall thermal conditions

$$\text{Either: } \dot{q}''_w = k \left.\frac{\partial t}{\partial r'}\right|_{r' = R} = \dot{q}''_w (z) \Big|_{\text{Given as data}}$$

$$\text{Or: } t_w = t_w (z) \Big|_{\text{Given as data}}$$

8.2.3 Dimensionless Form of the Equations

Equations (8.1) - (8.12) may be rendered dimensionless by using the substitutions defined in the nomenclature, giving Equations (8.13) - (8.24) respectively:-

$$\frac{\partial U}{\partial Z} + \frac{V}{r} + \frac{\partial V}{\partial r} = 0 \tag{8.13}$$

$$U \frac{\partial U}{\partial Z} + V \frac{\partial U}{\partial r} = - \frac{\partial P}{\partial Z} + \frac{1}{Re} \left[\eta_A \left(\frac{\partial^2 U}{\partial Z^2} + \frac{1}{r} \cdot \frac{\partial U}{\partial r} + \frac{\partial^2 U}{\partial r^2} \right) + \right.$$

$$\left. + \eta_B \left\{ 2 \frac{\partial T}{\partial Z} \cdot \frac{\partial U}{\partial Z} + \frac{\partial T}{\partial r} \left(\frac{\partial V}{\partial Z} + \frac{\partial U}{\partial r} \right) \right\} \right] - S \frac{\rho_m}{\rho_B} \cdot \frac{1}{Re^2} \{ G_r \cdot C04 + T(C05 + T \cdot C06) \} \tag{8.14}$$

$$U \frac{\partial V}{\partial Z} + V \frac{\partial V}{\partial r} = - \frac{\partial P}{\partial r} + \frac{1}{Re} \left[\eta_A \left(\frac{\partial^2 V}{\partial r^2} + \frac{1}{r} \cdot \frac{\partial V}{\partial r} - \frac{V}{r^2} + \frac{\partial^2 V}{\partial Z^2} \right) + \right.$$

$$\left. + \eta_B \left\{ 2 \frac{\partial T}{\partial r} \cdot \frac{\partial V}{\partial r} + \frac{\partial T}{\partial Z} \left(\frac{\partial V}{\partial Z} + \frac{\partial U}{\partial r} \right) \right\} \right] \tag{8.15}$$

$$U \frac{\partial T}{\partial Z} + V \frac{\partial T}{\partial r} = \frac{1}{Pr \cdot Re} \left(\frac{\partial^2 T}{\partial Z^2} + \frac{1}{r} \cdot \frac{\partial T}{\partial r} + \frac{\partial^2 T}{\partial r^2} \right) \tag{8.16}$$

$$\frac{\mu}{\mu_B} = (CO1 \cdot \frac{T}{G_r} + CO2)^{-CO3} \tag{8.17}$$

$$\frac{\rho}{\rho_B} = (CO4 + \frac{CO5}{G_r} \cdot T + \frac{CO6}{G_r} \cdot T^2) \tag{8.18}$$

$$\frac{1}{2} = \int_0^1 \rho/\rho_o \cdot U \cdot r \cdot dr \tag{8.19}$$

$$HFLUX = \frac{R^4 \cdot g \cdot C_5}{\nu_B^2 \cdot k \cdot M} \cdot \dot{q}''_w(z) \tag{8.20}$$

$$TWALL = \frac{R^3 \cdot g \cdot C_5}{\nu_B^2} \{t_w(z) - t_{in}\} \tag{8.21}$$

$$\frac{1}{2} \Delta T_{mean} = \frac{1}{Pr \cdot Re} \cdot \frac{\rho_m}{\rho_B} \int_{Z_n}^{Z_{n+1}} HFLUX(Z) \cdot dZ \tag{8.22}$$

where:-

$$TMEAN = 2 \int_0^1 \rho/\rho_o \cdot U \cdot T \cdot r \cdot dr \tag{8.23}$$

$$\Delta T_{mean} = TMEAN\Big|_{Z_{n+1}} - TMEAN\Big|_{Z_n} \tag{8.24}$$

Also:-

$$\eta_A = \frac{\mu}{\mu_B} = (CO1 \cdot \frac{T}{G_r} + CO2)^{-CO3}$$

$$\eta_B = \frac{d}{dT}(\eta_A) = \frac{CO1}{G_r} \cdot \left(CO1 \cdot \frac{T}{G_r} + CO2\right)^{-(CO3+1)}$$

8.2.4 Dimensionless Form of the Boundary Conditions

The four sets of boundary conditions become:-

(a) Entrance conditions, i.e. $Z = 0$, $0 \leq r \leq 1$

$$U = 1 \quad , \quad V = 0 \quad , \quad P = P_o \quad , \quad T = T_o$$

(b) At the axis, i.e. $Z > 0$, $r = 0$

$$\frac{\partial U}{\partial r} = 0 \quad , \quad V = 0 \quad , \quad \frac{\partial T}{\partial r} = 0 \quad , \quad \frac{\partial P}{\partial r} = 0$$

(c) The wall flow conditions, i.e. $Z > 0$, $r = 1$

$$U = 0 \quad , \quad V = 0$$

(d) The thermal conditions prescribed at the wall:

Either: HFLUX = HFLUX (Z)

Or: TWALL = TWALL (Z)

8.2.5 Procedure of the Solution

The solution is obtained by applying the finite-difference method to Equations (8.13) - (8.24). A grid of the form shown on Fig. (8.2) is used. The grid is a rectangular axial-radial one with suffices

n and m respectively. As the radius r is divided into M divisions:-

$$r = \frac{m - 1}{M}$$

and for m = 1 (at the axis) .... M + 1 (at the wall) the values of r = 0 and 1 are obtained.

By using a marching-forward technique, a set of linear finite-difference equations for the unknown level "n + 1" may be written. Then, these equations are solved by using the known values at the level "n" and "n - 1". In the solution whenever the product of two unknowns occurs, linearity is achieved by putting one of them equal to its value of the previous step, (i.e. $Z_{n+1} \rightarrow Z_n$). An approximation which should not be too serious.

The finite-difference form of Equations (8.13) - (8.24) is shown in Appendix (III). Here, only the boundary conditions are discussed.

8.2.6 Finite-Difference Form of the Boundary Conditions

(a) Entrance conditions, i.e. $Z = 0$, $0 \leq r \leq 1$

$$U_{1,m} = 1 \quad , \quad V_{1,m} = 0 \quad , \quad P_{1,m} = P_o \quad , \quad T_{1,m} = T_o$$

(b) At the tube axis, i.e. $Z > 0$, $r = 0$

$$U_{n,1} = U_{n,2} \quad , \quad V_{n,1} = 0 \quad , \quad P_{n,1} = P_{n,2} \quad , \quad T_{n,1} = T_{n,2}$$

(c) The wall flow conditions, i.e. $Z > 0$, $r = 1$

$$U_{n,M+1} = 0 \quad , \quad V_{n,M+1} = 0$$

(d) The wall thermal conditions, i.e. ($Z > 0$, $r = 1$)

In order to make the prescribed wall thermal conditions, $\dot{q}_w''' (z)$ or $t_w (z)$, suitable for the finite-difference approximation, their profiles are divided into infinitesimal axial strips and dealt with as follows:-

(d.1) Wall heat-flux profile, $\dot{q}_w''' (z)$ is prescribed

$$\text{Define: } \text{HFLUX}\Big|_{\text{Av. for } \Delta Z} = \frac{\int_{Z_n}^{Z_{n+1}} \text{HFLUX}\ (Z)\ .\ dZ}{Z_{n+1} - Z_n} \tag{8.25}$$

On the other hand:-

$$\text{HFLUX}\Big|_{\text{Av. for } \Delta Z} = \left|\frac{\partial T}{\partial r}\right|_{r=1} = \frac{T_{n,M+1} - T_{n,M}}{1/M} \tag{8.26}$$

Combining Equations (8.25) - (8.26):-

$$T_{n,M+1} = T_{n,M} + \frac{R^4\ .\ g\ .\ C_s}{\nu_B^2\ .\ k\ .\ M}\ .\ \dot{q}_w'''\Big|_{\text{Av. for } \Delta z} \tag{8.27}$$

As for the flat duct, Equation (8.27) shows how a prescribed wall heat-flux profile is turned into a boundary condition problem. Thus, if the flow specifications, i.e. U, V, P and T at the point Z_n are known, their corresponding

values at Z_{n+1} may now be calculated.

(d.2) Wall temperature profile, t_w (z) is prescribed

A similar procedure to that of the above-mentioned $\dot{q}_w'''$ case is followed. Define:-

$$TWALL\Big|_{\text{Av. for } \Delta Z} = \frac{\int_{Z_n}^{Z_{n+1}} TWALL\ (Z)\ .\ dZ}{Z_{n+1} - Z_n} \tag{8.28}$$

Combining Equations (8.21) and (8.28):-

$$T_{n,M+1} = \frac{R^3\ .\ g\ .\ C_5}{\nu_B^2} \{t_w\ (z) - t_{in}\}_{\text{Av. for } \Delta z} \tag{8.29}$$

8.2.7 Method of Solution

As with the flat duct solution, by assuming a second-order effect of the temperature on the flow-field (i.e. U, V, P) the latter is solved for first, and the solution is then used to solve the energy equation. This assumes the UVP solution is reasonable. As a check, and in view of the energy equation coefficients depending on the U values, the temperature solution so obtained is substituted into the UVP equations for a second solution of these and in turn a second temperature solution is found. Differences have usually been slight justifying the assumptions. This also implies that the temperature dependent viscosity and the density, appearing in the momentum equations, Equations (8.2) - (8.3), have virtually their correct values the second time round, rather than their values at the first step.

In more detail, Equations (8.13) - (8.15) and (8.19) were written for each radial position at the first axial step from the entry, and the known coefficients and the right-hand side values were evaluated. This gave (3M - 2) unknowns (i.e. U, V, P for each radial position and P_{M+1}), with the same number of equations. The solution, as for the flat duct, is by a standard Gaussian Elimination Method, suggested by McCormack and Salvadori (1964). The energy equation, Equation (8.16) is similarly written and solved with the U_{n+1} and V_{n+1} values from the first solution. Here (M - 1) equations, including Equation (8.22), solve for (M - 1) unknown T_{n+1} values. For the mixed-convection cases, where the energy and the momentum equations are linked, the semi-iterative check is carried out, i.e. the U, V, P matrix uses T_{n+1} values from the temperature solution and finally the temperature solution will be re-obtained.

Having completed the solution for one axial position, the marching forward is carried out by progression to the next axial step. This method has been executed by the computer program CIRCLE, see its Flow-Chart, Appendix (IV), and the predictions for several cases of prescribed $\dot{q}''_w$ or t_w profiles were obtained which will be discussed in the following.

8.3 Computer Predictions for Several Prescribed $\dot{q}''_w$ Profiles

8.3.1 The Wall Heat-Flux Profiles (I, II and III)

As mentioned in (8.1), three typical $\dot{q}''_w$ profiles are to be solved for. These are a uniform and two sinusoidal profiles described by the general formula:-

$$\dot{q}''_w(z') = \dot{q}''_{wo}\{b + c \cdot \sin(\tfrac{\pi z}{L})\} \qquad (8.30)$$

where the constants b and c differ for each profile. For the examples which will follow they are chosen in such a way that although the resultant profiles are different, the average wall heat-flux, $\dot{q}''_{w.av}$ is kept the same. The selected three profiles are:-

(i) Profile (I), uniform heating

which is obtained from Equation (8.30) by assuming:-

$$\begin{cases} b = 1 \ , \quad c = 0 \\ \dot{q}''_{wo} = \dot{q}''_{w.Av} = 1.34 \quad (w/cm^2) \end{cases}$$

Therefore:-

$$\dot{q}''_{w} \ (z) \ = 1.34 \tag{8.31}$$

where $\dot{q}''_{w}$ and z are measured in (w/cm^2) and cm respectively.

(ii) Profile (II), sinusoidal heating

By assuming: $b = 0.5$, $c = 1$, $\dot{q}''_{wo} = 1.179 \ (w/cm^2)$ in Equation (8.30):-

$$\dot{q}''_{w} \ (z) = 1.179 \ \{0.5 + \sin \ (\tfrac{\pi z}{L})\} \tag{8.32}$$

where $\dot{q}''_{w}$ and z are measured in (w/cm^2) and cm respectively.

Therefore:-

$$\begin{cases} \dot{q}''_{w.Av} = 1.34 \ (w/cm^2) \\ \dot{q}''_{w.Max}/\dot{q}''_{w.min} = 3.00 \end{cases}$$

(iii) Profile (III), sinusoidal heating

By taking b = 0.5, c = 2 and $\dot{q}''_{wo} = 0.755$ (w/cm^2) in Equation (8.30):-

$$\dot{q}''_w(z) = 0.755 \{0.5 + 2 \sin(\frac{\pi z}{L})\} \tag{8.33}$$

where $\dot{q}''_w$ and z are measured in (w/cm^2) and cm respectively.

So:-

$$\begin{cases} \dot{q}''_{w.Av} = 1.34 \text{ (w/cm}^2\text{)} \\ \dot{q}''_{w.Max}/\dot{q}''_{w.min} = 5.00 \end{cases}$$

It is noted that in these three profiles the ratio $\dot{q}''_{w.Max}/\dot{q}''_{w.min}$ assumes the values of 1, 3 and 5 respectively. These profiles are shown in Fig. (8.3) and were prescribed on a typical round tube, Fig. (8.1). The data for this tube is given in Table (8.1) and the computer predictions are discussed in the following.

8.3.2 Computer Predictions for a Prescribed Uniform Heating Case

These predictions are to be assessed by the examination of the axial variations of the four parameters namely: U, t, Nu and p which were obtained for the case where $\dot{q}''_w$ varies according to the Profile(I), Fig. (8.3).

(a) U Profile

Fig. (8.4) shows the U velocity profile along the tube for a forced-convection regime (i.e. when μ and ρ are constant). It is

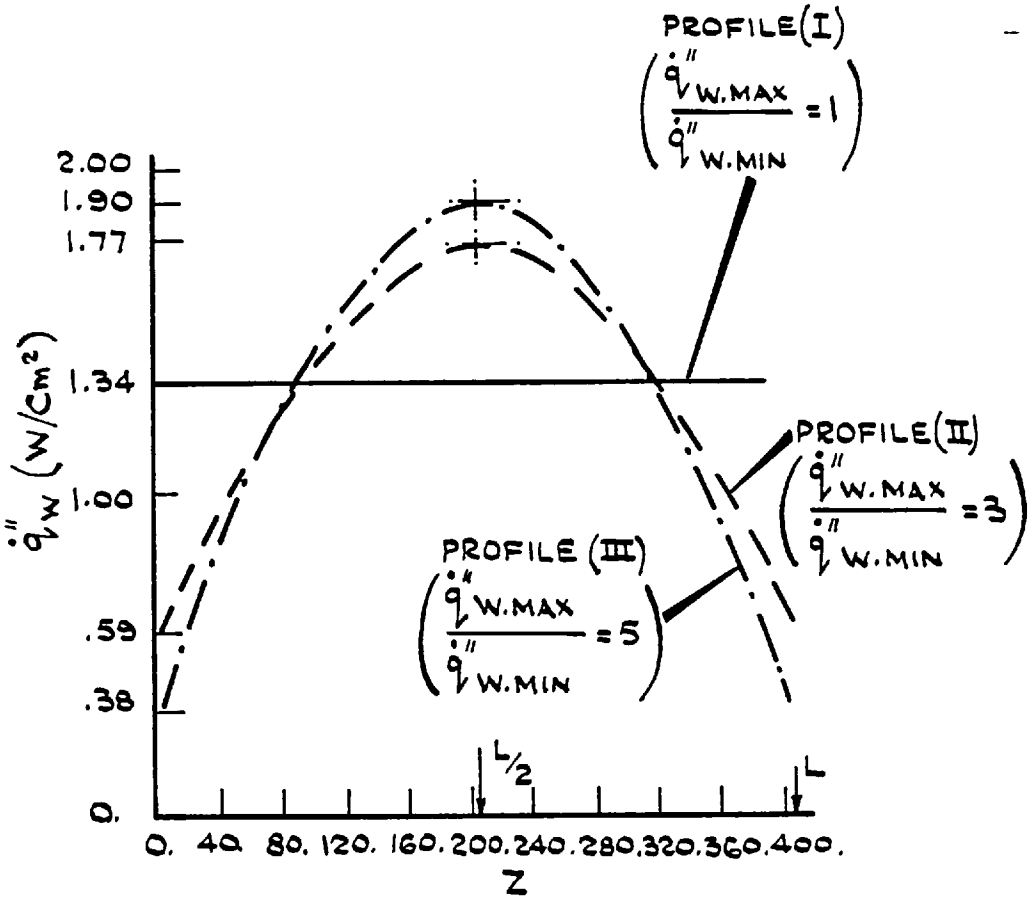

FIG(8.3) THE WALL HEAT-FLUX PROFILES.

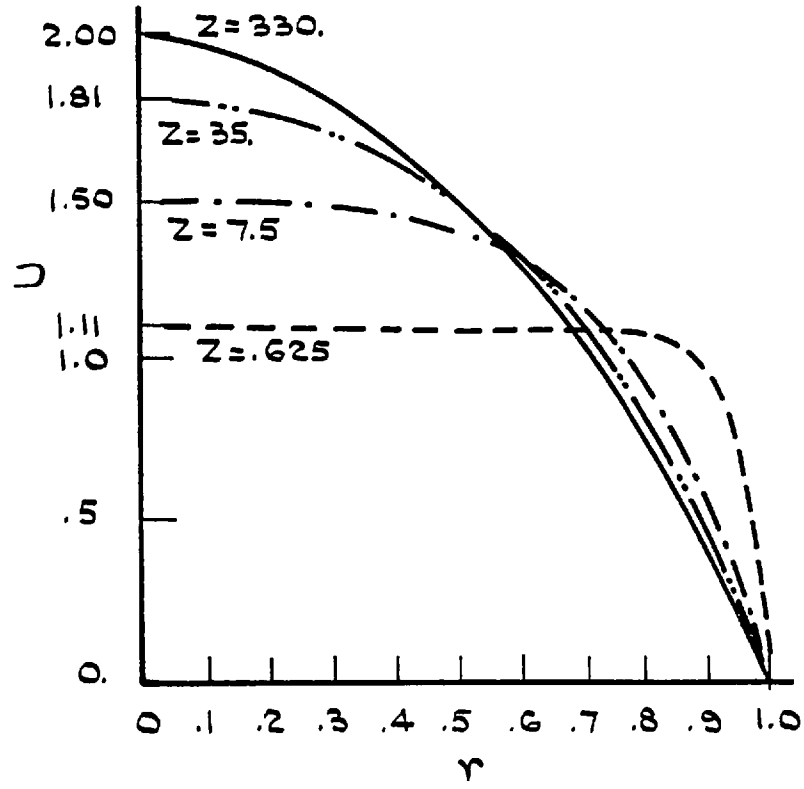

FIG(8.4) THE DEVELOPING U PROFILES ALONG THE TUBE.

TABLE (8.1)

DATA FOR THE TYPICAL ROUND TUBE

Data \ Reduced Data	Z_{max}	$\dot{Q}_{tot}(w)$	$\dot{m}(gr/sec)$	$\Delta t_{tot}(C^o)$	$t_m(C^o)$	$t_{out}(C^o)$	Pr	Re_o	Re_m	Re	Re_D	Gr_D	Gr_D/Re_D^2
u_o = 7.85 cm/sec D = 1.076 cm, L = 2.1875 m, t_{in} = 22.8 ^oC	406.6	990.9	6.94	34.3	40	57	6.503	437.2	600	419.7	839.4	1.381×10^6	1.96

noted that the profile continues to develop, from the uniform shape at the entrance, towards the parabolic shape of $U = 2(1 - r^2)$ far downstream.

In order to examine the effects of the variations of either of the viscosity and the density, the U profile is also obtained for when μ varies with temperature according to Equation (8.5) but ρ remains constant. Figs. (8.5) - (8.6) show the U profiles at Z = 60 and 310 respectively for both of these cases. It can be seen that the variable viscosity leads to a flatter U profile. The lower μ values near the heated wall reduce the resistance against the flow and result in higher velocities than those for the constant μ case. This is also reflected in the mass conservation equation, Equation (8.7), and leads to the lower velocities at the centre of the tube.

Fig. (8.7) shows the U profile along the tube for a mixed-convection regime, i.e. μ and ρ vary with temperature according to Equations (8.5) - (8.6). It is noted that here the profiles continue to develop in the same manner as those for the forced-convection case and $U_{\ell} = 1.57$ at Z = 35. But as the fluid moves further downstream, the density reduction becomes more apparent and the profile tends towards a flatter shape, e.g. at Z = 110 : $U_{\ell} = 1.15$ (c.f. $U_{\ell} = 1.981$ for the forced-convection). Further than this point, because of the higher rates of reduction in ρ and μ near the wall, the U values become increasingly larger there, to the extent that one of them even exceeds the U value at the centre of the tube, U_{ℓ}. This leads to the appearance of an inflexion point in the profile which distorts its parabolic shape. The increase in the U values near the wall is followed by the reduction in the U_{ℓ} values which continues until Z = 320 where it reaches zero.

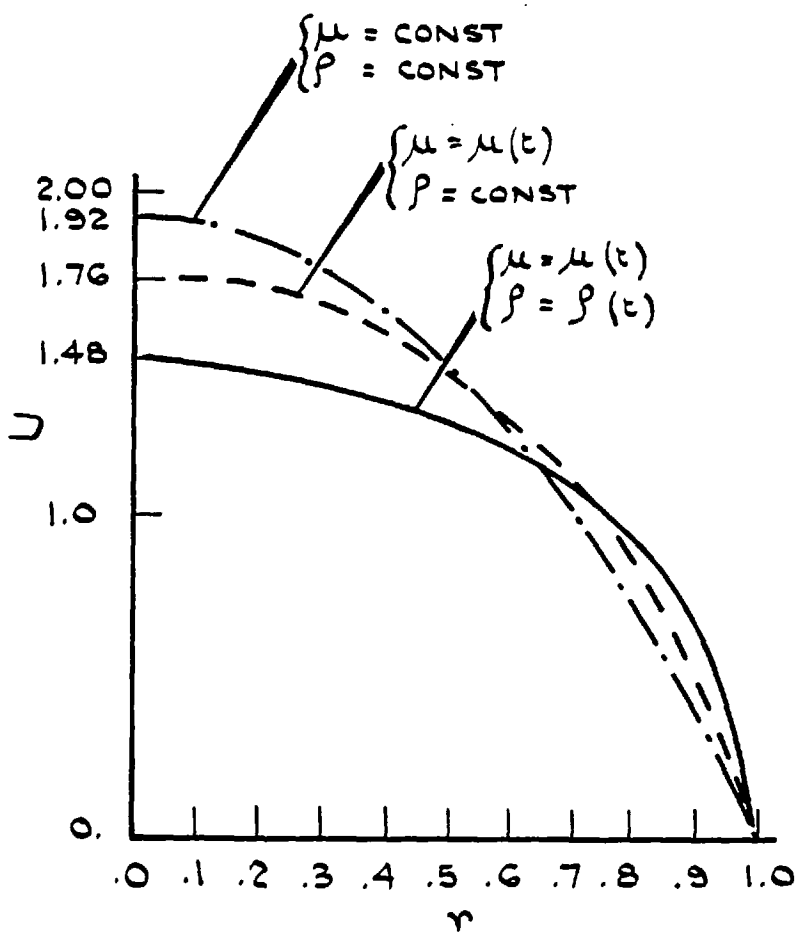

FIG(8.5) THE U PROFILES AT Z = 60.

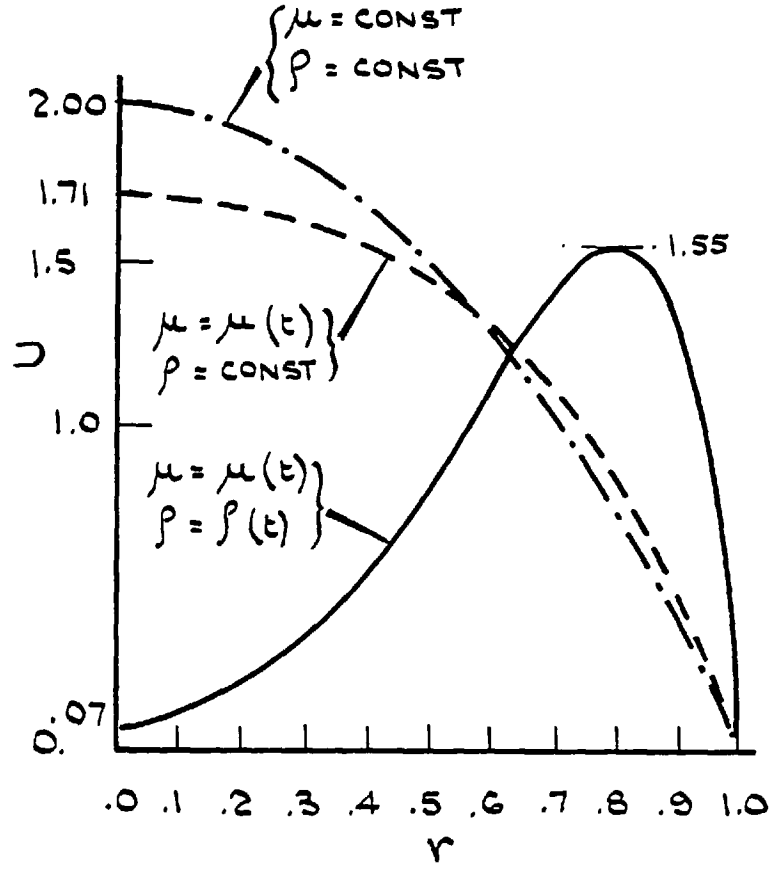

FIG(8.6) THE U PROFILES AT Z = 310.

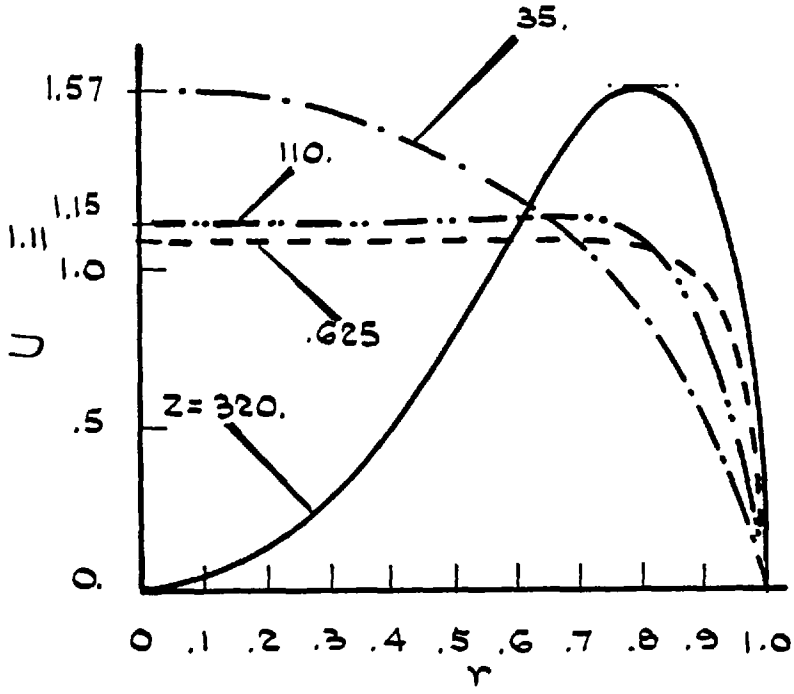

FIG(8.7) THE DEVELOPING U VELOCITY PROFILES.

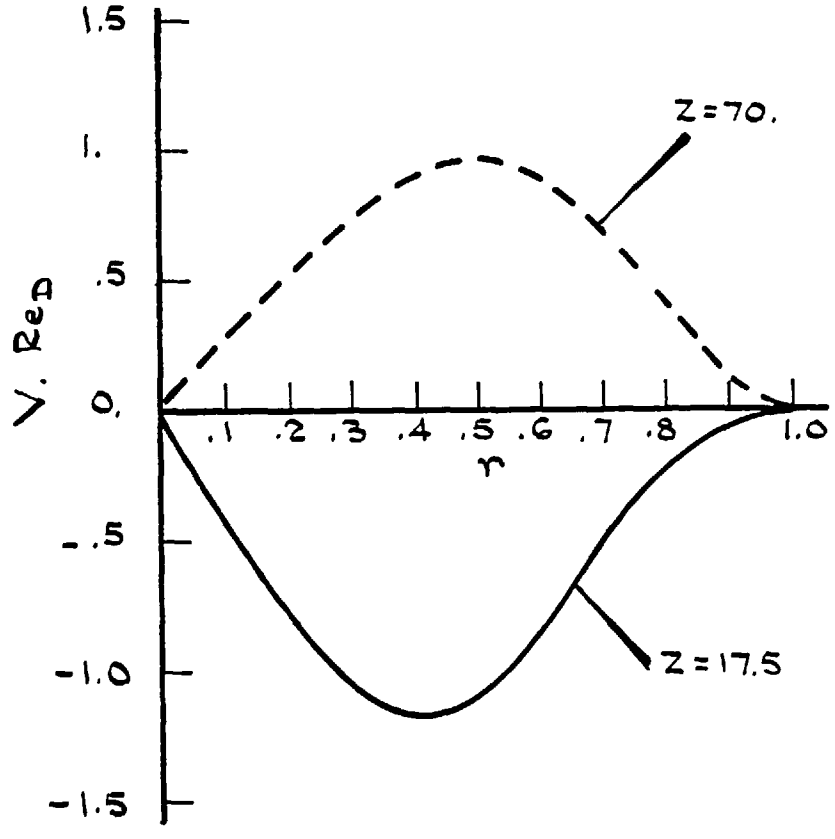

FIG(8.8) THE V PROFILES ALONG THE TUBE.

The development of the U profile along the tube may also be explained by the examination of the V velocity profile across the tube, Fig. (8.8). The negative values of the V profile at Z = 17.5 represent the radial movement of the fluid towards the centre of the tube. Conversely for Z = 70, where the V values are positive, the movement is towards the tube's wall. These movements are in agreement with the development of the U velocity profiles, Fig. (8.7), because up to Z = 35, where the peak U_{ℓ} occurs, the fluid layers near the centre are continuously assuming higher velocities (which requires the horizontal movement towards the centre). But, beyond this axial position, where the U velocity profiles are getting flatter, the increase in the U values will be transferred to the layers near the wall and accordingly the radial movement is reversed.

For comparison, the U profiles for the mixed-convection regime at two axial levels, Z = 60 and 310, are also shown on Figs. (8.5) - (8.6). It can be seen on Fig. (8.5) that when the variations of μ and ρ are both considered, the U profile is even flatter than that of the case where only μ varies with temperature. The reduction of the ρ values near the wall, which amplifies the effects of the lower viscosities, is responsible for obtaining a still flatter U profile.

In order to summarise the effects of μ and ρ variations along the tube, Fig. (8.9) is drawn. This figure shows the axial variations of the centreline velocity U_{ℓ} for the forced and the mixed-convection cases. According to the figure, for the forced-convection case, U_{ℓ} approaches its asymptotic value at Z = 120 where U_{ℓ} = 1.985. Further downstream the parabolic shape changes slightly and U_{ℓ} assumes values even closer to U_{ℓ} = 2 (e.g. U_{ℓ} = 1.995 at Z = 330). When μ variations with temperature are also allowed, the U profiles are flatter

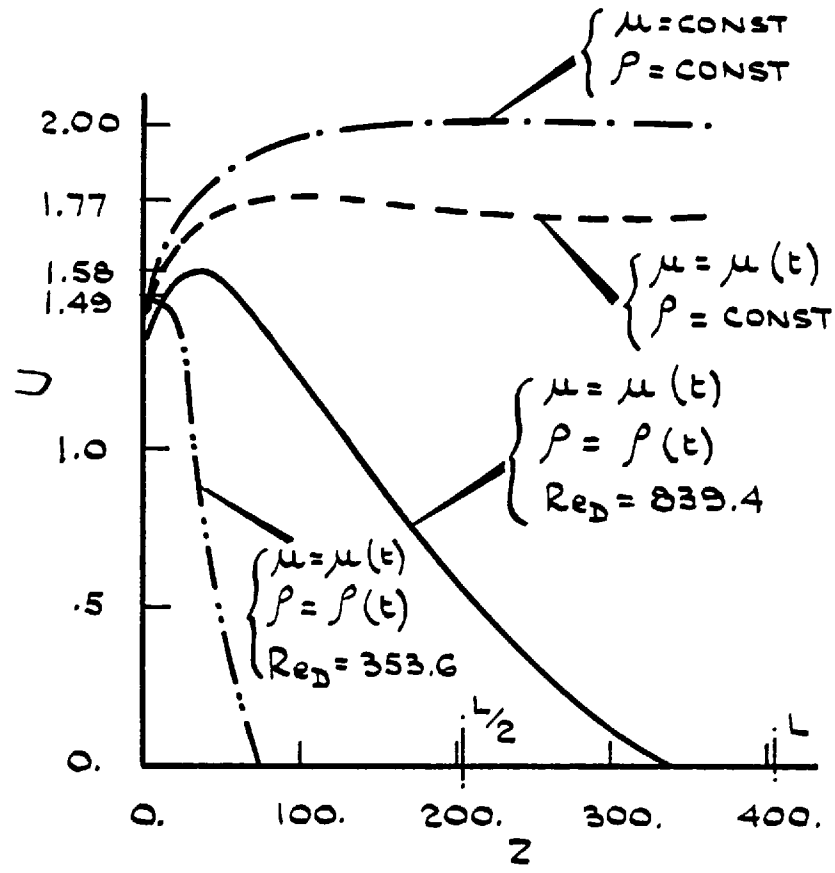

FIG (8.9) THE AXIAL VARIATIONS OF U_{ℓ} FOR THE UNIFORM HEATING CASE.

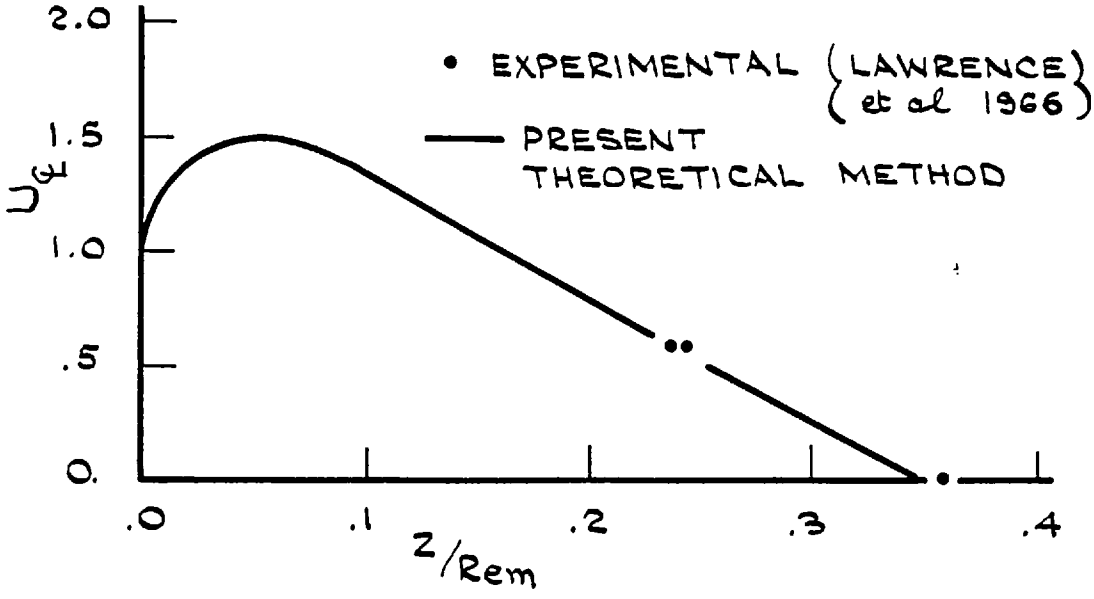

FIG (8.10) COMPARISON OF THE THEORETICAL AND EXPERIMENTAL VALUES OF U_{ℓ} ALONG THE TUBE.

and U_{ℓ} approaches to an asymptote value less than that of the forced-convection case, i.e. $U_{\ell} = 1.705$ at $Z = 320$. This occurs after U_{ℓ} passes through its peak value of $U_{\ell} = 1.763$ at $Z = 80$. For the mixed-convection, U_{ℓ} increases along the tube axis until $Z = 35$ (where $U_{\ell_{max}} = 1.500$). Further downstream, U_{ℓ} starts to decrease and after passing through the inflexion point, $U_{\ell} = 1.15$ at $Z = 110$, it continues towards the zero value at $Z = 320$.

The U_{ℓ} variations along the tube have been checked against a published experimental result of Lawrence et al (1966) for a case with $Re_D = 353.6$ and $Gr_D/Re_D^2 = 8.83$. The comparison, shown on Fig. (8.10), adds to the confidence about the present theoretical method.

(b) The Temperature Profile

Two temperature profiles are considered for discussion. These are the wall temperature along the tube and the temperature distributions across the tube radius. These profiles are shown on Figs. (8.11) - (8.12) respectively.

On Fig. (8.11) it is noted that throughout the tube the wall-temperature is lower for the mixed-convection case. As explained for the U profile, this is because of a higher velocity of the fluid layers near the tube wall which results in a better cooling process taking place. Also it may be seen that the effects of the density variations are more significant than those of the viscosity, although both of them contribute to the t_w reductions throughout the tube.

Fig. (8.12) shows the development of the temperature profile across the tube for the mixed-convection case. According to this figure, the profiles tend towards a parabolic shape far downstream and the increase in the t_{ℓ} values for the positions beyond $Z = 110$

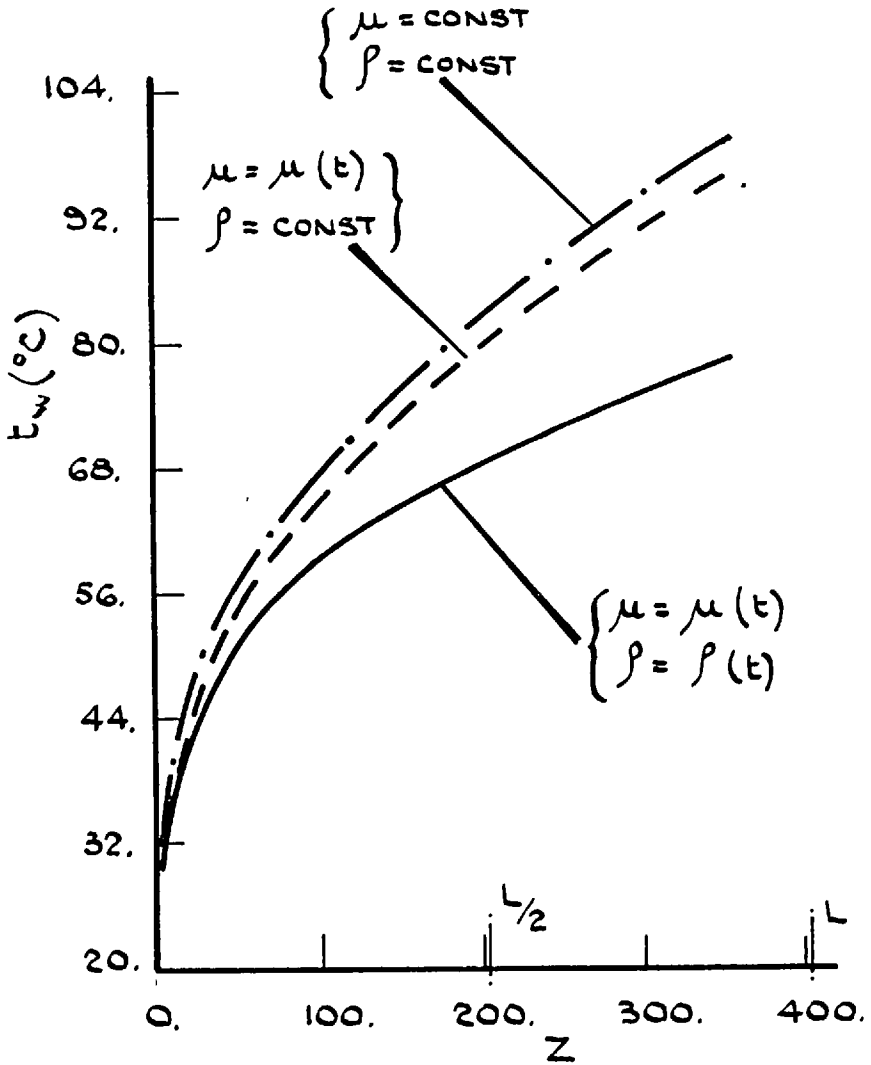

FIG (8.11) THE WALL TEMPERATURE DISTRIBUTIONS ALONG THE TUBE.

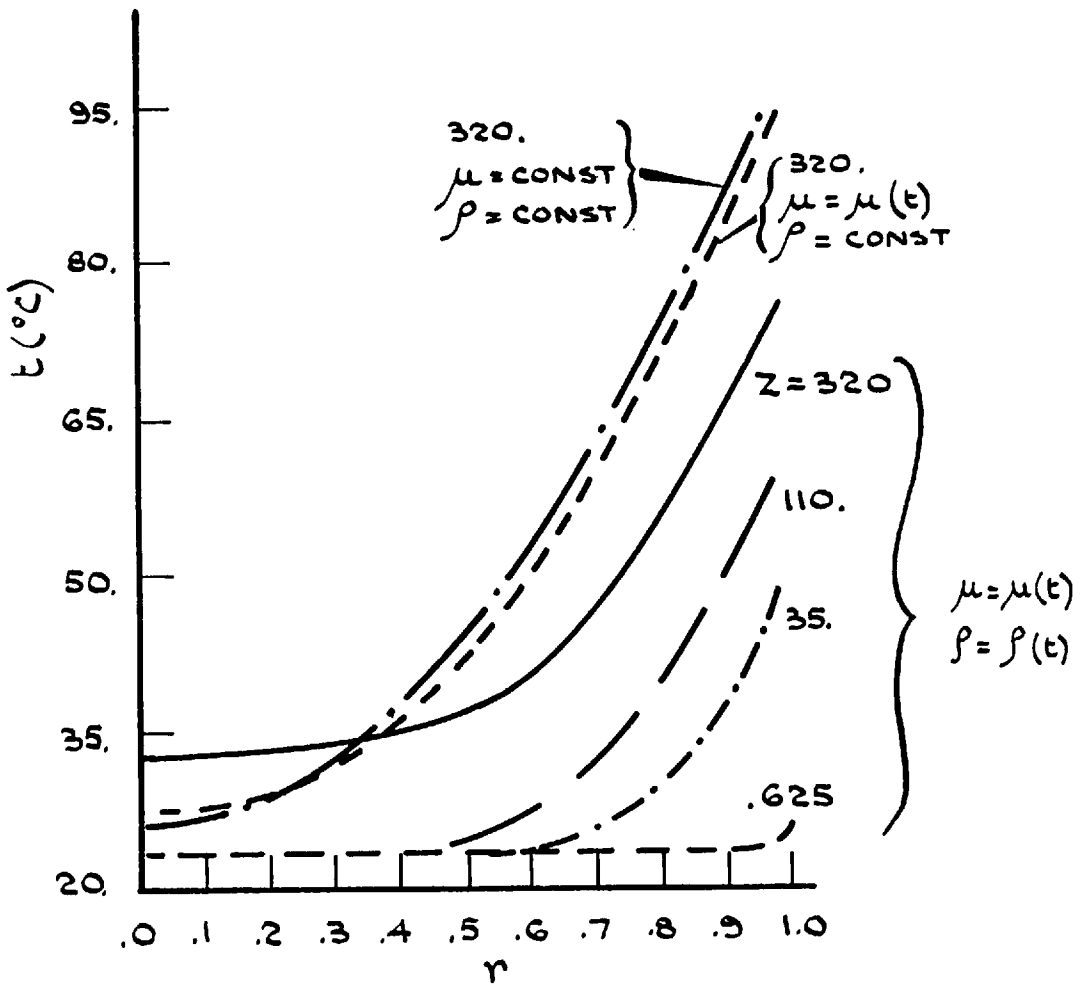

FIG (8.12) THE TEMPERATURE DISTRIBUTIONS ACROSS THE TUBE.

(where the inflexion occurs in the U profile) is considerable. Also on this figure are shown the temperature profiles for the forced-convection case and the case where only the variation of μ with temperature is allowed.

(c) Axial Variations of the Nusselt Number, Nu

Fig. (8.13) shows the Nusselt number along the tube. For the forced-convection case it starts with large values of Nu near the tube entry which decrease further downstream. At Z = 350, Nu = 4.800 and it is confirmed, by obtaining the predictions for larger Z values, that it approaches Nu = 4.364 which was theoretically obtained, among others, by Kays (1966). By allowing for the viscosity variations to take place the Nu values throughout the tube are slightly augmented. This is in agreement with the reduction in t_w and the increase of the U values near the above-mentioned wall (e.g. Nu = 5.170 at Z = 350).

For the mixed-convection regime, where the reduction in the density and the viscosity is allowed, the Nu values are even larger and the curve passes through a minimum value (Nu_{min} = 8.061 at Z = 140). This axial position is close to the position where the inflexion in the U profile occurs (i.e. Z = 110) and as a result, large U values will be assumed near the wall and the rate of heat transfer starts to improve. Due to ever-increasing U values near the wall, the Nusselt number continues to increase to the extent that Nu = 8.75 at Z = 320 which is considerably higher than the Nu = 4.87 obtained for its corresponding forced-convection case. Based on these comparisons, it can be said that because of the considerable increase in the heat transfer rate for the mixed-convection regime, any calculation for mixed-convection cases based on the fully-developed solution, i.e.

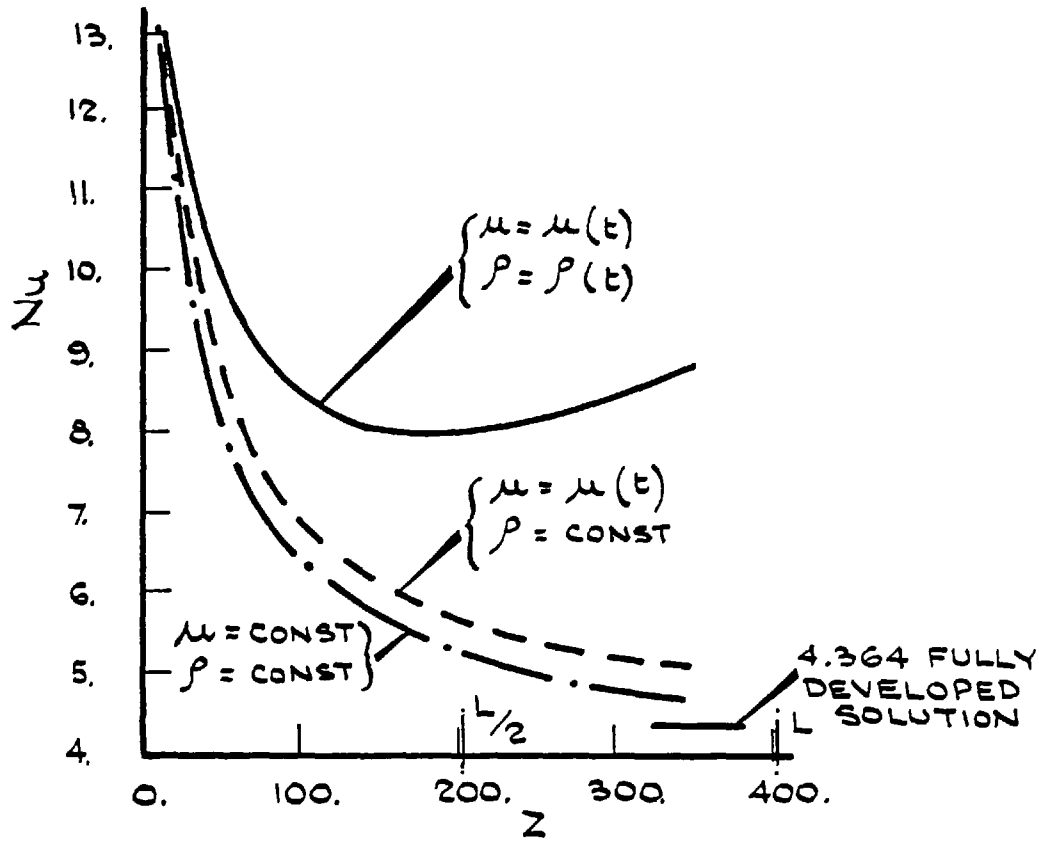

FIG(8.13) THE AXIAL VARIATIONS OF Nu.

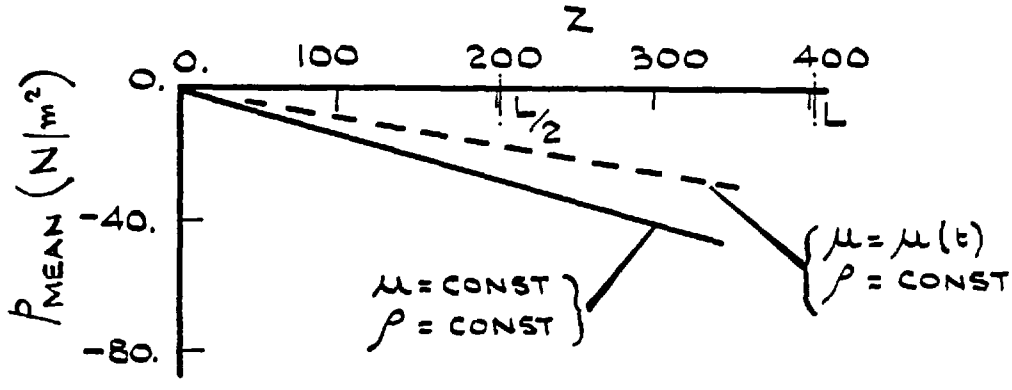

FIG(8.14) THE MEAN PRESSURE PROFILE ALONG THE TUBE.

Nu_H = 4.364, is subject to a considerable error.

(d) The Pressure Profiles

Fig. (8.14) shows the p_{mean} profile along the tube for the forced-convection case and for the case where the variation of μ with temperature is also considered. The profile, as expected, is linear and its slope, f_p approaches the fully-developed value of $f_p = 16/Re_D$ at the axial positions beyond the hydrodynamic entry length. Also on this figure, the effects of the variation of μ are appeared by the reduction of p_{mean} throughout the tube. According to this figure, for a forced-convective flow, the extra pressure needed at the tube entrance, $p_{o.Extra}$ must be at least equal to the value of p_{mean} at the end of the tube. For these two cases, the pressure profile across the tube is a straight line as shown on Fig. (8.15).

Fig. (8.16) shows axial variations of p_{mean} for the mixed-convection regimes. According to this figure the profile for the uniform heating case is almost linear. As for the flat duct, $p_{o.Extra}$ is calculated for different lengths of the tube, Fig. (8.17). It is noted that for the axial positions beyond Z = 140, $p_{o.Extra}$ starts to decrease and becomes zero at Z = 260. This length may be interpreted as the minimum length of the tube which is required for the natural-convection regime to take place in the tube. The mixed-convection index, i which is representative of the ratio of the buoyancy and the frictional pressure drops (defined in 5.3.3), is also predicted by CIRCLE and Fig. (8.18) shows its variations along the tube. The results shown on this figure are in agreement with those of Fig. (8.17) and particularly at Z = 260, where $p_{o.Extra} \cong 0$, the mixed-convection index i approaches 100.

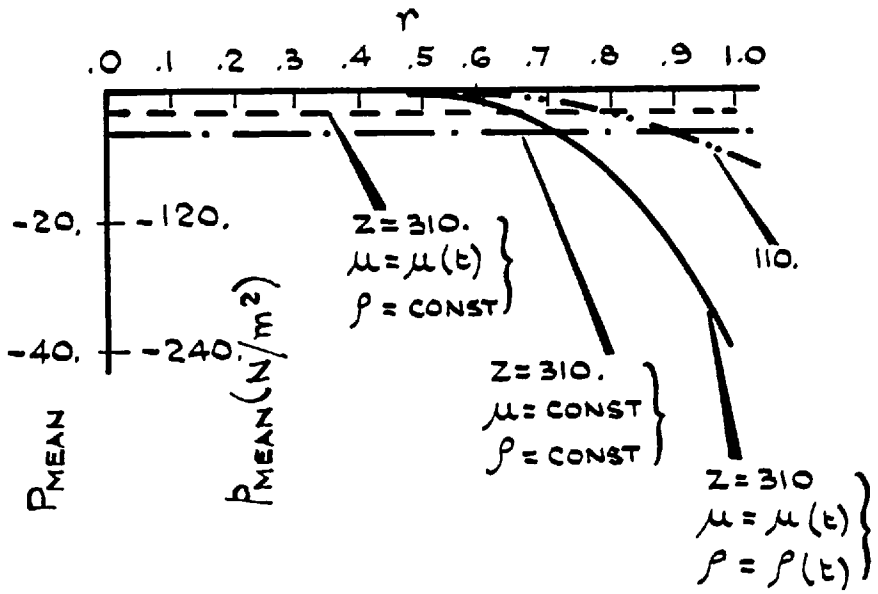

FIG(8.15) THE RADIAL DISTRIBUTIONS OF p_{MEAN}

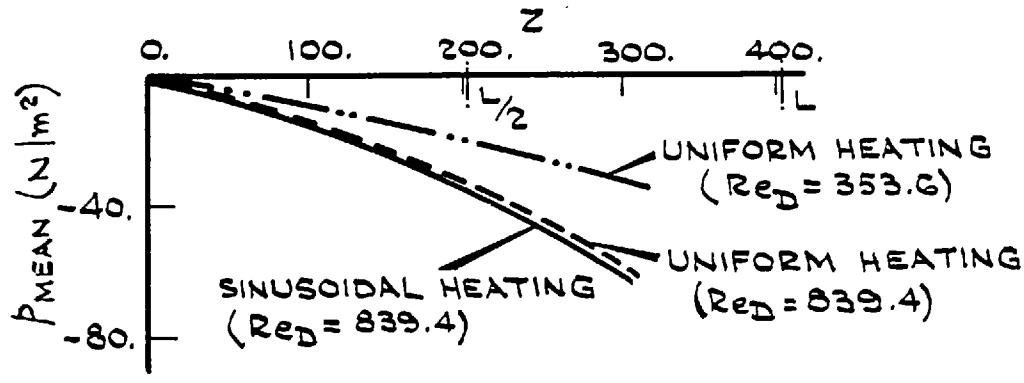

FIG(8.16) THE AXIAL DISTRIBUTIONS OF p_{MEAN}

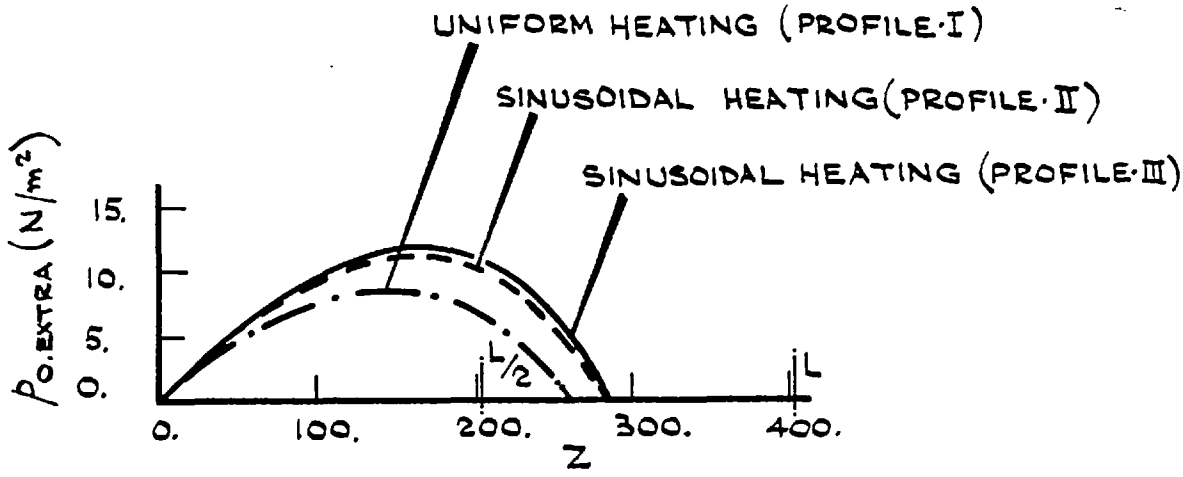

FIG(8.17) VARIATIONS OF $p_{o.EXTRA}$ FOR DIFFERENT LENGTHS OF TUBE.

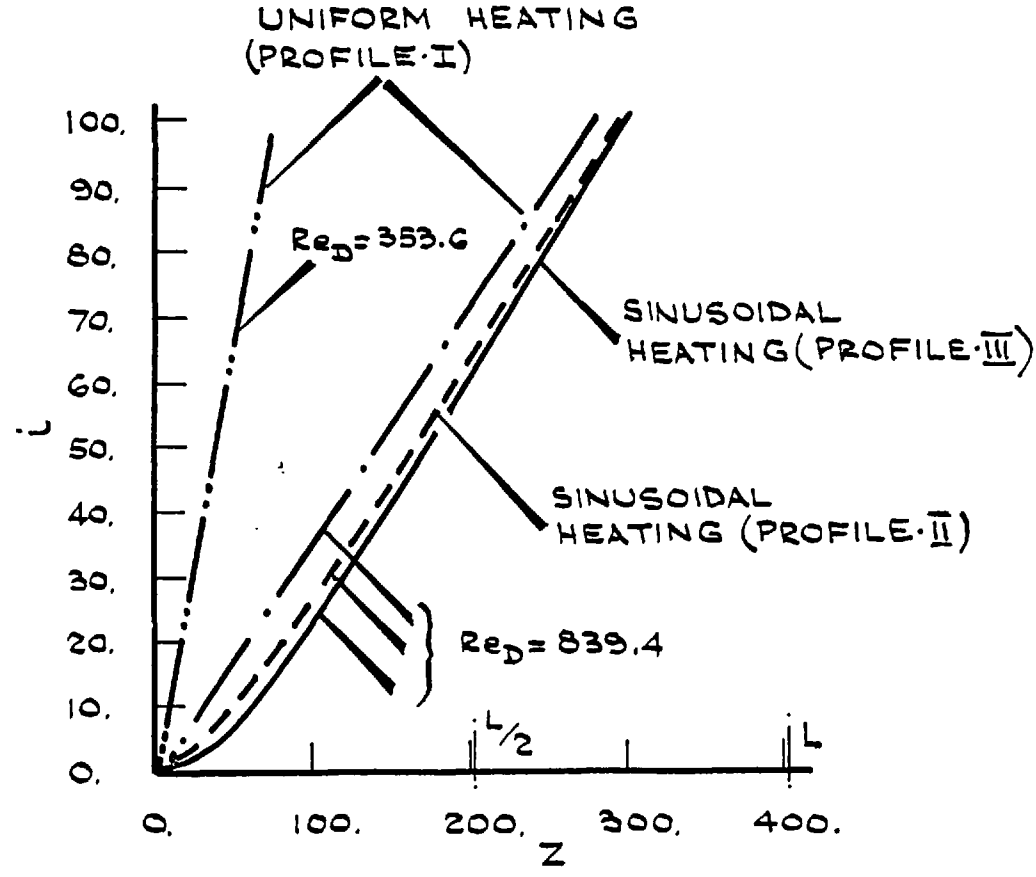

FIG(8.18) THE MIXED-CONVECTION INDEX VARIATIONS ALONG THE TUBE.

The pressure profile across the tube for the mixed-convection regime is also shown on Fig. (8.15). It is noted that near the wall, where the fluid temperature is higher than in the rest of the tube, the pressure is lower. This is expected because at this region the fluid is less dense. Conversely at the central region of the tube, where the fluid temperature is comparatively lower and the pressure is at its peak.

(e) Transition Into an Unstable Flow

The continuous development of the U profiles along the tube, and in particular the existence of an inflexion point in them at a certain axial distance, brings about the question of the possibility of transition from laminar flow to an unstable flow. The development of unstable flow is generally explained by the laminar instability theory, outlined by Pai (1956) and discussed in detail by Lin (1955). Their theory is based on the assumption that for any velocity profile there exists a Reynolds number such that above it the profile will be unstable to disturbances having wave numbers which lie within a certain range. Therefore, only the disturbances with these wave numbers will be amplified as they move downstream. The minimum Reynolds number at which a disturbance is amplified (so called "critical" Reynolds number) is the most important since below it the flow will be laminar for any disturbance. This Reynolds number depends only on the shape of the velocity profile. For developing profiles in poiseuille-flow, it would theoretically be possible to obtain a characteristic curve which, upon examination of different profiles along the tube, would show at what Reynolds number the profile would become unstable.

Lawrence and Chato (1966) adopted a method based on the

Lin (1955) theory which consists of taking three steps. First, the theoretical solution is used to obtain the developing U profiles for a number of cases with various Re_D's and Gr_D/Re_D^2 parameters (or Gr/Re_m in their paper). Second, using the experimental data to give the axial position at which instability began, the unstable profiles were obtained from the theoretical results for different Reynolds numbers. From these results they observed that transition always occurred after the profile had developed an inflexion point with the velocity at the centreline less than the velocity at some radial position, U_{peak}.

Based on this procedure, Lawrence and Chato (1966) have proposed a method to characterise these profiles so that a functional relationship exists between the characteristic parameter and the entrance Reynolds number, Re_o. Using trial and error, they have proposed a tentative parameter for giving the necessary functional relationship, which is:-

$$\text{Tran. Coef} = \frac{U_p + U_{\underline{\ell}}}{r_p} \cdot \mu_w$$

where U_p and $U_{\underline{\ell}}$ are respectively the peak and the centreline velocities, r_p being the dimensionless radial distance from the peak velocity to the wall and μ_w the fluid viscosity at the wall. These parameters, together with some experimental results of Lawrence and Chato (1966), are reproduced in Figs. (8.19) - (8.20).

In this chapter a trial is made to examine the possibility of transition into an unstable-flow based on this method. In particular, to assess the possiblity of extending it to cover the cases with sinusoidal heating.

Fig. (8.21) shows axial variations of the transition

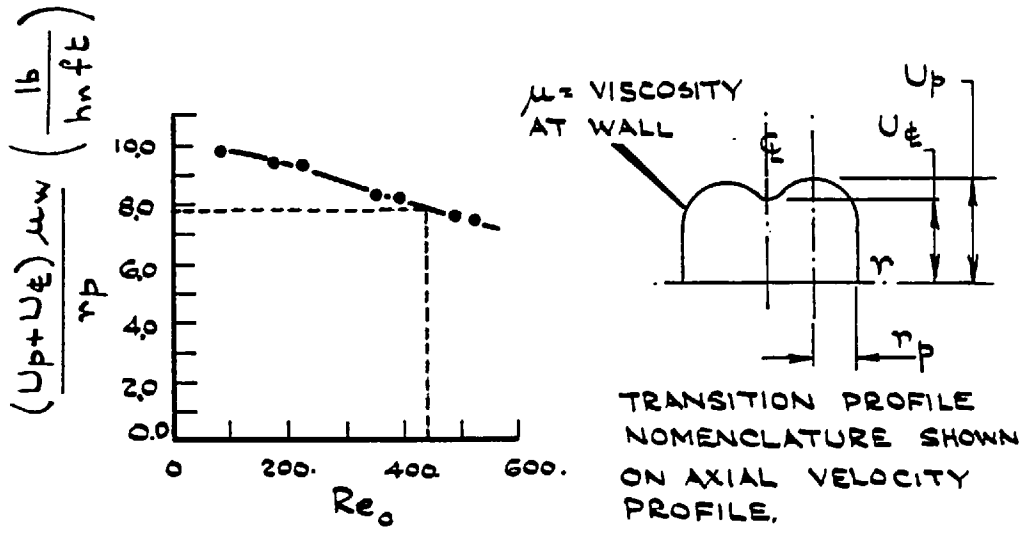

FIG (8.19) THE TRANSITION PARAMETER AS A FUNCTION OF Re_o (REPRODUCED FROM LAWRENCE et al 1966).

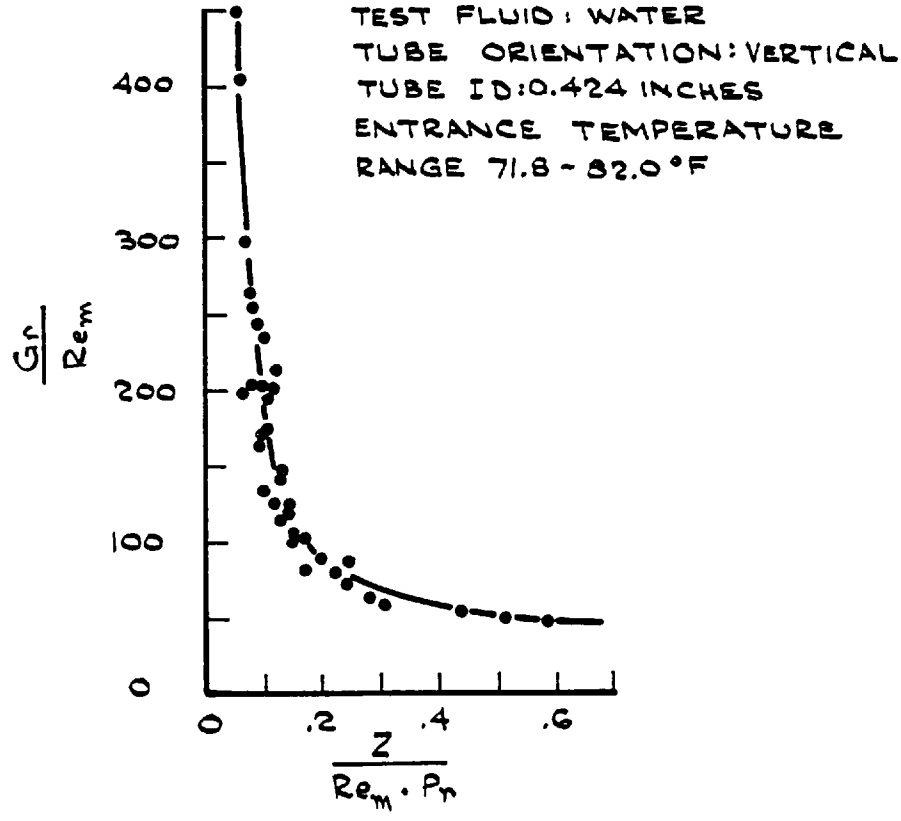

FIG (8.20) EXPERIMENTAL TRANSITION DATA (REPRODUCED FROM LAWRENCE et al 1966)

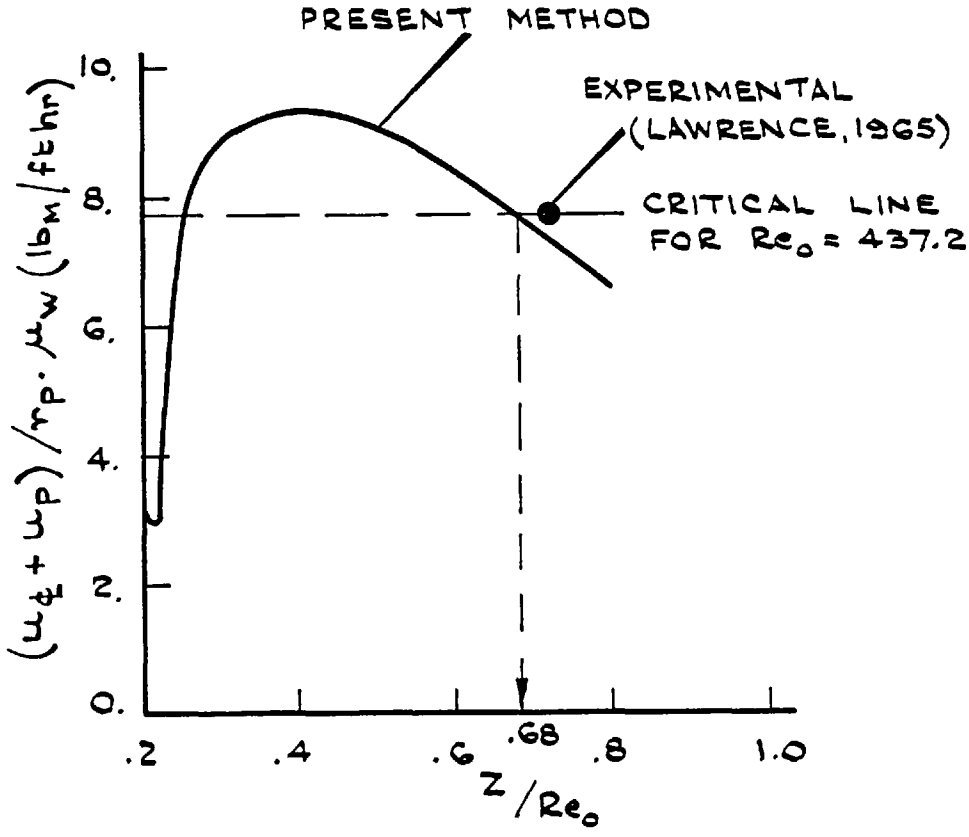

FIG(8.21) VARIATIONS OF THE TRANSITION-PARAMETER ALONG THE TUBE (FOR THE UNIFORM FLOW HEATING CASE).

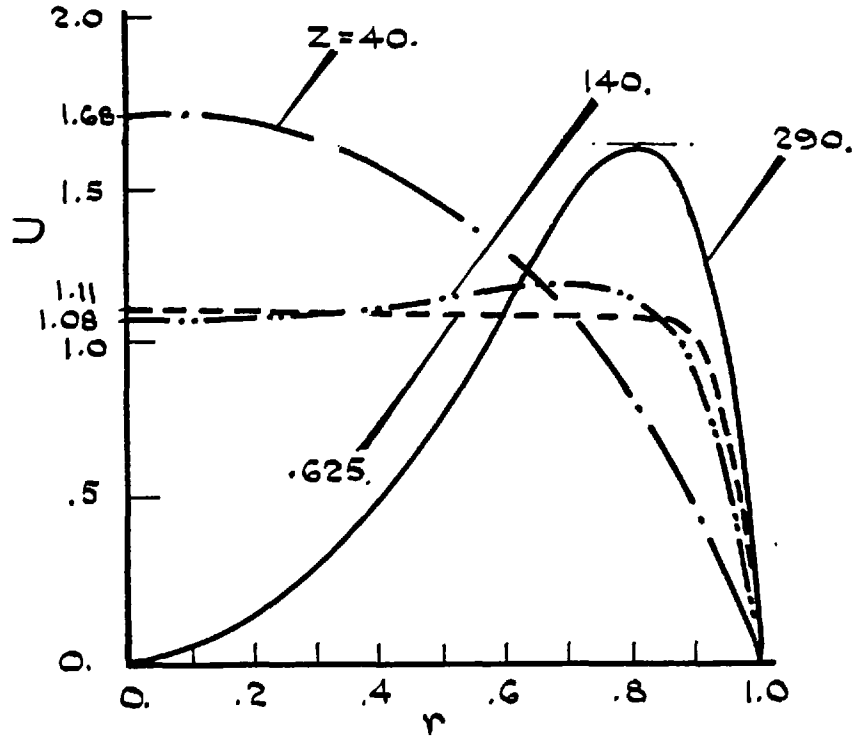

FIG(8.22) THE DEVELOPMENT OF THE U PROFILES ALONG THE TUBE FOR THE SINUSOIDAL HEATING CASE ACCORDING TO THE PROFILE II.

parameter for uniform heat-flux profile in the mixed-convection regime. It is noted that the parameter decreases from the entrance region of the tube up to the axial position where the U profile develops an inflexion point. Beyond that, it increases to a maximum value and falls again and passes through the critical-value line which was experimentally obtained by Lawrence and Chato (1966). Thus for a given Re_o the axial position where transition occurs may be found by repeating the procedure for every case. This method has its advantages over the other methods, which are generally based on correlations linked to the overall specifications of the flow, e.g. Hallman et al (1958). The main advantage is that the method is based only on the shape of the U velocity profile and thus may be extendable to non-uniform wall heating cases too.

For the data of the typical tube shown in Table (8.1), this method is attempted as follows:-

$$\begin{cases} Re_o = 437.2 \rightarrow \text{Fig. (8.19)} \rightarrow \text{Critical parameter} = 7.875 \\ \text{From Fig. (8.21)} \rightarrow Z/Re_o = 0.680 \end{cases}$$

Therefore:-

$$Z_{transition} = 297.2 \quad \left[\text{c.f. 320 experimentally obtained by Lawrence (1965)}\right]$$

This comparison shows that by following the present method the error will be 7.2%.

8.3.3 Computer Predictions for Sinusoidal Heating Cases

The main aim of this chapter is to study the computer predictions for sinusoidal heating cases. In what follows these predictions were obtained as a result of the prescription of the sinusoidal $\dot{q}_w''$ Profiles(II)and(III), shown on Fig. (8.3) , on the typical round tube of Table (8.1). The results for Profile II, in a mixed-convective regime, are to be presented together with those of the uniform heating case to facilitate the comparisons. At the end of this section, the results for Profile(III)are also given to generalise the conclusions.

8.3.3.1 The Results for the Sinusoidal $\dot{q}_w''$ Case According to the Profile (II)

(a) The U Profile

Fig. (8.22) shows the developing U profiles for this sinusoidal heating case. It is seen, as for the uniform heating case, that the profile develops along the tube towards the ideal parabolic shape of $U = 2(1 - r^2)$ in such a way that $U_{\ell} = U_{\ell_{max}} = 1.677$ at $Z = 40$. Beyond this axial position, due to the natural-convection effects, the profile starts to flatten and at $Z = 140$ it assumes an inflexion point. Further downstream, the natural-convection effects become ever more dominant and distort the shape of the U profile more significantly. At $Z = 290$, the centreline velocity U_{ℓ} reaches zero.

On Fig. (8.23) the U_{ℓ} profiles for this sinusoidal heating case and the uniform heating case, Profile(I), are shown.
By comparison the following points may be noted for the sinusoidal heating:-

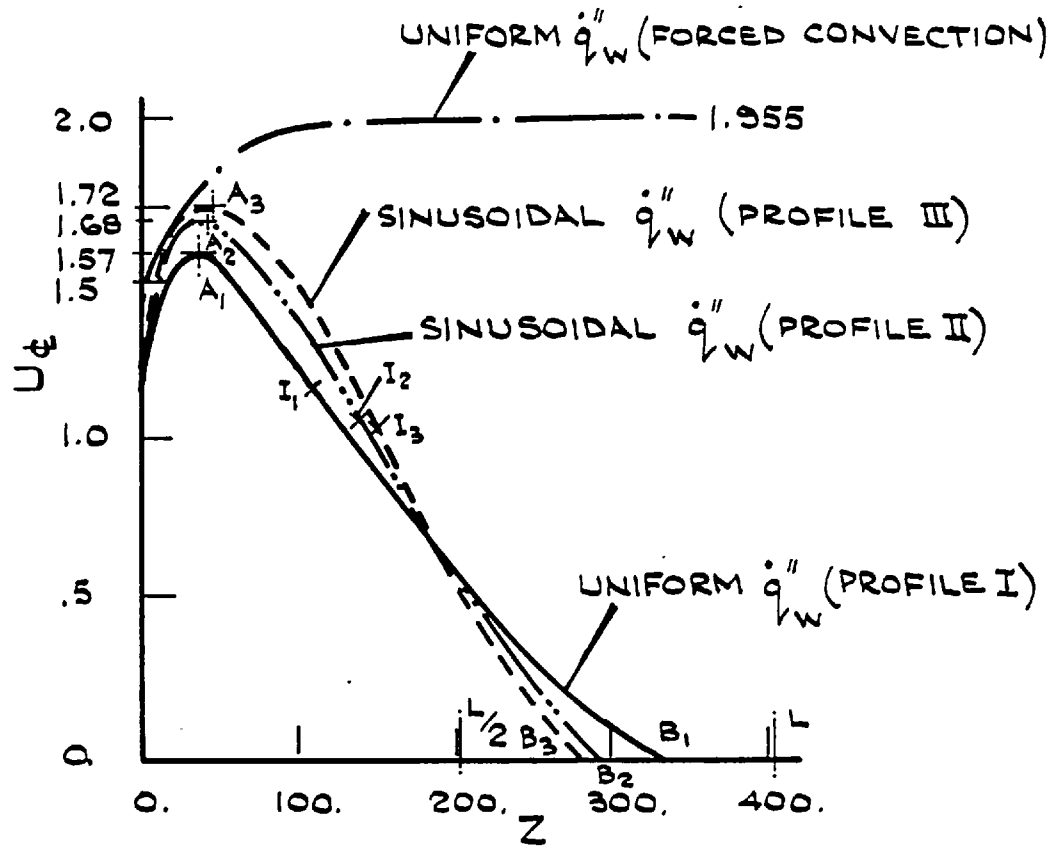

FIG(8.23) THE DEVELOPMENT OF U_ℓ ALONG THE TUBE FOR THE THREE HEATING CASES.

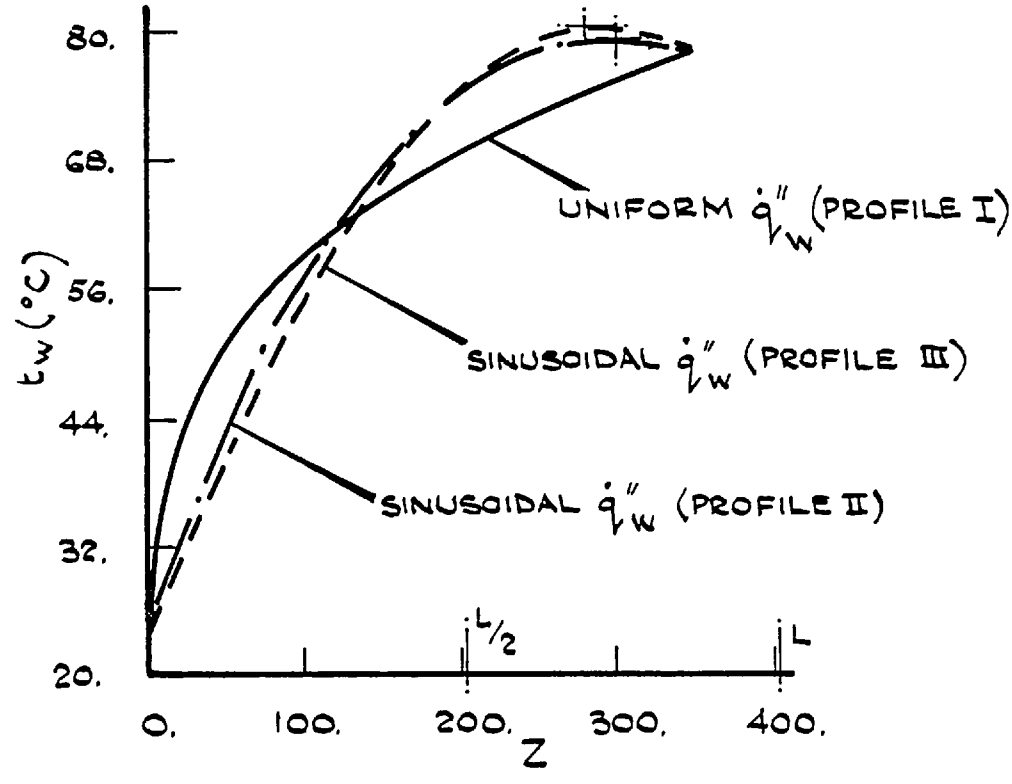

FIG(8.24) THE AXIAL VARIATIONS OF THE WALL TEMPERATURE.

(i) $U_{\ell_{max}}$ occurs at a larger distance from the tube entrance and its magnitude is larger, i.e.

$U_{\ell_{max}}$ = 1.677 at Z = 40 (c.f. $U_{\ell_{max}}$ = 1.570 at Z = 35)

(ii) Inflexion occurs at a larger axial distance with a lower magnitude, i.e.

$U_{\ell_{Inflexion}}$ = 1.08 at Z = 140 (c.f. $U_{\ell_{Inflexion}}$ = 1.15 at Z = 110)

(iii) The axial distance needed for the U_{ℓ} value to approach zero is smaller, i.e.

U_{ℓ} = 0.0 at Z = 290 (c.f. U_{ℓ} = 0.0 at Z = 320)

(b) The Temperature Profiles

Fig. (8.24) shows the axial variation of the wall temperature, t_w. It is noted that for the axial positions within the first quarter of the tube, t_w for this sinusoidal heating is lower. The reason seems to be that in this region the heat-input to the fluid is lower for the sinusoidal heating case than for the uniform heating case. Beyond Z = 120, t_w for the former case continues to increase until it passes through its maximum, $t_{w.Max}$ = 79 ^{o}C at Z = 300. It should be pointed out that this position is located at the second half of the tube and for the flat duct, Chapter (5), it is in accord with the results obtained by Ginn's equation. It is also noted that although the total heat addition up to Z = 203.3 (i.e. z = L/2) is

the same for both of the $\dot{q}''_w$ profiles, $t_{w.Max}$ for the sinusoidal heating case is larger.

Fig. (8.25) shows the radial temperature distribution of the flow along the tube for the sinusoidal $\dot{q}''_w$ case. It is seen that despite the considerable increase of t_w the centreline temperature does not increase at the same pace and its augmentation is even smaller in the axial positions smaller than the length needed for the inflexion in the U profile to appear. Half-way through the tube, at Z = 203.3 ($z = L/2$), the lower t_w value for the uniform $\dot{q}''_w$ case, together with the same total heat-input, forces its radial distribution profile to be flatter than that of the sinusoidal heating case.

Fig. (8.26) shows the mixed-mean temperature, t_{mean} along the channel for the three $\dot{q}''_w$ profiles. The curves on this figure may also be interpreted as representing the total heat-input at each axial position in the tube, $\dot{Q}_{tot}(z)$ (according to the ordinate placed at the right-hand side of the figure). As expected, t_{mean} for the sinusoidal heating cases is lower at the first half and higher at the second half. But as the flow continues towards the end of the tube, the curves become closer to each other in such a way that they will intersect at the end of the tube.

(c) The Axial Variations of Nu

Fig. (8.27) shows the profile for Nu along the tube for this sinusoidal heating case. For comparison the profiles for the uniform heating case in the mixed and the forced-convection regimes are also shown. As for the flat duct, the shape of the profile is close to a horizontally positioned letter s (i.e. ⊰). For the first half of the channel, Nu values always exceed their asymptotic value of 4.364,

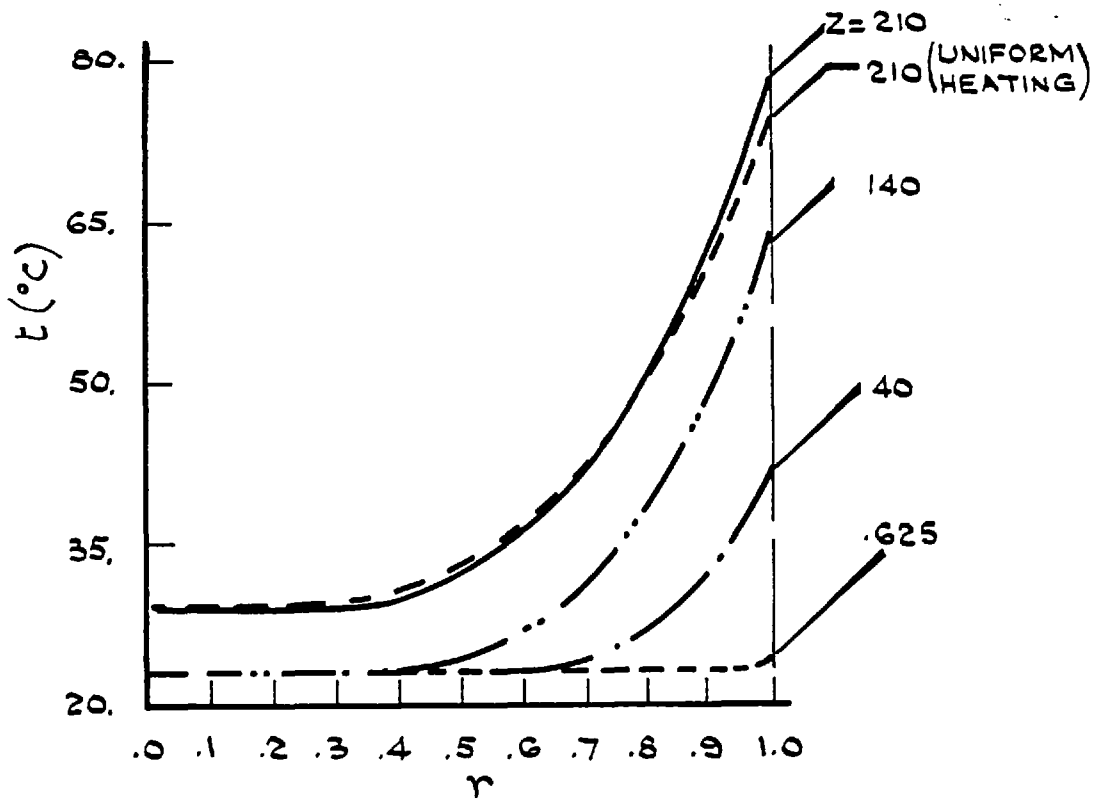

FIG(8.25) THE RADIAL DISTRIBUTION OF THE FLUID TEMPERATURE FOR THE SINUSOIDAL HEATING (PROFILE · II).

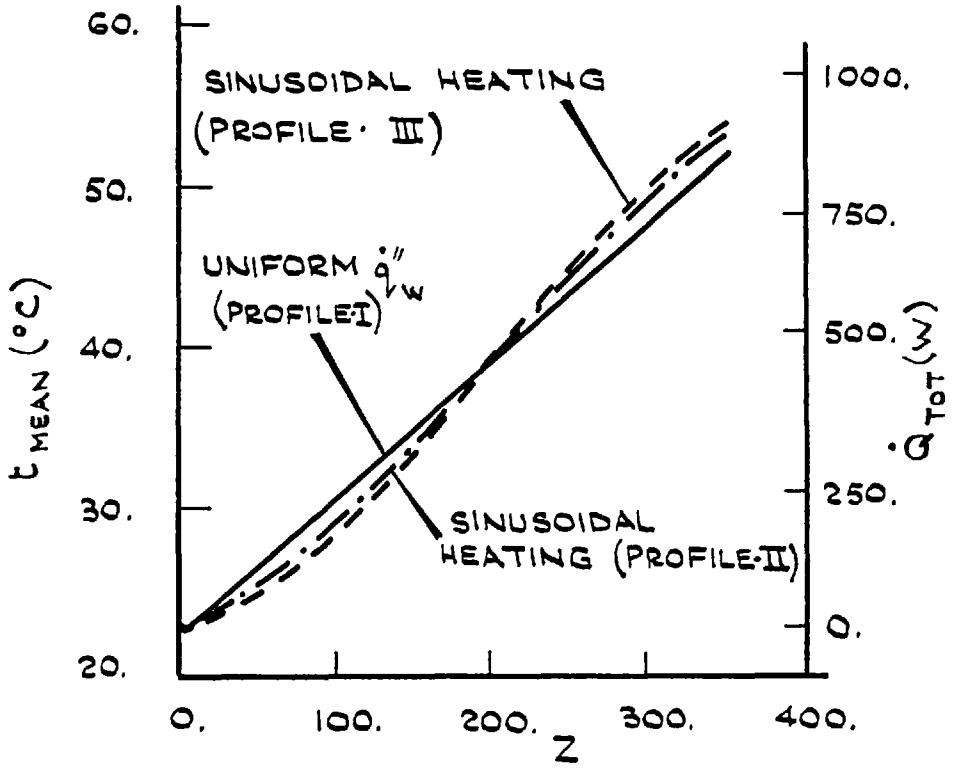

FIG (8.26) WATER MEAN TEMPERATURE, t_{MEAN} AND THE TOTAL HEAT INPUT, $\dot{Q}_{TOT}$ VARIATIONS ALONG THE TUBE.

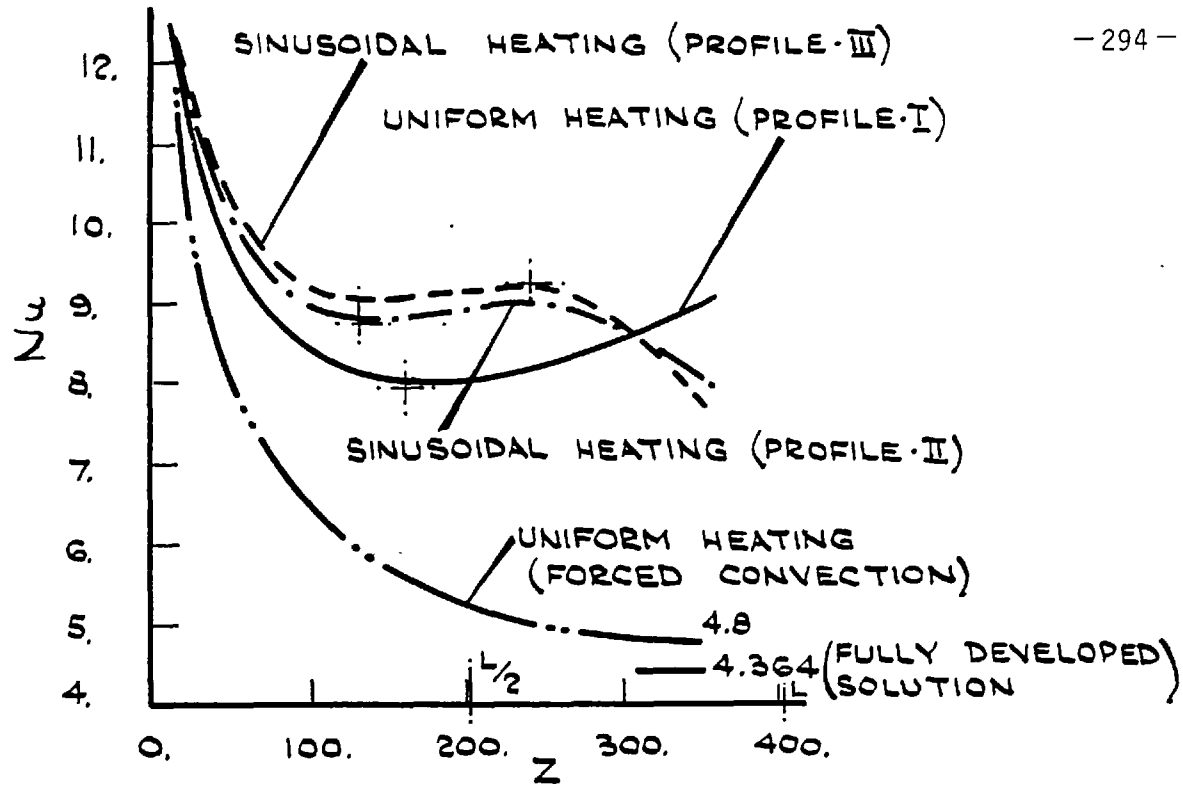

FIG (8.27) THE AXIAL VARIATIONS OF THE NUSSELT NUMBER IN THE TUBE.

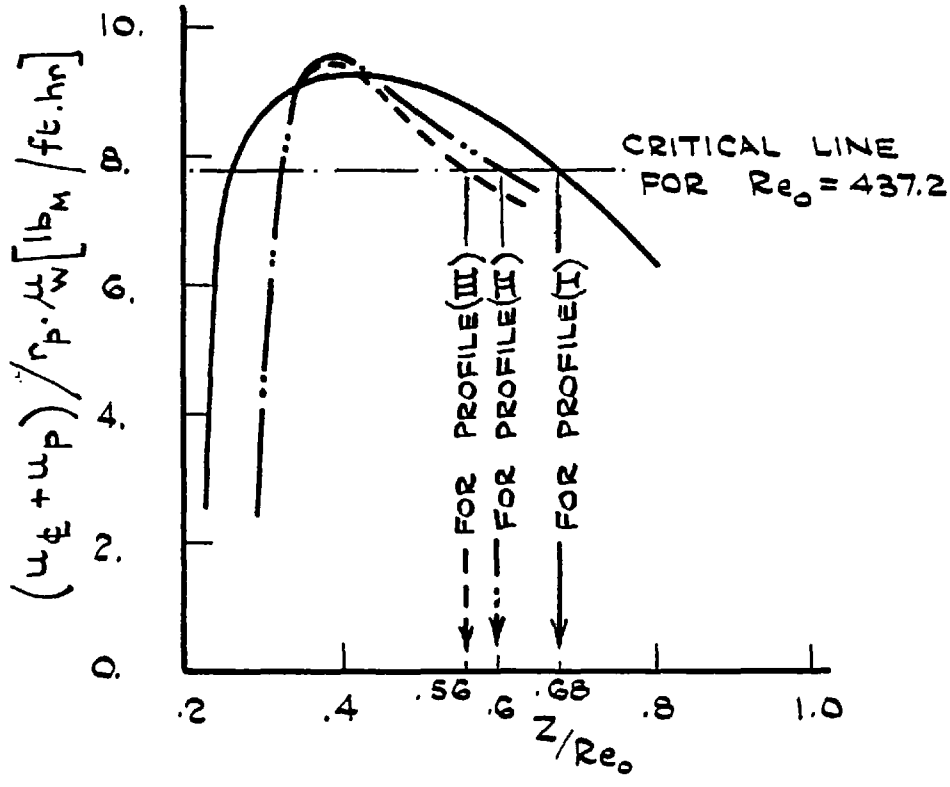

FIG (8.28) VARIATIONS OF THE TRANSITION PARAMETER ALONG THE TUBE FOR DIFFERENT WALL HEAT-FLUX PROFILES.

pertaining to the case of uniform wall heat flux for forced-convection. They also exceed their corresponding mixed-convection values to a large extent. From Z = 130 to Z = 240, the Nu values are fairly constant. In the region beyond Z = 240 (z/L = 0.6), which is characterised by an axial decrease of wall heat-flux, the Nusselt numbers begin to decrease to the extent that at Z = 350, the Nu values fall below the corresponding values for the uniform heating case in a mixed-convection regime. However, they still exceed the values obtained for a forced-convection case.

This comparison shows that the calculations for a mixed-convection regime in a tube, with prescribed sinusoidal $\dot{q}''_w$ profile should not be based on the asymptotic value of Nu = 4.364 because of the large error which will occur.

(d) Pressure Profiles

The axial variation of p_{mean} for this sinusoidal heating case is shown on Fig. (8.16). It is noted that the deviations from the nearly linear curve which is obtained for the uniform $\dot{q}''_w$ case are not significant although the p_{mean} values seem to be slightly lower.

On Figs. (8.17) - (8.18) the $p_{o.Extra}$ and i for this case are shown. It can be seen that the minimum length of the tube needed for: $p_{o.Extra}$ = 0 is enlarged because of the prescription of the sinusoidal $\dot{q}''_w$ profile. As for the mixed-convection index, i the values are less than their corresponding values for the uniform heating case. This is to be expected because of the shape of the total heat addition curve, $\dot{Q}_{tot}$ presented on Fig. (8.26). However, because the heat-addition throughout the tube, for all of these $\dot{q}''_w$ profiles, is the same, the index i will also be the same at the end of the tube, Fig. (8.18).

Radial pressure distributions will be of nearly the same shape as those for the uniform heating case, Fig. (8.15) although because of the lower t_w, for a fraction of the first half of the tube the pressure, p is slightly higher.

(e) Transition Length

For this sinusoidal $\dot{q}''_w$ case, Profile (II), the transition parameter is calculated and shown on Fig. (8.28). Following the same procedure as for the uniform $\dot{q}''_w$ case, the intersection between the characteristic curve of this case and the critical value of the parameter is at $Z/Re_o = 0.60$, i.e. $Z = 262.32$. It can be seen from Fig. (8.28) that this length is shorter than what was obtained for the uniform $\dot{q}''_w$ case (i.e. $Z = 297.2$) and may be interpreted as one of the effects of the prescription of a sinusoidal $\dot{q}''_w$ profile.

8.3.3.2 The Results for the Sinusoidal $\dot{q}''_w$ Profile According to the Profile (III)

As shown on Fig. (8.3) this $\dot{q}''_w$ profile is the same as the Profile (II) but with a higher ratio of $\dot{q}''_{w.Max}/\dot{q}''_{min}$, 5 c.f. 3 for the Profile (II). This profile has been chosen to confirm the trend of the results which were obtained for the other sinusoidal $\dot{q}''_w$ profile, specially for important design factors such as $t_{w.Max}$, Nu and to some extent, the transition length.

Fig. (8.23) shows the axial variation of U_{ℓ} for this $\dot{q}''_w$ case together with similar profiles for the other two cases. From this figure, it can be seen that for the Profile (III) in comparison with the other two $\dot{q}''_w$ profiles (I) and (II) of Fig. (8.3):-

(i) $U_{\ell_{max}}$ value is higher and occurs at a larger distance from the tube entrance, i.e.

$U_{\ell_{max}} = 1.713$ at $Z = 45$

c.f.
- $U_{\ell_{max}} = 1.677$ at $Z = 40$ For the Profile(II)
- $U_{\ell_{max}} = 1.570$ at $Z = 35$ For the Profile(I)

(ii) $U_{\ell_{Inflexion}}$ value is lower and occurs at a larger distance, i.e.

$U_{\ell_{Inflexion}} = 1.03$ at $Z = 150$

c.f.
- $U_{\ell_{Inflexion}} = 1.08$ at $Z = 140$ For the Profile(II)
- $U_{\ell_{Inflexion}} = 1.15$ at $Z = 110$ For the Profile(I)

(iii) The zero U_{ℓ} value occurs at a smaller axial distance, i.e.

$U_{\ell} = 0.00$ at $Z = 280$

c.f.
- $U_{\ell} = 0.00$ at $Z = 290$ For the Profile(II)
- $U_{\ell} = 0.00$ at $Z = 330$ For the Profile(I)

Fig. (8.24) shows the tube wall temperature profile along the tube for the three $\dot{q}''_w$ cases. It is noted that $t_{w.Max}$ is higher than that for the $\dot{q}''_w$ Profile (II) and occurs at a smaller distance from

the tube entry. i.e.:-

$$t_{w.Max} = 80.14\ ^{o}C \text{ at } Z = 290$$

c.f. $t_{w.Max} = 78.93\ ^{o}C$ at $Z = 300$ For the Profile (II)

Axial variations of Nu for all of these three $\dot{q}_w''$ profiles are shown on Fig. (8.27). It is noted that there exists a slight rise in the Nu values for the axial positions beyond the position where the inflexion in the U profile occurs. In more detail , for the Profile (III):-

$$Nu_{min} = 9.055 \text{ at } Z = 130 \text{ and } Nu_{Max} = 9.173 \text{ at } Z = 230$$

c.f. For the Profile (II):

$$Nu_{min} = 8.850 \text{ at } Z = 130 \text{ and } Nu_{Max} = 9.02 \text{ at } Z = 230$$

The mean pressure at each section, p_{mean} is not significantly affected by the sinusoidal heating. On Fig. (8.16) this is shown as for the other sinusoidal heating case.

The transition length, as defined in (8.3.2e) is predicted to be smaller for this sinusoidal heating case than that which was obtained for the other case, Profile (II). As shown on Fig. (8.28) for heating according to the Profile (III):-

$$Z/Re_o = 0.56 \rightarrow Z = 245$$

(c.f. 262.3 and 297.2 for the Profiles (II) and (I) respectively)

8.3.4 Effects of the Reynolds Number and the Parabolic Velocity Profile at the Tube Entrance on the Computer Predictions

(a) Reynolds Number

As for the flat duct, these effects are most significant for the pressure and its related parameters, i.e. p_{mean} and i. On Figs. (8.16) and (8.18) the axial variations of p_{mean} and i for the sinusoidal heating according to the Profile (II) are compared for two different Reynolds numbers (i.e. Re_D = 839.4 and 353.6). As expected, because of the reduction in the Re value while $\dot{Q}_{tot}$ is kept constant, p_{mean} reduces significantly throughout the tube. Conversely, due to stronger natural-convection effects, the index i increases considerably. These effects may also be seen by the examination of Fig. (8.9) where U_{ℓ} values along the tube are compared for these two Reynolds numbers.

(b) Parabolic U_o Profile

On Figs. (8.29) - (8.31) the axial variations of U_{ℓ}, t_w and Nu are compared for the following two U_o profiles:-

(i) $U_o = 1$ (Uniform U_o profile)

(ii) $U_o = 2(1 - r^2)$ (Parabolic U_o profile)

By examination of these figures, it can be suggested that for the parabolic U_o profile case, the U_{ℓ} and the t_w values are larger up to Z = 120 (i.e. $z/L \cong 0.3$) and Nu values at this region seem to be smaller. However, as for the flat duct geometry, the flow parameters such as U, t_w and Nu reach their corresponding values for the uniform U_o profile. This confirms that for the round tube also, the effects of

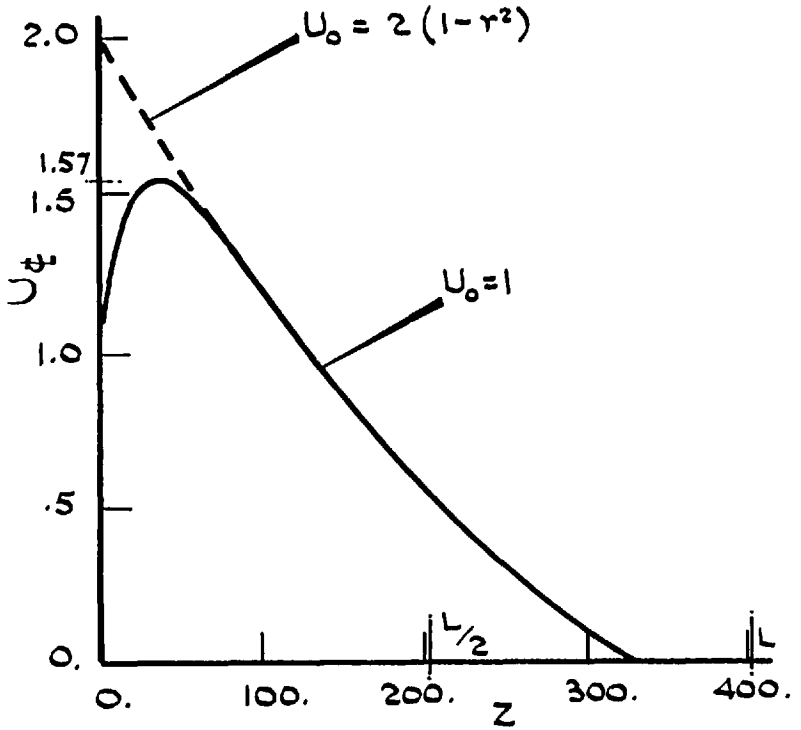

FIG(8.29) U_ℓ VARIATIONS ALONG THE TUBE FOR TWO DIFFERENT U_0 PROFILES.

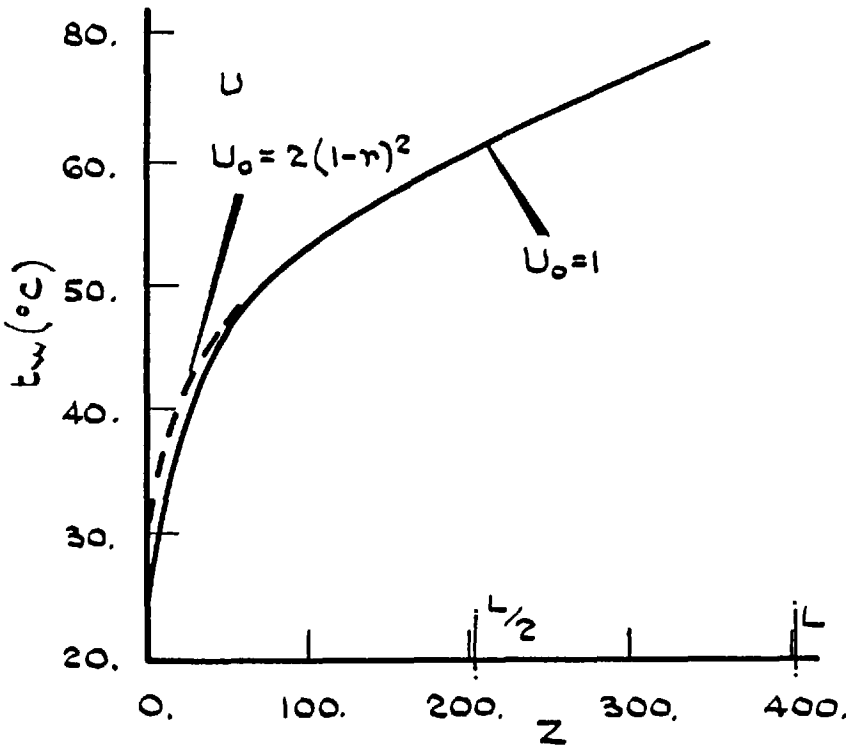

FIG(8.30) WALL TEMPERATURE VARIATIONS ALONG THE TUBE FOR TWO DIFFERENT U_0 PROFILES.

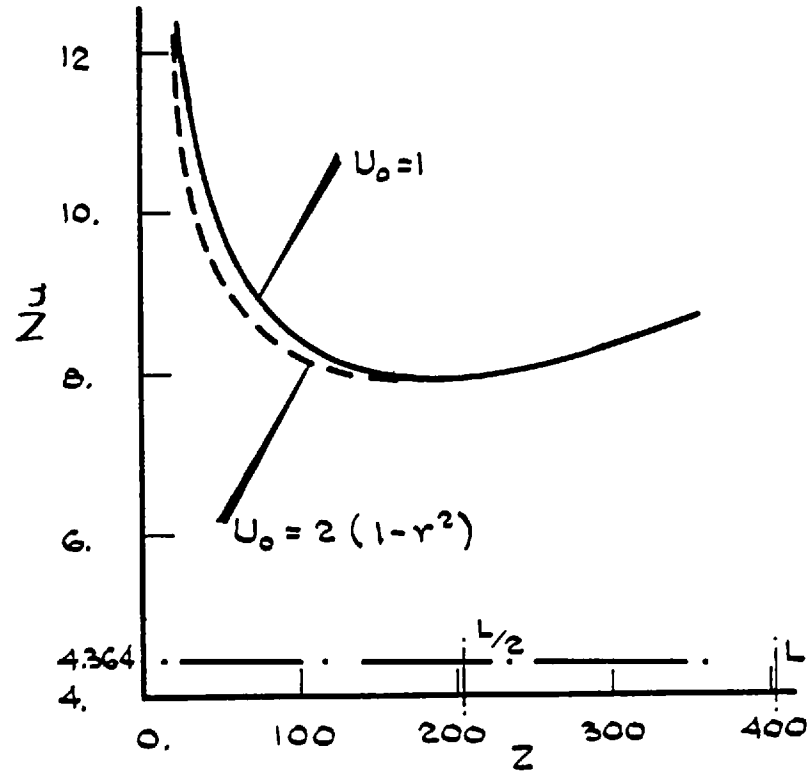

FIG (8.31) AXIAL VARIATIONS OF THE LOCAL NUSSELT NUMBER FOR TWO DIFFERENT U_o PROFILES.

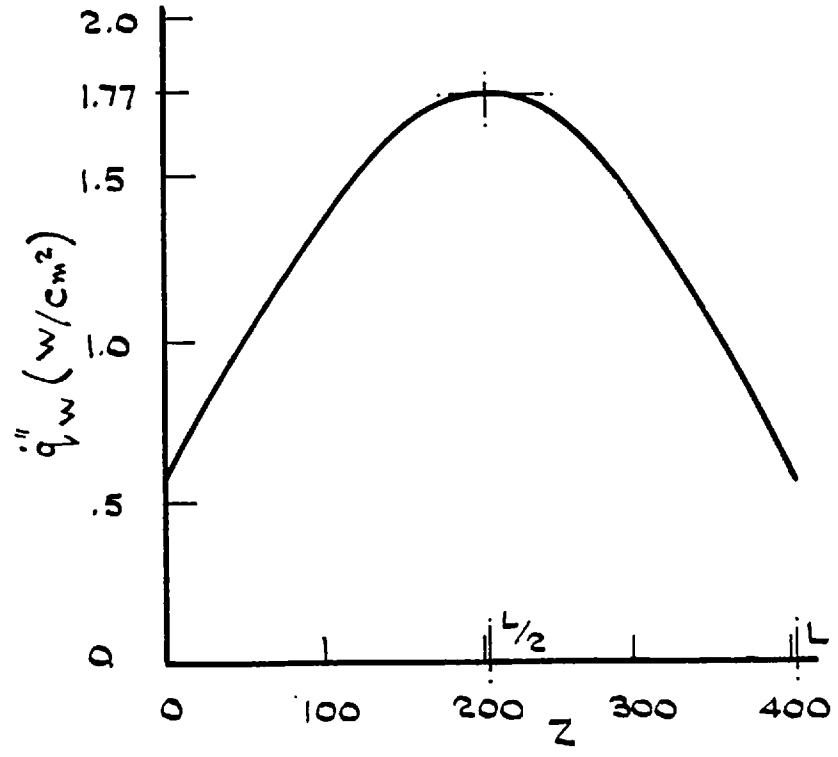

FIG (8.32) THE WALL HEAT-FLUX PROFILE OBTAINED FROM THE CROSS-CHECKING.

the parabolic U_o profile is limited to the entrance region of the channel.

8.4 Cross-Checking of the Computer Predictions for the Sinusoidal Heating Cases

In order to gain more confidence about the predictions for the sinusoidal heating cases, and also to test the computer program CIRCLE in solving the cases with prescribed t_w profiles, a cross-checking is attempted. This is done by taking the following three steps:-

1. The typical round tube of Fig. (8.1), with the data of Table (8.1), is solved by CIRCLE for a sinusoidal heating case according to Profile(II) in Fig. (8.3) and the t_w profile, shown in Fig. (8.24), is predicted.

2. This t_w profile is treated as the data for a prescribed wall temperature case applied on the same tube and CIRCLE is used to predict the $\dot{q}''_w$ profile for such a case.

3. A comparison between the $\dot{q}''_w$ profile predicted in the second step and the original $\dot{q}''_w$ profile, i.e. Profile (II), is made.

Fig. (8.32) shows the $\dot{q}''_w$ profile which was obtained when the above-mentioned steps were followed. A comparison between this profile and the sinusoidal $\dot{q}''_w$ according to the Profile (II) of Fig. (8.3) showed that they are virtually the same and the small difference at the

entrance region is less than 0.5%. This method also reproduces the other specifications of the flow (e.g. Nu, U, P, i, etc.) correctly. Therefore, as for the flat duct mentioned in (5.4), the present method for non-uniform wall conditions may also be used to solve for round tubes.

8.5 Comparison of the Computer Predictions for the Sinusoidal Heating Cases with Published Results

As mentioned in the literature review, Chapter (2) , there are published results for a sinusoidal heating case. These were obtained by the two following methods:-

(i) The superposition method, introduced by Hallman et al (1958) which takes the "thermal entrance region" solution, pertaining to the uniform wall heat-flux case as a starting point. Hsu (1965) used this method to calculate the local Nusselt number along the tube for a sinusoidal $\dot{q}''_w$ case.

(ii) The hybrid method, introduced by Nijsing et al (1973) which uses the superposition method together with an alternate method based on the numerical solution of the governing equations for the problem in a finite-difference form.

In this part of the thesis, the predictions of the computer program CIRCLE are to be checked against two sets of published results, one for each of the above-mentioned methods, and the differences will be discussed. It should be pointed out that both Hsu (1965) and Nijsing et al (1973) assumed the fully-developed U profile throughout the

tube and chose the parameter $\frac{D \cdot Pr \cdot Re_D}{L}$ to characterise each case. Therefore, their results correspond to the forced-convection cases. Also to comply with their assumptions the heat-flux distribution along the tube will be taken as half a complete sine wave, i.e.:-

$$\dot{q}''_w(z) = \dot{q}''_{wo} \sin \frac{\pi z}{L}$$

which may be obtained by putting b = 0 in the general formula:-

$$\dot{q}''_w(z) = \dot{q}''_{wo} \left(b + c \sin \frac{\pi z}{L}\right)$$

Fig. (8.33) shows the local Nusselt number, Nu along the tube for a laminar forced-convective flow with the sinusoidal $\dot{q}''_w$ distribution. Two cases with different values of $\frac{D \cdot Pr \cdot Re_D}{L}$ = 20 and 8 respectively are solved for. The agreement between the present predictions and those obtained by Hsu (1965) seems to be good and the Nu values are very close throughout the tube. However, the present method predicts the Nu values to be slightly lower in the first half of the tube and to be higher in the second half with the differences being less than 1%.

In order to examine the effects of the variations of μ and ρ with temperature, i.e. a mixed-convection regime, these variations were considered for the case of $\frac{D \cdot Pr \cdot Re_D}{L}$ = 20. Fig. (8.34) shows that the gain in the local Nusselt numbers along the tube is considerable, especially in the region of the middle of the tube. As mentioned for the flat duct geometry, Chapter (5), these are attributed to a better cooling process which takes place as a result of large velocities near the heated wall of the tube. It is noted that these gains are more

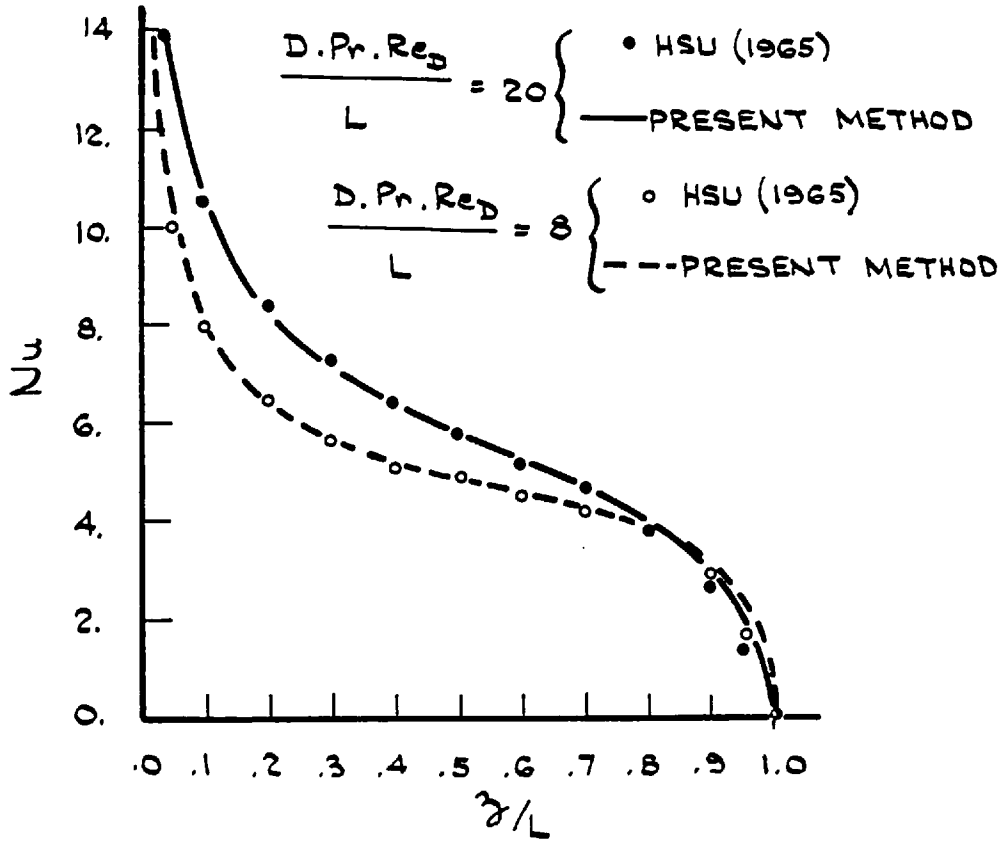

FIG(8.33) LOCAL NUSSELT NUMBER VS z/L FOR LAMINAR FORCED-CONVECTIVE FLOW WITH SINUSOIDAL WALL HEAT-FLUX DISTRIBUTION.

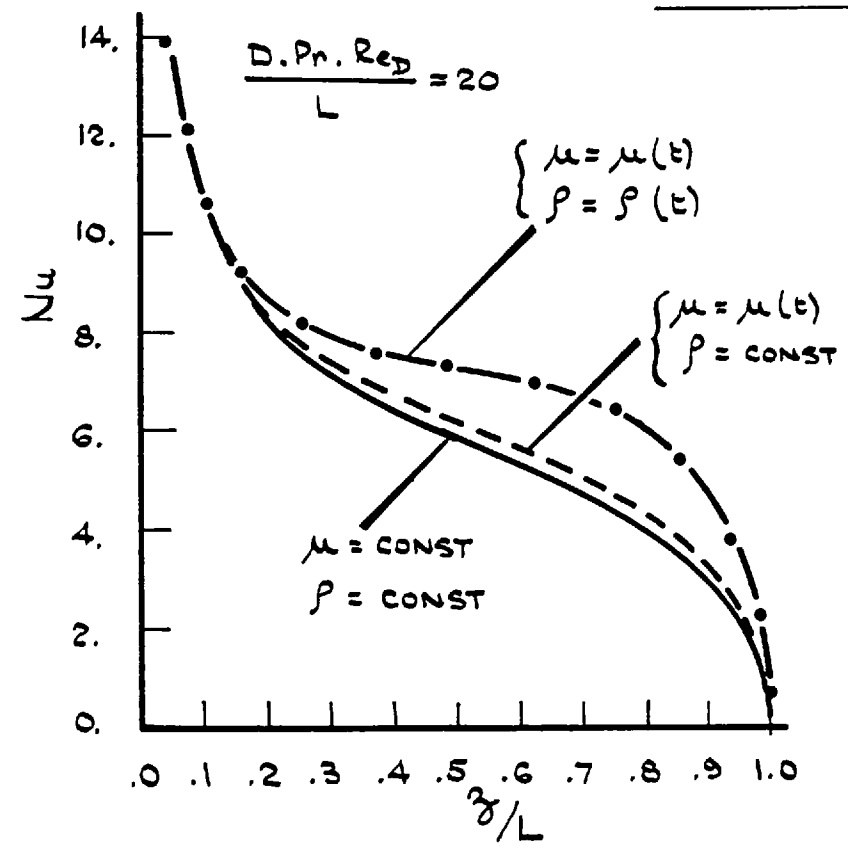

FIG(8.34) LOCAL NUSSELT NUMBERS FOR SINUSOIDAL WALL HEAT-FLUX VARIATION IN THE FORCED-CONVECTION AND THE MIXED-CONVECTION REGIMES.

significant after the inception of the inflexion in the U profile which causes large velocities near the wall, Fig. (8.22). In conclusion, as the fluid moves downstream, these gains in the Nu values become more significant and, consequently, the profile for the mixed-convection case will always be above that of the forced-convection case throughout the tube.

Fig. (8.34) shows that when the variations of μ with temperature are only considered, there will be some augmentation in the Nu values throughout the tube because in this case also the U profile will not be parabolic and will continue to develop along the tube.

Comparison of the computer predictions for the same problem but having $\frac{D \cdot Pr \cdot Re_D}{L} = 10$, with the published results of Nijsing et al (1973), Figs. (8.35) - (8.36), is also good. The gain in the local Nu values in the second half of the tube for the mixed-convection regime is more significant than the previous case. This is thought to be because of a lower value of $(Re_D \cdot Pr)$ which gives the natural-convection effects a stronger dominance throughout the tube.

8.6 Conclusions

The main conclusion is that the present method could solve for non-uniform prescribed wall conditions in round tubes. The predictions of the computer program CIRCLE, which is developed to execute the present method for sinusoidal and uniform wall heat-flux profiles, are in agreement with the published results of Hsu (1965), Nijsing et al (1973), Lawrence et al (1966) and Kays (1966). The predictions obtained by the application of several wall heat-flux profiles according to the general formula:-

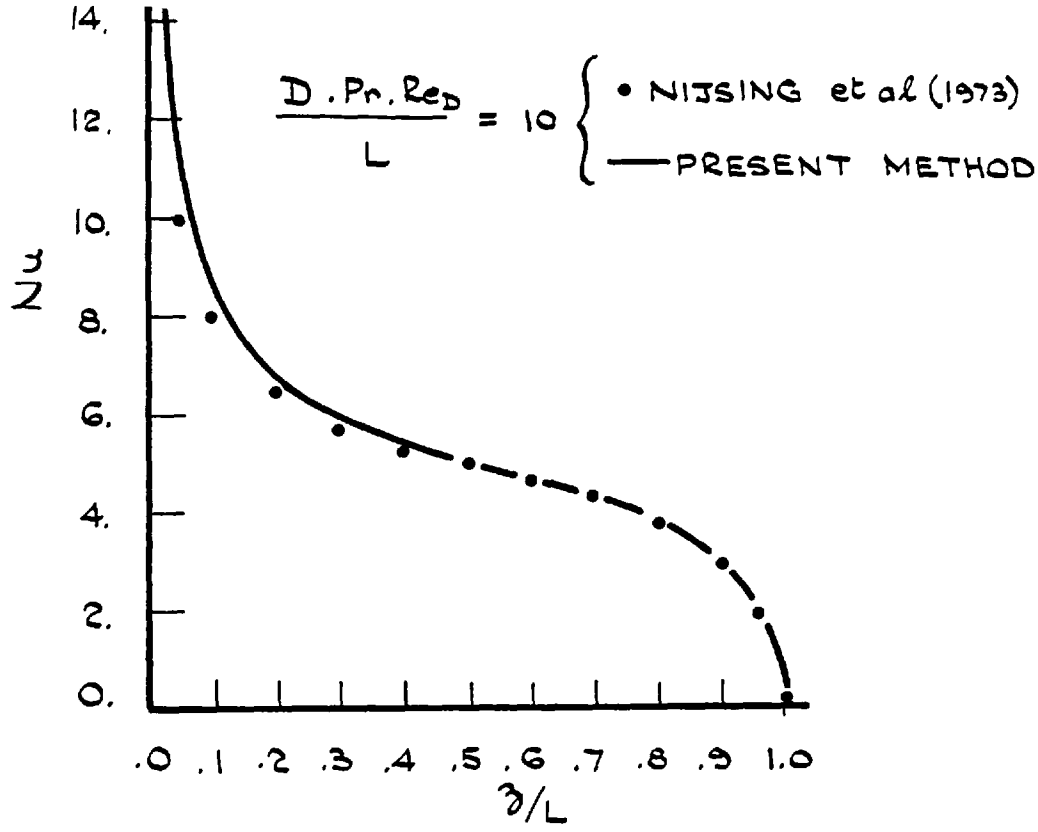

FIG(8.35) LOCAL NUSSELT NUMBER VS. z/L FOR LAMINAR FORCED - CONVECTIVE FLOW WITH SINUSOIDAL WALL HEAT-FLUX DISTRIBUTION.

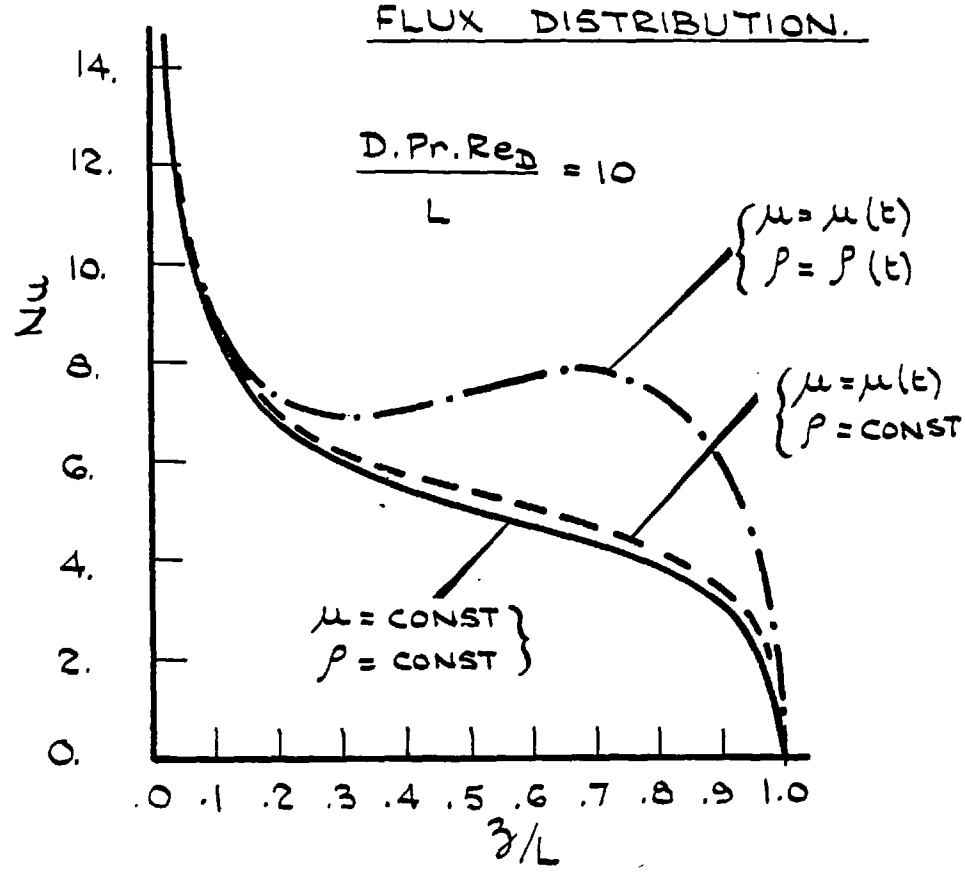

FIG(8.36) LOCAL NUSSELT NUMBER FOR SINUSOIDAL WALL HEAT-FLUX VARIATIONS IN THE FORCED-CONVECTION AND THE MIXED-CONVECTION REGIMES.

$$\dot{q}''_w(z) = \dot{q}''_{wo}\left(b + c \cdot \sin\frac{\pi z}{L}\right)$$

on a round tube lead to the following conclusions:-

1. For a mixed-convection regime the velocity and the temperature profiles continuously develop along the tube but never become fully-developed, Figs. (8.7), (8.9). This is shown to be due to the effects of the viscosity and the density variations with temperature. The study of these effects individually showed a stronger contribution of the density variations than of the viscosity on the profiles, Figs. (8.5) - (8.6). However, the fully-developed U and t profiles will be obtained only when μ and ρ are constant, i.e. in a forced-convection regime, Figs. (8.4) - (8.12), or when there is no heating, i.e. an adiabatic flow.

2. With the examination of the predictions for three prescribed heating cases, one with uniform and two with sinusoidal profiles shown on Fig. (8.3), it is noted that when the $\dot{q}''_{w.Max}/\dot{q}''_{w.min}$ increases:-

(a) $U_{\ell_{Max}}$ values decrease in contrast with U_{ℓ} .Inflexion while they occur at a larger axial distance z. Conversely, the tube length needed for $U_{\ell} = 0.00$ reduces, Fig. (8.23).

(b) Maximum wall temperature increases and occurs at a smaller distance from the tube entrance, Fig. (8.24).

(c) Mean pressure at a cross-section, p_{mean} does not

change significantly along the tube, Fig. (8.16). Also the mixed-convection index, i for the sinusoidal heating cases is less than its corresponding value for uniform heating, Fig. (8.18). The pressure profile across the tube is of a parabolic shape with higher pressures near the central layers, Fig. (8.15).

(d) The local Nusselt number, Nu increases throughout the tube, except near the exit where because of the shape of the $\dot{q}''_w$ profile it actually reduces, Fig. (8.27). However, in all of the cases Nu is above its fully-developed value of Nu = 4.364 which was obtained for the forced-convection case.

(d) Transition from laminar to an unstable-flow is predicted to occur at a smaller distance from the tube entry, Fig. (8.28). This prediction is based on the tentative transition parameter of Lawrence et al (1966) which depends only on the shape of the U profile and the entrance Reynolds number, Re_o.

3. By reducing the Re value while keeping the $\dot{Q}_{tot}$ constant, $U_{\ell} = 0.0$ occurs at a smaller axial distance, Fig. (8.9). Also p_{mean} reduces throughout the tube length, Fig. (8.16).

4. The effects of a parabolic entrance velocity profile, $U_o = 2(1 - r^2)$ on the flow specifications are not significant, Figs. (8.29) - (8.31), and the differences with those obtained for a uniform

U_o profile diminish downstream in the tube.

5. A cross-checking between the predictions for a typical sinusoidal heating case is made. This is done by treating the t_w profile, obtained for a sinusoidal $\dot{q}''_w$ profile, as data for a prescribed t_w case. A comparison between the $\dot{q}''_w$ profile obtained for the latter and the original sinusoidal $\dot{q}''_w$ profile adds to the confidence about the computer predictions, Fig. (8.32).

6. The computer predictions for a prescribed sinusoidal $\dot{q}''_w$ profile are compared with the analytical results of Hsu (1965) and Nijsing et al (1973) for the local Nusselt number distribution along the tube, Figs. (8.33), (8.35). Based on these comparisons, it is concluded that their results are valid only for a forced-convection regime, i.e. constant μ and ρ values with a fully-developed U profile. In mixed-convection regimes, the gain in the Nu values, particularly near the middle of the tube, is considerable, Figs. (8.34), (8.36).

CHAPTER 9

GENERAL REMARKS AND SUGGESTIONS FOR FUTURE WORK

9.1 General Remarks

Considering the conclusions at the end of Chapters (5) and (7) for flat ducts, and Chapter (8) for round tubes, the following remarks are made.

9.1.1 For Flat Duct Geometry

In laminar forced-convection flows, the present analysis assumes constant viscosity and density for the working fluid leading to fully-developed solutions for prescribed uniform heating cases. These consist of parabolic velocity and temperature profiles beyond the hydrodynamic and thermal entry lengths together with an asymptotic value for the local Nusselt number and the pressure-loss coefficient. For non-uniform heating cases, the present method solves the problem by dividing the prescribed boundary conditions into infinitesimal strips and treats them as uniform heating cases at each axial distance with the results of the previous position acting as initial conditions. Due to the assumption of constant ρ and μ values, the velocity profile will always assume its fully-developed shape beyond the hydrodynamic entry length regardless of the prescribed boundary conditions. Non-symmetrical heating cases were also considered. Important design parameters such as the local Nusselt number on both walls were obtained according to different ratios of the prescribed heat-fluxes (or temperatures) on the opposite walls.

For laminar mixed-convection flow, it is shown that the

effects of variations of viscosity and density should be considered. Consequently, the temperature and the velocity profiles will never become fully-developed and the local Nusselt numbers will assume values considerably higher as compared to their corresponding forced-convection values and do not approach an asymptotic value. Comparison of the present predictions for two uniformly heated flat ducts showed a good agreement with the published experimental results and also a marked improvement over the existing theoretical approaches. In sinusoidal heating cases, the simulation of the hot-channel of a plate-type nuclear fuel-element together with its neighbouring channels was treated with special interest.

Using the data of the University of London Reactor (ULR), the theoretical predictions for two different power levels (108.5 KW and 315 KW) showed that the nature of the flow in both of these cases will be of a mixed-convection nature. It was noted that even for the higher power level, the maximum wall temperature will still be less than that required for boiling and the axial velocity profile, although rather flat, will always remain without an inflexion point. The experimental results from a test-rig which was designed and successfully tested confirmed the validity of these theoretical predictions. In particular, the tests proved that the dominant parameter for the mixed-convection regimes is Gr_D/Re_D^2 and lead to the conclusion that a plan with Gr_D and Re_D as its co-ordinates with Gr_D/Re_D^2 as the governing parameter will facilitate the representation of the mixed-convection regimes and also the boundaries which exist between the forced, the mixed and the free-convection regimes. Experiments on the test-rig were conducted within the following constraints:-

$0.25 \leq \dot{q}''_w$ (w/cm^2) ≤ 1.66

$200 \leq Re_D \leq 600$

$0.50 \leq Gr_D/Re_D^2 \leq 2.50$

It should be pointed out that despite the efforts which were made, in terms of the design and the construction of the simulating heater plates, the thickness of these plates was still nearly three times larger than that of the actual ULR fuel-plate. This large thickness, it is believed, has contributed considerably to the longitudinal heat conduction which affected the present experimental results, and a thinner simulating plate would have produced more favourable results. Thus, the present theoretical predictions, e.g. wall temperature, are believed to be closer to the actual values than the experimental measurements. The present predictions for non-symmetrical heating cases show that the axial velocity profile will also be non-symmetrical, with the peak axial velocity occurring at a horizontal position between the centre of the duct and the wall with higher heating rate. The results for the case where one wall is sinusoidally heated while the other wall is insulated showed that the local Nusselt numbers will be larger than their corresponding forced-convection values but will still be smaller in comparison with the case where both of the walls were sinusoidally heated. For the mixed-convection cases, the present predictions show a larger pressure-loss coefficient than that conventionally assumed based on the average values of viscosity and density. Consequently, in a pure free-convection flow, the water flow rate for a given total heat-input to the duct will be reduced.

9.1.2 For Round Tube Geometry

The present method was shown to be successfully applicable to round tubes also. As for the flat duct, the laminar forced-convection results could have only been obtained when variations of μ and ρ with temperature were ignored. For several sinusoidal heating cases, these results were in good agreement with the published results of two other workers and it was shown that for mixed-convection regimes, the considerable increase in the local Nusselt number values must be considered. These increases were proved to be more significant when variations for both ρ and μ with temperature, rather than only for one of them, were considered. A review of the predictions obtained for three different prescribed $\dot{q}''_w$ profiles, according to the formula $\dot{q}''_w = \dot{q}''_{wo}\,(b + c \,.\, \sin\frac{\pi z}{L})$, on a typical round tube showed that by increasing the ratio $\dot{q}''_{w.Max}/\dot{q}''_{w.min}$ and at the same time keeping $\dot{q}''_{w.av}$ constant, the maximum wall temperature will be higher and as with the possible transition into an unstable flow, occurs at a smaller axial distance. Conversely, the centreline velocity and its value when the inflexion in the U profile occurs, although will be lower, is predicted to occur at larger axial distances. It is also noted that the mean pressure drop throughout the cross-section will not be significantly affected by the $\dot{q}''_{w.Max}/\dot{q}''_{w.min}$ ratio but the pressure-loss coefficient will still be larger than its conventional value based on the average viscosity and the density.

For round tube geometry, as for the flat duct, it is theoretically shown that a parabolic entrance velocity profile would only affect the predictions at the entrance region of the channel.

A cross-checking of the present predictions for a prescribed sinusoidal heating case in round tube geometry (and also for a prescribed

uniform heating case in flat duct geometry) added to the confidence about the present method.

9.2 Suggestions for Future Work

These suggestions are divided into two categories: one for theoretical; another for experimental. In what follows, these are explained in detail.

9.2.1 On the Theoretical Approach

The present approach for laminar flow is general and does not seem to require alterations in future work. However, in the execution of the approach, the following points are suggested:-

(a) Study of the prescribed $\dot{q}_w''$ (or t_w) profiles which were not specifically solved for in this thesis with the use of the computer programs DUCT and CIRCLE.

(b) As mentioned in Chapter (3), the conservation equations of mass and momentum are linked together in the present method. This requires that these equations be solved simultaneously and leads to a matrix which is non-symmetrical and not-banded. Consequently, the conventional methods for space saving, Cantin (1971), could have not been used for solution and regarding the largest available computer space (ULCC-CDC 7600), it has only been possible to choose up to 90 horizontal divisions. A recent paper by Hofmeister (1978) which contains a technique for solving this type of matrices on digital computers with restricted core size can be used in order to be able to increase the number of horizontal divisions. This will improve the slight non-symmetrical predictions for

the symmetrical heating cases with large $\dot{q}''_w$ values (c.f. 3.312 w/cm^2) and could lead to the possibility of being able to choose smaller axial increments (c.f. $\Delta Z = 0.625$).

(c) The computer programs DUCT and CIRCLE, for flat duct and round tube respectively, were used for the present theoretical predictions. Examination of the three principal conservation equations for these two geometries shows that those for the flat duct can be obtained from the equations for the round tube provided that the radius parameter r was replaced by the co-ordinate Y and also the terms with $\frac{1}{r}$ and $\frac{1}{r^2}$ were ignored. Those two provisions can be included in DUCT to make it suitable for solving round tube geometry too.

(d) The three principal conservation equations mentioned in Chapter (3) may also be written for an annular cross-section and solved for accordingly. Such a solution will have the advantage of covering the solution for annulus geometry in general and flat duct or round tube geometries as two extreme limits.

(e) The present experimental measurements, Chapter (7), show that for flat duct geometry, the assumption of a uniform wall temperature on the periphery of the cross-section is not strictly correct and a temperature profile seems to exist across the wall. This point will be more important if the solutions for flat ducts with smaller aspect ratios (c.f. w/d = 20.3) were sought. For round tube geometry, this will be of importance too because in some heating cases, the heat flux is unevenly distributed around the tube (e.g. a bank of tubes radiantly heated on one side) which leads to hot spots on the tube surface. These

effects can be acute for thin-walled tubes. A three-dimensional approach is suggested to deal with such cases.

(f) The scope of the work will be extended by solving the same set of equations (see Chapter.3) for turbulent flow where, depending on the turbulent-model, the eddy properties (instead of the fluid properties used in the present laminar solution) can be used for solution. The transition phenomenon could also be studied parallel with the turbulent flow solution.

9.2.2 On the Experimental Test-Rig

The utility of the present test-rig (see Chapter.6) can be extended by execution of the following suggestions:-

(a) Further tests of the present simulating heaters with larger values of heating rate, water flow rate and also the spacing of the test-channel.

(b) Non-symmetrical heating of the simulating plates and comparison of the results with the present predictions.

(c) Addition of a heat-exchanger to the water circuit in order to be able to recirculate the working fluid thus making it possible to test the apparatus with other working fluids.

(d) The narrow-sides of the test-channel may be made of a transparent material in order to be able to observe the flow inside the channel. Such arrangement will provide the possibility of measuring the velocity and the temperature profiles along the channel and

observing the appearance of an unstable flow.

(e) Other simulating plates with different wall heat-flux profiles will be useful to confirm the corresponding theoretical predictions. Also, insertion of heat-flux sensors in several axial positions of these plates will provide the data about the local heat-flux distribution along the test-channel.

(f) A pressure transducer may be placed at the entry to the test-section, Fig. (6.1), in order to facilitate the natural-convection tests in so far as showing the inlet pressure to the test-channel (which must be the same as that of the exit).

APPENDIX (I)

VALUES OF COEFFICIENTS FOR NUMERICAL INTEGRATION AND DIFFERENTIATION

TABLE (I.1)

VALUES OF COEFFICIENTS FOR NUMERICAL INTEGRATION - (REPRODUCED FROM SINGER (1954))

$$\frac{1}{Z_i - Z_o} \int_{Z_o}^{Z_i} F(Z) \cdot dZ = K \cdot e \sum_{J=0}^{N} C_J \cdot F(Z_J) \equiv a \sum_{J=0}^{N} C_J \cdot F(Z_J)$$

$$e = (Z_i - Z_o)/i$$

Exact for polynomials of max-degree	K	i \ J	0	1	2	3	4	5	6	7	8	9	10
4	$\frac{3}{10}$	6	11	- 44	96	- 84	41						
5	$\frac{3}{10}$	6	0	11	- 14	26	- 14	11					
6, 7	$\frac{1}{140}$	6	41	216	27	272	27	216	41	55			
5	$\frac{7}{1440}$	7	- 611	4277	- 9618	12782	- 8603	3213					
6	$\frac{7}{8640}$	7	751	- 640	8547	- 11648	14637	- 7224	4417				
7	$\frac{7}{17280}$	7	751	3577	1323	2989	2989	1323	3577	751			
8	$\frac{7}{518400}$	7	21361	116662	6958	155134	7840	105154	74578	31682	- 1169		
6	$\frac{8}{945}$	8	460	- 2760	8706	- 13904	13641	- 7464	2266				
7	$\frac{9}{945}$	8	0	460	- 954	2196	- 2459	2196	- 954	460			
8, 9	$\frac{4}{14175}$	8	989	5888	- 928	10496	- 4540	10496	- 928	5888	989		
7	$\frac{9}{4480}$	9	- 1787	16083	- 52839	105039	- 126801	98361	- 45069	11493			
8	$\frac{9}{44800}$	9	2857	- 4985	51966	- 110322	182680	- 177102	129666	- 50886	20727		
9	$\frac{9}{89600}$	9	2857	15741	1080	19344	5778	5778	19344	1080	15741	2857	
10	$\frac{9}{1971200}$	9	60259	372252	- 93015	736968	- 417834	781055	- 119332	335160	229527	89804	- 2595
9	$\frac{5}{4536}$	10	0	4045	- 11690	33340	- 55070	67822	- 55070	33340	- 11690	4045	
10 , 11	$\frac{5}{299376}$	10	16067	106300	- 48525	272400	- 260550	427368	- 260550	272400	- 48525	106300	16067

TABLE (1.2)

VALUES OF COEFFICIENTS FOR NUMERICAL DIFFERENTIATION - (REPRODUCED FROM SINGER (1964))

$$T'(Y)_i = \frac{K}{e} \sum_{J\ 0}^{N} C_J \cdot T(Y_j) \equiv d' \cdot M \sum_{J=0}^{N} C_j \cdot T(Y_j)$$

$$e = Y_{i+1} - Y_i$$

For polynomials of max-degree	i	j / K	0	1	2	3	4	5	6	7	8	9	10
2	0	1/2	- 3	4	- 1								
	1		- 1	0	1								
3	0	1/6	- 11	18	- 9	2							
	1		- 2	- 3	6	- 1							
4	0	1/12	- 25	48	- 36	16	- 3						
	1		- 3	- 10	18	- 6	1						
	2		1	- 8	0	8	- 1						
5	0	1/60	- 137	300	- 300	200	- 75	12					
	1		- 12	- 65	120	- 60	20	- 3					
	2		3	- 30	- 20	60	- 15	2					
6	0	1/60	- 147	360	- 450	400	- 225	72	- 10				
	1		- 10	- 77	150	- 100	50	- 15	2				
	2		2	- 24	- 35	80	- 30	8	- 1				
	3		- 1	9	- 45	0	45	- 9	1				
7	0	1/420	- 1089	2940	- 4410	4900	- 3675	1764	- 490	60			
	1		- 60	- 609	1260	- 1050	700	- 315	84	- 10			
	2		10	- 140	- 329	700	- 350	140	- 35	4			
	3		- 4	42	- 252	- 105	420	- 126	28	3			
8	0	1/840	- 2283	6720	- 11760	15680	- 14700	9408	- 3920	960	- 105		
	1		- 105	- 1338	2940	- 2940	2450	- 1470	588	- 140	15		
	2		15	- 240	- 798	1680	- 1050	560	- 210	48	- 5		
	3		- 5	60	- 420	- 378	1050	- 420	140	- 30	3		
	4		3	- 32	168	- 672	0	672	- 168	32	- 3		
9	0	1/2520	- 7129	22680	- 45360	70560	- 79380	63504	- 35280	12960	- 2835	280	
	1		- 280	- 4329	10080	- 11760	11760	- 8820	4704	- 1680	360	- 35	
	2		35	- 630	- 2754	5880	- 4410	2940	- 1470	504	- 105	10	
	3		- 10	135	- 1080	- 1554	3780	- 1890	840	- 270	54	- 5	
	4		5	- 60	360	- 1680	- 504	2520	- 840	240	- 45	4	
10	0	1/2520	- 7381	25200	- 56700	100800	- 132300	127008	- 88200	43200	- 14175	2800	- 252
	1		- 252	- 4609	11340	- 15120	17640	- 15876	10584	- 5040	1620	- 315	28
	2		28	- 560	- 3069	6720	- 5880	4704	- 2940	1344	- 420	80	- 7
	3		- 7	105	- 945	- 1914	4410	- 2646	1470	- 630	189	- 35	3
	4		3	- 40	270	- 1440	- 924	3024	- 1260	480	- 135	24	- 2
	5		- 2	25	- 150	600	- 2100	D*	2100	- 600	150	- 25	2

APPENDIX II

SIMULATION OF A SINUSOIDAL HEAT-FLUX WITH A PLATE WITH VARIABLE THICKNESS

Consider the variable thickness plate of Fig. (II.1) for simulation of the heat-flux profile, $\dot{q}''(z')$. If the voltage V_{AB} is exerted on this plate, the heating rate of the element dz' will be:-

$$d\{\dot{Q}(z')\} = I^2 \cdot d\{R'(z')\} \tag{II.1}$$

But:-

$$d\{R'(z')\} = \frac{\rho' \cdot dz'}{w \cdot \delta'(z')} \tag{II.2}$$

Combining Equations (II.1) - (II.2):-

$$d\{\dot{Q}(z')\} = I^2 \frac{\rho' \cdot dz'}{\delta'(z')} \tag{II.3}$$

This equation may be integrated throughout the plate to obtain $\dot{Q}_{tot}$:

$$\dot{Q}_{tot} = 2 \int_0^{L/2} I^2 \cdot \rho' \frac{dz'}{w \cdot \delta'(z')} \tag{II.4}$$

On the other hand, $\dot{Q}_{tot}$ may be calculated from the $\dot{q}''(z')$ profile:-

$$\dot{Q}_{tot} = 2 \int_0^{L/2} \dot{q}''(z') \cdot w \cdot dz' \tag{II.5}$$

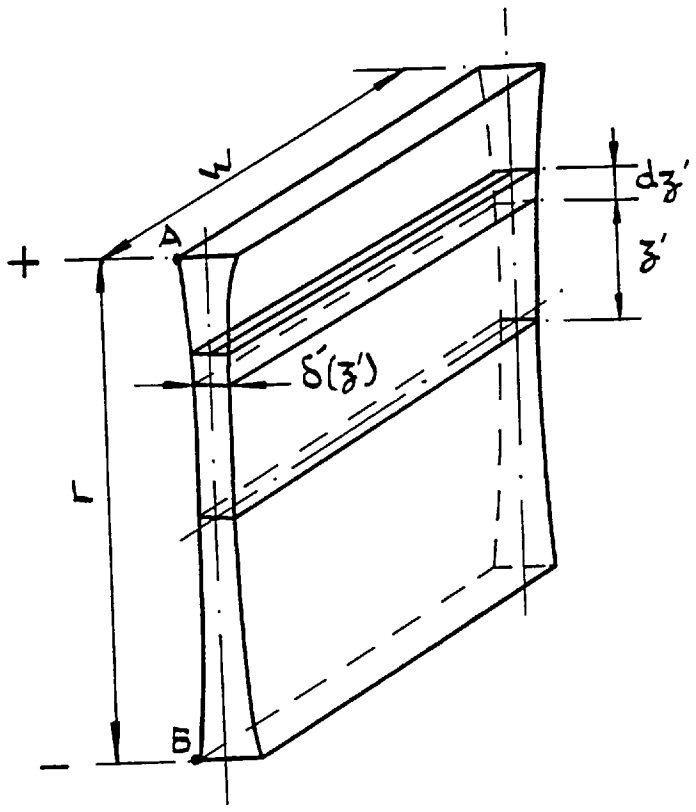

FIG. (II.1) THE VARIABLE THICKNESS PLATE.

Combination of Equations (II.4) - (II.5) leads to:-

$$\delta'(z') = \frac{I^2 \cdot \rho'}{w^2} \cdot \frac{1}{\dot{q}''' (z')} \qquad (II.6)$$

This equation shows that if the variable thickness plate is to simulate the prescribed $\dot{q}''' (z')$ profile, the $\delta' (z')$ and the $\dot{q}''' (z')$ functions vary in the opposite directions.

For the heat-flux profile: $\dot{q}''' (z') = \dot{q}'''_{max} \cdot \text{Cos} \frac{\pi z'}{L'}$.

Therefore:-

$$\delta'(z') = \frac{I^2 \cdot \rho'}{w^2 \cdot \dot{q}'''_{max}} \cdot \frac{1}{\text{Cos} \frac{\pi z'}{L'}} \qquad (II.7)$$

Equation (II.7) shows that the thickness $\delta'(z')$ is directly proportional to the square of the electric current and for reasonable thicknesses it must be quite high. This is because the rest of the parameters in Equation (II.7) lead to a comparatively small coefficient.

Assuming I = 416 A, and using the data of the 1950 W ULR fuel plate, Chapter (5), for a stainless steel simulating plate:-

$$\delta'(z') = \frac{0.902}{\text{Cos} \frac{\pi z'}{730}} \quad (\delta' \text{ and } z' \text{ are measured in mm})$$

Table (II.1) shows the thicknesses vary from 0.902 (mm) in the centre of the plate to 3.26 (mm) at the far-ends, which, despite the high electric current, (I = 416 A), are still very small.

TABLE (II.1)

z' (mm)	δ' (mm)
0.0	0.902
100.0	0.992
150.0	1.129
200.0	1.383
250.0	1.900
300.0	3.260

APPENDIX (III)

FINITE-DIFFERENCE FORM OF EQUATIONS (8.13) - (8.24)

These forms were obtained by using similar formulae for the partial differentiations as those used for the flat duct, Chapter (3). Obviously the variable Y in those formulae should be replaced by r.

The final form of Equations (8.13) - (8.16) and (8.22) are enclosed in the next pages. For Equations (8.17) - (8.21) and also (8.23) - (8.24), the procedure will be similar to those given for Equations (3.33) - (3.35), (3.24), (3.22) and (3.27) - (3.28) respectively.

$$\left\{\frac{2Mm\Delta Z}{m-1}\right\} V_{n+1,m} - (2\Delta ZM)\, V_{n+1,m-1} + (1)\, U_{n+1,m} + (1)\, U_{n+1,m-1} =$$

$$= (U_{n,m} + U_{n,m-1}) \tag{8.13}$$

$$\left[\frac{M^2}{2Re}\left\{\eta_A \frac{2m-1}{m-1} + \frac{\eta_B}{2}(T_{n+1,m+1} - T_{n+1,m-1})\right\} - \frac{M}{2} V_{n,m}\right] U_{n+1,m+1} +$$

$$+ \left[\frac{1}{Re}\left\{\eta_A \left(\frac{1}{\Delta Z^2} - 2M^2\right) + \frac{2\eta_B}{\Delta Z^2}(T_{n+1,m} - T_{n,m})\right\} - \frac{U_{n,m}}{\Delta Z}\right] U_{n+1,m} +$$

$$+ \left[\frac{M^2}{2Re} \cdot \left\{\eta_A \frac{2m-3}{m-1} - \frac{\eta_B}{2}(T_{n+1,m+1} - T_{n+1,m-1})\right\} + \frac{M}{2} V_{n,m}\right] U_{n+1,m-1} -$$

$$- \frac{P_{n+1,m}}{\Delta Z} = \left[\pm \frac{1}{Re^2}\left\{G_r \cdot C_{04} + T_{n+1,m}\,(C_{05} + C_{06} T_{n+1,m})\right\} \cdot \frac{\rho}{\rho_B} -\right.$$

$$- \frac{P_{n,m}}{\Delta Z} - \frac{U_{n,m^2}}{\Delta Z} + \frac{2U_{n,m}}{\Delta Z^2 \cdot Re}\left\{\eta_A + \eta_B(T_{n+1,m} - T_{n,m})\right\} - \frac{U_{n-1,m}}{\Delta Z^2 \cdot Re}\eta_A -$$

$$\left. - \frac{M\eta_B}{2Re\Delta Z}(T_{n+1,m+1} - T_{n+1,m-1}) \cdot (V_{n,m} - V_{n-1,m})\right] \tag{8.14}$$

$$\left[\frac{M^2}{2Re}\left\{\frac{\eta_A(2m-1)}{m-1} + \eta_B(T_{n+1,m+1} - T_{n+1,m-1})\right\} - \frac{M}{2} V_{n,m}\right] \cdot V_{n+1,m+1} +$$

$$+ \left[\frac{1}{Re}\left\{\eta_A \left(\frac{1}{\Delta Z^2} - \frac{(2m^2 - 4m + 3)\, M^2}{(m-1)^2}\right) + \frac{\eta_B}{\Delta Z^2}(T_{n+1,\,m} - T_{n,m})\right\} -\right.$$

$$- \frac{U_{n,m}}{\Delta z}\Bigg] V_{n+1,m} + \Bigg[\frac{M^2}{2Re}\{\eta_A \frac{2m-3}{m-1} - \eta_B (T_{n+1,m+1} - T_{n+1,m-1})\} +$$

$$+ \frac{M}{2} V_{n,m}\Bigg] V_{n+1,m-1} + (\frac{M}{12}) P_{n+1,m+2} - (\frac{2M}{3}) P_{n+1,m+1} + (\frac{2M}{3}) P_{n+1,m-1} -$$

$$- (\frac{M}{12}) P_{n+1,m-2} = \Bigg[- \frac{U_{n,m} \cdot V_{n,m}}{\Delta Z} + \frac{2V_{n,m} \cdot \eta_A}{Re \cdot \Delta Z^2} + \frac{V_{n-1,m}}{\Delta Z^2 \cdot Re}\{\frac{\eta_B}{2}(T_{n+1,m} -$$

$$- T_{n,m}) - \eta_A\} - \frac{M\eta_B}{2Re\Delta Z}(T_{n+1,m} - T_{n,m}) \cdot (U_{n,m+1} - U_{n,m-1})\Bigg] \qquad (8.15)$$

$$\eta_A = (CO1 \cdot T_{n+1,m}/G_r + CO2)^{-CO3}$$

$$\eta_B = \frac{d}{dT_{n+1,m}}(\eta_A)$$

$$\Bigg[\frac{M}{2} V_{n,m} + \frac{M^2(1-2m)}{2Pr \cdot Re(m-1)}\Bigg] T_{n+1,m+1} + \Bigg[\frac{U_{n,m}}{\Delta Z} + \frac{1}{Pr \cdot Re}\{2M^2 -$$

$$- \frac{1}{\Delta Z^2}\}\Bigg] T_{n+1,m} + \Bigg[\frac{M^2(3-2m)}{2Pr \cdot Re(m-1)} - \frac{M}{2} V_{n,m}\Bigg] T_{n+1,m-1} =$$

$$= \Bigg[(U_{n,m} - \frac{2}{Pr \cdot Re\Delta Z}) \cdot \frac{T_{n,m}}{\Delta Z} + \frac{T_{n-1,m}}{\Delta Z^2 \cdot Pr \cdot Re}\Bigg] \qquad (8.16)$$

Equation (8.22)

(i) When $\dot{q}''_w$ profile is prescribed:-

$$\sum_{m=2}^{M} \frac{\rho}{\rho_o} (m - 1)\, U_{n+1,m} \cdot T_{n+1,m} - \sum_{m=2}^{M} (m - 1) \cdot U_{n,m} \cdot T_{n,m} \cdot \frac{\rho}{\rho_o} =$$

$$= \frac{\Delta Z \cdot M^3}{Re \cdot Pr} \cdot \left| HFI \right|_{\text{Integrated between Z and Z + dZ}} \qquad (8.22)$$

(ii) When t_w profile is prescribed:-

$$\sum_{m=2}^{M} \frac{\rho}{\rho_o} (m - 1) \cdot U_{n+1,m} \cdot T_{n+1,m} - \sum_{m=2}^{M} (m - 1) \cdot U_{n,m} \cdot T_{n,m} \cdot \frac{\rho}{\rho_o} =$$

$$= \frac{\Delta Z \cdot M^2}{Re \cdot Pr} \cdot \left| \frac{dT}{dr} \right|_{r = 1} \qquad (8.22)$$

APPENDIX (IV)

FLOW-CHART OF THE 'CIRCLE' COMPUTER PROGRAM

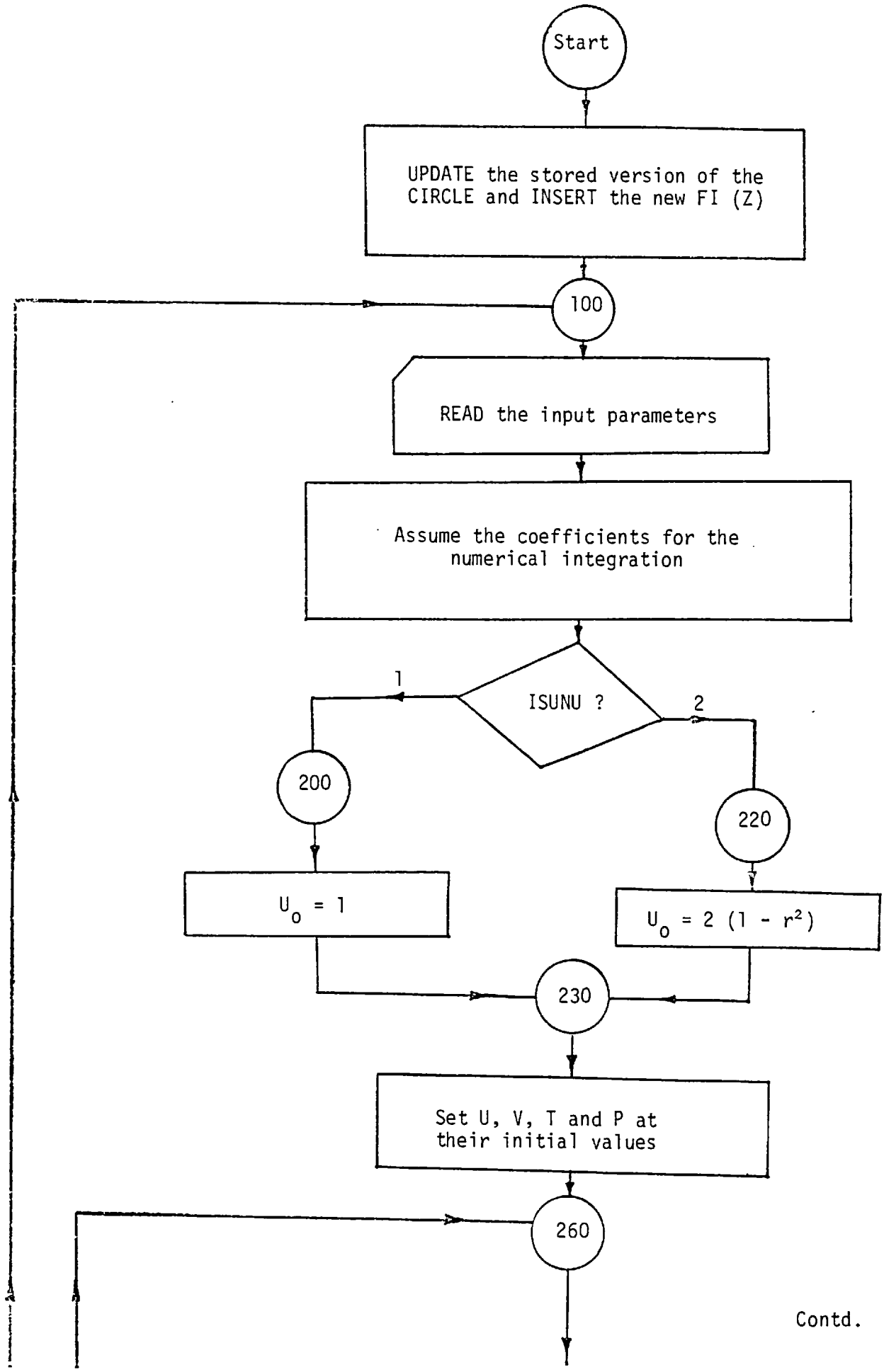

Contd.

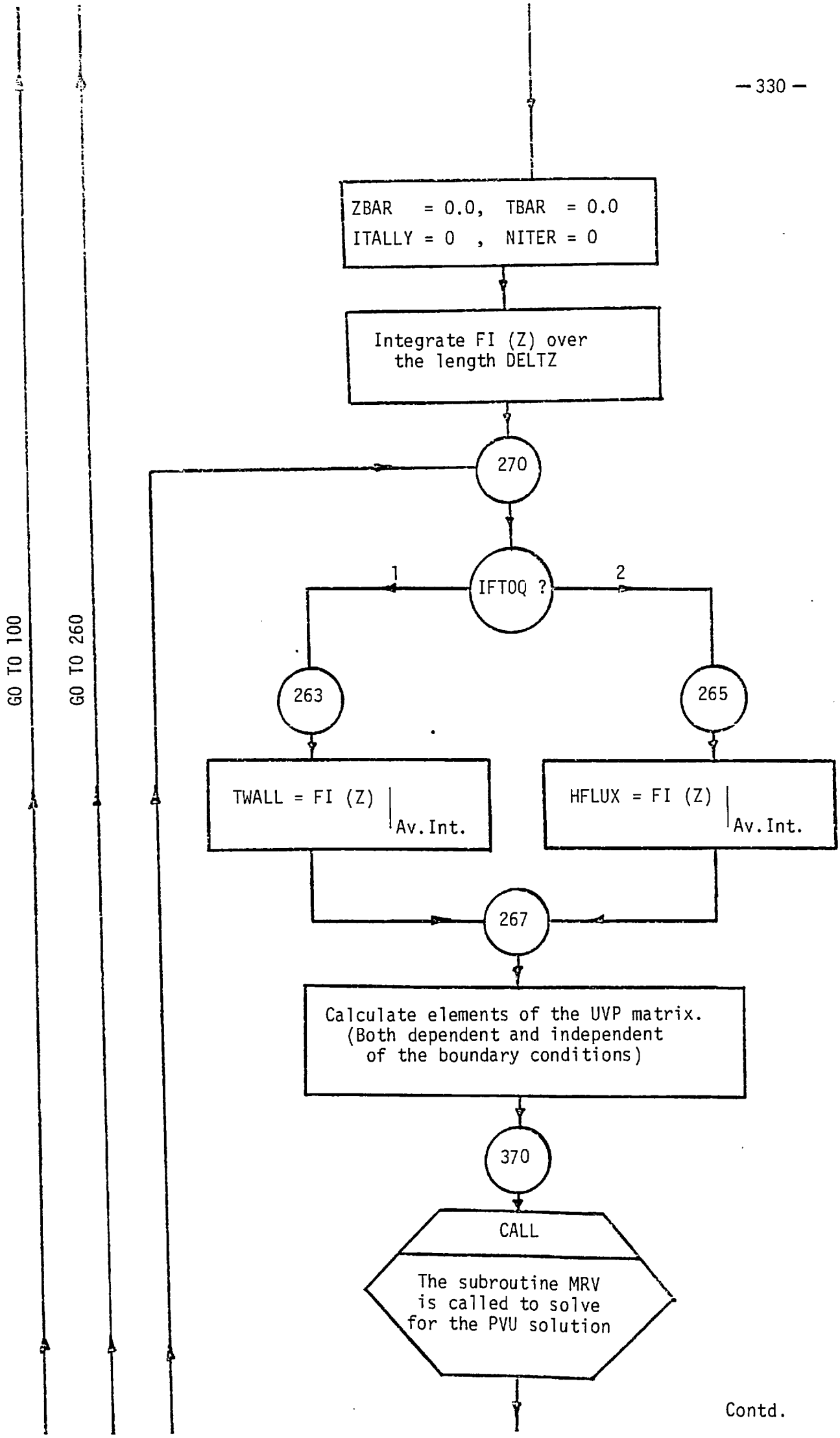
ZBAR = 0.0, TBAR = 0.0
ITALLY = 0 , NITER = 0
Integrate FI (Z) over the length DELTZ
270
IFTOQ ?
1
2
263
265
TWALL = FI (Z) | Av.Int.
HFLUX = FI (Z) | Av.Int.
267
Calculate elements of the UVP matrix. (Both dependent and independent of the boundary conditions)
370
CALL
The subroutine MRV is called to solve for the PVU solution
GO TO 100
GO TO 260

Contd.

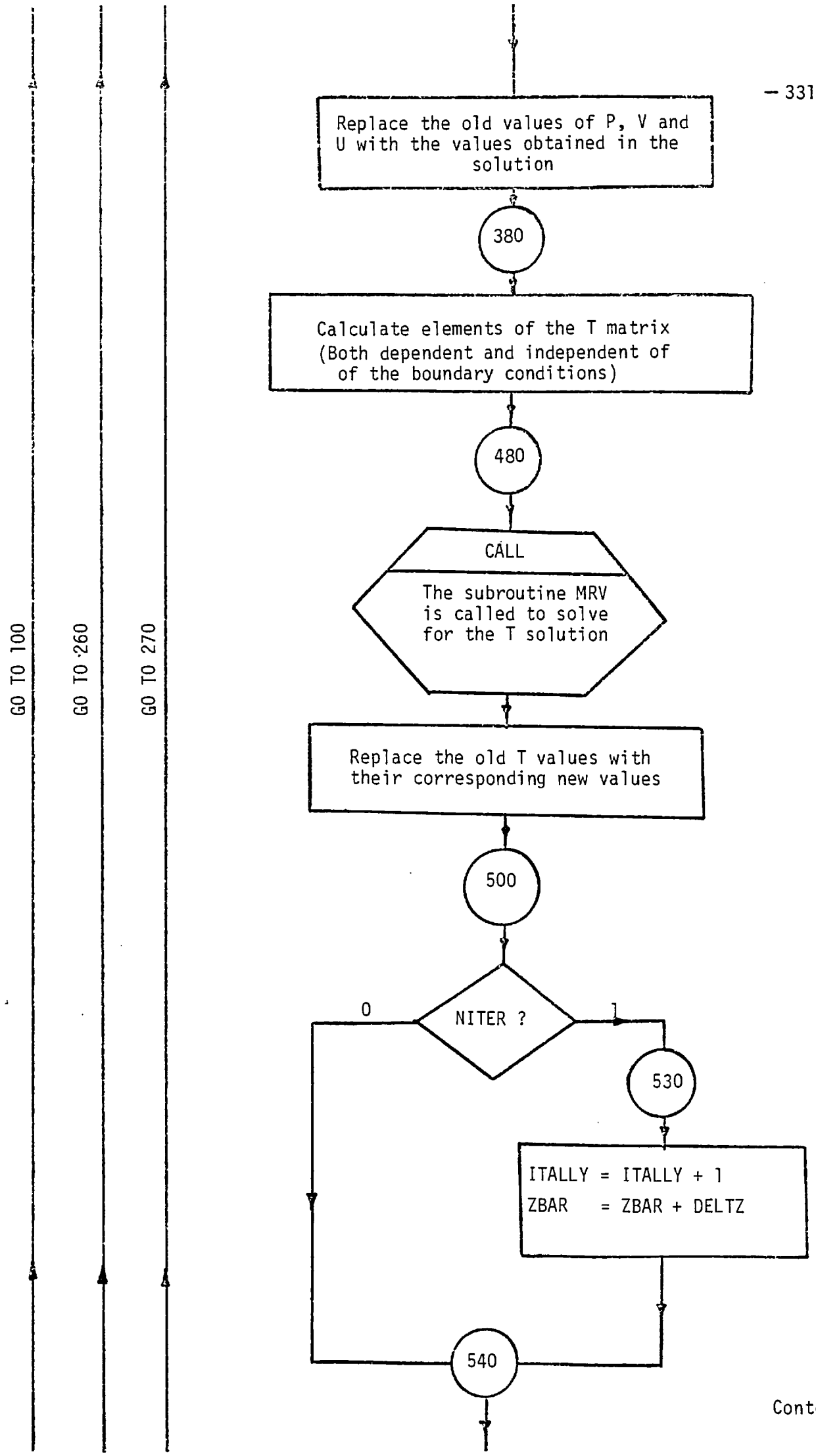
GO TO 100
GO TO 260
GO TO 270
Replace the old values of P, V and U with the values obtained in the solution
380
Calculate elements of the T matrix (Both dependent and independent of of the boundary conditions)
480
CALL
The subroutine MRV is called to solve for the T solution
Replace the old T values with their corresponding new values
500
NITER ?
0
1
530
ITALLY = ITALLY + 1
ZBAR = ZBAR + DELTZ
540

Contd.

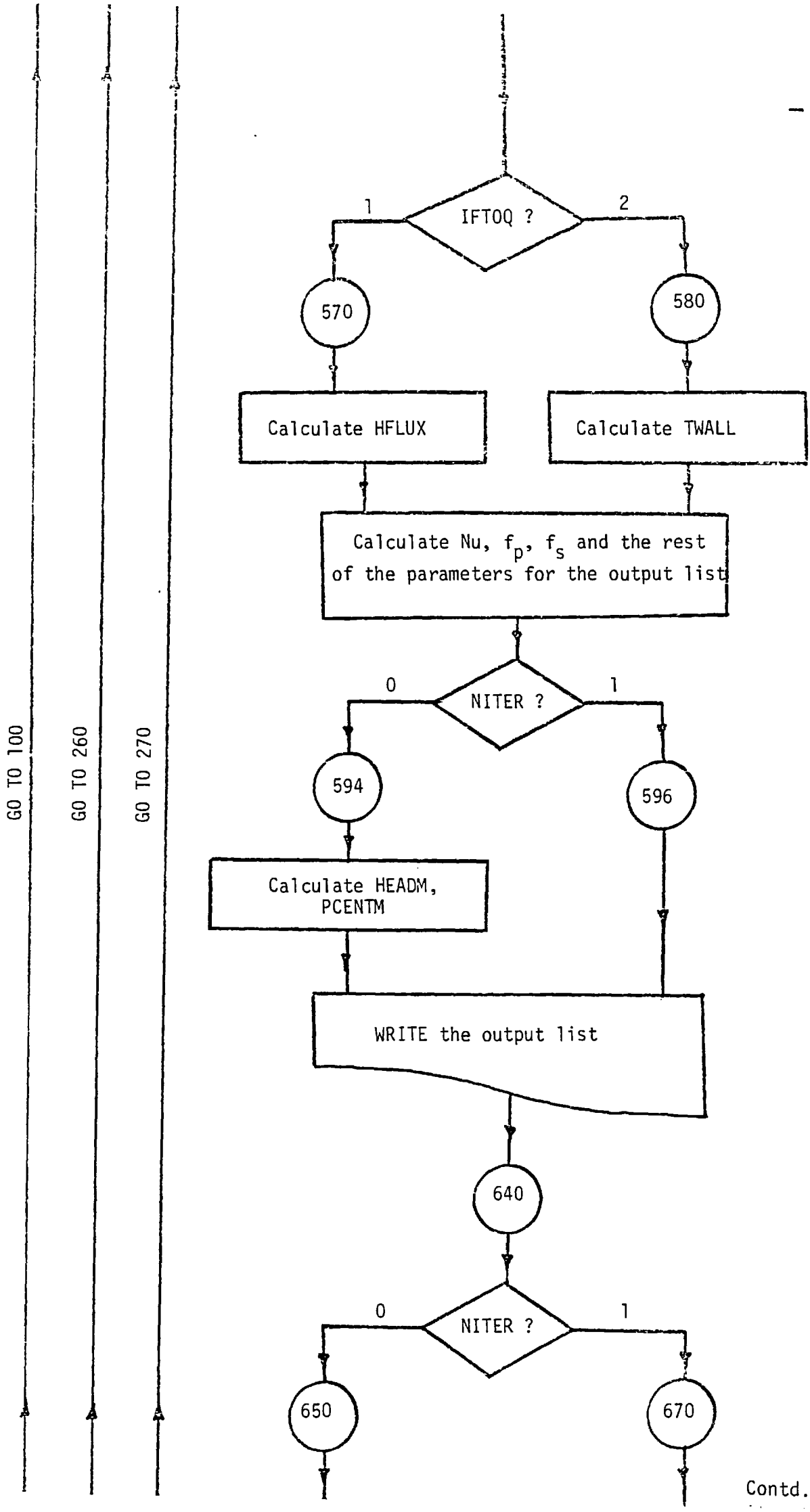
GO TO 100
GO TO 260
GO TO 270
IFTOQ ?
1
2
570
580
Calculate HFLUX
Calculate TWALL
Calculate Nu, f_p, f_s and the rest of the parameters for the output list
NITER ?
0
1
594
596
Calculate HEADM, PCENTM
WRITE the output list
640
NITER ?
0
1
650
670

Contd.

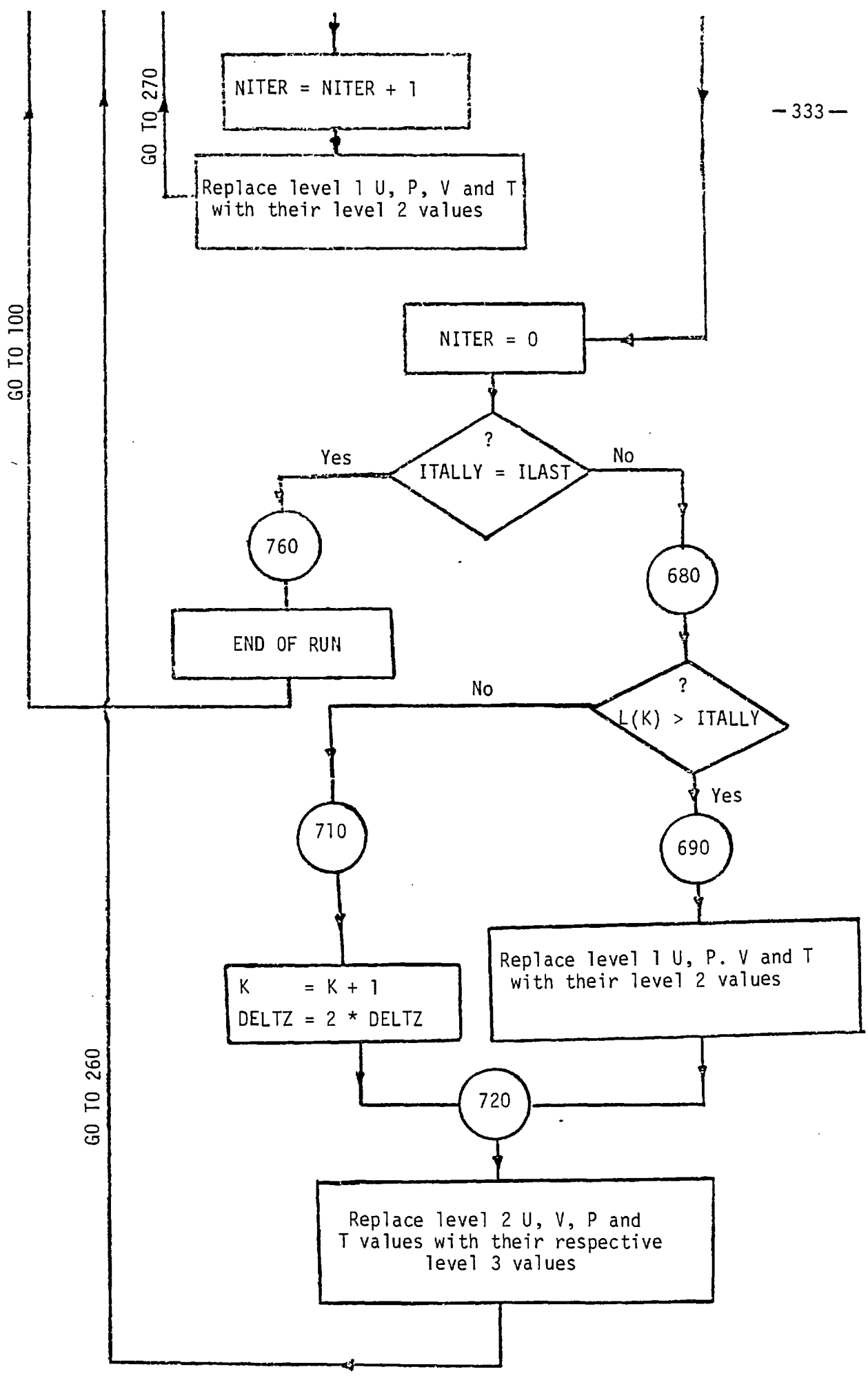
NITER = NITER + 1
GO TO 270
Replace level 1 U, P, V and T with their level 2 values
GO TO 100
NITER = 0
?
ITALLY = ILAST
Yes
No
760
680
END OF RUN
?
L(K) > ITALLY
No
Yes
710
690
K = K + 1
DELTZ = 2 * DELTZ
Replace level 1 U, P. V and T with their level 2 values
720
GO TO 260
Replace level 2 U, V, P and T values with their respective level 3 values

REFERENCES

ALLEN, D. N. and SOUTHWELL, R. V. (1955)
Quart. Jr. Mech. and Appl. Math. Part 2, Vol. 8, p. 129.

BANKSTON, C. A. and McELIGOT, D. M. (1969)
"Prediction of Tube Wall Temperature with Axial Variation of Heating Rate and Gas Property Variation". Nucl. Sci. and Engng., Vol. 37, pp. 157 - 162.

BODOIA, J. R. and OSTERLE, J. F. (1959)
"Finite Difference Analysis of Plane Poiseuille and Couette Flow Development". Appl. Sci. Res., pp. 265 - 276, Vol. A10.

BODOIA, J. R. and OSTERLE, J. F. (1962)
"The Development of Free Convection Between Heated Vertical Plates". Journal of Heat Transfer, TRANS.ASME, pp. 40 - 44.

BRITISH DRIVER-HARRIS (1974)
"Nickel-Chromium Resistance-Heating Alloys". The Nichrome Series, British Driver-Harris, Data Sheet No. 5.

BURHOLT, G. (1974)
"Proposed Replacement Fuel Elements For the University of London Reactor". ULRC, Reac. S/14/3, June.

CAMPBELL, W. D. and SLATTERY, J. C. (1936)
"Flow in the Entrance of a Tube". ASME Paper No. 62-Hyd-6.

CANTIN, G. (1971)
"An Equation Solver of Very Large Capacity". Int. J. for Num. Methods in Engng., Vol. 3, pp. 379 - 388.

CESS, R. D. and SHAFFER, E. C. (1958)
"Heat Transfer to Laminar Flow Between Parallel Plates With a Prescribed Wall Heat Flux". Appl. Sci. Res., Vol. A8, pp. 339 - 344.

CESS, R. D. and SHAFFER, E. C. (1960)
"Laminar Heat Transfer Between Parallel Plates With an Unsymmetrically Prescribed Heat Flux at the Walls". Appl. Sci. Res., Vol. A9, pp. 64 - 70.

CHATO, J. C. (1963)
"Natural Convection Flows in Parallel-Channel Systems". Journal of Heat Transfer, TRANS.ASME, pp. 339 - 345.

CHEN, T. S. and MUCOGLU, A. (1975)
"Buoyancy Effects on Forced Convection Along a Vertical Cylinder". Journal of Heat Transfer, TRANS.ASME, pp. 198 - 203.

CHEN, T. S. and MUCOGLU, A. (1976)
"Buoyancy Effects on Forced Convection Along a Vertical Cylinder with Uniform Surface Heat Flux". Journal of Heat Transfer, TRANS.ASME, pp. 523 - 525.

COLLINS, M. W. (1971)
"Combined Convection in Vertical Tubes". Inst. of Mech. Engrs. Proc. for Symposium, London, September.

COLLINS, M. W. (1975)
"An Analysis of Combined Natural and Forced Convection and Other Problems in Internal Laminar Flow". Ph.D. Thesis, City University, September.

DAVIS, L. P. and PERONA, J. P. (1971)
"Development of Free Convection Flow of a Gas in a Heated Vertical Circular Tube". Int. J. Heat and Mass Transfer, Vol. 14, pp. 889 - 903.

DIJKMAN, F. J. M. (1969)
"Some Hydrodynamic Aspects of a Boiling Water Channel". Dissertation for D. Engrg. Sci., Eindhoven University of Technology, December.

DYER, J. R. (1968)
"The Development of Natural Convection in a Vertical Circular Duct". Mech. Chem. Engng., TRANS Inst. Engrs., Aug. MC4, pp. 78 - 86.

DYER, J. R. (1975)
"The Development of Laminar Natural-Convective Flow in a Vertical Uniform Heat Flux Duct". Int. J. Heat and Mass Transfer, Vol. 18, pp. 1455 - 1465.

DZUNG, L. S. (1958a)
"Heat Transfer in a Round Duct with Sinusoidal Heat-Flux Distribution". 2nd U.N. Conference on Atomic Energy, A/Conf. 15/Pap. 253.

DZUNG, L. S. (1958b)
"Heat Transfer in a Flat Duct with Sinusoidal Heat Flux Distribution". 2nd U.N. Conference on Atomic Energy, A/Conf. 15/Pap. 254.

ELENBAAS, W. (1942a)
"Heat Dissipation of Parallel Plates by Free Convection". Physica, S'Grav., Vol. 9, pp. 1 - 28.

ELENBAAS, W. (1942b)
"The Dissipation of Heat by Free Convection (from) The Inner Surface of Vertical Tubes of Different Shapes of Cross-Section". Physica, S'Grav., Vol. 9, pp. 865 - 874.

GRAETZ, L. (1885)
Annalen d. Physik (N.F.), Vol. 25, p. 337.

GRIGULL, U. and TRATZ, H. (1965)
"Thermischer Einlauf In Ausgenbildeter Laminarer Rohrströmung". Int. J. of Heat and Mass Transfer, Vol. 8, pp. 669 - 678.

HALLMAN, T. M. (1956)
"Combined Forced and Free-Laminar Heat Transfer in Vertical Tubes With Uniform Internal Heat Generation". TRANS.ASME, pp. 1831 - 1841.

HALLMAN, T. M., SPARROW, E. M. and SIEGEL, R. (1958)
"Steady Laminar Heat Transfer in a Circular Tube With Prescribed Wall Heat Flux". Appl. Sci. Res., Vol. A7, pp. 386 - 392.

HALLMAN, T. M. (1961)
"Experimental Study of Combined Forced and Free Laminar Convection in a Vertical Tube". NASA.TN.D-1104, December.

HANRATTY, T. J., ROSEN, E. M. and KABEL, R. L. (1958)
"Effect of Heat Transfer on Flow Field at Low Reynolds Numbers in Vertical Tubes". Industrial and Engineering Chemistry, Vol. 50, No. 5, p. 815.

HANRATTY, T. J., ROSEN, E. M. and SCHEELE, G. F. (1960)
"Effects of Natural Convection on Transition to Turbulence in Vertical Pipes". The Canadian Journal of Chem. Engng., pp. 67 - 73, June.

HANRATTY, T. J. and ROSEN, E. M. (1961)
"Use of Boundary-Layer Theory to Predict the Effect of Heat Transfer on the Laminar-Flow Field in a Vertical Tube with a Constant-Temperature Wall". A.I.Ch.E. Journal, pp. 112 - 123, March.

HANRATTY, T. J. and SCHEELE, G. F. (1962)
"Effect of Natural Convection on Stability of Flow in a Vertical Pipe". Journal of Fluid Mechanics, Vol. 14, Part 2, pp. 244 - 256.

HEAD, J. L. (1962)
"Calculation of Coolant Mass Flow Through the Core and Fuel Plate Temperature". ULRC Special Report.

HOFMEISTER, L. D. (1978)
"An out-of Core Equation Solver For Full Unsymmetric Matrices". Int. J. of Num. Methods in Engng., Vol. 12, pp. 721 - 731.

HOLMAN, J. P. (1968)
"Heat Transfer". Text-book, McGraw-Hill Company, New York, pp. 202 - 205, 2nd. Ed.

HORNBECK, W. R. (1964)
"Laminar Flow in the Entrance Region of a Pipe". Appl. Sci. Res., Vol. A13, pp. 224 - 232.

HSU, C. J. (1965)
"Heat Transfer in a Round Tube with Sinusoidal Wall Heat-Flux Distribution". A.I.Ch.E. Journal, pp. 690 - 695, July.

HWANG, G. J. and SHEU, J. P. (1974)
"Effect of Radial Velocity Component in Laminar Forced Convection in Entrance Region of a Circular Tube". Int. J. of Heat and Mass Transfer, Vol. 17, pp. 372 - 375.

IQBAL, M., AGGARWALA, B. D. and ROKERYA, M. S. (1970)
"Viscous Dissipation Effects on Combined Free and Forced Convection Through Vertical Circular Tubes". Journal of Appl. Mechs., TRANS.ASME, pp. 931 - 935.

JACOB, M. (1949)
"Heat-Transfer". Vol. 1, John Wiley and Sons, New York, p. 451.

JOHNSON, H. A. and CLABAUGH, W. J. (1954)
TRANS.ASME., Vol. 76, No. 4.

KAYS, W. M. (1955)
TRANS.ASME., Vol. 77, p. 1265.

KAYS, W. M. and LEUNG, E. Y. (1963)
"Heat Transfer in Annular Passages - Hydrodynamically Developed Turbulent Flow with Arbitrary Prescribed Heat Flux". Int. J. of Heat and Mass Transfer, Vol. 6, pp. 537 - 557.

KAYS, W. M., REYNOLDS, W. C. and HEATON, H. S. (1964)
"Heat Transfer in Annular Passages. Simultaneous Development of Velocity and Temperature Fields in Laminar Flow". Int. J. of Heat and Mass Transfer, Vol. 7, pp. 763 - 781.

KAYS, W. M. (1966)
"Convective HEAT and MASS transfer". Text-book, McGraw-Hill Company, London.

KEMENY, G. A. and SOMERS, E. V. (1962)
"Combined Free and Forced-Convective Flow in Vertical Circular Tubes - Experiments With Water and Oil". Journal of Heat Transfer, TRANS.ASME, pp. 339 - 346.

KNUDSON and KATZ (1958)
"Fluid Mechanics and Heat Transfer". Text-book, McGraw-Hill, pp. 99 - 105, New York.

LANGHAAR, H. L. (1942)
Journal of Applied Mechs., TRANS.ASME. Vol. 64, A55.

LAWRENCE, W. T. (1965)
"Entrance Flow and Transition From Laminar to Turbulent Flow in Vertical Tubes With Combined Free and Forced Convections". Sc.D. Thesis, M.I.T.

LAWRENCE, W. T. and CHATO, J. C. (1966)
"Heat-Transfer Effects on the Developing Laminar Flow Inside Vertical Tubes". Journal of Heat Transfer, TRANS.ASME, pp. 214 - 222.

LIN, C. C. (1955)
"Hydrodynamic Stability". Cambridge University Press, London.

LUNDBERG, R. E., REYNOLDS, W. C. and McCUEN, P. A. (1963)
"Heat Transfer in Annular Passages. General Formulation of the Problem for Arbitrarily Prescribed Wall Temperatures or Heat-Fluxes". Int. J. Heat and Mass Transfer, Vol. 6, pp. 483 - 493.

LUNDBERG, R. E., McCUEN, P. A. and REYNOLDS, W. C. (1963)
"Heat Transfer in Annular Passages. Hydrodynamically Developed Laminar Flow with Arbitrarily Prescribed Wall Temperatures or Heat-Fluxes". Int. J. Heat and Mass Transfer, Vol. 6, pp. 495 - 529.

MARTIN, B. W. (1973)
"Viscous Heating and Varying Viscosity Effects on Developing Laminar Flow in a Circular Pipe". Proc. Inst. Mech. Engrs., Vol. 187, pp. 435 - 445.

McCORMACK, J. M. and SALVADORI, M. G. (1964)
"Numerical Methods in Fortran". Prentice Hall.

McCUEN, P. A. (1962)
"Heat Transfer With Laminar and Turbulent Flow Between Parallel Planes With Constant and Variable Wall Temperature and Heat Flux". Ph.D. Thesis, Stanford University, April.

METIAS, B. and ECKERT, R. G. (1964)
"Forced, Mixed, and Free Convection Regimes". Journal of Heat Transfer, TRANS.ASME, pp. 295 - 296.

MUZZY, R. J., BURNETTE, G. W., NILSSON, K. A., SOZZI, G. L., WALKER, J. P. and WING, K. D. (1974)
"Task B Topical Report : Evaluation of Direct Heaters and Hydrodynamic Measurement Techniques Under Simulated LOCA Conditions in a Single-Loop Test Apparatus". GEAP-20512, June.

NAYAK, A. L. and PING CHENG (1975)
"Finite Element Analysis of Laminar Convective Heat Transfer in Vertical Ducts with Arbitrary Cross-Section". Int. J. Heat and Mass Transfer, pp. 227 - 236, February.

NIJSING, R. (1972)
"Heat Exchange and Heat Exchangers with Liquid Metals". Lecture Series No. 57 on Heat Exchangers, AGARD, Paris.

NIJSING, R. and EIFLER, W. (1973)
"The Hybrid Method, a New Method For Accurate Heat Transfer Predictions In Channels With Axially Variable Heat Flux". Appl. Sci. Res., Vol. 28, pp. 401 - 418, December.

OLUSOJI, O. F. I. and HETHERINGTON, H. J. (1977)
"Application of the Finite Element Method to Natural Convection Heat Transfer From the Open Vertical Channel". Int. J. Heat and Mass Transfer, Vol. 20. pp. 1195 - 1204.

OOSTHUIZEN, P. H. (1973)
"A Numerical Study of Laminar Combined Convective Flow Over Flat Plates". Journal of Heat Transfer, TRANS.ASME, pp. 60 - 63.

ORNATSKIY, A. P., CHERNOBAY, V. A., VASIL'YEV, A. F. and PERKOV, S. V. (1975)
"Heat Transfer Crisis In Annuli with Cosinusoidal Heat Release Along the Length". Heat Transfer - Soviet Research, Vol. 7, No. 3, May - June.

OSTRACH, S. (1952)
"Combined Natural and Forced Convection Laminar Flows and Heat Transfer of Fluids With and Without Heat Sources in Channels With Linearly Varying Wall Temperatures". NACA-TN. 2863.

PAI, S. (1956)
"Viscous Flow Theory". Vol. 1; D. Van Nostrand Co. Inc., Princeton, New Jersey, p. 309.

PATANKAR, S. V., SPARROW, E. M. and ABDEL-WAHED, R. M. (1976)
"Mixed Convection On a Vertical Plate With an Unheated Starting Length". Journal of Heat Transfer, TRANS.ASME, pp. 576 - 580.

PETROVICHEV, V. I. (1960)
"Heat Transfer to Mercury in a Circular Tube and Annular Channels With Sinusoidal Heat Load Distribution". Int. J. Heat Mass Transfer, Vol. 1, pp. 115 - 120.

PIGFORD, R. L. (1955)
"Nonisothermal Flow and Heat Transfer Inside Vertical Tubes". Chem. Eng. Proc. Symp. Ser., Vol. 51, No. 17, p. 79.

REISMAN, O. I. and PARKER, R. O. (1977)
"Laminar Heat Transfer Data with a Step-Varying Wall Heat Flux". Nucl. Sci. and Engng., Vol. 63, pp. 188 - 218.

REYNOLDS, W. C., McCUEN, P. A., LUNDBERG, R. E., LEUNG, Y. W. and HEATON, H. S. (1960)
"Heat Transfer in Annular Passages with Variable Wall Temperature and Heat-Flux". Stanford University, Dept. Mech. Engng., Rep. No. AHT-1, May.

RILEY, J. A. (1970)
"Combined Convective Heat Transfer In a Vertical Channel of Rectangular Cross-Section". Journal of the British Nuclear Energy Society, Vol. 9, No. 4, pp. 235 - 243, October.

SAVINO, J. M. and SIEGEL, R. (1964)
"Laminar Forced Convection in Rectangular Channels With Unequal Heat Addition on Adjacent Sides". Int. J. Heat and Mass Transfer, Vol. 7, pp. 733 - 741.

SAVKAR, S. D. (1970)
"Developing Forced and Free Convective Flows Between Two Semi-Infinite Parallel Plates". 4th International Heat Transfer Conference, Versailles.

SCHILLER, L. (1921)
Z. angew. Math. Mech., Vol. 2, p. 96.

SCHMIDT , W. P. M. (1967)
Int. J. Heat Mass Transfer, Vol. 10, p. 541.

SCHMITZ, R. A. and ULRICHSON, D. L. (1965)
"Laminar-Flow Heat Transfer In The Entrance Region of Circular Tubes". Int. J. Heat Mass Transfer, Vol. 8, pp. 253 - 258.

SELLARS, J. R., TRIBUS, M. and KLEIN, J. S. (1956)
"Heat Transfer to Laminar Flow in a Round Tube or Flat Conduit - The Graetz Problem Extended". TRANS.ASME, pp. 441 - 448, February.

SINCLAIR and BUDD (1975)
"CDC UPDATE Reference Manual". Imperial College Computer Centre, June.

SINGER, J. (1964)
"Elements of Numerical Analysis". Academic Press.

STEIN, R. P. (1966)
Advances in Heat Transfer, Vol. 3, pp. 101 - 174, Academic Press Inc., New York.

TRIBUS, M. and SLEICHER, C. A. (1957)
"Heat Transfer In a Pipe with Turbulent Flow and Arbitrary Wall-Temperature Distribution". TRANS.ASME, Vol. 79, pp. 789 - 797.

VERNIER, P. H. (1962)
"Natural Convection In a Uniformly Heated Vertical Channel With Rectangular Cross-Section". C.E.A. Rep. No. 2197, E.I.S. Translation No. T13409.

ZELDIN, B. and SCHMIDT , F. W. (1970)
"Laminar Heat Transfer In The Entrance Region of Ducts". Appl. Sci. Res., Vol. 23, pp. 73 - 94, October.

ZELDIN, B. and SCHMIDT , F. W. (1972)
"Developing Flow with Combined Forced-Free Convection in an Isothermal Vertical Channel". Journal of Heat Transfer, TRANS.ASME, pp. 211 - 223.

ZIENKIEWICZ, O. C. and TAYLOR, C. (1975)
"Finite Elements in Fluids". Text-book, John Wiley & Sons.